

## Electromagnetic and acoustic waves in layered organic conductors (a review)

O. V. Kirichenko and V. G. Peschansky

*B. Verkin Institute for Low Temperature Physics and Engineering, National Academy of Sciences of Ukraine, 310164 Kharkov, Ukraine\**)

(Submitted April 8, 1999; revised May 21, 1999)

Fiz. Nizk. Temp. **25**, 1119–1144 (November 1999)

The review is devoted to theoretical investigations of propagation of electromagnetic and acoustic waves in layered conductors of organic origin. Attention is focussed on spectroscopic possibilities for studying the electron structure of organic quasi-two-dimensional conductors, which is of great importance for understanding physical processes in these materials. High-frequency and magnetoacoustic effects considered in this review are typical of quasi-two-dimensional conductors and quite informative. The analysis of these effects makes it possible to study in detail the electron energy spectrum and relaxation properties of charge carriers in layered conductors. © 1999 American Institute of Physics. [S1063-777X(99)00111-5]

### 1. INTRODUCTION

The search for new materials in the sixties attracted the attention of researchers to conductors of organic origin with a layered or filamentary structure. Intense experimental investigations of physical properties of organic conductors were stimulated in the hope of obtaining superconductors with high critical parameters just among quasi-one-dimensional filamentary conductors in which a superconducting transition can theoretically occur at high temperatures. Many years of efforts made by physicists and chemists to obtain a large number of new organic conductors culminated in the synthesis of organic quasi-one-dimensional conductors with a superconducting transition temperature  $T_c$  of the order of several kelvins as well as layered organic superconductors with a record-high superconducting transition temperature  $T_c \cong 13$  K. Although these values of  $T_c$  are lower than for some intermetallic compounds, the interest towards the electronic properties of organic conductors remains unabated.

Layered conductors of organic origin are attractive for experimenters to a considerable extent due to their peculiar behavior in strong magnetic fields and a number of phase transitions under comparatively low pressures. Their electrical conductivity along layers is several orders of magnitude higher than electrical conductivity along the normal  $\mathbf{n}$  to the layers, and the critical magnetic field at which superconductivity is violated depends considerably on its orientation relative to the layers. Under the action of applied pressure, the superconducting transition temperature of the  $\beta$ -modification of tetrathiafulvalene salt (BEDT-TTF)<sub>2</sub>JBr<sub>2</sub> increases approximately by a factor of three.<sup>1</sup> Such a sensitive reaction of the system of charge carriers to crystal deformation indicates that acoustoelectronic phenomena in layered conductors with a quasi-two-dimensional electron energy spectrum apparently possess peculiar properties.

The interest in investigations of organic conductors with a layered structure is also due to the variety of various phase

states of these compounds and the possibility of changing the ground state with external agencies.

Shubnikov–de Haas magnetoresistance oscillations observed in tetraselenotetracene halides and a large family of tetrathiafulvalene-based ion-radical salts with a charge transport in magnetic fields of the order of several tens tesla indicate that these compounds possess the metal-type conductivity. This allows us to describe the electron processes in such conductors on the basis of the concept of quasiparticles carrying an electric charge  $e$ , which are similar to conduction electrons in metals. Strong anisotropy of the electrical conductivity of a layered conductor is apparently associated with strong anisotropy of the velocity of charge carriers  $\mathbf{v} = \partial \varepsilon(\mathbf{p}) / \partial \mathbf{p}$  on the Fermi surface  $\varepsilon(\mathbf{p}) = \varepsilon_F$ , i.e., their energy  $\varepsilon(\mathbf{p})$  weakly depends on the momentum component  $p_z = \mathbf{p} \cdot \mathbf{n}$  along the normal  $\mathbf{n}$  to the layers.

The Fermi surface of quasi-two-dimensional conductors is open and weakly corrugated along the  $p_z$ -axis. The corrugated planes can be rolled into a cylinder whose base lies in a unit cell of the momentum space so that the Fermi surface of layered conductor can be presented as a system of weakly corrugated cylinders or a system of planes corrugated weakly along the  $p_z$ -axis. Small closed cavities belonging to anomalously small groups of charge carriers can also be present.

The mean free path  $l$  of charge carriers in experimentally investigated layered conductors attains values of several micrometers, and the radius of curvature  $r$  of conduction electrons in strong magnetic fields that may be induced in actual practice can be much smaller than  $l$ . Under these conditions, it is appropriate to formulate the inverse problem of reconstruction of the electron energy spectrum with the help of experimental investigation of kinetic phenomena in a magnetic field.

Galvanomagnetic phenomena and quantum oscillation effects in low-dimensional conductors of organic origin have been investigated experimentally by many authors. In recent years, several publications appeared,<sup>2–7</sup> in which the results of experimental studies of high-frequency phenomena were reported (including the discovery of cyclotron resonance in

the layered conductor  $\alpha$ -(BEDT-TTF)<sub>2</sub>KHg(SCN).

High-frequency parameters of layered and filamentary conductors are undoubtedly quite informative, and their analysis will make it possible to determine in fine details the electron energy spectrum and relaxation properties of charge carriers. Here we shall consider the propagation of electromagnetic and acoustic oscillations in organic quasi-two-dimensional conductors, choosing these oscillations from the variety of waves that can propagate in current-carrying media.

**2. ENERGY SPECTRUM OF LAYERED CONDUCTORS**

A unit cell of a crystal in layered organic conductors contains a large number of atoms, and the separation  $a$  between layers is much larger than atomic spacing in a layer. As a result, the overlapping of wave functions for electrons belonging to different layers is quite small, and we can use the strong-coupling approximation for dispersion relations for charge carriers:

$$\varepsilon(\mathbf{p}) = \sum_{n=0}^{\infty} \varepsilon_n(p_x, p_y) \cos\left(\frac{anp_z}{h}\right). \tag{2.1}$$

Here  $h$  is Planck's constant and  $\varepsilon_n(p_x, p_y)$  are assumed to be arbitrary functions of their arguments. However, the maximum values  $\varepsilon_n^{\max}$  at the Fermi surface decrease significantly with increasing  $n$  so that  $\varepsilon_1^{\max} = \eta\varepsilon_F \ll \varepsilon_F$ , and  $\varepsilon_{n+1}^{\max} \ll \varepsilon_n^{\max}$ , where  $\eta$  is the quasi-two-dimensionality parameter of the spectrum.

Shubnikov-de Haas quantum oscillations are observed virtually for all organic conductors of the family of tetrathiafulvalene salts.<sup>8-19</sup> This points to the presence of closed sections of the Fermi surface by the plane  $p_H = \mathbf{p} \cdot \mathbf{H}/H$  for such conductors, and the large value of the oscillation amplitude suggests the presence of a group of charge carriers for which the states with the Fermi energy are located on weakly corrugated cylinder in the momentum space, such a group of conduction electrons dominating over the remaining charge carriers with the Fermi energy.

The model of a Fermi surface of a quasi-two-dimensional conductor in the form of a weakly corrugated cylinder (Figs. 1 and 2) is in good agreement with the experimental investigations of galvanomagnetic phenomena and Shubnikov-de Haas oscillations in many layered complexes of organic origin with charge transport. Among other things, the results of theoretical calculations based on this model are in complete accord with the experimentally observed quantum oscillations of magnetoresistance of tetrathiafulvalene salts (BEDT-TTF)<sub>2</sub>JBr<sub>2</sub> and (BEDT-TTF)<sub>2</sub>J<sub>3</sub>. However, the substitution of the complex MHg(SCN)<sub>4</sub> for halogens in these salts, where M is a metal of the group (K, Rb, Tl), leads to a more complex dependence of resistance on magnetic field. According to band analysis of the electron energy spectrum,<sup>20</sup> the Fermi surface of (BEDT-TTF)<sub>2</sub>MHg(SCN)<sub>4</sub> salts contains, apart from a weakly corrugated cylinder, two quasi-one-dimensional sheets. Although the presence of a magnetic field affect the dynamic properties of charge carriers with a quasi-one-dimensional spectrum only slightly, the existence of such a

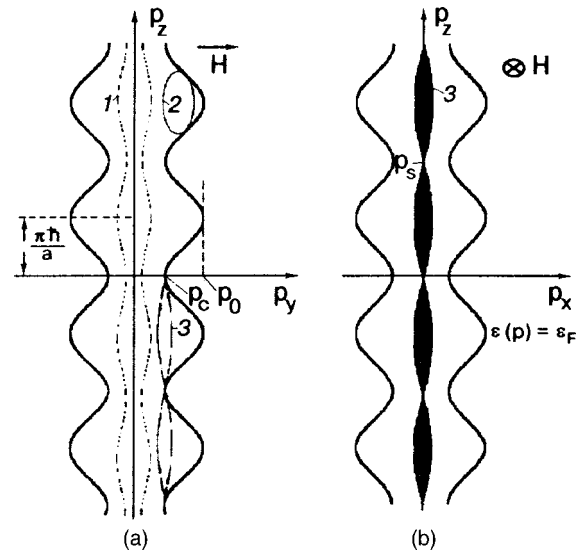


FIG. 1. Various types of electron trajectories in momentum space in a magnetic field parallel to the layers: open trajectories (curves 1), closed electron orbits (curve 2), and a self-intersecting orbit containing a saddle point  $p_c$  (curve 3). The cross section of the Fermi surface by the plane  $p_y = p_c$  separates the regions of open and closed electron trajectories; (a) and (b) show different projections of the Fermi surface.

charge carrier group can change significantly the dependence of electromagnetic and acoustic impedances on the magnitude of a strong magnetic field.

Yamagiji<sup>21</sup> used a rather simplified model of the Fermi surface in theoretical calculations of the magnetoresistance anisotropy of layered conductors, while Zimbovskaya<sup>22</sup> analyzed the rf properties by using the energy spectrum of

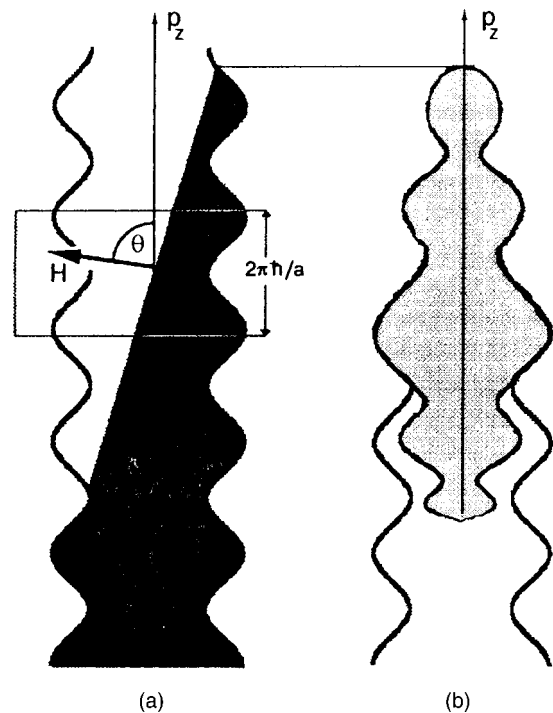


FIG. 2. Electron trajectories in momentum space in a magnetic field ( $\theta$  is the angle formed by the magnetic field vector with the normal to the layers); (a) and (b) show different projections of the Fermi surface.

charge carriers of an exotic form with kinks on the Fermi surface. Under such assumptions, spectroscopic potentialities of studying electron processes in organic conductors in a magnetic field were underestimated or even disregarded altogether. We shall consider here the high-frequency and magnetoacoustic effects in organic conductors under the most general assumptions concerning the form of quasi-two-dimensional electron energy spectrum (2.1).

The quasi-one-dimensional energy spectrum of charge carriers will not be specified either. We shall only assume that the coefficients  $A_{000}$  and  $A_{100}$  in the expression for the dependence of energy on quasimomentum

$$\varepsilon_l(\mathbf{p}) = \sum_{nml} A_{nml} \cos\left(\frac{a_1 n p_x}{h}\right) \cos\left(\frac{a_2 m p_y}{h}\right) \cos\left(\frac{a l p_z}{h}\right) \quad (2.2)$$

are much larger than all the remaining coefficients  $A_{nml}$ . The dimensions  $a_1$  and  $a_2$  of a unit cell of the crystal lattice in the  $xy$  plane of the layers can also differ considerably. In the case when these planes are not the symmetry planes of the crystal, we must take into account additional phase in the arguments of the cosines in formulas (2.1) and (2.2), which changes sign upon the substitution of  $-\mathbf{p}$  for  $\mathbf{p}$ . This will not alter the wave spectrum in layered conductors considerably, and so there is no need to complicate the solution of the given problem. Thus, we shall use below the dispersion relation for charge carriers in the form (2.1) and (2.2), assuming that the coefficients  $A_{nml}$  and the functions  $\varepsilon_n(p_x, p_y)$  are arbitrary.

### 3. COMPLETE SET OF EQUATIONS

An acoustic wave in a conductor always generates a varying electromagnetic field accompanying it. However, the perturbation of the electron subsystem of a conductor by an electromagnetic wave incident on its surface can also excite elastic oscillations in it. Consequently, the system of equations describing the propagation of waves in a conductor contains the equation of the theory of elasticity for ionic displacement  $\mathbf{u}$ , i.e.,

$$\rho \frac{\partial^2 u_i}{\partial t^2} = \lambda_{ijlm} \frac{\partial u_{lm}}{\partial x_j} + F_i, \quad (3.1)$$

as well as Maxwell's equations

$$\text{curl } \mathbf{H} = \frac{4\pi}{c} \mathbf{j} + \frac{1}{c} \frac{\partial \mathbf{E}}{\partial t}; \quad \text{curl } \mathbf{E} = -\frac{1}{c} \frac{\partial \mathbf{B}}{\partial t}; \quad \text{div } \mathbf{B} = 0. \quad (3.2)$$

Here  $\rho$  and  $\lambda_{ijlm}$  are the density and elastic tensor of the crystal,  $u_{lm} = (1/2)(\partial u_l / \partial x_m + \partial u_m / \partial x_l)$  is the strain tensor, and  $c$  the velocity of light.

In view of a quite high number density of charge carriers, Poisson's equation can be reduced to the electroneutrality condition of the conductor, and hence the continuity condition for charge flux in the asymptotic approximation in reciprocal density of conduction electrons assumes the form

$$\text{div } \mathbf{j} = 0. \quad (3.3)$$

The magnetization  $\mathbf{M}$  induced by an external magnetic field in conductors without a spontaneous magnetic moment is usually small, and there is no need to distinguish between the magnetic induction  $\mathbf{B}$  and the magnetic field  $\mathbf{H} = \mathbf{B} - 4\pi\mathbf{M}(\mathbf{B})$  except at ultra-low temperatures. At quite low temperatures, when the inclusion of charge carrier energy quantization in a magnetic field is significant, the amplitude of quantum oscillations of magnetization as a function of  $1/B$  can become comparable with  $\mathbf{B}$ , and the difference  $\mathbf{B} - 4\pi\mathbf{M}(\mathbf{B})$  can become an infinitely small quantity. In this case, the wave process is essentially nonlinear even for small wave amplitude.<sup>23,24</sup>

If  $M(\mathbf{B}) \ll B$ , Eqs. (3.2) can be reduced to a high degree of accuracy to the equation

$$\text{curl } \text{curl } \mathbf{E} - \frac{\omega^2}{c^2} \mathbf{E} = \frac{4\pi i \omega}{c^2} \mathbf{j}. \quad (3.4)$$

In the case of a small wave amplitude, it is sufficient to confine the analysis to the linear approximation in weak perturbation of the electron system, and the wave process can be regarded as monochromatic with frequency  $\omega$  so that the differentiation with respect to time is equivalent to multiplication by  $(-i\omega)$ , which is taken into account in Eq. (3.4). This assumption does not violate in any way the generality of the problem since in view of the linearity of equations relative to the displacement of ions, the electric field  $\mathbf{E}(\mathbf{r}, t)$ , and the magnetic field of the wave, the generalization to the case of an arbitrary time dependence of the fields is trivial and can be reduced to the summation of various harmonics of the solution of the system of equations (3.1)–(3.3).

The perturbation of the electron system by crystal deformation leads to a renormalization of the conduction electron energy,<sup>25</sup> i.e.,

$$\delta\varepsilon = \lambda_{ij}(\mathbf{p}) u_{ij} \quad (3.5)$$

and to the emergence of the force

$$F_i = \frac{1}{c} [\mathbf{j} \times \mathbf{H}]_i + \frac{m}{e} i \omega j_i + f_i^d, \quad (3.6)$$

exerted by electrons on the crystal lattice.

The electric current density

$$j_i = -\frac{2}{(2\pi\hbar)^3} \int e v_i \psi \frac{\partial f_0}{\partial \varepsilon} d^3 p \equiv \langle e v_i \psi \rangle \quad (3.7)$$

and the deforming force density<sup>26,27</sup>

$$f_i^d = \frac{\partial}{\partial x_k} \langle \Lambda_{ik} \psi \rangle, \quad (3.8)$$

characterizing the response of the electron system to perturbation are functionals of the charge carrier distribution function  $f = f_0\{\varepsilon(\mathbf{p}) + i\omega\mathbf{p} \cdot \mathbf{u}\} - \psi \partial f_0 / \partial \varepsilon$ , where  $f_0\{\varepsilon(\mathbf{p}) + i\omega\mathbf{p} \cdot \mathbf{u}\}$  is the equilibrium Fermi function in a reference frame moving with the vibrating lattice at a velocity  $-i\omega\mathbf{u}$ . The nonequilibrium correction to this velocity should be determined by solving the kinetic equation closing the complete system of equations of the problem and having the form

$$\mathbf{v} \frac{\partial \psi}{\partial \mathbf{r}} + \frac{\partial \psi}{\partial t} + \left( \frac{1}{\tau} - i\omega \right) \psi = g. \quad (3.9)$$

Here the function  $g = -\omega \Lambda_{ij}(\mathbf{p}) u_{ij} + e \tilde{\mathbf{E}} \cdot \mathbf{v}$  takes into account the perturbation of the system of charge carriers by the electric field

$$\tilde{\mathbf{E}} = \mathbf{E} - \frac{i\omega}{c} [\mathbf{u} \times \mathbf{H}] + \frac{m\mathbf{u}\omega^2}{e} \quad (3.10)$$

and by crystal deformation.

The components  $\lambda_{ij}(\mathbf{p})$  of the deformation potential tensor in the kinetic equation (3.9) and in expression (3.8) for the deforming force density are given in the form taking into account the conservation of the number of charge carriers, i.e.,

$$\Lambda_{ik}(\mathbf{p}) = \lambda_{ik}(\mathbf{p}) - \langle \lambda_{ik}(\mathbf{p}) \rangle / \langle 1 \rangle. \quad (3.11)$$

The collision operator in the equation for  $\psi$  is taken in the approximation of the relaxation time  $\tau$  for charge carriers, and the time  $t$  is a coordinate in momentum space, which indicates the position of a charge on its trajectory in a magnetic field in accordance with the equation of motion

$$\frac{\partial \mathbf{p}}{\partial t} = \frac{e}{c} [\mathbf{v} \times \mathbf{H}]. \quad (3.12)$$

The kinetic equation must be supplemented with the boundary condition taking into account the scattering of charge carriers at the conductor surface coinciding, say, with the plane  $x=0$ :

$$\begin{aligned} \psi(\mathbf{p}_+, 0) = & q(\mathbf{p}_-) \psi(\mathbf{p}_-, 0) + \int d^3 p W(\mathbf{p}, \mathbf{p}_+) \\ & \times \{1 - \Theta[v_x(\mathbf{p})]\} \psi(\mathbf{p}, 0). \end{aligned} \quad (3.13)$$

Here the specular reflection parameter  $q(\mathbf{p})$  is the probability that a conduction electron incident on the sample surface with a momentum  $\mathbf{p}_-$  has after reflection a momentum  $\mathbf{p}_+$  connected with  $\mathbf{p}_-$  through the specular reflection condition presuming the conservation of the energy of the charge and of the component of its momentum along the scattering boundary. The specular reflection parameter is connected with the scattering indicatrix  $W(\mathbf{p}, \mathbf{p}_+)$  through the relation<sup>28,29</sup>

$$q(\mathbf{p}_-) = 1 - \int d^3 p W(\mathbf{p}, \mathbf{p}_+) \{1 - \Theta[v_x(\mathbf{p})]\}, \quad (3.14)$$

where  $\Theta(\zeta)$  is the Heaviside function.

In a bulk conductor whose size is much larger than the mean free path  $l$  of charge carriers, most of them do not collide with the sample surface during their mean free time. If we are interested in "bulk" effects that are not associated with interaction of a small group of charge carriers with the sample surface, there is no need to use the boundary condition, and the function  $\psi$  can be presented in the form

$$\psi = \int_{-\infty}^t dt' g[x+x(t')-x(t)] \exp[\nu(t'-t)], \quad (3.15)$$

where  $\nu = 1/\tau - i\omega$ , and  $x(t) = \int^t v_x(t) dt$ .

Let us suppose that a wave propagates along the normal to the surface of a conductor occupying the half-space  $x \geq 0$ . Using the Fourier method, we continue evenly  $\mathbf{u}(x)$  and  $\tilde{\mathbf{E}}(x)$  to the region of negative values of  $x$  and obtain for the Fourier component

$$u_i(k) = 2 \int_0^\infty dx u_i(x) \cos kx \quad (3.16)$$

of ion displacement and for the electric field

$$\tilde{E}_i(k) = 2 \int_0^\infty dx \tilde{E}_i(x) \cos kx \quad (3.17)$$

the following system of algebraic equations:

$$\frac{4\pi i\omega}{c^2} j_\alpha(k) = 2E'(0) + k^2 E_\alpha(k) - \left( \frac{\omega}{c} \right)^2 E_\alpha(k), \quad (3.18)$$

$$\alpha = y, z,$$

$$j_x(k) = 0 \quad (3.19)$$

$$\begin{aligned} -\omega^2 \rho u_i(k) = & -\lambda_{ixix} [2u'_\alpha(0) + k^2 u_i] + (im\omega/e) j_i(k) \\ & + c^{-1} [\mathbf{j}(k) \times \mathbf{H}]_i + ik \langle \Lambda_{ix} \psi \rangle. \end{aligned} \quad (3.20)$$

The fluxes characterizing the response of the electron system to a perturbation can be presented with the help of the solution of the kinetic equation in the following form:

$$j_i(k) = \sigma_{ij}(k) \tilde{E}_j(k) + a_{ij}(k) k \omega u_j(k), \quad (3.21)$$

$$\langle \Lambda_{ix} \psi(k) \rangle = b_{ij}(k) \tilde{E}_j(k) + c_{ij}(k) k \omega u_j(k), \quad (3.22)$$

where the Fourier transforms of electrical conductivity  $\sigma_{ij}(k)$  and of acoustoelectronic tensors  $a_{ij}(k), b_{ij}(k)$  and  $c_{ij}(k)$  are defined as

$$\sigma_{ij}(k) = \langle e^2 v_i \hat{R} v_j \rangle; \quad a_{ij}(k) = \langle e v_i \hat{R} \Lambda_{jx} \rangle, \quad (3.23)$$

$$b_{ij}(k) = \langle e \Lambda_{ix} \hat{R} v_j \rangle; \quad c_{ij}(k) = \langle \Lambda_{ix} \hat{R} \Lambda_{jx} \rangle. \quad (3.24)$$

Here

$$\begin{aligned} \hat{R} g \equiv & \int_{-\infty}^t dt' g(t') \exp\{ik[x(t') - x(t)] + \nu(t' - t)\}, \\ g(t) = & \omega \Lambda_{ji}(t) k_i u_j(k) + e \mathbf{v}(t) \cdot \tilde{\mathbf{E}}(k). \end{aligned} \quad (3.25)$$

Substituting expressions (3.21) and (3.22) into Eqs. (3.18)–(3.20), we obtain a system of linear algebraic equations in  $u_i(k)$  and  $\tilde{E}_i(k)$ . The problem of distribution of electric field and the field of displacement of ions in a conductor will be solved completely if we apply the inverse Fourier transformation to its solutions.

The condition for the existence of a nontrivial solution of the obtained system of equations (i.e., the equality to zero of its determinant) is a dispersion equation. The imaginary components of the roots of the dispersion equation determine the damping factors of the acoustic and electromagnetic waves, while the real components of these roots describe renormalizations of the velocities of the waves.

#### 4. PROPAGATION OF ELECTROMAGNETIC WAVES IN LAYERED CONDUCTORS

The equations in the theory of elasticity and Maxwell's equations turn out to be coupled weakly when the mutual transformation of electromagnetic and acoustic waves is hampered. In this case, the propagation of acoustic waves in conductors can be investigated without using Maxwell's equations, and the problem of propagation of electromagnetic waves can be solved to a sufficiently high degree of accuracy without using equations in the theory of elasticity.

We consider the propagation of electromagnetic waves in a layered conductor. Their attenuation length depends considerably on the polarization of the incident wave. A linearly polarized wave with the electric field directed along the normal to the layers penetrates into the conductor to a considerably larger depth than a wave with the electric field directed along the layers.

The surface impedance and the penetration depth of the varying electric field of the wave can easily be determined by solving the system of equations (3.18), (3.7), and (3.9) with the boundary condition (3.13). The solution of the kinetic equation (3.9) allows us to find the relation between the Fourier transforms of current density and electric field:

$$j_i(k) = \sigma_{ij}(k)E_j(k) + \int dk' Q_{ij}(k, k')E_j(k'), \quad (4.1)$$

where

$$\begin{aligned} \sigma_{ij}(k) &\equiv 2e^3 H/c(2\pi h)^3 \\ &\times \int dp_H \int_0^T dt v_i(t, p_H) \int_0^t dt' v_j(t', p_H) \\ &\times \exp\{\nu(t' - t)\} \cos k\{x(t', p_H) - x(t, p_H)\} \\ &\equiv \langle e^2 v_i \hat{R} v_j \rangle. \end{aligned} \quad (4.2)$$

The kernel of the integral operator  $Q_{ij}(k, k')$  depends considerably on the state of the sample surface, i.e., on the probability of specular reflection of charge carriers at the surface.

In the cases when the relation between the Fourier transforms of current density and electric field is local, i.e., the contribution of electrons colliding with the sample boundary to the alternating current is considerably smaller than the contribution from "bulk" electrons, the electric field attenuation length is determined by the imaginary component of the roots of the dispersion equation

$$\det \left\{ \left( k^2 - \frac{\omega^2}{c^2} \right) \delta_{\alpha\beta} - \frac{4\pi i \omega}{c^2} \bar{\sigma}_{\alpha\beta}(k) \right\} = 0, \quad (4.3)$$

where

$$\bar{\sigma}_{\alpha\beta}(k) = \sigma_{\alpha\beta}(k) - \frac{\sigma_{\alpha x}(k)\sigma_{x\beta}(k)}{\sigma_{xx}(k)}; \quad \alpha, \beta = (y, z). \quad (4.4)$$

Under the conditions of normal skin effect, when the mean free path of charge carriers is smaller than the skin depth, the relation between current density and electric field is local to a high degree of accuracy, i.e.,

$$j_i(x) = \sigma_{ij} E_j(x), \quad (4.5)$$

and the component of the electrical conductivity matrix  $\sigma_{ij} = \sigma_{ij}(0)$  have the same form as in a uniform electric field. The electrical conductivity  $\sigma_{zz} = \eta^2 \sigma_0$  across the layers is proportional to the square of the quasi-two-dimensionality parameter of the electron energy spectrum, and  $\sigma_0$  has the same order of magnitude as the electrical conductivity along the layers in a uniform electric field. In this case, the dispersion equation (4.3) implies that the attenuation depth  $\delta_{\parallel}$  of the electric field  $E_z(\mathbf{r})$  is larger than the attenuation depth  $\delta_{\perp}$  of the electric field along the layers by a factor of  $1/\eta$ , i.e.,

$$\delta_{\perp} = \delta_{\parallel} \eta. \quad (4.6)$$

Under the conditions of anomalous skin effect, when the skin depth  $\delta_{\parallel}$  is much smaller than the mean free path  $l$  of charge carriers, the relation between  $\delta_{\perp}$  and  $\delta_{\parallel}$  has the form

$$\delta_{\perp} = \delta_{\parallel} \eta^{2/3}, \quad (4.7)$$

since the tensor components  $\sigma_{ij}(k)$  are inversely proportional to the wave number  $k$  for  $kl \gg 1$ .

In a magnetic field, the relations between  $\delta_{\perp}$  and  $\delta_{\parallel}$  are more diversified.

Let us consider the propagation of electromagnetic waves in a layered conductor in a magnetic field  $\mathbf{H} = (H \sin \varphi, H \cos \varphi \sin \theta, H \cos \varphi \cos \theta)$ , tilted by the angle  $\varphi$  to the conductor surface  $x_s = 0$ .

The integral term in the boundary condition (3.13) ensures the absence of current through the sample surface, but in the range of high frequencies  $\omega$ , the solution of the kinetic equation weakly depends on this functional.<sup>30</sup> Disregarding this functional for  $\varphi = 0$  and assuming the absence of charge carrier drift along the  $x$ -axis along open electron orbits, we can write the solution of the kinetic equation in the form

$$\begin{aligned} \psi(t, p_H, x) &= \int_{\lambda}^t dt' e\nu(t', p_H) \cdot \mathbf{E}[x(t', p_H) - x(\lambda, p_H)] \\ &\times \exp\{\nu(t' - t)\} + q(\lambda, p_H)[1 - q(\lambda, p_H)] \\ &\times \exp\{\nu(2\lambda - T)\}^{-1} \int_{\lambda}^{T-\lambda} dt' \\ &\times e\nu(t', p_H) \cdot \mathbf{E}[x(t', p_H) - x(\lambda, p_H)] \\ &\times \exp\{\nu(t' - t + 2\lambda - T)\}, \end{aligned} \quad (4.8)$$

where  $T = 2\pi/\Omega = 2\pi m^*c/eH$  is the period of motion of a charge in the magnetic field,  $m^*$  the effective cyclotron mass of conduction electrons, and  $\lambda$  is the root of the equation

$$x(t, p_H) - x(\lambda, p_H) = \int_{\lambda}^t v_x(t', p_H) dt' = x. \quad (4.9)$$

which is nearest to  $t$ .

Conduction electrons for which  $\{x(t, p_H) - x_{\min}\} < x$  do not collide with the sample surface, and we must put  $\lambda = -\infty$  for such electrons.

In a magnetic field tilted to the sample surface, conduction electrons either penetrate to the bulk of the sample after several collisions with the boundary, or tend to approach this surface. The relative fraction of the latter electrons is not

large, and they make a small contribution to the alternating current. The contribution of the remaining electrons to the current for  $\varphi \cong 1$  is naturally determined by the type of their interaction with the sample surface, but the state of the surface affects only insignificant factor of the order of unity in the expression for surface impedance.

#### 4.1. Normal skin effect

We shall apply the term normal skin effect to penetration of an electromagnetic field to the bulk of a sample under the condition when the current density  $\mathbf{j}(\mathbf{r})$  is determined to a high degree of accuracy by the value of the electric field  $\mathbf{E}(\mathbf{r})$  at the same point  $\mathbf{r}$ . In a strong magnetic field parallel to the conductor surface, charge carriers with closed orbits drift in the momentum space along the sample surface. If the diameter  $2r$  of their orbits is much smaller than the skin depth, the main contribution to rf current comes from carriers separated from the surface  $x_s=0$  by a distance greater than  $2r$ . These conduction electrons do not collide with the sample surface, and it is expedient to use the approximation of local coupling between the current density and the electric field of the wave to calculate the surface impedance in the asymptotic approximation in the small parameter  $r/\delta$  in the absence of open cross sections of the Fermi surface.

The asymptotic expression for the tensor component  $\sigma_{ij}(k)$  for  $kr \ll 1$  has the same form as in a uniform electric field so that the electric current  $E_y$  for  $kr \ll 1$  attenuates at distances

$$\delta_{\perp} \cong \delta_0 = c(2\pi\omega\sigma_0)^{-1/2} \quad (4.10)$$

for any relation between the mean free path of charge carriers and the skin depth.

For  $\eta \ll 1$ , each of the components  $\sigma_{zx}$  and  $\sigma_{xz}$  is at least proportional to  $\eta^2$  so that  $\bar{\sigma}_{zz} \cong \sigma_{zz}$ . The asymptotic form of  $\sigma_{zz}(k)$  for small angles  $\theta$  is equal to  $\sigma_0 \eta^2$  in order of magnitude, and the attenuation length  $\delta_{\parallel}$  of the electric field  $E_z$  is larger than  $\delta_{\perp}$  by a factor of  $1/\eta$  as in zero magnetic field if the corrugation of the Fermi surface is not very small and  $\eta \gg \delta_0 \omega/c$ . For  $\omega \gg \sigma_0 \eta^2$ , the skin depth

$$\delta_{\parallel} = \frac{\delta_0^2 \omega}{c \eta^2} \left( 1 + \frac{r^2 \omega^2}{c^2} \right)^{-1/2} \quad (4.11)$$

increases with the magnetic field, attaining its limiting value  $\omega \delta_0^2 / c \eta^2$ .<sup>31,32</sup>

For significant values of  $\theta$ , there exists a sequence of values of  $\theta = \theta_c$  for which the asymptotic behavior of  $\sigma_{zz}$  changes considerably, as well as the behavior of the quantity<sup>33-35</sup>  $\bar{\sigma}_{zz}$  which satisfies the expression

$$\begin{aligned} \bar{\sigma}_{zz}(k, \eta, \theta) = & \frac{ae^3 \tau TH \cos \theta}{4 \pi^2 h^4 c} \sum_n n^2 I_n^2 + \sigma_0 \eta^2 \{ \eta^2 f_1(\theta) \\ & + \gamma^2 f_2(\theta) + (kr)^2 f_3(\theta) \}, \end{aligned} \quad (4.12)$$

where the  $f_i$  stand for functions of  $\theta$  of the order of unity, and

$$I_n(\theta) = \int_0^T dt \varepsilon_n(t) \cos\{anp_y(t) \tan \theta/h\}. \quad (4.13)$$

For  $\theta = \theta_c$ , when  $I_1(\theta_c)$  vanishes, the value of  $\bar{\sigma}_{zz}$  decreases abruptly for small  $\eta$ ,  $\gamma = (\Omega\tau)^{-1}$ ,  $\omega/\Omega$ , and  $kr$ .

As a result, the penetration depth for the electric field  $E_z$  increases considerably for  $\theta = \theta_c$ , and the angular dependence of impedance acquires a series of narrow peaks. For  $\tan \theta \gg 1$ , these peaks are repeated periodically, with a period determined by the separation between the stationary phase points on the electron orbit, where  $\mathbf{k} \cdot \mathbf{v} = \omega$ , which are close to turning points ( $v_x = 0$ ). Since the phase velocity of the wave  $v_{\varphi} = \omega/k = (\omega\tau)^{-1/2} \omega c / \omega_0 \eta$  is much smaller than the Fermi velocity  $v_F$  of conduction electrons, the separation between stationary phase points on the electron orbit can be regarded to be equal to the diameter of the orbit to a high degree of accuracy.

The height of sharp peaks for  $\theta = \theta_c$  in pure conductors at low temperatures, when  $l\eta^2 > \delta_0$ , decreases with increasing magnetic field, and conversely, for  $l\eta^2 < \delta_0$ , it increases in proportion to  $l\delta_0/r\eta$  if  $l\eta < r < \delta_0/\eta$ . At not very high frequencies, when the displacement current is smaller than the conduction current, the solution of the dispersion equation (4.3) for  $\theta = \theta_c$  can be represented in the form of the interpolation formula

$$\delta_{\parallel} = l \left( \frac{r^2 + \delta_0^2 \eta^{-2}}{r^2 + l^2 \eta^2} \right)^{1/2}. \quad (4.14)$$

In the case of extremely low electrical conductivity along the normal to the layers, when  $\omega > \sigma_0 \eta^2 (\eta^2 + r^2/l^2)$ , the skin depth  $\delta_{\parallel}$  has the form

$$\begin{aligned} \delta_{\parallel} = & (\delta_0/\eta^2) \{ 1 + (r/l\eta)^2 + (r\omega/c\eta)^2 \}^{-1/2} \\ & \times \{ 1 + (r\eta/\delta_0)^2 \}, \end{aligned} \quad (4.15)$$

and the electric field attenuation depth along the normal to the layers is again equal to  $\delta_0/\eta^2$  in a strong magnetic field when  $r < (l^2 \eta^2 + \delta_0^2/\eta^2)^{1/2}$ . In the range of moderate magnetic fields in which the relation  $\delta_0/\eta \ll r \ll \delta_{\parallel}$  holds for  $\theta = \theta_c$ , the impedance as a function of magnetic field has a minimum since for  $r \gg l\eta$  the skin depth

$$\delta_{\parallel} = lr\eta/\delta_0 \quad (4.16)$$

is inversely proportional to the magnetic field, i.e., decreases with increasing magnetic field.<sup>32-35</sup>

For  $\delta_{\perp} \ll r \ll \delta_{\parallel}$ , the attenuation length of the electric field  $E_z(x)$  depends weakly on the type of reflection of charge carriers at the sample surface as before, but the penetration depth for the electric field  $E_y(x)$  is quite sensitive to the state of the conductor surface if the value of  $\delta_{\perp}$  is smaller than or comparable to the mean free path of charge carriers. In this range of magnetic fields, normal skin effect can take place only for  $\delta_{\perp} \gg l$ , when the local relation between the current density and electric field is observed for any polarization of the wave. The asymptotic expression  $\bar{\sigma}_{yy}(k)$  for  $kl \ll 1$  coincides with  $\sigma_0$  to within a numerical factor of the order of unity, and hence  $\delta_{\perp}$  coincides in order of magnitude with  $\delta_0$ . However, the penetration depth of the electric field  $E_z(x)$  in the sample depends considerably on the magnetic field orientation.

A peculiar dependence of the attenuation length of the electric field  $E_z(x)$  is observed for  $\theta = \pi/2$ , when, apart from

the drift of charge carriers along the magnetic field, a fan of various drift directions is possible in the  $xy$  plane for conduction electrons belonging to open cross sections of the Fermi surface. In this case, the dependence of  $\sigma_{zz}$  on the magnitude of a strong magnetic field ( $\gamma_0 = 1/(\Omega_0\tau) \ll 1$ , where  $\Omega_0$  is the frequency of electron rotation in a magnetic field orthogonal to the layers) can be presented by the following interpolation formula:

$$\sigma_{zz} = \sigma_0 \gamma_0^2 \eta^2 (\gamma_0^2 + \eta)^{-1/2}, \quad (4.17)$$

which is valid for any orientation of the magnetic field in the  $xy$  plane, i.e., for any angle of its inclination to the sample surface  $x_s = 0$ .

Using formulas (4.3) and (4.17), we can easily verify that the value of  $\delta_{\parallel}$  increases with the magnetic field in proportion to  $H^{1/2}$  for  $\eta^{1/2} \ll \gamma_0 \ll 1$ , while the attenuation length  $\delta_{\parallel} \cong \delta_0 / \gamma_0 \eta^{3/4}$  of the electric field along the normal to the layers increases linearly with the magnetic field for  $\eta^2 \ll \gamma_0 \ll \eta^{1/2}$ .

The solution of the dispersion equation (4.3) for  $\varphi$  differing from zero has the form

$$k = \frac{(2\pi\omega)^{1/2}(1+i)}{2c} \{ \sigma_0^{-1} + \sigma_{zz}^{-1} \pm [(\sigma_{zz}^{-1} - \sigma_0^{-1})^2 - (2H \cos \theta \sin \varphi / Nec)^2]^{1/2} \}^{-1/2}, \quad (4.18)$$

where  $N$  is the charge carrier density.

This formula shows that in the extremely strong magnetic field, when  $\gamma_0 \ll \eta^2$ , helicoidal waves can propagate. For  $\varphi \cong 1$ , one of the roots of the dispersion equation describes attenuation of electric field along the layers at distances of the order of

$$\delta_{\perp} = \delta_0 \left( 1 + \frac{\sigma_{zz}}{\sigma_0 \gamma_0^2} \right)^{1/2}. \quad (4.19)$$

It can easily be seen that the penetration depth for the electric field  $E_y$  increases as the magnetic field increases in proportion to  $H$  when  $\gamma_0 \ll \eta$ . The electric field directed along the normal to the layers for  $\gamma_0 \gg \eta^2$  attenuates at distances<sup>35</sup>

$$\delta_{\parallel} = \delta_0 (\sigma_0 / \sigma_{zz})^{1/2}, \quad (4.20)$$

i.e., at distances of the order of  $\delta_0 / \eta$  as in zero magnetic field.

In the presence of an additional group of charge carriers with a quasi-one-dimensional energy spectrum, high-frequency properties of layered conductors are quite sensitive not only to the polarization of the incident wave, but also to the direction of propagation of electromagnetic field in the plane of the layers.<sup>36-38</sup> If the reflection of charge carriers at the conductor surface is close to specular, the relation between the Fourier transforms of current density and electric field can be regarded as local to a fairly high degree of accuracy even for an indefinitely large mean free path of charge carriers:

$$j_i(k) = \{ \sigma_{ij}(k) + \sigma_{ij}^{(1)}(k) \} E_j(k). \quad (4.21)$$

Here  $\sigma_{ij}^{(1)}(k)$  is the contribution to the rf electrical conductivity from charge carriers with the energy spectrum (2.2), in which we retain only a few terms by putting

$$A_{100} = U, \quad A_{010} = \eta_1 U \ll U, \quad A_{001} = \eta_2 U \ll U.$$

The contribution to  $\tilde{\sigma}_{\alpha\beta}(k)$  from charge carriers with a quasi-one-dimensional energy spectrum is mainly determined by the component  $\sigma_{xx}^{(1)}(k)$  which has the following form accurate to small corrections proportional to  $\eta_1^2$  and  $\eta_2^2$ :

$$\sigma_{xx}^{(1)}(k) = \sigma_1(k) = \frac{\sigma_1}{1 + (kl_1)^2}, \quad (4.22)$$

where  $l_1 = v_{01}\tau_1 / (1 - i\tau_1)$ ;  $\sigma_1$  is the contribution of this group of charge carriers to electrical conductivity along the  $x$ -axis in a uniform electric field,  $\tau_1$  the mean free time of charge carriers with the energy spectrum (2.2), and  $v_0 = (Ua_1/h) \sin[(\epsilon_F - A_{000})/U]$ .

The magnetic field dependence of  $\sigma_{ij}^{(1)}(k)$  is manifested only in the next terms of expansion into a power series in the small parameters  $\eta_1$  and  $\eta_2$ :

$$\sigma_{yy}^{(1)}(k) = \sum_{\pm} \frac{\eta_1^2 \sigma_1 a_2^2 U^2 / 4h^2 v_0^2}{1 + (k \pm eHa_2 \cos \theta / ch)^2 l_1^2}, \quad (4.23)$$

$$\sigma_{zz}^{(1)}(k) = \sum_{\pm} \frac{\eta_2^2 \sigma_1 a^2 U^2 / 4h^2 v_0^2}{1 + (k \pm eHa \sin \theta / ch)^2 l_1^2}, \quad (4.24)$$

whose inclusion does not affect significantly the skin depth of electromagnetic field attenuation.

The asymptotic behavior of the components of  $\tilde{\sigma}_{\alpha\beta}(k)$  in strong magnetic fields ( $\gamma = 1/\Omega\tau \ll 1$ ), i.e.,

$$\tilde{\sigma}_{yy}(k) = \frac{\sigma_1(k) \{ \gamma^2 \sigma_0 + \sigma_{zz} \tan^2 \theta \} + \gamma^2 \sigma_0^2}{\sigma_1(k) + \gamma^2 \sigma_0}, \quad (4.25)$$

$$\tilde{\sigma}_{yz}(k) = \tilde{\sigma}_{zy}(k) = \frac{\sigma_1(k)}{\sigma_1(k) + \gamma^2 \sigma_0} \sigma_{zz} \tan \theta, \quad (4.26)$$

$$\tilde{\sigma}_{zz}(k) = \sigma_{zz} + \sigma_{zz}^{(1)}(k). \quad (4.27)$$

is very sensitive to the emergence of a group of charge carriers with a quasi-one-dimensional energy spectrum.

We have omitted here insignificant numerical factors of the order of unity and small corrections of the order of  $(kr)^2$  in the expression for  $\sigma_{zz}$ , i.e., the contribution of charge carriers with a quasi-two-dimensional spectrum to the current is taken into account, as before, in the approximation valid for normal skin effect.

If  $\sigma_1$  and  $\sigma_0$  are of the same order of magnitude, the value of  $\tilde{\sigma}_{yy}(k)$  does not attain saturation in strong magnetic fields as in the case of  $\sigma_1 = 0$  and turns out to be much smaller than  $\sigma_0$  in a fairly wide range of magnetic fields. This leads to a considerable increase in the conductor transparency.

The dispersion equation (4.3) taking into account relations (4.25)–(4.27) makes it possible to determine the length of attenuation of electromagnetic fields in a strong magnetic field:

$$\delta_1 \cong \delta_0 / \eta, \quad \delta_2 \cong \delta_0 / \gamma, \quad (4.28)$$

where  $\delta_0 = \{c/2\pi\omega(\sigma_0 + \sigma_1)\}^{1/2}$ .

If  $\sigma_1$  is much smaller than  $\sigma_0$ , but  $\sigma_1 \geq \gamma^2 \sigma_0$ , the expression for  $\delta_2$  should be supplemented with the small factor  $(\sigma_1/\sigma_0)^{1/2}$ . For  $\sigma_1 \ll \gamma^2 \sigma_0$ , the attenuation lengths for the electric fields  $E_z(x)$  and  $E_y(x)$  differ significantly ( $\delta_{\parallel} = \delta_1$  and  $\delta_{\perp} \equiv \delta_0$ , respectively), by the electric fields along and across the layers for  $\sigma_1 \geq \gamma^2 \sigma_0$  contain both components with considerably different attenuation lengths  $\delta_1$  and  $\delta_2$ . Consequently, in pure conductors for which  $l\eta \gg \delta_0$ , not only the field  $E_z(x)$ , but also the field  $E_y(x)$  attenuate over distances considerably longer than the mean free path of charge carriers in magnetic fields for which  $r \ll \delta_0$ .

When an electromagnetic wave propagates along the  $y$ -axis, the presence of a group of charge carriers with a quasi-one-dimensional energy spectrum does not affect significantly the attenuation length of electromagnetic waves. As in the case of a single group of charge carriers with the dispersion relation (2.1), the electric field along the layers attenuates over distances of the order of  $\delta_0$ , and the electric field along the normal to the layers penetrates a quasi-two-dimensional conductor to the depth  $\delta_{\parallel}$  for which the above formulas (4.11), (4.14)–(4.16) are valid. The effect of charge carriers with spectrum (2.2) on the propagation of electromagnetic waves becomes significant when  $\cos \alpha \gg \gamma^2 \sigma_0/\sigma_1$ , where  $\alpha$  is the angle between the wave vector and the predominant direction of the velocity of charge carriers with a quasi-one-dimensional energy spectrum.

Thus, analyzing the dependence of surface impedance on the magnetic field during the propagation of an electromagnetic wave in two different directions in the plane of the layers, we can determine unambiguously the presence of a quasi-one-dimensional cavity on the Fermi surface and its contribution of the electrical conductivity of an organic conductor.

**4.2. Anomalous skin effect**

With increasing frequency of an electromagnetic wave, the skin depth  $\delta$  decreases, and the relation between current density and electric field becomes essentially nonlocal for  $\delta \leq 2r$ . In this case, Maxwell’s equations are of the integral type even in the Fourier representation.<sup>39</sup> Hartmann and Luttinger<sup>40</sup> proposed a correct solution of these equations in a magnetic field for some special cases. If we disregard numerical factors of the order of unity, we can obtain a reasonable solution of the physical problem, i.e., determine the dependence of surface impedance and other characteristics of waves in a conductor on physical parameters, with the help of a correct estimation of the contribution of the integral term in formula (4.1) to the Fourier transform of the high-frequency current. In a magnetic field parallel to the sample surface, for  $\delta_{\perp} \leq r$ , the contribution of charge carriers colliding with the sample surface to the current is significant. In the case of a nearly specular reflection of charge carriers by the sample boundary (the width of scattering indicatrix for charge carriers  $w \ll r^{3/2}/l\delta_{\perp}^{1/2}$ ), the contribution of conduction electrons ‘‘sliding’’ along the sample surface and remaining in the skin layer to the rf current is quite large. In this case, the asymptotic expression for  $\tilde{\sigma}_{yy}(k)$  for large  $k$  has the form

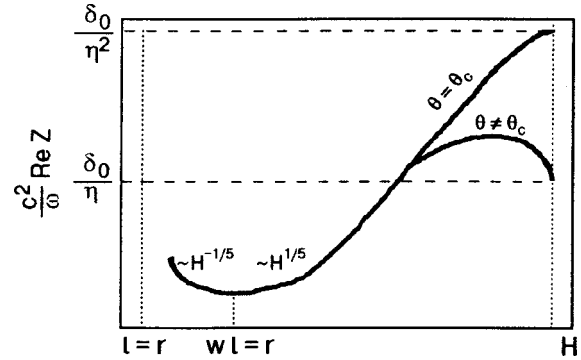


FIG. 3. Dependence of surface impedance on the magnitude of a strong magnetic field ( $r \ll l$ ) parallel to the surface of the conductor  $x_s = 0$ . The width  $w$  of the indicatrix of charge carrier scattering at the sample surface can be determined from the position of the minimum.

$$\tilde{\sigma}_{yy}(k) = \frac{\omega_0^2}{\Omega(kr)^{1/2}(w+r/l)}. \tag{4.29}$$

Using the dispersion equation (4.3), we can easily determine the attenuation length of electric fields, i.e.,

$$\delta_{\perp} = \delta_0^{6/5} r^{-1/5} (w+r/l)^{2/5}; \quad \delta_{\parallel} = \delta_0 / \eta. \tag{4.30}$$

In the range of not very strong magnetic fields, where  $\delta_{\perp} \ll r \ll l$ , the impedance has a minimum for  $r = wl$ , and its position determines uniquely the width of indicatrix of charge carrier scattering at the sample boundary (Fig. 3).

Under the conditions of extremely anomalous skin effect, when the depth of electromagnetic wave penetration in the conductor is the smallest parameter of the problem having the dimensions of length (i.e., not only  $\delta_{\perp}$ , but also  $\delta_{\parallel}$  is much smaller than  $r$  and  $l$ ), the values of  $\delta_{\perp}$  and  $\delta_{\parallel}$  are connected through a universal relation in a magnetic field parallel to the sample surface for  $w \ll r^{3/2}/l\delta_{\parallel}^{1/2}$ .<sup>33</sup>

$$\delta_{\perp} = \delta_{\parallel} \eta^{4/5}. \tag{4.31}$$

If  $w \gg r^{3/2}/l\delta_{\perp}^{1/2}$  and  $\delta_{\perp} \ll r \ll l$ , the contribution to the rf current mainly comes from charge carriers that do not interact with the sample surface, and the relation between  $\delta_{\perp}$  and  $\delta_{\parallel}$  has the form (4.7).

In the intermediate case when  $r^{3/2}/l\delta_{\parallel}^{1/2} \ll w \ll r^{3/2}/l\delta_{\perp}^{1/2}$ , only  $\delta_{\perp}$  depends considerably on  $w$  for  $w \geq r/l$ :

$$\delta_{\parallel} = r^{1/3} (\delta_0 / \eta)^{2/3}, \quad \delta_{\perp} = w^{2/5} \delta_0^{6/5} r^{-1/5}. \tag{4.32}$$

In the absence of open electron orbits, conduction electrons carry information on the field in the skin layer to the bulk of the conductor in the form of narrow spikes predicted by Azbel.<sup>41</sup> The transport of electromagnetic field to the bulk of the conductor and the screening of the incident wave at the surface  $x_s = 0$  are mainly accomplished by charge carriers moving in phase with the wave almost parallel to the sample surface. For  $\eta \leq \delta/r$ , almost all of charge carriers participate in the formation of electromagnetic field spikes.<sup>42</sup> The intensity of the spikes at distances from the sample surface multiple to the diameter of the electron orbit in the direction of the  $x$ -axis has the same order of magnitude in the collisionless limit. The inclusion of scattering of conduction electrons in the bulk of the conductor leads to field attenua-

tion in a spike at distances of the order of the mean free path of charge carriers. Thus, there are two scales of electromagnetic field attenuation length under the conditions of anomalous skin effect. Apart from the skin depth, the electromagnetic field penetrates into the bulk of the sample to a depth of the order of the mean free path of charge carriers.

For  $\eta \gg \delta/r$ , only an insignificant fraction of charge carriers of the order of  $(\delta/r\eta)^{1/2}$  participates in the formation of spikes. The spread in the diameters of orbits of such carriers in the vicinity of the extremal diameter is comparable with the skin depth. As a result, with increasing distance from the surface  $x_s=0$ , the intensity of each next spike acquires an additional small factor  $(\delta/r\eta)^{1/2}$  apart from the exponential factor  $\exp\{-x/l\}$  taking into account attenuation of waves in the spike over the mean free path  $l$ .

As the angle  $\theta$  approaches  $\pi/2$ , closed electron orbits become strongly elongated along the  $x$ -axis, and the spike mechanism of penetration of electromagnetic field in the bulk of the sample is replaced by the electron transport of the varying field in the form of Reuter–Sondheimer weakly attenuating quasi-waves<sup>39,43–46</sup> when the diameter of the orbits in this direction exceeds the mean free path  $l$ .

### 4.3. Weakly attenuating Reuter–Sondheimer waves

The drift of charge carriers along the normal to the sample surface facilitates the transport of electromagnetic field from the skin layer to the bulk of the conductor over a distance smaller than or of the order of the mean free path  $l$  of charge carriers. For  $\theta = \pi/2$ , the drift of charge carriers along open trajectories leads to penetration of electromagnetic field over a distance  $x \leq l$  even in a magnetic field parallel to the surface  $x_s=0$ .

In order to determine the electric field in the bulk of the sample with the help of inverse Fourier transformation

$$E_j(x) = \frac{1}{2\pi} \int_{-\infty}^{+\infty} dk E_j(k) \exp\{-ikx\} \quad (4.33)$$

we continue  $E_j(k)$  analytically to the entire complex  $k$ -plane and close the integration contour in formula (4.33) with an arc of infinitely large radius in the half-plane where  $\text{Im} k \geq 0$ . The skin depth is determined by the poles of the integrand in formula (4.33), while weakly attenuating waves are associated with integration along the cuts drawn from the branching point of the function  $E_j(k)$ . It can easily be verified that the tensor component  $\sigma_{ij}(k)$  for indefinitely small  $\eta$  display a root singularity of the form

$$\sigma_{zz}(k) = (\omega_0^2 \eta^2 / \nu) \{ (\alpha_+^2 - 1)^{-1/2} + (\alpha_-^2 - 1)^{-1/2} \}; \quad (4.34)$$

$$\Delta \sigma_{yy}(k) = \nu (\omega_0 / k \nu)^2 \{ (k \nu / \nu)^2 + 1 \}^{1/2}, \quad (4.35)$$

where  $\omega_0$  is the frequency of plasma oscillations of charge carriers,  $\nu = v_x^{\text{max}} \cong v_F$ , and  $\alpha_{\pm} = i(k \nu \pm \Omega) / \nu$ . For  $\eta \ll 1$ , the time variation of the electron velocity  $v_x$  in the magnetic field  $\mathbf{H} = (0, H, 0)$  does not exceed  $\nu \eta^{1/2}$  so that away from the saddle points on the Fermi surface, charge carriers move in the momentum space along the  $p_z$ -axis virtually without acceleration over a distance equal to the period of a unit cell

during the time  $T = 2\pi \hbar c / aeH v_x$ . In this case,  $\Omega$  appearing in the expression for  $\alpha_{\pm}$  is equal to  $aeH \nu / \hbar c$ .

The kernel of the integral operator  $Q_{ij}(k, k')$  as a function of  $k$  also possesses a similar singularity.

The electromagnetic field decreases in proportion to  $x^{-3/2} \exp(-x/l)$  over distances from the sample surface which exceed considerably either  $r = \nu / \Omega$ , or the displacement of an electron during the wave period  $2\pi \nu / \omega$ . For  $\Omega \gg \omega$ , the slowly decreasing varying electric field

$$E_z(x) = E_z(0) \eta^{-4/3} (c / \omega_0)^{4/3} (\nu / \omega)^{2/3} r^{-1/2} x^{-3/2} \times \exp\{ix/r - x/l\} \quad (4.36)$$

oscillates upon variation of  $H$  at large distances  $x \gg r$ .

The attenuation of the electric field  $E_y(x)$  over the mean free path of charge carriers for  $\eta \leq 1$  has the form

$$E_y(x) = E_y(0) (c / \omega_0)^{4/3} (\nu / \omega)^{2/3} (\nu / \nu)^{1/2} x^{-3/2} \times \exp\{-x/l + ix\omega / \nu\}, \quad (4.37)$$

$$\nu / \omega \ll x \ll \nu / \omega \eta$$

and is independent of the magnetic field.

The oscillatory dependence of  $E_y(x)$  on the magnetic field is manifested only in small corrections proportional to  $\eta^2$ .

For values of  $\eta$  that are not small in zero magnetic field, the functions  $\sigma_{yy}(k)$  and  $\sigma_{zz}(k)$  have a logarithmic singularity for  $k_1 = i\nu / v_1$  and  $k_2 = i\nu / v_2$ , where  $v_1$  is the electron velocity at the reference point on the Fermi surface in the  $x$ -direction and  $v_2$  the projection of the velocity  $v_x$  at the saddle point of the Fermi surface, at which connectedness of the line  $v_x = \text{const}$  changes.<sup>44</sup> For indefinitely small  $\eta$ , these branching points of the rf conductivity tensor component become closer, and the logarithmic singularity changes into a root singularity for  $\eta = 0$ .<sup>47</sup> For small  $\eta$ , we choose the integration contour in the  $k$ -plane along the cut lines drawn from the branching points  $k_1$  and  $k_2$  parallel to the imaginary axis so that we can bypass both branching points simultaneously. In this case, the electric field  $E_z(x)$  away from the skin layer assumes the form

$$E_z(x) = -2E_z'(0) \left\{ \int_{k_1}^{k_1+i\infty} dk \left[ k^2 - \frac{\omega^2}{c^2} - \frac{4\pi i \omega}{c^2} \sigma_{zz1}(k) \right]^{-1} \times \exp(ikx) + \int_{k_2+i\infty}^{k_2} dk \left[ k^2 - \frac{\omega^2}{c^2} - \frac{4\pi i \omega}{c^2} \sigma_{zz2}(k) \right]^{-1} \exp(ikx) \right\}. \quad (4.38)$$

We can neglect the integral along lines connecting the branching points  $k_1$  and  $k_2$  and assume that  $\sigma_{zz1}(k)$  is the value of the function  $\sigma_{zz}(k)$  at the left bank of the cut drawn from the point  $k_1$ , while  $\sigma_{zz2}(k)$  is its value at the right bank of the cut drawn from the point  $k_2$ . For definiteness, we assume that  $v_1$  is greater than  $v_2$ . If we disregard anisotropy of the dispersion relation (2.1) for charge carriers in the plane of the layers, the diagonal components of the rf electrical conductivity tensor for  $k_1 \leq k \leq k_2$  assume the form

$$\sigma_{yy}(k) = \frac{\omega_0^2 \eta}{\pi^3} \int_0^\pi d\alpha \int_0^{\pi/2} d\varphi \frac{\sin^2 \varphi}{\nu + ik\nu \cos \varphi (1 + \eta \cos \alpha)^{1/2}}. \quad (4.39)$$

$$\sigma_{zz}(k) = \frac{\omega_0^2 \eta^2}{\pi^3} \int_0^\pi \sin^2 \alpha d\alpha \times \int_0^{\pi/2} d\varphi \frac{1}{\nu + ik\nu \cos \varphi (1 + \eta \cos \alpha)^{1/2}}. \quad (4.40)$$

It can easily be seen that the rf electrical conductivity component  $\sigma_{zz}(k)$  is proportional to  $(\nu + ik\nu)^{-1/2}$ , for  $\eta \ll 1$ , while  $\sigma_{yy}(k)$  is proportional to  $(\nu + ik\nu)^{1/2}$ , i.e., both component have a root singularity for  $k = i\nu/\nu$ . In the case of a considerable corrugation of the Fermi surface, when  $\eta \cong 1$ , the root singularity is replaced by a logarithmic singularity for  $k = i\nu/\nu(1 + \eta)^{1/2}$  and  $k = i\nu/\nu(1 - \eta)^{1/2}$ . After the integration with respect to  $\varphi$ , the integrands in (4.39) and (4.40) have a root singularity for  $k = i\nu/\nu(1 + \eta \cos \alpha)^{1/2}$ . As a result of simple calculations, we arrive at the following expression for the electric field component weakly attenuating at large distances from the skin layer:

$$E_y(x) = E_y(0)(c/\omega_0)^{4/3}(\nu/\omega)^{2/3}x^{-3/2}(\nu/\nu)^{1/2} \times \int_0^\pi d\alpha \exp\left\{-\frac{\nu x}{\nu(1 + \eta \cos \alpha)^{1/2}}\right\}. \quad (4.41)$$

At large distances from the sample surface, the electric field along the normal to the layers can be described by the same formula if we supplement the integrand in the integral with respect to  $\alpha$  with the factor  $\eta^{-4/3} \sin^2 \alpha$ . For  $x \gg \nu/\omega\eta$ , the integrand in formula (4.41) is a rapidly oscillating alternating function, and the main contribution to this integral comes from small neighborhoods of the stationary phase point  $\alpha = (0, \pi)$ . As a result of simple calculations, we obtain

$$E_y(x) = E_y(0)(c/\omega_0)^{4/3}(\nu/\omega)^{2/3}x^{-2}\eta^{-1/2} \times \left[ \exp\left\{-\frac{\nu x}{\nu(1 + \eta)^{1/2}}\right\} + \exp\left\{-\frac{\nu x}{\nu(1 - \eta)^{1/2}}\right\} \right], \quad (4.42)$$

$x \gg \nu/\omega\eta.$

In the above formulas, we have omitted insignificant numerical factors of the order of unity. The pre-exponential factor in formula (4.42) is inversely proportional to  $x^2$  as in normal metals. Such an asymptotic behavior in quasi-two-dimensional conductors is observed only in the range of high frequencies, where  $\omega\tau \gg 1/\eta$ . Essentially different asymptotic forms of electric fields at such frequencies can be explained by tracing the phase of the wave carried by conduction electrons with different velocity components  $\mathbf{v}_x$  from the skin layer. At the instant  $t$ , electrons carry over a distance  $x$  the information on electromagnetic wave with a phase lag  $\omega\Delta t = \omega x/\mathbf{v}_x$ . Averaging over different values of  $\mathbf{v}_x$  by the formula

$$E(x) \sim \int d\mathbf{v}_x \exp\{-i\omega t + i\omega x/\mathbf{v}_x\} \quad (4.43)$$

we can easily see that a weakly attenuating wave which propagates with the electron velocity  $\mathbf{v}_1$  at the reference point of the Fermi surface is formed by charge carriers whose velocity  $\mathbf{v}_x$  differs from  $\mathbf{v}_1$  by the quantity  $\Delta\mathbf{v}_x \ll \mathbf{v}_1^2/\omega x$ . If  $\mathbf{v}_1 - \mathbf{v}_2 \cong \nu\eta$  is smaller than  $\Delta\mathbf{v}_x$ , i.e.,  $x \ll \nu/\omega\eta$ , formula (4.37) is valid for  $E_y(x)$ , while in the opposite limiting case, when  $\Delta\mathbf{v}_x \ll \nu\eta$ , weakly attenuating waves described by formula (4.42) are formed by electrons from small neighborhoods on the Fermi surface near the saddle and reference points.

In a magnetic field, charge carriers belonging to one of the "banks" of the central open cross section of the Fermi surface, on which the velocity  $\mathbf{v}_x$  varies with time periodically in the interval between  $\mathbf{v}_2$  and  $\mathbf{v}_1$ , move most rapidly to the bulk of the sample. Weakly attenuating waves propagate at a velocity equal to the extremal value  $\bar{\mathbf{v}}_x$  and are described by formulas (4.36) and (4.37).

Weakly attenuating waves in a magnetic field tilted from the plane of the layers have a similar form. If the magnetic field lies in the  $xy$  plane, i.e.,  $\theta = \pi/2$ , a weakly attenuating wave with  $\varphi$  differing noticeably from zero propagates at a velocity  $\bar{\mathbf{v}}_x$  equal to the drift velocity of charge carriers belonging to the open cross section of the Fermi surface containing the reference point along the  $p_x$ -axis. The asymptotic form of the electric field  $E_y(x)$  is described by (4.37), and its oscillatory dependence on the magnetic field orthogonal to the axis of the corrugated cylinder is manifested, as before, only in small corrections proportional to  $\eta^2$ .

When electromagnetic waves propagate along the normal to the layers (along the  $z$ -axis), charge carriers can carry information on the field in the skin layer to the bulk of the sample only over a distance of the order of  $l\eta$ , which exceeds the skin depth only for very small values of  $\eta$ .

The weakly attenuating electric field component can easily be determined with the help of relation (4.33) in which  $x$  should be replaced by  $z$ . Without a loss in generality of the given problem, we shall confine our analysis only to the first two terms in expression (2.1) for  $\varepsilon(\mathbf{p})$ , assuming that  $\varepsilon_1(p_x, p_y)$  is a constant quantity equal to  $\eta\nu_0 h/a$ , where  $\nu_0$  coincides in order of magnitude with the characteristic Fermi velocity  $\mathbf{v}_F$  of charge carriers along the layers.

If the magnetic field is orthogonal to the layers, the Fourier components  $\sigma_{ij}(k)$  of the electrical conductivity tensor assume the form

$$\sigma_{ij}(k) = \frac{2e^2}{(2\pi\hbar)^3} \times \sum_n \int dp_z 2\pi m^* \frac{\mathbf{v}_i^{(-n)} \mathbf{v}_j^{(n)}}{\nu + ik\nu_F \eta \sin(ap_z/h) + in\Omega}. \quad (4.44)$$

After simple calculations, we obtain

$$\sigma_{ij}(k) = \omega_0^2 \sum_n C_{ij}^{(n)} \{(k\nu_0\eta)^2 + (\gamma_n\Omega)^2\}^{-1/2}, \quad (4.45)$$

where

$$\gamma_n = \gamma + in,$$

$$v^{(n)} = (1/T) \int_0^T dt v_i(t, p_z) \exp(-in\Omega t),$$

and  $C_{ij}^{(n)}$  are numerical factors of the order of unity. For  $i = j$ , all these factors are real-valued and positive, while in Hall's nondissipative components they are imaginary as a rule and change sign upon inversion of  $i$  and  $j$  so that a helicoidal wave attenuating over a distance  $l_{\text{hel}} = \delta_0(\Omega\tau)^{3/2}$  is formed in a strong magnetic field for  $\Omega \gg kv_0\eta$ .

For moderate magnetic fields in which  $kr\eta \gg 1$ , Hall's nondissipative Fourier components  $\sigma_{ij}(k)$  are of the same order of magnitude as the dissipative diagonal components, and all of them possess a root singularity for  $k = k_{\pm} = (\omega \pm \Omega + i/\tau)/(v_F\eta)$ . In this region of magnetic fields, electromagnetic field penetrates in the bulk of the sample only in the form of a Reuter–Sondheimer quasiwave

$$\mathbf{E}(z) = \mathbf{E}(0) \left(\frac{c}{\omega_0}\right)^{4/3} \left(\frac{v\eta}{\omega}\right)^{1/6} z^{-3/2} \exp\{ik_{\pm}z\},$$

$$z \gg v\eta/\omega. \tag{4.46}$$

#### 4.4. Cyclotron resonance

In all organic conductors synthesized at present, the mean free path  $l$  of charge carriers is not large ( $l \leq 10 \mu\text{m}$ ) so that the frequency of electromagnetic waves in the rf and microwave regions is much lower than the electron collision frequency  $1/\tau$ , and the time dispersion can be disregarded while calculating the skin depth. However, the frequency of electromagnetic wave in the millimeter and submillimeter regions at low temperatures can be comparable to the collision frequency for charge carriers, and the interaction of conduction electrons with electromagnetic field is of resonant type, when the wave frequency  $\omega$  is equal or multiple to the frequency  $\Omega$  of their rotation in a magnetic field.

In a magnetic field orthogonal to the sample surface  $z_s = 0$ , cyclotron resonance can take place at multiple frequencies  $\omega = n\Omega$  in the case of essentially anisotropic spectrum of charge carriers in the plane of the layers. The shape of the resonance curve can be determined easily by using formula (4.45) for  $\sigma_{ij}(k)$ . Resonance takes place for  $r\eta \ll \delta_0$ , but it is manifested most clearly when  $l\eta \leq \delta_0$ . If  $l\eta \ll r$  in this case, all charge carriers with a quasi-two-dimensional energy spectrum participate in the formation of resonance effect. In the case of an isotropic spectrum of charge carriers in the plane of the layers, i.e., for  $\varepsilon_0(p_x, p_y) = \varepsilon_0(p_{\perp})$ , where  $p_{\perp} = (p_x^2 + p_y^2)^{1/2}$ , we have only one resonance value of the magnetic field satisfying the condition  $\omega = \Omega$ .

Diagonalizing the tensor  $\sigma_{ij}(k)$ , we obtain the following expression for the diagonal components of surface impedance:

$$Z_{\mu} = -\frac{8i\omega}{c^2} \int_0^{\infty} \frac{dk}{k^2 - 4\pi i\omega c^{-2}\sigma_{\mu}(k)}. \tag{4.47}$$

Under favorable conditions for cyclotron resonance, i.e., for  $l\eta \ll \{r, \delta_0\}$ , the resonance value of the impedance is  $Z_{\mu}^{\text{res}} = 8\pi\omega\delta_0/c^2$ , and the resonance line width is  $(H - H^{\text{res}})/H^{\text{res}} \cong \gamma$ . Away from the resonance we have  $Z_{\mu}$

$\cong \gamma^{-1}Z_{\mu}^{\text{res}}$ . If  $l\eta \gg \delta_0$ , both terms in the braces of formula (4.45) have the same order of magnitude, and the resonance line is ‘‘blurred.’’

The detection of cyclotron resonance at multiple frequencies would make it possible to analyze in detail the energy spectrum of charge carriers, but the observation of this effect requires long mean free paths of charge carriers. The cyclotron resonance observed by Polisski *et al.*<sup>6</sup> in (BEDT–TTF)<sub>2</sub>ReO<sub>4</sub>(H<sub>2</sub>O) for only one resonance value of magnetic field cannot be regarded as an evidence of isotropic spectrum of charge carriers in the plane of the layers. The information on the dispersion relation of charge carriers in this compound can be refined by analyzing the Azbel–Kaner resonance<sup>48</sup> in a magnetic field parallel to the sample surface, at which the cyclotron resonance at multiple frequencies takes place for any shape of the electron energy spectrum.

#### 5. PROPAGATION OF ACOUSTIC WAVES

In an analysis of sound absorption in ordinary metals, the inclusion of electromagnetic waves accompanying an acoustic wave is essential in the range of strong magnetic fields, when the radius of curvature  $r$  of charge carrier trajectories is much smaller than not only the mean free path of the carriers, but also the acoustic wave length  $k^{-1}$ . If, however, the inequality

$$1 \ll kr \ll kl. \tag{5.1}$$

is satisfied, the attenuation of sound in a metal is mainly determined by the deformation mechanism associated with the renormalization of electron energy in the field of the wave. In low-dimensional conductors, the role of electromagnetic fields excited by sound is significant in a wider range of magnetic fields, including fields satisfying the inequality (5.1). In this region of magnetic fields, the sound absorption coefficient  $\Gamma$  oscillates upon a change in reciprocal magnetic field. If the magnetic field is orthogonal to the wave vector  $\mathbf{k}$ , and the trajectories of charge carriers in the momentum space are closed, the amplitude of oscillations in a normal metal is small in comparison with the smoothly varying component of  $\Gamma$  since oscillations are formed by a small group of charge carriers with a diameter of orbits close to the extremal diameter. This effect predicted by Pippard<sup>49</sup> is associated with periodic repetition of the conditions of effective interaction of a charge with an acoustic wave, when the number of wave lengths corresponding to the diameter of the electron orbit changes by unity. If the vectors  $\mathbf{k}$  and  $\mathbf{H}$  are not orthogonal, the average velocity of a charge in the direction of propagation of the sound differs from zero for any shape of the Fermi surface, i.e., charge carriers drift in the direction of wave propagation. The existence of points at which the interaction with the wave is most effective on such a trajectory leads to a resonant dependence of the sound absorption coefficient on reciprocal magnetic field. In ordinary metals, periodic variations of  $\Gamma$  with  $1/H$ , which are not associated with quantization of the motion of charge carriers with an amplitude much larger than the minimum value of  $\Gamma$ , are possible only in the presence of drift along  $\mathbf{k}$ .<sup>50</sup>

In contrast to conventional metals, the formation of Pipard oscillations in low-dimensional conductors involves virtually all charge carriers on the Fermi surface since the diameters of their orbits are close in value. As a result, the amplitude of periodic variations of electrical conductivity and other acoustoelectronic coefficients with  $1/H$  increases abruptly, and absorption is of the resonant type.<sup>51–54</sup> In this case, we cannot obtain even an order-of-magnitude estimate of the sound absorption coefficient without taking into account electromagnetic fields correctly.

### 5.1. Longitudinal wave propagating along the layers

Let us consider a longitudinal acoustic wave ( $\mathbf{u} = (u, 0, 0)$ ) propagating along the layers in a quasi-two-dimensional conductor in a magnetic field  $\mathbf{H}$ . Using formulas (3.19)–(3.21), we can write the system of equations (3.18) after elimination of the field  $\tilde{E}_x$  in the form

$$\begin{aligned} (\tilde{a}_{yx}k\xi + iH_z/c)\omega u + (\xi\sigma_{yy} - 1)\tilde{E}_y + \xi\tilde{\sigma}_{yz}\tilde{E}_z &= 0, \\ (\tilde{a}_{zx}k\xi - iH_z/c)\omega u + \xi\tilde{\sigma}_{zy}\tilde{E}_y + (\xi\sigma_{zz} - 1)\tilde{E}_z &= 0, \\ (\omega^2 - s^2k^2)\rho u + [ik\tilde{c}_{xx} + c^{-1}(\tilde{a}_{yx}H_z - \tilde{a}_{zx}H_y)]k\omega u \\ + [ik\tilde{b}_{xy} + c^{-1}(\tilde{\sigma}_{yy}H_z - \tilde{\sigma}_{zy}H_y)]\tilde{E}_y + [ik\tilde{b}_{xz} \\ + c^{-1}(\tilde{\sigma}_{yz}H_z - \tilde{\sigma}_{zz}H_y)]\tilde{E}_z &= 0, \end{aligned} \quad (5.2)$$

where

$$\begin{aligned} s &= (\lambda_{xxxx}/\rho)^{1/2}, \quad \xi = 4\pi i\omega/(k^2c^2 - \omega^2), \\ \tilde{\sigma}_{\alpha\beta} &= \sigma_{\alpha\beta} - \frac{\sigma_{\alpha x}\sigma_{x\beta}}{\sigma_{xx}}, \quad \tilde{a}_{\alpha j} = a_{\alpha j} - \frac{a_{xj}\sigma_{\alpha x}}{\sigma_{xx}}, \\ \tilde{b}_{i\beta} &= b_{i\beta} - \frac{b_{ix}\sigma_{x\beta}}{\sigma_{xx}}, \quad \tilde{c} = c_{ij} - \frac{b_{ix}a_{xj}}{\sigma_{xx}}, \\ \alpha, \beta &= y, z. \end{aligned}$$

For  $\omega\tau \ll 1$ , the root of the dispersion equation describing an acoustic wave is close to  $\omega/s$ , and we can write it in the form

$$k = \omega/s + k_1. \quad (5.3)$$

In the case of weak corrugation of the Fermi surface ( $\eta \ll 1$ ), the expression for  $k_1$  has the form

$$\begin{aligned} k_1 &= \frac{ik^2}{2\rho s} \frac{1}{1 - \xi\tilde{\sigma}_{yy}} \left\{ \xi(\tilde{a}_{yx}\tilde{b}_{xy} - \tilde{c}_{xx}\tilde{\sigma}_{yy}) + [\tilde{c}_{xx} - i(\tilde{a}_{yx} \right. \\ &\quad \left. - \tilde{b}_{xy})] \frac{H_z}{kc} + \tilde{\sigma}_{yy} \frac{H_z^2}{k^2c^2} \right\} \Bigg|_{k=\omega/s}. \end{aligned} \quad (5.4)$$

Vectors  $\mathbf{H}$  and  $\mathbf{k}$  are orthogonal. In a magnetic field  $\mathbf{H} = (0, H \sin \theta, H \cos \theta)$  orthogonal to the direction of wave propagation, the solution of the kinetic equation in the Fourier representation can be written in the form

$$\begin{aligned} \psi &= \frac{\int_{t-T}^t dt' g(t') \exp\{i\mathbf{k}[x(t') - x(t)] + \nu(t' - t)\}}{1 - \exp(-\nu T)} \\ &\equiv \hat{R}g, \end{aligned} \quad (5.5)$$

where  $T$  is the period of rotation of charges in the magnetic field. In the range of magnetic fields for which the inequality (5.1) is satisfied, the interaction with the acoustic wave is most effective for charge carriers moving in phase with the wave. Such carriers make the main contribution to the components of acoustoelectronic tensors which can easily be calculated with the help of the stationary phase method. The amplitude of their oscillations with  $1/H$  is large if the quasi-two-dimensionality parameter  $\eta$  satisfies the condition  $kr\eta \ll 1$  for which the spread in the diameter of electron orbits  $\Delta D \cong 2r\eta$  becomes much smaller than the acoustic wave length. Let a charge pass through two stationary phase points at which  $k v_x = \omega$  during the period of motion  $T$ . Then the following expressions hold<sup>55</sup> for  $\sigma_{yy}$  and  $a_{yx}$  for  $\eta \rightarrow 0$ :

$$\begin{aligned} \sigma_{yy}(k) &= (G/kD)(1 - \sin kD); \\ a_{yx}(k) &= -i(G\Lambda_{xx}/e v kD) \cos kD, \end{aligned} \quad (5.6)$$

where  $D = cD_p/(eH \cos \theta)$ ,  $D_p$  being the averaged diameter of the Fermi surface along the  $p_y$  axis,  $G = 4vD_p e^2 \tau / [ac(2\pi h)^2]$ , and  $\Lambda_{xx}$  the value of the quantity  $\Lambda_{xx}(\mathbf{p})$  at the stationary phase points.

It can easily be verified that the value of  $\tilde{\sigma}_{yy}$  is mainly determined by the  $\sigma_{yy}$  component, and hence the denominator in formula (5.4) for  $k_1$  decreases significantly for  $kD = 2\pi(n + 1/4)$ . This leads to the emergence of sharp peaks of the sound absorption coefficient  $\Gamma$ , which are repeated periodically with the period

$$\Delta \left( \frac{1}{H} \right) = \frac{2\pi e \cos \theta}{kcD_p}. \quad (5.7)$$

The height

$$\Gamma_{\text{res}} = \frac{\omega\tau}{D} = \frac{\omega}{v} \Omega \tau \quad (5.8)$$

of these resonance peaks is proportional to  $H$  for  $l \ll kr^2$ .

Regions of high acoustic transparency in which the absorption coefficient has the form

$$\Gamma = \frac{\omega\tau}{D} \left[ \left( \frac{D}{l} \right)^2 + (kD\eta)^2 \right]. \quad (5.9)$$

are situated away from the resonance (in regions where  $\sin kD$  differs considerably from unity).

We can easily obtain explicit expressions for  $\Gamma$  for arbitrary  $kr\eta$ . Let us consider by way of an example a layered quasi-two-dimensional conductor for which the dispersion relation for charge carriers has the form

$$\varepsilon(\mathbf{p}) = \frac{p_x^2 + p_y^2}{m} + \eta \frac{h}{a} v_0 \cos \left( \frac{ap_z}{h} \right), \quad v_0 = 2\varepsilon_F/m, \quad (5.10)$$

and the deformation potential tensor components  $\Lambda_{ik}(\mathbf{p})$  can be represented in the form

$$\Lambda_{ik}(\mathbf{p}) = \Lambda_{ik}^{(0)}(\mathbf{p}) + \eta L_{ik} \cos \left( \frac{ap_z}{h} \right), \quad (5.11)$$

where

$$\Lambda_{ik}^{(0)}(\mathbf{p}) = -\frac{1}{m} \begin{bmatrix} p_x^2 - m\varepsilon_F & p_x p_y & 0 \\ p_x p_y & p_y^2 - m\varepsilon_F & 0 \\ 0 & 0 & 0 \end{bmatrix},$$

the matrix components  $L_{ik}$  coinciding the Fermi energy in the order of magnitude.

Let us write the expressions for some components of acoustoelectronic tensors obtained in the main approximation in the small parameters  $\gamma = (\Omega\tau)^{-1}$  and  $(kD)^{-1}$  for a magnetic field orthogonal to the layers.<sup>52,53</sup>

$$\begin{aligned} \sigma_{yy} &= \frac{4Ne^2}{m\nu\pi kD} [1 - J_0(\zeta)\sin kD], \\ \sigma_{yx} &= -\sigma_{xy}^{(2)} = \frac{4Ne^2}{m\nu\pi kD} J_0(\zeta)\cos kD, \\ c_{xx} &= \frac{Nm v_0}{\nu\pi kD} [1 + J_0(\zeta)\sin kD], \end{aligned} \quad (5.12)$$

where  $N$  is the number density of charge carriers with a quasi-two-dimensional dispersion relation,  $J_0$  Bessel's function of  $\zeta = kR\eta$ , and  $R = 2hc/(eHa)$ . The diameter  $D$  of the electron orbit in the case under investigation has the form  $D = 2c v_0 m / (eH)$ .

For  $\zeta \gg 1$ , the corrugation of the Fermi surface is quite strong, and absorption coefficient behaves as in an ordinary isotropic metal:

$$\Gamma = \Gamma_0 \Omega_0 \tau \left[ 1 + \left( \frac{2}{\pi\zeta} \right)^{1/2} \cos \left( \zeta - \frac{\pi}{4} \right) \sin(kD) \right] \Big|_{k=\omega/s}, \quad (5.13)$$

where  $\Omega_0 = eH/(mc)$ ;  $\Gamma_0 = Nm\omega v_0 / (4\pi\rho s^2)$  is the energy absorption coefficient for acoustic waves in zero magnetic field.

For  $\zeta \ll 1$ , specific features of the quasi-two-dimensional conductor are manifested, and  $\Gamma$  is given by

$$\begin{aligned} \Gamma &= \Gamma_0 \Omega_0 \tau \\ &\times \operatorname{Re} \left[ \frac{(\pi\gamma)^2 + \zeta^2/2 + i\mu[1 + \sin kD]}{1 - \sin kD + (\pi\gamma)^2/2 + \zeta^2/2 + 9/8(kD)^{-2} + i\mu} \right] \Big|_{k=\omega/s}, \end{aligned} \quad (5.14)$$

where  $\mu = \pi v_0 c^2 \omega / 2s^3 \omega_0^2 \Omega \tau$ ,  $\omega_0$  being the frequency of plasma oscillations. If the latter is comparable with the value typical of ordinary metal ( $10^{15} - 10^{16} \text{ s}^{-1}$ ), the parameter  $\mu$  in the ultrasonic frequency range is quite small, and periodic variations of  $\Gamma(1/H)$  have the form of giant resonance oscillations (Fig. 4). Such a behavior of  $\Gamma$  is typical of any conductor with a quasi-two-dimensional dispersion relation for charge carriers.

*Vectors  $\mathbf{H}$  and  $\mathbf{k}$  are not orthogonal.* Let us now consider the case when the magnetic field  $\mathbf{H} = (H \sin \varphi, 0, H \cos \varphi)$  is not orthogonal to the vector  $\mathbf{k}$ . In this case, the value of the velocity component  $\bar{v}_x$  along the direction of the wave vector averaged over the period differs from zero, and the solution of the kinetic equation has the form

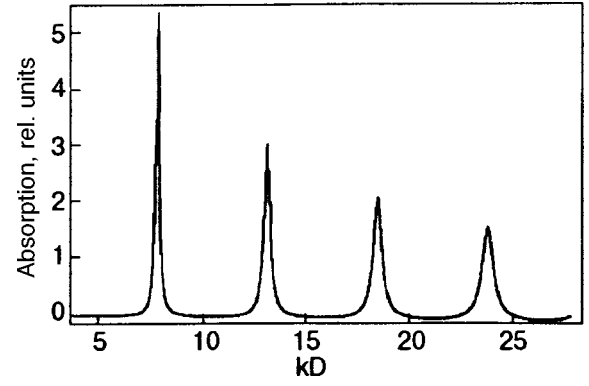


FIG. 4. Dependence of the absorption coefficient of a longitudinal acoustic wave on the reciprocal magnetic field  $D \propto 1/H$  in relative units.

$$\begin{aligned} \psi &= \frac{\int_{t-T}^t dt' g(t') \exp\{i\mathbf{k}[x(t') - x(t)] + \nu(t' - t)\}}{1 - \exp[-\nu T - i\mathbf{k}\bar{v}_x T]} \\ &\equiv \hat{R}g. \end{aligned} \quad (5.15)$$

It follows from the equation of motion (3.9) for a charge with the dispersion relation (2.1) that its velocity components averaged over the period  $T$  satisfy the relation

$$\bar{v}_x = \tan \varphi \bar{v}_z; \quad \bar{v}_\alpha = \frac{1}{T} \int_0^T v_\alpha(t_H) dt_H. \quad (5.16)$$

The displacement of an electron over the period of motion along the wave vector is given by

$$\begin{aligned} \bar{v}_x T &= -\tan \varphi \sum_{n=1}^{\infty} \frac{an}{h} \int_0^T dt \varepsilon_n(t, p_H) \sin \frac{anp_z}{h} \\ &= -\tan \varphi \sum_{n=1}^{\infty} \frac{an}{h} \int_0^T dt \varepsilon_n(t, p_H) \sin \left[ \frac{anp_H}{h \cos \theta} \right. \\ &\quad \left. - \frac{1}{h} anp_x(t, p_H) \tan \varphi \right]. \end{aligned} \quad (5.17)$$

If we take into account the fact that  $p_x$  and  $p_y$ , and hence  $\varepsilon_n$  depends weakly on the integral of motion  $p_H = p_x \sin \varphi + p_z \cos \varphi$  in a magnetic field, the drift velocity of electrons along  $\mathbf{k}$  in the main approximation in the small parameter  $\eta$  of quasi-two-dimensionality of the electron energy spectrum assumes the form

$$\bar{v}_x = -\tan \varphi \operatorname{Im} \sum_{n=1}^{\infty} \frac{an}{h} \exp \left\{ \frac{ianp_H}{h \cos \varphi} \right\} I_n(\tan \varphi), \quad (5.18)$$

where

$$I_n(\tan \varphi) = \frac{1}{T} \int_0^T dt \varepsilon_n(t) \exp \left\{ -\frac{i}{h} anp_x(t) \tan \varphi \right\}. \quad (5.19)$$

These relations are valid for  $\Omega\tau \equiv (eH\tau \cos \varphi / mc) \gg 1$ , i.e., when  $\cos \varphi$  differs from zero considerably.

It can be easily seen that the main term in formula (5.18) proportional to  $I_1(\tan \varphi)$  vanishes for certain values of  $\tan \varphi$ , and there exists a large number of values of the angle  $\varphi = \varphi_c$  in the vicinity of zeros of the function  $I_1(\tan \varphi)$ , for

which the drift velocity  $\bar{v}_x$  of charge carriers along the acoustic wave vector coincides with the velocity  $s$  of propagation of the acoustic wave, and their interaction with the wave is most effective. As a result, we can expect the presence of narrow peaks in the dependence of the damping decrement of acoustic waves on the angle  $\varphi$ .

Using the stationary phase method, we can easily calculate the acoustoelectronic tensor components in the presence of electron drift along  $\mathbf{k}$  also. For example, for the dispersion relation (5.10) for charge carriers, we obtain the following expression for  $\sigma_{yy}$  for small  $\eta$ :

$$\sigma_{yy} = \frac{4Ne^2}{\pi m \nu k D} \left\{ \frac{1 - \sin kD}{(1 + \alpha^2)^{1/2}} + \frac{(\pi \gamma)^2}{3} \left( 1 + \frac{1}{2} \sin kD \right) + \pi \gamma \sin kD \left( 1 - \frac{1}{(1 + \alpha^2)^{1/2}} \right) \right\}. \quad (5.20)$$

Here  $D = 2v_0/\Omega$ ,  $\alpha = kl\eta \tan \varphi J_0(ah^{-1}m\nu \tan \varphi)$ . The component  $\sigma_{yy}$  oscillates with reciprocal magnetic field, and its complex periodic dependence on the angle  $\varphi$  can be described in terms of the quantity  $\alpha$ . The remaining acoustoelectronic coefficients behave similarly.

For  $\alpha \ll 1$ , we can easily obtain the following expression for  $k_1$ <sup>56,57</sup>:

$$k_1 = \frac{i\omega N m \nu}{4\pi \rho s^2} \times \frac{2\pi \sin^2 kD [1 - (1 + \alpha^2)^{-1/2}] + \pi^2 \gamma}{1 - \sin kD + [(\pi \gamma)^2/2](1 + \alpha^2)^{1/2} + \pi \gamma [(1 + \alpha^2)^{1/2} - 1]}. \quad (5.21)$$

If  $\alpha \ll 1$ , we obtain

$$k_1 = \frac{i\omega N m \nu}{4\pi \rho s^2} \frac{\pi \alpha^2 \sin^2 kD + \pi^2 \gamma}{1 - \sin kD + (\pi \gamma)^2/2 + \pi \gamma \alpha^2/2}. \quad (5.22)$$

For  $\gamma^{1/2} \ll \alpha \ll 1$ , the oscillating terms exceed the smoothly varying terms not only in the denominator, but also in the numerator of formula (5.21). This leads to giant oscillations of the sound absorption coefficient  $\Gamma = \text{Im } k_1$  upon a variation of the reciprocal magnetic field as well as the angle  $\varphi$  between  $\mathbf{H}$  and  $\mathbf{n}$ . In the case, when the displacement of charge carriers along  $\mathbf{k}$  during their mean free time is much larger than the acoustic wave length, these oscillations also take place. Then we can write the following expression for  $k_1$ :

$$k_1 = \frac{i\omega N m \nu}{4\pi \rho s^2} \frac{2\pi \sin^2 kD + \pi^2 \gamma}{1 - \sin kD + \pi \gamma \alpha}, \quad 1 \ll \alpha \ll 1/\gamma. \quad (5.23)$$

Thus, the existence of even a small displacement of charge carriers along  $\mathbf{k}$  affects significantly the sound absorption  $\Gamma$ . For  $\sin kD = 1$ , the function  $\Gamma(H)$  attains its maximum value

$$\Gamma_{\max} = \frac{\Gamma_0 \Omega \tau}{(1 + \alpha^2)^{1/2}}. \quad (5.24)$$

A slight deviation of  $\sin kD$  from unity leads to a strong decrease in  $\Gamma$  which has the minimum value  $\Gamma_{\min} = \Gamma_0/\Omega\tau$  for  $\sin kD = -1$  if  $\alpha^2 \ll \gamma \ll 1$ . For  $\gamma \leq 3\alpha^2/2 \ll 1$ , the minimum of  $\Gamma(H)$  is shifted towards the values of  $H$  for which  $\sin kD$  is

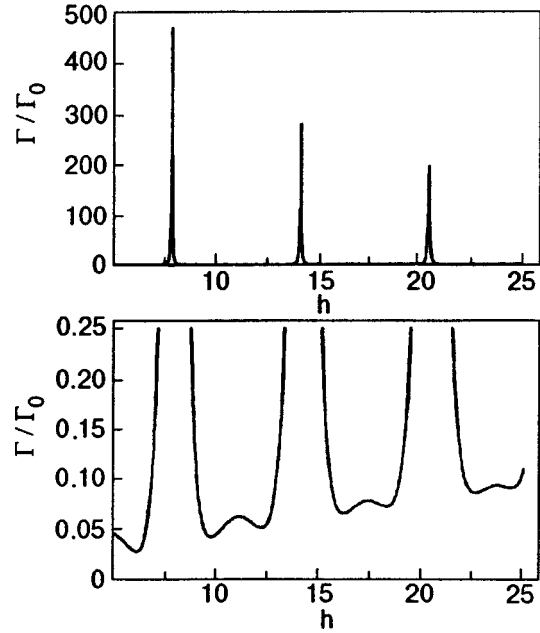


FIG. 5. Dependence of the absorption coefficient  $\Gamma/\Gamma_0$  on  $h = H_0/H$  ( $H_0 = 2\omega cm v_0/es$ ) for  $kl = 10^3$ ,  $\eta = 10^{-2}$ ,  $x = \tan \varphi = 1.5 \times 10^{-2}$ . The upper and lower figures differ in scale.

close to zero, and the function  $\Gamma(H)$  has a local peak  $\Gamma = \Gamma_0 \alpha^2$  for  $\sin kD = -1$ . This peak increases with  $\alpha$  and attains the value  $\Gamma_0$  of the sound absorption coefficient in zero magnetic field for  $\alpha \geq 1$ . At the same time, the main peak decreases with increasing  $\alpha$  and approaches the local maximum. For  $\sin kD = -1$ , the absorption coefficient oscillates with a large amplitude exceeding the minimum value of  $\Gamma$  by a factor of  $\Omega\tau$ .

Figures 5, 6, and 7 show the dependence of absorption coefficient on the quantity  $h = H_0/H$  ( $H_0 = 2\omega v_0 mc/se$ )

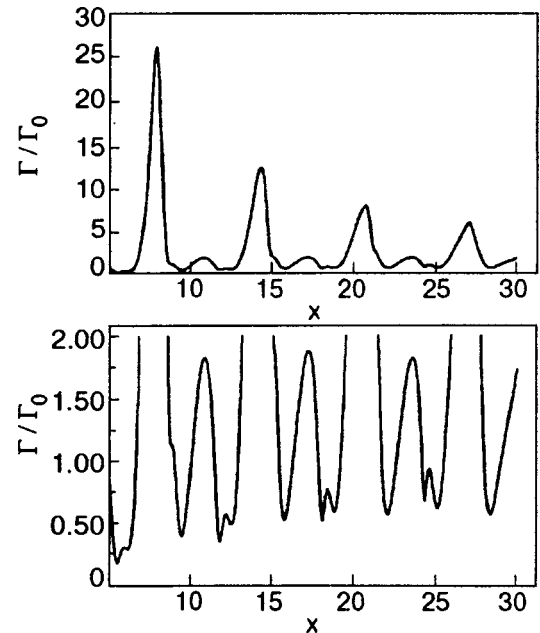


FIG. 6. Dependence of the absorption coefficient  $\Gamma/\Gamma_0$  on  $x = \tan \varphi$  for  $kl = 10^2$ ,  $\eta = 10^{-2}$ . The upper and lower figures differ in scale.

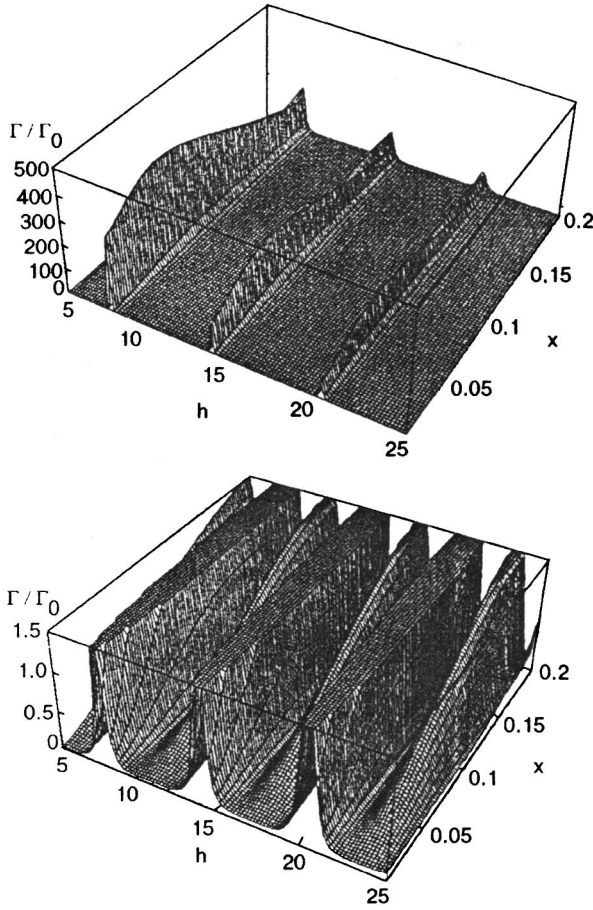


FIG. 7. Dependence of the absorption coefficient  $\Gamma/\Gamma_0$  on  $h$  and  $x = \tan \varphi$  for  $kl = 10^3$ ,  $\eta = 10^{-2}$ . The upper and lower figures differ in scale.

and on  $\tan \varphi$ .

It can easily be seen that the dependence of  $\Gamma$  on  $1/H$  and  $\tan \varphi$  described above remains valid for an arbitrary form of the quasi-two-dimensional electron energy spectrum. If the electron orbit contains only two stationary phase points, the value of  $D = cD_p/eH$  is determined by the diameter  $D_p$  of the Fermi surface in a direction orthogonal to the vectors  $\mathbf{k}$  and  $\mathbf{H}$ .

Noticeable manifestation of the effect of drift of charge carriers on the oscillatory dependence of  $\Gamma$  on  $1/H$  at ultrasonic frequencies ( $\omega \cong 10^8 \text{ s}^{-1}$ ) is determined by certain requirements. For example, we must use perfect samples with a large mean free path of charge carriers and strong magnetic fields of the order of 10 T. In this range of magnetic fields, the Shubnikov–de Haas effect is manifested clearly in compounds of tetrathiafulvalene, which indicates that the condition  $\Omega \tau \gg 1$  is satisfied, and at the same time the separation between quantized electron energy levels is much smaller than not only the Fermi energy, but also the quantity  $\eta \varepsilon_F$ . Under these conditions, a semiclassical description of non-equilibrium processes is valid. In stronger magnetic fields, the quantization of electron energy levels is significant, but the effects described above must also be observed.

*Presence of a quasi-one-dimensional group of charge carriers.* In order to clarify the role of a quasi-one-dimensional group of charge carriers in attenuation of acous-

tic waves, we consider a simple model of the energy spectrum for a two-band conductor. We assume that the dispersion relation (5.10) is valid for one group of charge carriers, while the other group has a quasi-one-dimensional dispersion relation of the form

$$\varepsilon_1(\mathbf{p}) = \pm \mathbf{p} \cdot \mathbf{N} v_1 + \eta_1 \frac{h}{a} v_1 \cos\left(\frac{a n p_z}{h}\right). \quad (5.25)$$

Here  $\eta_1 \ll 1$  and  $v_1$  is the velocity of an electron with the Fermi energy on a quasi-one-dimensional sheet of the Fermi surface. The vector  $\mathbf{N} = (\cos \beta, \sin \beta, 0)$  is oriented in the plane of the layers and forms an angle  $\beta$  with the direction of wave propagation.

In this case, for calculating acoustoelectronic tensors, we must carry out integration in formulas (3.21) over all sheets of the Fermi surface, and each component is the sum of the contributions from quasi-two-dimensional and quasi-one-dimensional ( $\sigma_{ij}^{(1)}, a_{ij}^{(1)}, b_{ij}^{(1)}, c_{ij}^{(1)}$ ) groups of charge carriers.

The existence of preferred direction of the velocities of charge carriers in the quasi-one-dimensional group is manifested in the dependence of their deformation potential  $\Lambda_{ij}^{(1)}$  on the angle  $\beta$ . If crystal deformation does not lead to a redistribution of charges between electron groups, we can naturally assume [bearing in mind relation (3.12)] that  $\Lambda_{ij}^{(1)}$  vanishes in the main approximation in the small parameter  $\eta_1$ . If we put  $\Lambda_{xx}^{(1)} = \eta_1 \varepsilon_F \cos \beta$ , the expressions for the contributions to acoustoelectronic coefficients from the electrons of the quasi-one-dimensional group assume the form

$$\sigma_{ij}^{(1)} = h_\beta \frac{N_1^2 e^2 v_1^2}{\nu \varepsilon_F} N_i N_j, \quad i, j = x, y;$$

$$c_{xx}^{(1)} = \eta_1^2 h_\beta \frac{N_1 \varepsilon_F \cos^2 \beta}{\nu},$$

$$a_{xx}^{(1)} = b_{xx}^{(1)} = i \eta_1 h_\beta \frac{N_1 e v_1}{\nu} kl \cos^3 \beta,$$

$$a_{yx}^{(1)} = b_{xy}^{(1)} = i \eta_1 h_\beta \frac{N_1 e v_1}{\nu} kl \cos^2 \beta \sin \beta,$$

$$h_\beta = [1 + (kl)^2 \cos^2 \beta]^{-1}. \quad (5.26)$$

Here  $l = v_1 \tau$  and  $N_1$  is the number density of charge carriers with the quasi-one-dimensional dispersion relation. The contribution to the acoustoelectronic coefficients from the quasi-two-dimensional group of charge carriers have the form of (5.12) and similar relations.

In the main approximation in the small parameters  $(\Omega \tau)^{-1}$ ,  $(kD)^{-1}$ , the absorption coefficient for a longitudinal acoustic wave has the form<sup>58</sup>

$$\Gamma = \Gamma_0 \Omega_0 \tau \frac{1 - J_0^2(\zeta) + kD g_\beta [1 + J_0(\zeta) \sin kD] + \eta_1^2 kD f_\beta^2 \cos^2 \beta [1 - J_0(\zeta) \sin kD]}{1 - J_0(\zeta) \sin kD + kD g_\beta} \Big|_{k=\omega/s} \quad (5.27)$$

The functions

$$f_\beta = \frac{N_1}{N} \frac{(kl)^2 \cos^2 \beta}{1 + (kl)^2 \cos^2 \beta} \quad \text{and} \quad g_\beta = \frac{N_1}{N} \frac{\sin^2 \beta}{1 + (kl)^2 \cos^2 \beta}$$

do not exceed unity when the number densities of charge carriers of both electron groups are equal. In expression (5.4), we have neglected unity in comparison with the quantity  $|\xi \bar{\sigma}_{yy}|$ . This corresponds to the inequality  $c^2 \omega^2 D / s^3 \omega_0^2 \tau \ll 1$  which is satisfied in the ultrasonic frequency range if the frequency of plasma oscillations  $\omega_0$  in a quasi-two-dimensional conductor is of the same order of magnitude as in an ordinary metal. Insignificant numerical factors in formula (5.27) have been omitted.

The presence of a group of charge carriers with a quasi-one-dimensional dispersion relation leads to considerable anisotropy in attenuation of an acoustic wave in the plane of the layers. If the wave propagates along the preferred direction of velocities of electrons belonging to this group ( $\beta = 0$ ), the sound absorption coefficient can be represented in the form

$$\Gamma = \Gamma_0 \left( \Omega_0 \tau \frac{1 - J_0^2(\zeta)}{1 - J_0(\zeta) \sin kD} + \eta_1^2 \frac{N_1}{N_2} \frac{\omega \tau}{s} v_0 \right) \Big|_{k=\omega/s} \quad (5.28)$$

For  $\zeta \ll 1$ , the corrugation of the quasi-two-dimensional cavity on the Fermi surface is quite small, and the first term in formula (5.28) assumes the form of sharp resonance peaks. The resonant dependence of  $\Gamma$  on  $H^{-1}$  can be observed by measuring the derivative of  $\Gamma$  with respect of reciprocal magnetic field. In this case, charge carriers belonging to the quasi-one-dimensional group make a contribution to the ‘‘background’’ component of  $\Gamma$ .

When the angle  $\beta$  deviates from zero, the resonant nature of the dependence  $\Gamma(H^{-1})$  is preserved as long as the inequality  $\pi/2 - \beta > (kD)^{1/2}/kl$  is satisfied. When the value

of the angle  $\beta$  approaches  $\pi/2$ , the resonant behavior of the sound absorption coefficient changes for giant oscillations which assume the following form for  $\beta = \pi/2$ :

$$\Gamma = \Gamma_0 \Omega_0 \tau \{1 + J_0(\zeta) \sin kD\} \cong \Gamma_0 \Omega_0 \tau \left\{ 1 + \sin kD - \frac{\zeta^2}{4} \sin kD \right\} \Big|_{k=\omega/s} \quad (5.29)$$

For  $\sin kD = -1$ , the absorption coefficient  $\Gamma$  assumes its minimum value which is the smaller, the weaker the corrugation of the Fermi surface.

Figures 8 and 9 show the dependence of absorption coefficient on  $h$  and  $\cos \beta$ .

The peaks on the experimentally observed dependence of  $\Gamma$  on the magnitude and orientation of magnetic field are considerably less sharp than those in Figs. 5–9 since the value of  $kl$  in the layered conductors studied at present considerably exceeds unity only in the region of hypersonic frequencies.

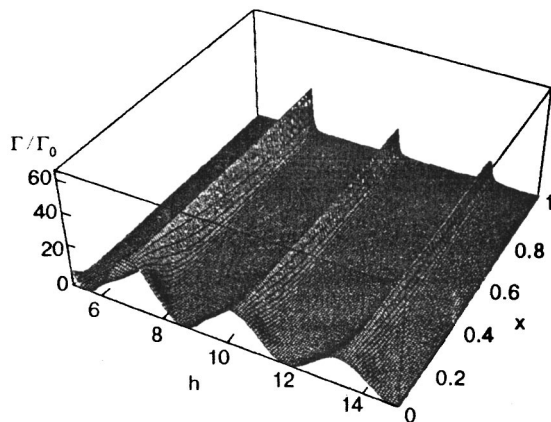


FIG. 8. Dependence of the absorption coefficient  $\Gamma/\Gamma_0$  on  $h=H_0/H$  ( $H_0=2\omega cm v_0/es$ ) and  $x=\cos \beta$  for  $\eta=\eta_1=10^{-2}$ ,  $N_1/N_2=1$ , and  $kl=10^2$ .

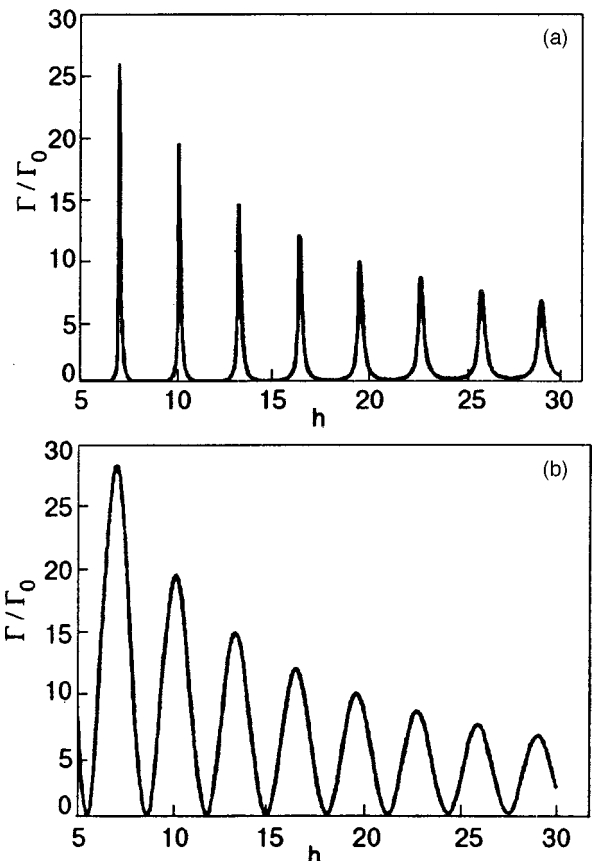


FIG. 9. Cross sections of the curve in Fig. 8 by the planes  $x=1$ (a) and  $x=0$ (b).

**5.2. Transverse wave propagating along the layers**

In the case of transverse polarization of an acoustic wave  $\mathbf{u}=(0, u_y, u_z)$ , the magnetic field  $\mathbf{H}=(0, H \sin \theta, H \cos \theta)$  oriented perpendicularly to the wave vector appears in Maxwell's equations

$$\tilde{E}_\alpha = \frac{m\omega^2}{e} u_\alpha + \xi j_\alpha; \quad \alpha=y, z \tag{5.30}$$

only in expressions for acoustoelectric coefficients. Using formulas (3.21), we can write these equations in the form

$$j_y(1 - \xi \tilde{\sigma}_{yy}) - j_z \xi \tilde{\sigma}_{yz} = \left( k\omega \tilde{a}_{yy} + \frac{m\omega^2}{e} \tilde{\sigma}_{yy} \right) u_y + \left( k\omega \tilde{a}_{yz} + \frac{m\omega^2}{e} \tilde{\sigma}_{yz} \right) u_z,$$

$$-j_y \xi \tilde{\sigma}_{zy} + j_z(1 - \xi \tilde{\sigma}_{zz}) = \left( k\omega \tilde{a}_{zy} + \frac{m\omega^2}{e} \tilde{\sigma}_{zy} \right) u_y + \left( k\omega \tilde{a}_{zz} + \frac{m\omega^2}{e} \tilde{\sigma}_{zz} \right) u_z. \tag{5.31}$$

Let us consider the propagation of a transverse acoustic wave in a conductor with one group of charge carriers possessing a quasi-two-dimensional energy spectrum. Supplementing Eqs. (5.31) with equations (3.2) from the theory of elasticity, we obtain a system of equation whose compatibility condition

$$\begin{vmatrix} 1 - \xi \tilde{\sigma}_{yy} & -\xi \tilde{\sigma}_{yz} & \chi_{yy} & \chi_{yz} \\ -\xi \tilde{\sigma}_{zy} & 1 - \xi \tilde{\sigma}_{zz} & \chi_{zy} & \chi_{zz} \\ (i\omega m/e) + ik\xi \tilde{b}_{yy} & ik\xi \tilde{b}_{yz} & (\omega^2 - s_y^2 k^2)\rho + \varphi_{yy} & \varphi_{yz} \\ ik\xi \tilde{b}_{zy} & (i\omega m/e) + ik\xi \tilde{b}_{zz} & \varphi_{zy} & (\omega^2 - s_z^2 k^2)\rho + \varphi_{zz} \end{vmatrix} = 0 \tag{5.32}$$

is the dispersion equation of the problem. Here  $s_y = (\lambda_{yzyx}/\rho)^{1/2}$  and  $s_z = (\lambda_{zxzx}/\rho)^{1/2}$  are the velocities of acoustic waves polarized along the y- and z-axes, respectively, and

$$\chi_{\alpha\beta} = -k\omega \tilde{a}_{\alpha\beta} - \frac{m\omega^2}{e} \tilde{\sigma}_{\alpha\beta},$$

$$\varphi_{\alpha\beta} = ik \left[ k\omega \tilde{c}_{\alpha\beta} + \frac{m\omega^2}{e} \tilde{b}_{\alpha\beta} \right]. \tag{5.33}$$

The elastic moduli tensor components  $\lambda_{yxzx}$  and  $\lambda_{zyyx}$  vanish if the xy plane is the symmetry plane of the crystal.<sup>59</sup> Otherwise, these components must be taken into account, but this does not change the final results significantly.

In view of strong anisotropy of the energy spectrum for charge carriers, the absorption of acoustic waves polarized along and across the layers has essentially different forms. It can easily be verified that the series expansion in small  $\eta$  of acoustoelectronic tensor components with at least one index z starts with quadratic or higher-order terms in  $\eta$ . Retaining only quadratic terms in  $\eta$  in Eq. (5.31), we obtain

$$\left\{ [(\omega^2 - s_y^2 k^2)\rho + \varphi_{yy}](1 - \xi \tilde{\sigma}_{zz})\chi_{yy} \left( i \frac{\omega m}{e} + ik\xi \tilde{b}_{yy} \right) \right\} \times [(\omega^2 - s_z^2 k^2)\rho + \varphi_{zz}] \left( 1 - \xi \tilde{\sigma}_{zz} - \chi_{zz} i \frac{\omega m}{e} \right) = 0. \tag{5.34}$$

The multiplicity of this equation implies that in the approximation quadratic in  $\eta$ , acoustic waves polarized along the y- and z-axes do not interact with each other. Equating the ex-

pression in the braces in (5.34) to zero, we obtain the dispersion equation for the wave polarized along the y-axis. Its solution can be presented in the form  $k = \omega/s_y + k_2$ , where

$$k_2 = \frac{i}{2\rho s_y^2 (1 - \xi \tilde{\sigma}_{yy})} \left[ \xi k\omega (\tilde{a}_{yy} \tilde{b}_{yy} - \tilde{c}_{yy} \tilde{\sigma}_{yy}) + \frac{m\omega^2}{e} (\tilde{a}_{yy} + \tilde{b}_{yy})k\omega \tilde{c}_{yy} + \frac{m^2 \omega^3}{k e^2} \tilde{\sigma}_{yy} \right]_{k=\omega/s_y}. \tag{5.35}$$

The denominator in this expression has the same form as in formula (5.4) for  $k_1$ . It follows hence that the absorption of a transverse acoustic wave polarized along the y-axis in a conductor with a single quasi-two-dimensional group of charge carriers is of resonance type like the absorption of a longitudinal wave.

The deviation of the second root of Eq. (5.34) from  $\sigma/s$  is described by the formula

$$k_3 = \frac{i}{2\rho s_z^2} \left[ \frac{m\omega^2}{e} \left( \frac{\tilde{a}_{zz}}{1 - \xi \tilde{\sigma}_{zz}} + \tilde{b}_{zz} \right) + \left( \frac{m\omega}{e} \right)^2 \frac{s_z \tilde{\sigma}_{zz}}{1 - \xi \tilde{\sigma}_{zz}} + \frac{\omega^2}{s_z} \tilde{c}_{zz} \right]_{k=\omega/s_z}. \tag{5.36}$$

It can easily be verified that the last term in the brackets in formula (5.36) has the highest order of magnitude. Its contribution to the absorption coefficient is decisive and has the form

$$\Gamma \cong \Gamma_0 \eta^2 \frac{l}{D} (1 + \sin kD). \tag{5.37}$$

The peculiarity of quasi-two-dimensional energy spectrum of charge carriers for waves with the above polarization is manifested in stronger magnetic fields also, when  $kD \ll 1$ . In this case, the orientation magnetoacoustic effect is manifested in a strong oscillatory dependence of absorption coefficient on the angle formed by the magnetic field with the normal to the layers.<sup>53,60</sup>

Electron orbits in the momentum space are cross sections of the Fermi surface by the plane  $p_H = \text{const}$ , where  $p_H$  is the momentum component along the magnetic field. Consequently, integrating over the Fermi surface for calculating acoustoelectronic tensors by formulas (3.21), we can conveniently use the variables  $\varepsilon, t$ , and  $p_H$ . If we substitute  $p_z = p_H / \cos \theta - p_y \tan \theta$  into the integrands containing the expressions

$$\begin{aligned}\Lambda_{zz}(\mathbf{p}) &= \sum_{n=1}^{\infty} \Lambda_n(p_x, p_y) \cos \frac{anp_z}{h}, \\ v_z(\mathbf{p}) &= - \sum_{n=1}^{\infty} n \varepsilon_n(p_x, p_y) \frac{a}{h} \sin \frac{anp_z}{h},\end{aligned}\quad (5.38)$$

it can easily be verified that the corresponding acoustoelectronic coefficients are complex periodic functions of the angle  $\theta$  formed by the directions of magnetic field and the normal to the layers. All the orbits in a quasi-two-dimensional conductor are almost indistinguishable, and hence the momentum components  $p_x$  and  $p_y$  depend on  $p_H$  weakly. This allows us to obtain explicit dependence of acoustoelectronic coefficients on  $\theta$  and to make sure that they vanish for certain values of the angle  $\theta = \theta_c$  in the approximation quadratic in the parameter  $\eta$ . When  $\tan \theta \gg 1$ , but  $\cos \theta \gg 1/\Omega\tau$ , the values of  $\theta_c$  are repeated with a period  $\Delta(\tan \theta) = 2\pi h/D_p$ . These oscillations are associated with the motion of charge carriers in strongly elongated orbits in the momentum space, which intersect a large number of unit cells in the reciprocal lattice, and the period of oscillations is connected with a change in this number by unity.

In the case when the dispersion relation for charge carriers has the form (5.10), and the deformation potential is described by formula (5.11), the absorption coefficient has the form

$$\Gamma = \eta^2 \Gamma_0 \frac{\omega \tau v_0}{s} J_0^2(\xi). \quad (5.39)$$

where  $\xi = (a v_0 m/h) \tan \theta$ . At points where Bessel's function  $J_0(\xi)$  vanishes, we must take into account the next terms in the expansion in small parameters  $kD$  and  $s/v$ .

### 5.3. Acoustic wave propagating across the layers

In order to solve the system of equations (3.1)–(3.3) in the case when a wave propagates across the layers, we must carry out Fourier transformations in the coordinate  $z$  considering that the solution of the kinetic equation has the form

$$\psi = \int_{-\infty}^t dt' g[(z + z(t') - z(t)) \exp[\nu(t' - t)]],$$

$$z(t) = \int^t v_z(t') dt'. \quad (5.40)$$

We consider the propagation of a longitudinal acoustic wave  $\mathbf{u} = (0, 0, u)$  in a magnetic field  $\mathbf{H} = (0, H \sin \theta, H \cos \theta)$ . The system of equations for the Fourier components of ion displacement and electric field in this case has the form

$$\begin{aligned}(\tilde{a}_{xz} k \xi + i H_y / c) \omega u + (\xi \sigma_{xx} - 1) \tilde{E}_x + \xi \tilde{\sigma}_{xy} \tilde{E}_y &= 0, \\ \tilde{a}_{yz} k \xi \omega u + \xi \tilde{\sigma}_{yx} \tilde{E}_x + (\xi \sigma_{yy} - 1) \tilde{E}_y &= 0, \\ (\omega^2 - s^2 k^2) \rho u + [ik \tilde{c}_{zz} + c^{-1} \tilde{a}_{xz} H_y] k \omega u + [ik \tilde{b}_{zx} \\ + c^{-1} \tilde{\sigma}_{xx} H_y] \tilde{E}_x + [ik \tilde{b}_{zy} + c^{-1} \tilde{\sigma}_{xy} H_y] \tilde{E}_y &= 0,\end{aligned}\quad (5.41)$$

where

$$\begin{aligned}\tilde{\sigma}_{\alpha\beta} &= \sigma_{\alpha\beta} - \frac{\sigma_{\alpha z} \sigma_{z\beta}}{\sigma_{zz}}, \quad \tilde{a}_{\alpha z} = a_{\alpha z} - \frac{a_{zz} \sigma_{\alpha z}}{\sigma_{zz}}, \\ \tilde{b}_{z\beta} &= b_{z\beta} - \frac{b_{zz} \sigma_{z\beta}}{\sigma_{zz}}, \quad \tilde{c}_{zz} = c_{zz} - \frac{b_{zz} a_{zz}}{\sigma_{zz}}, \\ s &= (\lambda_{zzzz} / \rho)^{1/2}.\end{aligned}$$

Acoustoelectronic coefficients are defined by formulas (3.21) in which

$$\hat{R}g = \int_{-\infty}^{\tau} dt' g(t') \exp\{ik[z(t') - z(t)] + \nu(t' - t)\}.$$

We shall describe the results of analysis of the dispersion equation of the system (5.41), which is carried out for  $\omega\tau \ll 1$  for an acoustic wave propagating, as before, along the layers.

If the magnetic field is directed along the normal to the layers ( $\theta = 0$ ), the absorption is mainly determined by renormalization of the charge carrier energy under the action of deformation. In the case when the deformation potential is described by formula (5.11), the absorption coefficient satisfies the following expression:

$$\Gamma = \Gamma_0 \frac{1}{kl} \{ [1 + (\eta kl)^2]^{1/2} - 1 \}, \quad (5.42)$$

which has the form

$$\Gamma = \Gamma_0 \eta^2 kl. \quad (5.43)$$

for  $kl\eta \ll 1$ . Here  $l = \tau v_0$ .

If, however, the angle  $\theta$  differs from zero, but is not very close to  $(\pi/2)(\cos \theta \gg 1/\Omega_0\tau)$ , the absorption coefficient for  $kl\eta \ll 1$  is described by the formula

$$\Gamma = \frac{\Gamma_0}{2} \left\{ \eta^2 kl J_0^2(\xi) + \frac{\sin^2 \theta}{kl} \left( \frac{\Omega_0 \omega c^2}{\omega_0^2 s^2} \right) \right\}, \quad (5.44)$$

which coincides with formula (5.43) for  $\theta = 0$ .

The first term in formula (5.44) is determined by deformation interaction of electrons with the acoustic wave and describes angular oscillations of absorption coefficient. The second term is associated with the electromagnetic field excited by the acoustic wave and differs from zero even for

$\eta \rightarrow 0$ . For values of angles for which Bessel's function  $J_0(\xi)$  does not vanish, the dependence of  $\Gamma$  on  $kl$  has a minimum for

$$kl\eta = \frac{\sin \theta}{J_0(\xi)} \frac{\Omega_0 \omega c^2}{\omega_0^2 s^2},$$

associated with the competition between the two mechanisms of absorption.

If the magnetic field is oriented along the plane of the layers ( $\theta = \pi/2$ ), almost all charge carriers move in open orbits, and the attenuation of the acoustic wave for  $kR\eta \ll 1$  [ $R = hc/(aeH)$ ] is described by the formula

$$\Gamma = \Gamma_0 \eta^2 kR. \quad (5.45)$$

Thus, the dependences of  $\Gamma$  on the magnitude and direction of the applied magnetic field are quite diverse and can give rich information for studying the properties of charge carriers in low-dimensional conducting structures.

## 6. CONCLUSION

Wave processes in layered organic conductors in a strong magnetic field are quite sensitive to the form of the electron energy spectrum, and their experimental study will provide detailed and reliable information on the dispersion relation and relaxation properties of charge carriers.

Organic conductors are also interesting for applications owing to the diversity of high-frequency and magnetoacoustic phenomena typical of conductors with low-dimensional electron energy spectra. The acoustic transparency stimulated by a magnetic field undoubtedly facilitates the perfection of acoustoelectronic devices. Such a strong dependence of the intensity of the wave penetrating in the bulk of the sample on its polarization makes it possible to use even thin plate of layered conductors, whose thickness is considerably larger than the skin depth, but smaller than or of the order of the mean free path of charge carriers, as filters through which waves with a definite polarization can pass. We shall consider our task to be fulfilled and the publication of this review as expedient if the variety of weakly attenuating waves typical of quasi-two-dimensional conductors considered by us here draws the attention of experimenters.

\*E-mail: vpeschansky@ilt.kharkov.ua

- <sup>1</sup>I. F. Shchegolev, V. N. Laukhin, Yu. V. Sushko, and E. V. Kostyuchenko, *Pis'ma Zh. Éksp. Teor. Fiz.* **42**, 294 (1985) [*JETP Lett.* **42**, 363 (1985)].
- <sup>2</sup>J. Singleton, F. L. Pratt, M. Doportó *et al.*, *Phys. Rev. Lett.* **68**, 2500 (1992).
- <sup>3</sup>S. Hill, J. Singleton, F. L. Pratt *et al.*, *Synth. Met.* **55**, 2566 (1993).
- <sup>4</sup>S. V. Demishev, A. V. Semeno, N. E. Sluchanko, and N. A. Samarin, *Pis'ma Zh. Éksp. Teor. Fiz.* **61**, 299 (1995) [*JETP Lett.* **61**, 313 (1995)].
- <sup>5</sup>S. V. Demishev, A. V. Semeno, N. E. Sluchanko *et al.*, *Phys. Rev. B* **53**, 12794 (1996).
- <sup>6</sup>A. Polisski, J. Singleton, and N. D. Kushch, *Czech. J. Phys.* **46**, Suppl. S5 (1996) (Proceeding, LT 21, Prague, Aug. 8–14 1996).
- <sup>7</sup>S. V. Demishev, A. V. Semeno, N. E. Sluchanko *et al.*, *Zh. Éksp. Teor. Fiz.* **111**, 979 (1997) [*JETP* **84**, 540 (1997)].
- <sup>8</sup>M. V. Kartsovnik, V. N. Laykhin, V. N. Nizhankovskii, and A. A. Ignat'ev, *Pis'ma Zh. Éksp. Teor. Fiz.* **47**, 302 (1988) [*JETP Lett.* **47**, 363 (1988)].
- <sup>9</sup>M. V. Kartsovnik, P. A. Kononovich, V. N. Laykhin, and I. F. Shchegolev,

- Pis'ma Zh. Éksp. Teor. Fiz.* **48**, 498 (1988) [*JETP Lett.* **48**, 541 (1988)].
- <sup>10</sup>I. D. Parker, D. D. Pigram, R. H. Friend *et al.*, *Synth. Met.* **27**, A387 (1988).
- <sup>11</sup>K. Oshima, T. Mori, H. Inokuchi *et al.*, *Phys. Rev. B* **38**, 938 (1988).
- <sup>12</sup>N. Toyota, T. Sasaki, K. Murata *et al.*, *J. Phys. Soc. Jpn.* **57**, 2616 (1988).
- <sup>13</sup>W. Kang, G. Montambaux, J. R. Cooper *et al.*, *Phys. Rev. Lett.* **62**, 2559 (1989).
- <sup>14</sup>I. F. Shchegolev, P. A. Kononovich, M. V. Kartsovnik *et al.*, *Synth. Met.* **39**, 357 (1990).
- <sup>15</sup>R. Yagi, Y. Iye, T. Osada, and S. Kagoshima, *J. Phys. Soc. Jpn.* **59**, 3069 (1990).
- <sup>16</sup>N. D. Kushch, L. I. Buravov, M. V. Kartsovnik *et al.*, *Synth. Met.* **46**, 271 (1992).
- <sup>17</sup>A. I. Kovalev, M. V. Kartsovnik, R. P. Shibaeva *et al.*, *Solid State Commun.* **89**, 575 (1994).
- <sup>18</sup>M. V. Kartsovnik, A. I. Kovalev, V. N. Laykhin *et al.*, *Synth. Met.* **70**, 811 (1995).
- <sup>19</sup>S. I. Pessotskii, R. B. Lyubovskii, M. V. Kartsovnik *et al.*, *Zh. Éksp. Teor. Fiz.* **115**, 205 (1999) [*JETP* **88**, 114 (1999)].
- <sup>20</sup>R. Rossenau, M. L. Doublet, E. Canadell *et al.*, *J. Phys. (Paris)* **6**, 1527 (1996).
- <sup>21</sup>K. Yamagji, *J. Phys. Soc. Jpn.* **58**, 1520 (1989).
- <sup>22</sup>N. A. Zimbovskaya, *Zh. Éksp. Teor. Fiz.* **113**, 2229 (1998) [*JETP* **86**, 1220 (1998)].
- <sup>23</sup>V. G. Peschansky and D. I. Stepanenko, *Zh. Éksp. Teor. Fiz.* **112**, 1841 (1997) [*JETP* **85**, 1007 (1997)].
- <sup>24</sup>V. G. Peschansky and D. I. Stepanenko, *Fiz. Nizk. Temp.* **25**, 277 (1999) [*Low Temp. Phys.* **25**, 203 (1999)].
- <sup>25</sup>A. I. Akhiezer, *Zh. Éksp. Teor. Fiz.* **8**, 1338 (1938).
- <sup>26</sup>V. P. Silin, *Zh. Éksp. Teor. Fiz.* **38**, 977 (1960) [*Sov. Phys. JETP* **11**, 703 (1960)].
- <sup>27</sup>V. M. Kontorovich, *Zh. Éksp. Teor. Fiz.* **45**, 1633 (1963) [*sic*].
- <sup>28</sup>L. A. Fal'kovskii, *Zh. Éksp. Teor. Fiz.* **58**, 1830 (1970) [*Sov. Phys. JETP* **31**, 981 (1970)].
- <sup>29</sup>V. I. Okulov and V. V. Ustinov, *Fiz. Nizk. Temp.* **5**, 213 (1979) [*Sov. J. Low Temp. Phys.* **5**, 101 (1979)].
- <sup>30</sup>V. G. Peschansky, *Sov. Sci. Rev. A* **16**, 1 (1992).
- <sup>31</sup>V. G. Peschansky, J. A. Roldan Lopez, and Toji Gnado Jao, *J. Phys. (Paris)* **1**, 1469 (1991).
- <sup>32</sup>V. G. Peschansky, S. N. Savel'eva, and H. Kheir Bek, *Fiz. Tverd. Tela (St. Petersburg)* **34**, 1640 (1992) [*Sov. Phys. Solid State* **34**, 864 (1992)].
- <sup>33</sup>V. G. Peschansky, H. Kheir Bek, and S. N. Savel'eva, *Fiz. Nizk. Temp.* **18**, 1012 (1992) [*Sov. J. Low Temp. Phys.* **18**, 711 (1992)].
- <sup>34</sup>V. G. Peschansky, H. Kheir Bek, S. N. Savel'eva, and D. A. Torjanik, *Phys. Low-Dimens. Semicond. Struct.* **8**, 81 (1994).
- <sup>35</sup>V. G. Peschansky, *Phys. Rep.* **288**, 305 (1997).
- <sup>36</sup>V. M. Gokhfeld, V. G. Peschansky, and D. A. Torjanik, *Fiz. Nizk. Temp.* **24**, 371 (1998) [*Low Temp. Phys.* **24**, 281 (1998)].
- <sup>37</sup>V. G. Peschansky, *Zh. Éksp. Teor. Fiz.* **114**, 676 (1998) [*JETP* **87**, 369 (1998)].
- <sup>38</sup>V. G. Peschansky, S. N. Savel'eva, and D. A. Torjanik, *Fiz. Tverd. Tela (St. Petersburg)* **40**, 1401 (1998) [*Phys. Solid State* **40**, 1272 (1998)].
- <sup>39</sup>G. E. H. Reuter and E. H. Sondheimer, *Proc. Roy. Soc. (London)* **195**, 36 (1948).
- <sup>40</sup>L. E. Hartmann and L. M. Luttinger, *Phys. Rev.* **151**, 430 (1966).
- <sup>41</sup>M. Ya. Azbel, *Zh. Éksp. Teor. Fiz.* **39**, 400 (1960) [*Sov. Phys. JETP* **12**, 283 (1960)].
- <sup>42</sup>M. A. Lur'e, V. G. Peschansky, and K. Yiasemides, *J. Low Temp. Phys.* **56**, 277 (1984).
- <sup>43</sup>E. A. Kaner and V. G. Skobov, *Adv. Phys.* **17**, 605 (1968).
- <sup>44</sup>V. G. Peschansky, M. Dassanaeke, and E. V. Tsybulina, *Fiz. Nizk. Temp.* **11**, 297 (1985) [*Sov. J. Low Temp. Phys.* **11**, 162 (1985)].
- <sup>45</sup>V. G. Peschansky and S. N. Savel'eva, *Fiz. Tverd. Tela (Leningrad)* **32**, 937 (1990) [*Sov. Phys. Solid State* **32**, 554 (1990)].
- <sup>46</sup>V. M. Gokhfeld and V. G. Peschansky, *Ukr. Fiz. Zh.* **37**, 1593 (1992).
- <sup>47</sup>V. G. Peschansky, J. A. Roldan Lopez, and D. A. Torjanik, *Fiz. Nizk. Temp.* **23**, 784 (1997) [*Low Temp. Phys.* **23**, 591 (1997)].
- <sup>48</sup>M. Ya. Azbel and E. A. Kaner, *Zh. Éksp. Teor. Fiz.* **32**, 896 (1957) [*Sov. Phys. JETP* **5**, 730 (1957)].
- <sup>49</sup>A. B. Pippard, *Philos. Mag.* **2**, 1147 (1957).
- <sup>50</sup>E. A. Kaner, V. G. Peschansky, and I. A. Privorotskii, *Zh. Éksp. Teor. Fiz.* **40**, 214 (1961) [*Sov. Phys. JETP* **13**, 147 (1961)].
- <sup>51</sup>O. V. Kirichenko and V. G. Peschansky, *J. Phys. (Paris)* **4**, 823 (1994).

- <sup>52</sup>O. V. Kirichenko and V. G. Peschansky, *Fiz. Nizk. Temp.* **20**, 574 (1994) [*Low Temp. Phys.* **20**, 323 (1994)].
- <sup>53</sup>V. M. Gokhfeld, O. V. Kirichenko, and V. G. Peschansky, *Zh. Éksp. Teor. Fiz.* **108**, 2147 (1995) [*JETP* **81**, 1171 (1995)].
- <sup>54</sup>O. V. Kirichenko and V. G. Peschansky, *Pis'ma Zh. Éksp. Teor. Fiz.* **64**, 845 (1996) [*JETP Lett.* **64**, 903 (1996)].
- <sup>55</sup>O. Galbova, G. Ivanovsky, O. V. Kirichenko, and V. G. Peschansky, *Fiz. Nizk. Temp.* **23**, 173 (1997) [*Low Temp. Phys.* **23**, 127 (1997)].
- <sup>56</sup>O. V. Kirichenko, D. Krstovska, and V. G. Peschansky, *Fiz. Nizk. Temp.* **24**, 367 (1998) [*Low Temp. Phys.* **24**, 278 (1998)].
- <sup>57</sup>G. Ivanovsky, O. V. Kirichenko, D. Krstovska, and V. G. Peschansky, *J. Phys.: Condens. Matter* **10**, 11765 (1998).
- <sup>58</sup>O. V. Kirichenko and V. G. Peschansky, *Fiz. Nizk. Temp.* **24**, 677 (1998) [*Low Temp. Phys.* **24**, 514 (1998)].
- <sup>59</sup>L. D. Landau and E. M. Lifshitz, *Theory of Elasticity*, 3rd Eng. Ed., Pergamon, Oxford, 1986.
- <sup>60</sup>V. M. Gokhfeld, O. V. Kirichenko, and V. G. Peschansky, *Fiz. Nizk. Temp.* **19**, 456 (1993) [*Low Temp. Phys.* **19**, 321 (1993)].

Translated by R. S. Wadhwa

## QUANTUM LIQUIDS AND QUANTUM CRYSTALS

### Time correlation functions and generalized transport coefficients of semiquantum helium

V. V. Ignatyuk\*<sup>1</sup> and M. V. Tokarchuk

*Institute for Condensed Matter Physics, National Academy of Sciences of the Ukraine, 290011 Lviv, Ukraine*

I. M. Mryglod

*Institute for Condensed Matter Physics, National Academy of Sciences of the Ukraine, 290011 Lviv, Ukraine; Institute of Theoretical Physics, University Linz, A-4040 Linz, Austria*

(Submitted April 6, 1999)

Fiz. Nizk. Temp. **25**, 1145–1153 (November 1999)

The dynamic properties of semiquantum  $^4\text{He}$  are analyzed at two temperatures above the point of superfluid phase transition. Investigations are carried out in the framework of the dynamic thermal viscous model for low and intermediate values of the wave vector. The “momentum–momentum” and “enthalpy–enthalpy” time correlation functions are evaluated and the partial contributions of the collective excitations to these functions are separated. The recurrent relations for memory kernels are used to calculate the time–space dispersion of the generalized transport coefficients. © 1999 American Institute of Physics.  
[S1063-777X(99)00211-X]

#### 1. INTRODUCTION

The dynamic properties of various (simple,<sup>1,2</sup> multicomponent,<sup>3,4</sup> polar,<sup>5</sup> and quantum<sup>6,7</sup>) liquids have drawn the attention of experimental and theoretical scientists for a long time. Experiments aimed at studying the nonequilibrium characteristics of such objects are mainly connected with the scattering of neutrons.<sup>8</sup> In spite of the fact that a large body of data has been accumulated, several characteristic features still await an adequate interpretation.

One such unanswered question concerns the kinetic properties of semiquantum liquids, i.e., liquids whose temperature exceeds the quantum degeneracy value, but is much smaller than the Debye temperature.<sup>9</sup> In this case, the situation is complicated by the fact that there is no appropriate model for describing equilibrium as well as nonequilibrium properties of liquids except for a small number of simplest liquids.<sup>9,10</sup> The difficulties arise because of the need to use the quantum-mechanical apparatus, and also because the anharmonicity of the Hamiltonian with respect to the operators of creation and annihilation of particles must be taken into account. The situation with  $^4\text{He}$  below the  $\lambda$ -point is simpler because explicit expressions for the susceptibility can be obtained in spite of the presence of the Bose condensate and the need to introduce quasimean values. Moreover, the chain of equations for the Green's functions can also be analyzed in this case (at least in the hydrodynamic approximation<sup>11,12</sup>).

Studies of the dynamics properties of the above-mentioned objects are also interesting for experimenters since they provide a better understanding of the processes of initiation of Bose condensation as a result of violation of the system symmetry. Thus the problem involves the

construction of a microscopic picture of events, including the separation and description of certain time and space intervals corresponding to processes of different origin.

One such model, which proved to be quite useful for describing the classical liquids<sup>13,14</sup> is the thermal model including hydrodynamic densities (which are essentially the most slowly varying quantities) as well as the kinetic variables corresponding to the microscopic fluxes of heat and momentum (longitudinal component of the microscopic stress tensor). This model was used by de Schepper *et al.*<sup>14</sup> in the theory of generalized collective modes, and is a generalization of the hydrodynamic model of liquids.<sup>2</sup> It leads to exact expressions in the hydrodynamic limit (when the wave vector  $k$  and the frequency  $\omega$  are small) which correctly describe the region of intermediate values of  $k$  and  $\omega$ . The model becomes especially attractive for constructing computer-adapted theories to describe the dynamics of liquids without using any fitting parameters when the static correlation functions (SCF) and correlation relaxation times serve as the initial parameters and all computations boil down to the eigenvector and eigenvalue problem. Moreover, physical processes of different durations (slow hydrodynamic processes and fast kinetic processes) are separated from the very beginning in the thermal viscous model.

This paper is a logical continuation of our earlier publication<sup>15</sup> in which we calculated the spectra of collective excitations of semiquantum  $^4\text{He}$  at temperatures 4 and 8 K, as well as the symmetrized dynamic structural factor. Data of independent thermodynamic measurements and neutron scattering were used for verification of results and evaluation of the initial parameters of the model. The aim of our investi-

gations is to use the thermal viscous model for studying other time correlation functions which are interesting for experimental studies as well as for computer simulation. Among other things, we shall consider partial contributions to the ‘‘momentum–momentum’’ and ‘‘energy–energy’’ correlation functions. The Fourier transform of the first of these functions may be obtained from experiments on scattering, while the second function is important for interpretation of the molecular dynamics data.

Another interesting problem concerns the space–time dispersion of transport coefficients, and its solution provides a correct description of the nonlocal processes of momentum and energy transport. The computation of space–time characteristics of the transport coefficients can also be carried out effectively by using the thermal viscous model.

In this context, we can mention that Crevecoeur *et al.*<sup>16,17</sup> also used the thermal viscous model, but later simplified it to reduce the number of dynamic variables. They used the damped harmonic oscillator model, and many peculiarities of the dynamic behavior remained outside the range of this model. Moreover, the justification of some of the assumptions raises questions. For example, the initial dynamic matrix used by Crevecoeur<sup>16,17</sup> does not take into consideration the nondiagonal memory functions that play a significant role in the range of intermediate values of  $k$  and  $\omega$ .

The present paper consists of the following parts. In Sec. 2, we shall calculate the ‘‘momentum–momentum’’ and ‘‘enthalpy–enthalpy’’ time correlation functions taking into consideration the contribution from each collective mode. In Sec. 3, the recurrent relations for the memory functions are used to compute the space–time dispersion for the transport coefficients. The last section will be devoted to a discussion of the obtained results.

## 2. TIME CORRELATION FUNCTIONS OF SEMIQUANTUM <sup>4</sup>He

In our earlier publication,<sup>15</sup> we derived a system of equations for time correlation functions (TCF)  $\Phi_{AB}(k, t)$  which can be defined as follows<sup>1</sup>:

$$\begin{aligned} \Phi_{AB}(k, t) &= [\hat{A}(\mathbf{k}, t), \hat{B}(-\mathbf{k})]_0 \\ &= \int_0^1 d\tau \text{Sp}[\rho_0 \Delta \hat{A}(\mathbf{k}, t + i\beta\hbar\tau) \Delta \hat{B}(-\mathbf{k})], \quad (1) \end{aligned}$$

$$\Delta \hat{A}(\mathbf{k}, t) = \hat{A}(\mathbf{k}, t) - \text{Sp}[\rho_0 \hat{A}(0, 0)],$$

where  $\rho_0$  is the equilibrium statistical operator,  $\beta = 1/k_B T$  is the inverse temperature,  $k_B$  the Boltzmann constant, and the time dependence is introduced in terms of the Heisenberg representation. We used the 5-variable thermal viscous model which contains the hydrodynamic number densities of particles  $\hat{n}_{\mathbf{k}}$ , the longitudinal component  $\hat{J}_{\mathbf{k}}$  of momentum, and the generalized enthalpy  $\hat{h}_{\mathbf{k}}$ , as well as the variables  $\hat{\pi}_{\mathbf{k}}$  and  $\hat{Q}_{\mathbf{k}}$ , connected with the longitudinal component of the microscopic viscous stress tensor and the enthalpy flux, respectively, from which the linear combination of hydrody-

namic variables  $\hat{n}_{\mathbf{k}}$ ,  $\hat{J}_{\mathbf{k}}$ , and  $\hat{h}_{\mathbf{k}}$  has been subtracted. In this sense,  $\hat{\pi}_{\mathbf{k}}$  and  $\hat{Q}_{\mathbf{k}}$ , being fast variables, are defined as kinetic variables.

The system of equations for Laplace transforms of TCF

$$\tilde{\Phi}_{AB}(k, z) = \int_0^\infty \exp(-zt) \Phi_{AB}(k, t) dt$$

( $z = i\omega + \varepsilon$ ,  $\varepsilon = +0$ ) can be represented in matrix form as follows:<sup>18,19</sup>

$$z\tilde{\Phi}(k, z) - i\Omega(k)\tilde{\Phi}(k, z) + \tilde{\varphi}(k, z)\tilde{\Phi}(k, z) = \Phi(k), \quad (2)$$

where the notation

$$\begin{aligned} i\Omega_{ij}(k) &= [i\hat{L}\tilde{Y}_i(\mathbf{k}), \hat{Y}_j(-\mathbf{k})]_0 [\hat{Y}_j(\mathbf{k}), \hat{Y}_i(-\mathbf{k})]_0^{-1}; \\ \hat{Y}_i(\mathbf{k}) &= \{\hat{n}_{\mathbf{k}}, \hat{J}_{\mathbf{k}}, \hat{h}_{\mathbf{k}}, \hat{\pi}_{\mathbf{k}}, \hat{Q}_{\mathbf{k}}\} \end{aligned} \quad (3)$$

has been used for elements of the frequency matrix  $i\Omega(k)$  and

$$\begin{aligned} \tilde{\varphi}_{ij}(k, z) &= \left( (1 - \mathcal{P})\hat{Y}_i(\mathbf{k}), \frac{1}{z - (1 - \mathcal{P})i\hat{L}} \right. \\ &\quad \left. \times (1 - \mathcal{P})\hat{Y}_j(-\mathbf{k}) \right)_0 (\hat{Y}_j(\mathbf{k}), \hat{Y}_i(-\mathbf{k}))_0^{-1} \quad (4) \end{aligned}$$

for elements of the matrix of memory functions  $\tilde{\varphi}(k, z)$ . In formulas (3) and (4), the Liouville operator  $i\hat{L}$  is defined in the standard manner

$$\hat{A} \equiv i\hat{L}\hat{A} = \frac{i}{\hbar} [\hat{A}, \hat{H}] \quad (5)$$

through a commutator with the Hamiltonian

$$\hat{H} = \sum_{\mathbf{p}} \frac{\mathbf{p}^2}{2m} \hat{a}_{\mathbf{p}}^+ \hat{a}_{\mathbf{p}} + \frac{1}{2V} \sum_{\mathbf{k}} \sum_{\mathbf{p}} v(\mathbf{k}) \hat{a}_{\mathbf{p}+\mathbf{k}/2}^+ \hat{n}_{\mathbf{k}} \hat{a}_{\mathbf{p}-\mathbf{k}/2}, \quad (6)$$

where  $\hat{a}_{\mathbf{p}}^+$  and  $\hat{a}_{\mathbf{p}}$  are the operators of creation and annihilation of quasiparticles with momentum  $\mathbf{p}$  satisfying the commutation relations  $[\hat{a}_{\mathbf{p}}^+, \hat{a}_{\mathbf{q}}] = \delta_{\mathbf{p}\mathbf{q}}$ ;  $[\hat{a}_{\mathbf{p}}, \hat{a}_{\mathbf{q}}] = [\hat{a}_{\mathbf{p}}^+, \hat{a}_{\mathbf{q}}^+] = 0$ ;  $v(\mathbf{q}) = \int \exp(i\mathbf{q}\cdot\mathbf{r}) \Phi(|\mathbf{r}|) d\mathbf{r}$  is the Fourier transform of the potential  $\Phi(|\mathbf{r}|)$  of interaction between particles,  $V$  the volume of the system and  $N$  the number of particles, while  $\mathcal{P}$  is the Mori projection operator defined on the complete basic set of dynamic variables  $Y_i(\mathbf{k}) = \{\hat{n}_{\mathbf{k}}, \hat{J}_{\mathbf{k}}, \hat{h}_{\mathbf{k}}, \hat{\pi}_{\mathbf{k}}, \hat{Q}_{\mathbf{k}}\}$ , which can also be written in the secondary quantization representation. Note that the TCF  $\Phi_{nn}(k, t)$  constructed on the particle density operators is connected directly with the symmetrized dynamic structural factor  $S_{\text{sym}}(k, \omega)$ .<sup>15</sup>

The chain of equations (2) for TCF is not closed. For the memory functions  $\tilde{\varphi}_{ij}(k, z)$ , we can also write a system of equations containing higher derivatives of the initial basic variables.<sup>20</sup> The natural requirement is the uncoupling of this system. Considering that the relaxation times of the memory functions (4) constructed on ‘‘fast’’ (kinetic) variables are much smaller than the characteristic time scales of evolution of hydrodynamic quantities, we normally use the Markov approximation for  $\tilde{\varphi}_{ij}(k, z)$ , assuming that

$$\tilde{\varphi}_{ij}(k, z) \approx \tilde{\varphi}_{ij}(k, 0) = \int_0^\infty \varphi_{ij}(k, t) dt. \quad (7)$$

The system of equations (2) can then be presented in the form

$$\tilde{T}(k) = \begin{bmatrix} 0 & -i\Omega_{nJ} & 0 & 0 & 0 \\ -i\Omega_{Jn} & 0 & -i\Omega_{Jh} & -i\Omega_{J\pi} & 0 \\ 0 & -i\Omega_{hJ} & 0 & 0 & -i\Omega_{hQ} \\ 0 & -i\Omega_{\pi J} & 0 & \tilde{\varphi}_{\pi\pi} & -i\Omega_{\pi Q} + \tilde{\varphi}_{\pi Q} \\ 0 & 0 & -i\Omega_{Qh} & -i\Omega_{Q\pi} + \tilde{\varphi}_{Q\pi} & \tilde{\varphi}_{QQ} \end{bmatrix}. \quad (9)$$

In the Markov approximation, the solution of the system of equations for TCF can be written in an analytic form in terms of the eigenvalues  $z_\alpha$  and eigenvectors  $X_\alpha = \|X_{i\alpha}\|$  of the matrix  $\tilde{T}(k)$ ,<sup>13,19</sup> i.e.,

$$\tilde{\Phi}_{il}(k, z) = \sum_{\alpha=1}^5 \frac{G_\alpha^{il}(k)}{z + z_\alpha(k)}, \quad (10)$$

where the amplitudes  $G_\alpha^{il}(k)$  can be represented in the form

$$G_\alpha^{il}(k) = X_{i\alpha}(k) [X(k)]_{l\alpha}^{-1} \Phi_{il}(k, 0), \quad (11)$$

$X^{-1}$  is the matrix inverse to  $X = \|X_{i\alpha}\|$ .

It should be emphasized that the Markov approximation (7) is exact in the limit  $k \rightarrow 0$ . Moreover, it was shown<sup>21</sup> that the use of 5-variable thermal viscous model leads to exact expressions for the frequency moments of the dynamic structural factor right up to and including the fourth order. In their most comprehensive form, formulas (8)–(11) essentially describe the thermal viscous model of a liquid and can be used for any fixed value of  $k$ . The problem is simplified considerably for small and intermediate values of the wave vector, since most elements of the matrix  $\tilde{T}(k)$  can be expressed in terms of thermodynamic quantities and hydrodynamic transport coefficients. It should also be noted that, according to the results of computer calculations for a Lennard–Jones liquid,<sup>13</sup> there is no need for a further extension of the description level, i.e., an increase in the number of dynamic basic variables, since the results for the thermal viscous model are close to those obtained for the 7-variable model.

In our previous publication,<sup>15</sup> we analyzed in detail the spectrum of collective modes of semiquantum <sup>4</sup>He in the quasi-hydrodynamic region and their contribution to the dynamic structural factor. An interesting feature of the spectrum is that the dispersion curve of the kinetic propagating excitation at  $T = 4$  K intersects the acoustic curve and the phenomenon of ‘‘fast sound’’ is observed.<sup>3</sup> Another characteristic feature is the disappearance of the central (thermal) peak which may serve as an indication of the onset of symmetry breaking in the Bose system. At  $T = 8$  K, the behavior of  $S_{\text{sym}}(k, \omega)$  was more classical and a Rayleigh–Brillouin triplet was observed in the entire range of wave vectors  $k = 1 - 3 \text{ nm}^{-1}$ . It was also found that, at this temperature, the

$$z\tilde{\Phi}(k, z) + \tilde{T}(k)\tilde{\Phi}(k, z) = \Phi(k), \quad (8)$$

where the generalized hydrodynamic matrix  $\tilde{T}(k)$  has the following structure:

kinetic mode, which becomes a propagating mode for smaller values of the wave vector, participates in the formation of the central peak together with the thermal mode.

Naturally, it should be interesting to consider the behavior of the other TCF also. In particular, the ‘‘momentum–momentum’’ TCF is connected with the dynamic structural factor through the simple relation

$$\tilde{\Phi}_{JJ}(k, \omega) = \frac{m^2 \omega^2}{k^2} S_{\text{sym}}(k, \omega), \quad (12)$$

and can also be obtained from the results of neutron scattering experiments. The ‘‘energy–energy’’ TCF was not measured directly in experiments, but can be calculated from molecular dynamics.

Figures 1 and 2 show the results of calculation of the ‘‘momentum–momentum’’ TCF and the ‘‘enthalpy–enthalpy’’ TCF which is connected with the ‘‘energy–energy’’ TCF through the simple relation

$$\begin{aligned} \tilde{\Phi}_{hh}(k, \omega) = & \tilde{\Phi}_{\varepsilon\varepsilon}(k, \omega) - \frac{\Phi_{n\varepsilon}(k)}{\Phi_{nn}(k)} \\ & \times \left( 2\tilde{\Phi}_{n\varepsilon}(k, \omega) - \frac{\Phi_{n\varepsilon}(k)}{\Phi_{nn}(k)} \tilde{\Phi}_{nn}(k, \omega) \right), \quad (13) \end{aligned}$$

where  $\Phi_{n\varepsilon}(k)$  and  $\Phi_{\varepsilon\varepsilon}(k)$  are static correlation functions.<sup>15</sup>

The same figures also show the contribution of each collective excitation to the corresponding TCF. Analyzing the partial contribution of collective modes to the ‘‘momentum–momentum’’ TCF, we note that the thermal mode does not make any contribution to  $\tilde{\Phi}_{JJ}(k, \omega)$  in the limit of small  $k$  since the corresponding weight factor is proportional to  $k^2$  and the form of the spectral function lines is determined completely by acoustic excitation. This peculiarity observed at  $T = 4$  K is preserved for intermediate values of the wave numbers although the contribution from kinetic excitations is clearly visible for  $k = 2$  and  $3 \text{ nm}^{-1}$ . On the other hand, the contribution from the thermal mode is significant in gaseous <sup>4</sup>He at low frequencies for  $T = 8$  K and  $k = 2 \text{ nm}^{-1}$ , while its amplitude decreases sharply for  $k = 3 \text{ nm}^{-1}$ . However, the kinetic propagating excitation gives a hardly perceptible resonance at the frequency  $\omega = 0.7 \text{ ps}^{-1}$ .

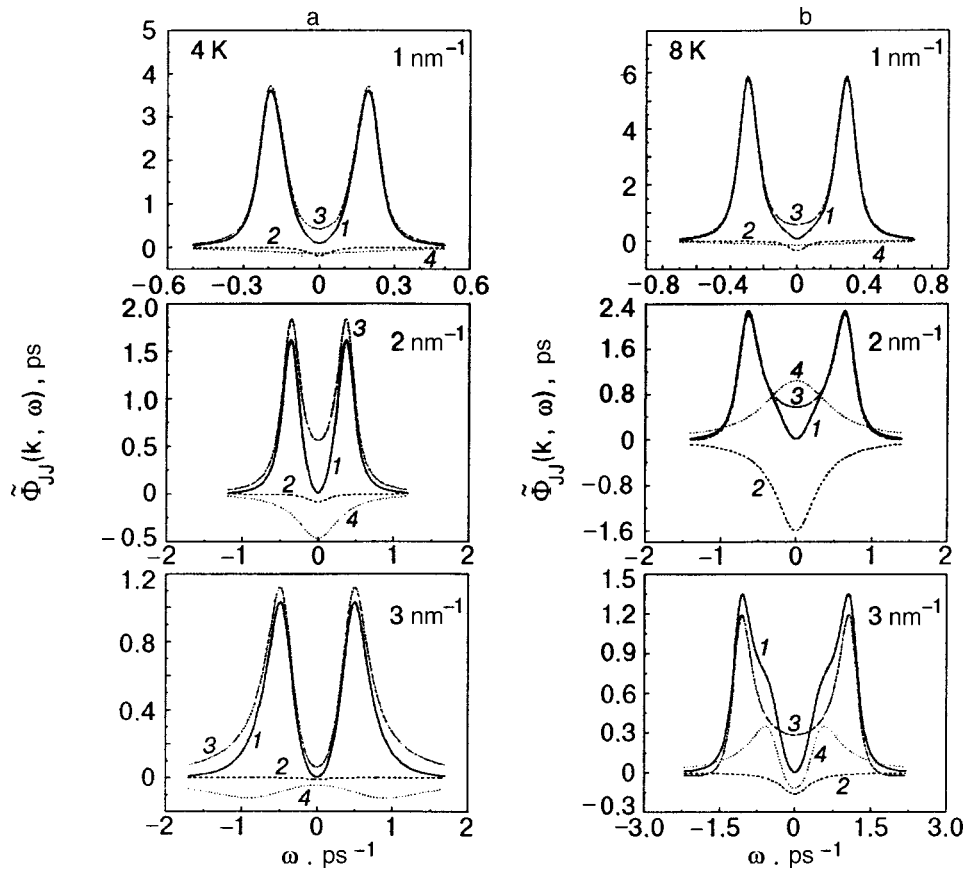


FIG. 1. Time correlation function  $\tilde{\Phi}_{JJ}(k, \omega)$  (curve 1) for  ${}^4\text{He}$  at  $T=4$  K (a) and  $T=8$  K (b) for  $k=1, 2$  and  $3 \text{ nm}^{-1}$ . Curve (2) corresponds to the thermal mode contribution to  $\tilde{\Phi}_{JJ}(k, \omega)$ , while the contributions from the acoustic mode and kinetic mode are shown by curves 3 and 4, respectively.

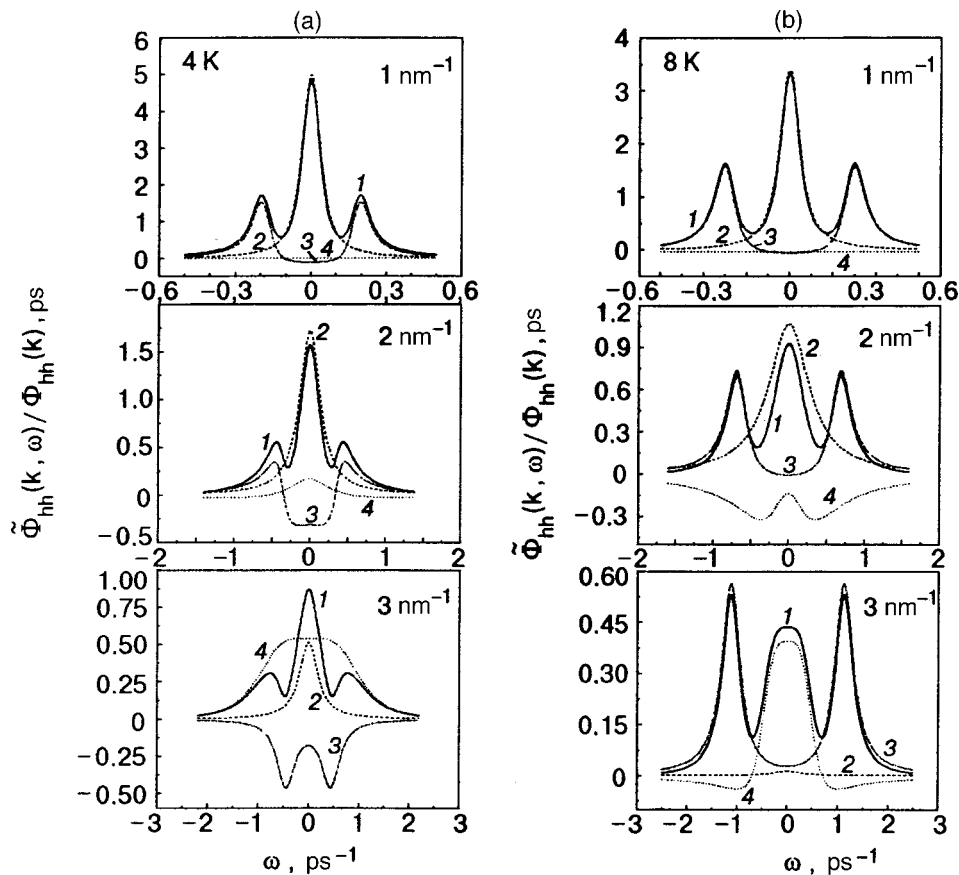


FIG. 2. Normalized time correlation function  $\tilde{\Phi}_{hh}(k, \omega) / \Phi_{hh}(k)$  (curve 1) for  ${}^4\text{He}$  at  $T=4$  K (a) and  $T=8$  K (b) for  $k=1, 2$ , and  $3 \text{ nm}^{-1}$ . Curves 2, 3 and 4 correspond to the contribution to  $\tilde{\Phi}_{hh}(k, \omega) / \Phi_{hh}(k)$  from the thermal, acoustic, and kinetic mode, respectively.

As regards the normalized TCF  $\tilde{\Phi}_{hh}(k, \omega)/\Phi_{hh}(k)$  is concerned, the thermal mode determines the shape of the central peak for small values of  $k$ , the acoustic mode determines the form of the side peaks, while the contribution from kinetic excitations can be disregarded since their weight factor is proportional to  $k^4$ . The situation is identical to the case of  $S_{\text{sym}}(k, \omega)$ .<sup>15</sup> However, in contrast to the result for dynamic structural factor in which the contribution from thermal excitation disappears at  $T=4$  K in the region of  $k=2-3 \text{ nm}^{-1}$ , a decrease in the amplitude of the thermal mode becomes noticeable only for  $k=3 \text{ nm}^{-1}$ , when the shape of the lines  $\tilde{\Phi}_{hh}(k, \omega)/\Phi_{hh}(k)$  is determined equally by all types of excitations. An interesting fact is a sharp decrease of the thermal mode amplitude almost to zero at  $T=8$  K,  $k=3 \text{ nm}^{-1}$ , when the shape of the central resonance is completely determined by kinetic excitation.

The following circumstance is worth noting. The position of the side peak is not always related to the frequency of a certain propagating excitation. In particular, it can be seen clearly from Fig. 2 ( $T=4$  K,  $k=3 \text{ nm}^{-1}$ ) that, since the weight factor for the acoustic mode is negative, the frequency of the acoustic excitation determines the position of the local minimum rather than the peak of the ‘‘enthalpy–enthalpy’’ TCF. Analytically, such a result can be explained by considering the expressions (10) and (11). The extrema of a TCF on the frequency scale are determined by the modes as well as amplitudes of collective excitations. In this example, we can notice the difference between the ‘‘intuitive’’ definition of the collective excitation in terms of the position and shape the extremum of a certain TCF and a more rigorous definition of collective excitations directly as poles of the appropriate Green’s functions. Note that the Fourier transform of the TCF (1) is directly associated with the retarded Green’s correlation functions.<sup>18,22</sup>

Thus, the conclusions drawn by Montfrooij *et al.*<sup>23</sup> that the additional side peak in semiquantum <sup>4</sup>He at  $T=13.3$  K is associated with the thermal wave for intermediate  $k$  is disputable since the ‘‘energy–energy’’ TCF resonance peaks

studied by these authors are determined by a number of factors as mentioned above. Even more astonishing is the statement that the generalized thermal wave is transformed into a normal acoustic wave in the limit  $k \rightarrow 0$ . It is also worthwhile to note that the dispersion of propagator excitations obtained by Montfrooij *et al.*<sup>23</sup> is qualitatively similar to the results obtained in Ref. 15 for  $T=8$  K, i.e., the curve for the kinetic mode lies below the dispersion curve for generalized acoustic excitation. In this context, it should be quite interesting to investigate semiquantum helium at other temperatures in the interval 3–8 K in order to determine unambiguously whether the ‘‘fast sound’’ is an indispensable feature of the low-temperature semiquantum <sup>4</sup>He or is a result of processing of the experimental data only for a certain thermodynamic point.

### 3. SPACE–TIME DISPERSION OF TRANSPORT COEFFICIENTS

Using the method of the nonequilibrium statistical operator (NSO),<sup>18</sup> we can obtain a system of transport equations for Fourier transforms of dynamic variables  $\langle \Delta Y_i(k) \rangle^\omega = \{ \langle \Delta \hat{n}_k \rangle^\omega, \langle \Delta \hat{J}_k \rangle^\omega, \langle \Delta \hat{h}_k \rangle^\omega, \langle \Delta \hat{\pi}_k \rangle^\omega, \langle \Delta \hat{Q}_k \rangle^\omega \}$ , averaged over NSO:

$$i\omega \langle \Delta \hat{Y}(k) \rangle^\omega - i\Omega(k) \langle \Delta \hat{Y}(k) \rangle^\omega + \tilde{\varphi}(k, \omega) \langle \Delta \hat{Y}(k) \rangle^\omega = 0. \tag{14}$$

The structure of this system is reminiscent of the system of equations (2) for TCF. Note that the system of 3 equations constructed on a hydrodynamic basis has an analogous form. In this case, the memory functions  $\tilde{\varphi}_{JJ}(k, \omega)$ ,  $\tilde{\varphi}_{hh}(k, \omega)$  and  $\tilde{\varphi}_{hJ}(k, \omega)$  are no longer equal to zero and define the generalized coefficients of longitudinal viscosity, thermal conductivity, and thermal viscosity, respectively. Solving Eqs. (14) in  $\langle \Delta \hat{\pi}_k \rangle^\omega$  and  $\langle \Delta \hat{Q}_k \rangle^\omega$ , substituting the obtained results into the first three equations of the system and grouping the terms containing  $\langle \Delta \hat{J}_k \rangle^\omega$  and  $\langle \Delta \hat{h}_k \rangle^\omega$ , we arrive at the following recurrent relations for the generalized transport coefficients:<sup>22</sup>

$$(4/3) \eta(k, \omega) + \zeta(k, \omega) = \frac{nm}{k^2} \frac{-i\Omega_{\pi J}(k)}{i\omega + \tilde{\varphi}_{\pi\pi}(k, \omega) - [ -i\Omega_{\pi Q}(k) + \tilde{\varphi}_{\pi Q}(k, \omega) ] [ -i\Omega_{Q\pi}(k) + \tilde{\varphi}_{Q\pi}(k, \omega) ] / [ i\omega + \tilde{\varphi}_{QQ}(k, \Omega) ]} \tag{15}$$

for the generalized longitudinal viscosity, where  $\eta(k, \omega)$  is the generalized shear viscosity and  $\zeta(k, \omega)$  is the generalized bulk viscosity;

$$\lambda(k, \omega) = \frac{nc_V}{k^2} \frac{-i\Omega_{Qh}(k)}{i\omega + \tilde{\varphi}_{QQ}(k, \omega) - [ i\Omega_{\pi Q}(k) + \tilde{\varphi}_{\pi Q}(k, \omega) ] [ -i\Omega_{Q\pi}(k) + \tilde{\varphi}_{Q\pi}(k, \omega) ] / [ i\omega + \tilde{\varphi}_{\pi\pi}(k, \omega) ]} \tag{16}$$

for the generalized thermal conductivity  $\lambda(k, \omega)$ , ( $c_V = (1/k_B T^2) (\hat{h}_k \hat{h}_{-k})_0$  is the generalized specific heat at constant volume), and

$$\xi(k, \omega) = \frac{nm}{k^2} \frac{i\Omega_{\pi J}(k)}{-i\Omega_{\pi Q}(k) + \tilde{\varphi}_{\pi Q}(k, \omega) + (i\omega + \tilde{\varphi}_{\pi\pi})(i\omega + \tilde{\varphi}_{QQ}) / (-i\Omega_{Q\pi}(k) + \tilde{\varphi}_{Q\pi}(k, \omega))} \tag{17}$$

for the generalized thermal viscosity  $\xi(k, \omega)$ .

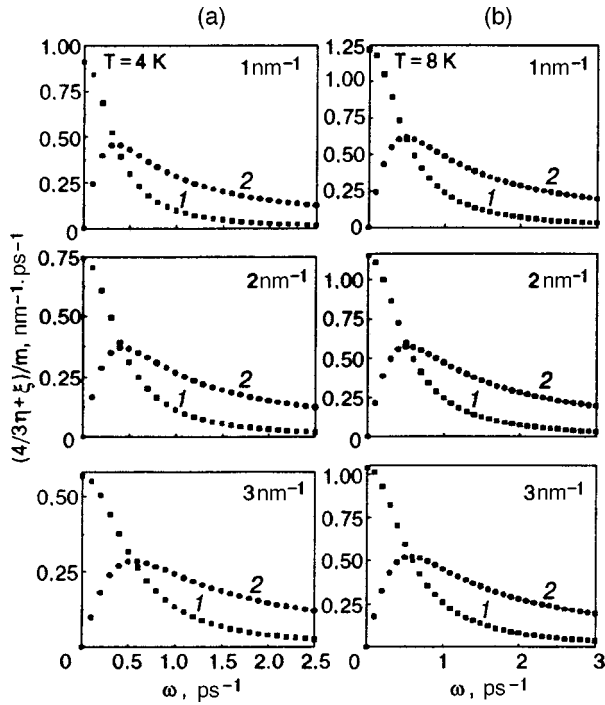


FIG. 3. Real (1) and imaginary (2) parts of the generalized longitudinal viscosity coefficient  $(4/3)\eta(k, \omega) + \zeta(k, \omega)$  for  ${}^4\text{He}$  at  $T=4$  K (a) and  $T=8$  K (b) for  $k=1, 2$ , and  $3 \text{ nm}^{-1}$ .

In these expressions, we have used the Markov approximation (7) for the memory functions. In the denominators of Eqs. (15)–(17), we have confined to terms linear in frequency since the higher-order terms can be disregarded by putting  $\tilde{\varphi}_{ij}(k, \omega) = \tilde{\varphi}_{ij}(k, 0) + o(\omega^2)$ . The spatial dependence is determined completely by nondiagonal elements. Note that the diagonal memory functions  $[\tilde{\varphi}_{\pi\pi}(k, 0) = \tilde{\varphi}(0, 0) + o(k^2)]$ , also give the same order in  $k$ . However, in this case we must analyze their spatial dispersion in greater detail. From the point of view of the approach used by us, this corresponds to the introduction of two additional fitting parameters. We took into account such a dependence on  $k$  through nondiagonal memory functions.

Analyzing the structure of Eqs. (15)–(17), it can be noted easily that the generalized transport coefficients also have the Lorentz form [cf. Eq. (10)]. In particular, putting  $-i\Omega_{\pi Q}(k) + \tilde{\varphi}_{\pi Q}(k, 0) = -ikT_{\pi Q}$ ,  $-i\Omega_{Q\pi}(k) + \tilde{\varphi}_{Q\pi}(k, 0) = -ikT_{Q\pi}$  and  $i\Omega_{Qh}(k) = k^2\omega_{Qh}$  for small values of the wave vector, we can write for the real part of  $\lambda(k, \omega)$

$$\text{Re } \lambda(k, \omega) = \frac{\lambda(k)}{[\omega\tau_{hh}(k)]^2 + 1}, \quad \lambda(k) = \frac{\lambda(0,0)}{(L_{hh}k)^2 + 1}, \quad (18)$$

where

$$\tau_{hh}(k) = \left( \tilde{\varphi}_{QQ}(0,0) + \frac{k^2 T_{\pi Q} T_{Q\pi}}{\tilde{\varphi}_{\pi\pi}(0,0)} \right)^{-1},$$

$$L_{hh} = \left( \frac{T_{\pi Q} T_{Q\pi}}{\tilde{\varphi}_{\pi\pi}(0,0)} \right)^{1/2}, \quad \lambda(0,0) = n c_V \omega_{Qh} \tau_{hh}(0). \quad (19)$$

The results of calculations of the generalized transport coefficients are shown in Figs. 3, 4 and 5. It can be seen that

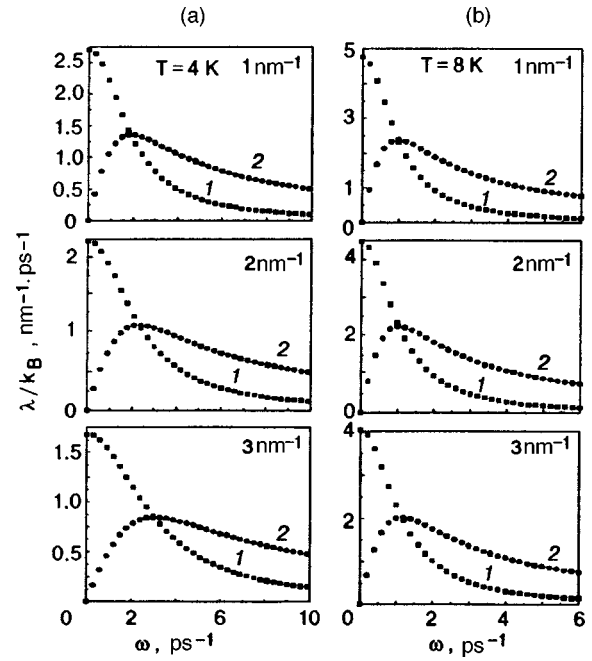


FIG. 4. Real (1) and imaginary (2) parts of the generalized thermal conductivity  $\lambda(k, \omega)$  for  ${}^4\text{He}$  at  $T=4$  K (a) and  $T=8$  K (b) for  $k=1, 2$ , and  $3 \text{ nm}^{-1}$ .

the coefficient of thermal viscosity has ‘‘inverse’’ parity relative to the diagonal transport coefficients: for  $\omega=0$ , only the imaginary part is nonzero, while in the limit  $k \rightarrow 0$  it tends to zero in complete accord with the Curie principle.<sup>18</sup> Moreover, the value of this coefficient is an order of magnitude smaller than the generalized thermal conductivity.

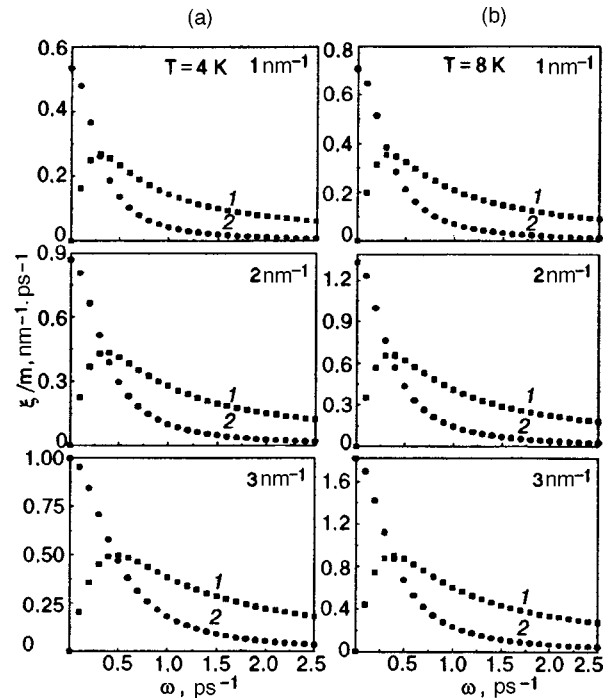


FIG. 5. Real (1) and imaginary (2) parts of the generalized thermal viscosity coefficient  $\xi(k, \omega)$  for  ${}^4\text{He}$  at  $T=4$  K (a) and  $T=8$  K (b) for  $k=1, 2$ , and  $3 \text{ nm}^{-1}$ .

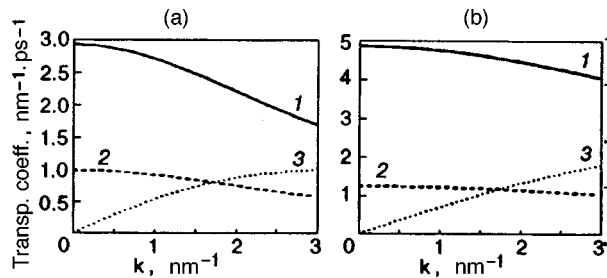


FIG. 6. Generalized coefficients of thermal conductivity  $\lambda(k,0)$  (curve 1), longitudinal viscosity  $(4/3)\eta(k,0) + \zeta(k,0)$  (curve 2), and thermal viscosity  $\xi(k,0)$  (curve 3) for  ${}^4\text{He}$  at  $T=4$  K (a) and  $T=8$  K (b).

Figure 6 shows the spatial dispersion of the generalized transport coefficients. The dependence (18) is observed for the diagonal coefficients, while  $\xi(k, \omega=0)$  increases in proportion to  $k$  in the region of small wave numbers. In the limit  $k \rightarrow 0$ , we can disregard the thermal viscosity coefficient  $\xi(k, \omega=0)$ . However, it increases quite rapidly in the region of intermediate  $k$ , which leads to an additional dynamic interaction between elastic and thermal processes. Conventional hydrodynamics contains only static interaction proportional to the thermal expansion coefficient  $\alpha$ .

## 5. CONCLUSION

In this work, we have used the 5-variable thermal viscosity model to analyze the behavior of the ‘‘momentum–momentum’’ and ‘‘enthalpy–enthalpy’’ TCF for semiquantum  ${}^4\text{He}$  at  $T=4$  and 8 K in the quasihydrodynamic limit taking into account the partial contributions of all collective excitations. The ‘‘momentum–momentum’’ TCF is directly connected with the dynamic structural factor measured in neutron scattering experiment. The results for the ‘‘enthalpy–enthalpy’’ TCF can be obtained from computer simulation.

An important problem concerns the study of transport processes. In the general case, the transport equations are nonlocal, hence it becomes necessary to calculate the space–time dispersion of the transport coefficients. In this work, the  $(k, \omega)$ -dependent coefficients were obtained from the recurrent relations by successive elimination of fast (kinetic) variables.

In order to interpret the experimental data for the intermediate values of the wave vector, we must take into consideration the spatial dispersion of collective modes defining the position and width of the TCF resonances, as well as eigenvectors in the spectral problem characterizing the resonance amplitudes. Only such a complex analysis makes it possible to determine the origin of collective excitations in semiquantum liquids.

The analysis presented here does not claim to be exact or comprehensive since the authors do not have any information about the spatial dispersion of SCF. This information is usually obtained from molecular dynamic computations.<sup>13</sup> Such an analysis becomes more complicated in the quantum case<sup>24</sup> since computer techniques for calculating higher-order SCF have not been developed to such an extent. However,

the description of semiquantum objects can be carried out successfully by using the computer-adapted theories developed for various classical liquids.<sup>4,5,13</sup>

This research was financed partially by the Fonds zur Forderung der wissenschaftlichen Forschung (Austria), Project P12423 TPH (I.M.M.). One of the authors (V.V.I.) wishes to thank the President of Ukraine for granting a stipend for young scientists.

\*E-mail: ignat@icmp.lviv.ua

<sup>1</sup>We shall also use the notation TCF for Fourier and Laplace transforms of the corresponding time-correlation functions.

- <sup>1</sup>J. R. D. Copley and S. W. Lovesey, *Rep. Prog. Phys.* **38**, 461 (1975).
- <sup>2</sup>J. P. Boon and S. Yip, *Molecular Hydrodynamics* McGraw-Hill, New York (1980).
- <sup>3</sup>N. H. March and M. P. Tosi, *Atomic Dynamics in Liquids*, Macmillan Press, London (1976).
- <sup>4</sup>T. M. Bryk, I. M. Mryglod, and G. Kahl, *Phys. Rev. E* **56**, 2903 (1997).
- <sup>5</sup>I. P. Omelyan, *Physica A* **247**, 121 (1997).
- <sup>6</sup>D. L. Price, in *The Physics of Liquid and Solid Helium* [Ed. by J. B. Ketterson and K. H. Bennemann], Wiley Interscience, New York (1978).
- <sup>7</sup>H. R. Glyde, *Excitations in Liquid and Solid Helium*, Clarendon Press, Oxford (1994).
- <sup>8</sup>S. W. Lovesey, *Theory of Neutron Scattering from Condensed Matter*, Clarendon Press, Oxford (1984).
- <sup>9</sup>A. F. Andreev, *Pis'ma Zh. Éksp. Teor. Fiz.* **28**, 603 (1978) [*JETP Lett.* **28**, 556 (1978)].
- <sup>10</sup>L. L. Buishvili and A. I. Tugushi, *Zh. Éksp. Teor. Fiz.* **84**, 970 (1983) [*Sov. Phys. JETP* **57**, 563 (1983)].
- <sup>11</sup>Yu. A. Tserkovnikov, *Teor. Mat. Fiz.* **93**, 412 (1992).
- <sup>12</sup>D. N. Zubarev and Yu. A. Tserkovnikov, *Proc. Steklov Inst. Math.* **2**, 139 (1988).
- <sup>13</sup>I. M. Mryglod, I. P. Omelyan, and M. V. Tokarchuk, *Mol. Phys.* **84**, 235 (1995).
- <sup>14</sup>I. M. de Schepper, E. G. D. Cohen, C. Bruin *et al.*, *Phys. Rev. A* **38**, 271 (1988).
- <sup>15</sup>V. V. Ignatyuk, I. M. Mryglod, and M. V. Tokarchuk, *Fiz. Nizk. Temp.* **25**, 407 (1999) [*Low Temp. Phys.* **25**, 295 (1999)].
- <sup>16</sup>R. M. Crevecoeur, R. Verberg, I. M. de Schepper *et al.*, *Phys. Rev. Lett.* **74**, 5052 (1995).
- <sup>17</sup>R. M. Crevecoeur, H. E. Smorenburg, and I. M. de Schepper, *J. Low Temp. Phys.* **105**, 149 (1996).
- <sup>18</sup>D. Zubarev, V. Morozov, and G. Röpke, *Statistical Mechanics of Non-equilibrium Processes* Vol. 2, Relaxation and Hydrodynamic Processes, Akademie Verlag, Berlin (1996).
- <sup>19</sup>V. V. Ignatyuk, I. M. Mryglod, and M. V. Tokarchuk, Preprint ICMP-98-08E, Lviv (1998).
- <sup>20</sup>R. Zwanzig, *Lectures in Theoretical Physics*, Interscience, New York (1961).
- <sup>21</sup>I. M. Mryglod, *Ukr. Fiz. Zh. (Russ. Ed.)* **43**, 252 (1998).
- <sup>22</sup>I. M. Mryglod and A. M. Hachkevych, *Chin. Phys.* **5**, 105 (1995).
- <sup>23</sup>W. Montfrooij, L. A. de Graaf, and I. M. de Schepper, *Phys. Rev. B* **45**, 3111 (1992).
- <sup>24</sup>M. C. Payne, M. P. Teter, D. C. Allan *et al.*, *Rev. Mod. Phys.* **64**, 1045 (1992).

## SUPERCONDUCTIVITY, HIGH-TEMPERATURE SUPERCONDUCTIVITY

### On the self-consistent theory of Josephson effect in ballistic superconducting microconstrictions

M. Zareyan

*Institute for Advanced Studies in Basic Sciences, 45195-159, Gave Zang, Zanjan, Iran*

Yu. A. Kolesnichenko and A. N. Omelyanchouk

*B. Verkin Institute for Low-Temperature Physics and Engineering, National Academy of Sciences of Ukraine, 47 Lenin Ave., 310164 Kharkov, Ukraine\**

*Fiz. Nizk. Temp.* **25**, 1154–1160 (November 1999)

The microscopic theory of current-carrying states in the ballistic superconducting microchannel is presented. The effects of the contact length  $L$  on the Josephson current are investigated. For the temperatures  $T$  close to the critical temperature  $T_c$  the problem is treated self-consistently, with allowance for the distribution of the order parameter  $\Delta(\mathbf{r})$  inside the contact. The closed integral equation for  $\Delta$  in strongly inhomogeneous microcontact geometry ( $L \lesssim \xi_0$ , where  $\xi_0$  is the coherence length at  $T=0$ ) replaces the differential Ginzburg–Landau equation. The critical current  $I_c(L)$  is expressed in terms of the solution of this integral equation. The limiting cases of  $L \ll \xi_0$  and  $L \gg \xi_0$  are considered. With increasing length  $L$ , the critical current decreases, although the ballistic Sharvin resistance of the contact remains the same as at  $L=0$ . For ultrashort channels with  $L \lesssim a_D$  ( $a_D \sim v_F/\omega_D$ , where  $\omega_D$  is the Debye frequency) the corrections for the value of the critical current  $I_c(L=0)$  are sensitive to the strong-coupling effects. © 1999 American Institute of Physics. [S1063-777X(99)00311-4]

#### 1. INTRODUCTION

Weak superconducting links<sup>1</sup> include the tunnel structures *SIS* (superconductor–insulator–superconductor) and the contacts with direct conductivity, *SNS* ( $N$  is the normal layer) and *ScS* ( $c$  is a geometrical constriction). Superconducting constrictions can be modeled as an orifice with diameter  $d$  in an impenetrable sheet for electrons between two superconducting half spaces (point contact) or as a narrow channel with length  $L$  in contact with superconducting banks (microbridge). Aslamazov and Larkin<sup>2</sup> have shown on the basis of a solution of the Ginzburg–Landau (GL) equations that in the dirty limit and for small sizes of the constriction  $L$ ,  $d \ll \xi(T)$  [ $\xi(T)$  is the GL coherence length] the *ScS* contact can be described by a Josephson model with the current-phase relation

$$I = I_c \sin \varphi, \quad I_c = \pi \Delta_0^2(T) / (4eR_N T_c), \quad (1)$$

where  $I_c$  is the Josephson critical current,  $\Delta_0$  is the absolute value of the order parameter in the bulk banks,  $T_c$  is the critical temperature, and  $R_N$  is the normal-state resistance of the dirty microbridge. The critical current of the microbridge (1) depends on the bridge length as  $I_c \sim 1/L$ . The expression (1) is valid within the domain of applicability of the GL approach, i.e., for temperatures  $T$  close to  $T_c$  and  $L$ ,  $d \gg \xi_0$  ( $\xi_0 \approx v_F/T_c$  is the coherence length at  $T=0$ , and  $v_F$  is the Fermi velocity).

The present level of technology has made it possible to study the ultrasmall Josephson weak links with the

dimensions up to interatomic size. For example, they can be nanosize microchannels produced by means of a scanning tunneling microscope<sup>3</sup> or point contacts and microchannels obtained by using the mechanical, controllable, break technique.<sup>4–6</sup> The microchannels between two superconductors can also arise spontaneously as microshorts in tunnel junctions,<sup>7</sup> with the length  $L$  determined by the thickness of an insulator layer. The value of the critical current  $I_c$  of such microshorts is of special interest in the case of tunnel structures based on high- $T_c$  metal-oxide compounds. Small microconstrictions with dimensions of the order or smaller than the coherence length  $\xi_0$ , when the expression (1) for the critical current  $I_c \sim 1/L$  is not valid, require the microscopic consideration even for  $T$  near  $T_c$ . Such microscopic theory of stationary Josephson effect in microconstrictions was developed in Ref. 8 for the ballistic channel of zero length,  $L=0$ , in the model of the orifice with diameter  $d \ll \xi_0$ . The Josephson current in this case is given by

$$I = \frac{\pi \Delta_0(T)}{eR_0} \sin \frac{\varphi}{2} \tanh \frac{\Delta_0(T) \cos(\varphi/2)}{2T}, \quad (2)$$

$$-\pi < \varphi < \pi,$$

$$R_0^{-1} = \frac{1}{2} S e^2 v_F N(0), \quad (3)$$

where  $S = \pi d^2/4$  is the contact cross-sectional area, and  $N(0) = mp_F/(2\pi^2)$  is electron density of states at the Fermi surface. At temperatures  $T_c - T \ll T_c$  expression (2) coincides

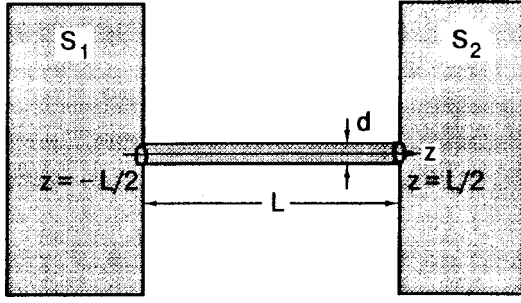


FIG. 1. Model of  $ScS$  contact as narrow superconducting channel is in contact with bulk superconductors  $S_1$  and  $S_2$ .

with the Aslamazov–Larkin result [Eq. (1)], in which instead of the normal resistance  $R_N$  for dirty metal, the ballistic Sharvin resistance<sup>9</sup>  $R_0$  (3) is substituted.

In this article we present a microscopic theory of current-carrying states in the ballistic microbridges of arbitrary length  $L$  in the scale of the coherence length  $\xi_0$ . We have investigated the dependence of the Josephson critical current on the ratio  $L/\xi_0$  and analyzed the transition from the case of  $I_c(L=0)$  [Eq. (2)] to  $I_c \sim 1/L$  [Eq. (1)] with increasing length  $L$ .

In Sec. 2 we formulate the model of a microbridge and the microscopic equations for Green's functions with boundary conditions at the bridge edges. In studying the effects on the critical current of the length of the microconstriction, the crucial point, as always, in the inhomogeneous superconducting state is the self-consistent treatment of the order parameter distribution  $\Delta(\mathbf{r})$  inside the weak link. In Sec. 3 the closed integral equation for the order parameter  $\Delta$  in the microchannel is derived for temperatures near  $T_c$ , which in a strongly inhomogeneous ( $L \sim \xi_0$ ) microcontact geometry replaces the differential GL equation. The critical current  $I_c(L)$  is expressed in terms of the solution of this integral equation. The limiting cases of  $L \ll \xi_0$  and  $L \gg \xi_0$  are considered. We will show that in addition to the characteristic scale  $\xi_0$ , there is the length  $a_D \approx v_F/\omega_D$  ( $\omega_D$  is the Debye frequency) in the case of an ultrasmall channel. The length  $L \sim a_D$  is the length at which the frequency of the ballistic flight of an electron from one bank to another becomes comparable with the frequency  $\omega_D$ , which characterizes the retardation of the electron-phonon interaction. In conventional superconductors the value of the coherence length  $\xi_0$ , about  $10^{-4}$  cm, is much larger than  $a_D \sim 100$  Å. In high- $T_c$  metal-oxide compounds, however, we have a situation in which  $\xi_0$  is comparable with  $a_D$ . Thus, in high- $T_c$  compounds the critical current of the contact with dimensions  $\sim a_D \sim \xi_0$  is sensitive to the effects of strong coupling.

## 2. MODEL AND BASIC EQUATIONS

We consider the model of a contact in the form of a filament (narrow channel) that joins two superconducting half-spaces (massive banks) (Fig. 1). The length  $L$  and the diameter  $d$  of the channel are assumed to be large as compared with the Fermi wavelength  $\lambda_F$ , so we can apply

the quasi-classical approximation. In the ballistic case, we proceed from the quasi-classical Eilenberger equation for the energy-integrated Green's function:<sup>10</sup>

$$\mathbf{v}_F \frac{\partial \hat{G}}{\partial \mathbf{r}} + [\omega \hat{\tau}_3 + \hat{\Delta}, \hat{G}] = 0, \quad (4)$$

where

$$G(\omega, \mathbf{v}_F, \mathbf{r}) = \begin{pmatrix} g_\omega & f_\omega \\ f_\omega^+ & -g_\omega \end{pmatrix}$$

is the matrix Green's function which depends on the Matsubara frequency  $\omega$ , the electron velocity on the Fermi surface  $\mathbf{v}_F$ , and the spatial variable  $\mathbf{r}$ ;

$$\hat{\Delta}(\mathbf{r}) = \begin{pmatrix} 0 & \Delta \\ \Delta^* & 0 \end{pmatrix}$$

is the superconducting pair potential;  $\hat{\tau}_i$  ( $i=1,2,3$ ) are Pauli matrices. Equation for the matrix Green's function (4) is supplemented by the normalization condition<sup>11</sup>

$$\hat{G}^2 = 1. \quad (5)$$

The off-diagonal potential  $\Delta(\mathbf{r})$  must be determined from the self-consistency equation

$$\Delta(\mathbf{r}) = \lambda 2\pi T \sum_{\omega>0} \langle f \rangle, \quad (6)$$

in which  $\langle \dots \rangle$  stands for averaging over directions of  $\mathbf{v}_F$  on the Fermi surface, and  $\lambda$  is the electron-phonon coupling constant. In the BCS model the summation over  $\omega$  contains the cutoff on the frequency  $\omega_D$ , which is of the order of the Debye frequency.

The equations (4) and (6) are supplemented by the values of the Green's functions and  $\Delta$  in the bulk superconductors  $S_1$  and  $S_2$  far from the channel ends:

$$\hat{G}_{1,2} = \frac{\omega \hat{\tau}_3 + \hat{\Delta}_{1,2}}{\Omega}, \quad (7)$$

$$\hat{\Delta}_{1,2} = \Delta_0 (\cos(\varphi/2) \hat{\tau}_1 \pm \sin(\varphi/2) \hat{\tau}_2).$$

Thus the phase  $\varphi$  is the total phase difference at the contact. We also must determine the boundary conditions concerning the reflection of the electrons from the surface of the superconductors  $\mathbf{r}_S$ . For simplicity we assume that at  $\mathbf{r}_S$  electrons undergo the specular reflection. Then for quasiclassical Green's function we have the boundary condition (Ref. 8)

$$G(\mathbf{v}_F, \mathbf{r}_S) = G(\mathbf{v}'_F, \mathbf{r}_S), \quad (8)$$

in which  $\mathbf{v}_F$  and  $\mathbf{v}'_F$  are the velocities of the incident and specular reflected electron. These velocities are related by the conditions, which conserve the component of  $\mathbf{v}_F$  parallel to the reflecting surface  $\mathbf{r}_S$  and changes the sign of the normal component.

The solutions of Eqs. (4) and (6) allow us to calculate the current density  $\mathbf{j}$ :

$$\mathbf{j}(r) = -4i\pi e N(0) T \sum_{\omega>0} \langle \mathbf{v}_F g_\omega \rangle. \quad (9)$$

In the case of the microconstriction shown in Fig. 1, under the conditions  $d \ll \xi_0$  and  $L \gg d$  ( $d$  is the contact diameter) inside the filament we can solve the one-dimensional Eilenberger equations with  $\Delta = \Delta(z)$ . The banks of the bridge are equivalent here to certain boundary conditions for the Green's function  $\hat{G}(v_z, z)$  at the points  $z = \pm L/2$ . Following the procedure which was described in Ref. 8, we find the Green's functions at the end points ( $z = \pm L/2$ ) from the general solutions of Eq. (4) in superconducting half-spaces  $S_1$  and  $S_2$  with conditions (5). They are given by

$$\begin{aligned} \hat{G}(z = \mp L/2) = & \hat{G}_{1,2} + A_{1,2} [\Delta_0 \hat{\tau}_3 - [\omega \cos(\varphi/2) \\ & + i \eta \Omega \sin(\varphi/2)] \hat{\tau}_1 \mp [\omega \sin(\varphi/2) \\ & - i \eta \Omega \cos(\varphi/2)] \hat{\tau}_2, \end{aligned} \quad (10)$$

where  $\Omega = \sqrt{\omega^2 + \Delta_0^2}$ , and  $\eta = \text{sign}(v_z)$ . The arbitrary constants  $A_{1,2}$  must be determined by matching these boundary conditions with the solution for  $\hat{G}(v_z, z)$  inside the channel.

Using the off-diagonal components in Eq. (4), we have the following first-order differential equations for the anomalous Green's functions:

$$\begin{aligned} v_z \frac{df_\omega}{dz} + 2\omega f_\omega = 2\Delta(z) g_\omega, \\ -v_z \frac{df_\omega^+}{dz} + 2\omega f_\omega^+ = 2\Delta^*(z) g_\omega. \end{aligned} \quad (11)$$

The normal Green's function  $g_\omega$ , as follows from condition (5), is expressed in terms of  $f_\omega$  and  $f_\omega^+$ :

$$g_\omega = \sqrt{1 - f_\omega f_\omega^+}. \quad (12)$$

From Eqs. (6), (9), (11), and (12) we obtain the symmetry relations

$$f_\omega^+(v_z, z) = [f_\omega(-v_z, z)]^*, \quad \Delta^*(z) = \Delta(-z) \quad (13)$$

and the current conservation inside the channel  $dj/dz = 0$ .

### 3. JOSEPHSON CURRENT AND ORDER PARAMETER DISTRIBUTION IN SUPERCONDUCTING MICROCHANNEL

In the present paper we consider the case of temperatures  $T$  close to the critical temperature  $T_c$ . Near the phase-transition curve the order parameter  $\Delta_0(T)$  in the banks is small. In order to find the Josephson current in the lowest order in  $\Delta_0$  we linearize Eqs. (11) for  $\Delta$  and obtain  $f_\omega \sim \Delta_0(T)$ ,  $g_\omega \sim 1 - 1/2 f_\omega f_\omega^+ \sim 1 - O(\Delta_0^2)$ ,  $j \sim \Delta_0^2$ . The equation for  $f_\omega$  near  $T_c$  takes the form

$$v_z \frac{df_\omega}{dz} + 2\omega f_\omega = 2\Delta(z), \quad (14)$$

with linearized boundary conditions (10)

$$\begin{aligned} f_\omega(v_z > 0, z = -L/2) = \frac{\Delta_0}{\omega} e^{-i\varphi/2}, \\ f_\omega(v_z < 0, z = +L/2) = \frac{\Delta_0}{\omega} e^{+i\varphi/2}. \end{aligned} \quad (15)$$

Its solution for arbitrary function  $\Delta(z)$  is given by

$$\begin{aligned} f_\omega(v_z, z) = \frac{\Delta_0}{\omega} e^{-i\eta\varphi/2} e^{-(2\omega/v_z)(z + \eta L/2)} \\ + e^{-2\omega z/v_z} \int_{-\eta L/2}^z dz' \frac{2\Delta(z')}{v_z} e^{2\omega z'/v_z}. \end{aligned} \quad (16)$$

The Green's function  $f_\omega^+(v_z, z)$  is obtained from expression (14) with the help of relations (15).

Substituting the function  $f_\omega(v_z, z)$  (16) in the self-consistency equation (6), we obtain the integral equation for the space-dependent order parameter inside the contact

$$\Delta(z) = A(z) + \int_{-L/2}^{L/2} dz' \Delta(z') K(|z - z'|), \quad (17)$$

where

$$A(z) = \lambda 2 \pi T \sum_{\omega > 0} \frac{\Delta_0}{\omega} \left\langle e^{-\omega L/v_z} \cosh\left(\frac{2\omega z}{v_z} + i\frac{\varphi}{2}\right) \right\rangle_{v_z > 0}, \quad (18)$$

$$K(z) = \lambda 2 \pi T \sum_{\omega > 0} \left\langle \frac{1}{v_z} e^{-2\omega z/v_z} \right\rangle_{v_z > 0}. \quad (19)$$

The averaging  $\langle \dots \rangle_{v_z > 0}$  denotes

$$\langle F(v_z = v_F \cos \theta) \rangle_{v_z > 0} = \int_0^1 d(\cos \theta) F(\cos \theta).$$

In the case of strongly inhomogeneous microcontact problem the integral equation for the order parameter  $\Delta$  replaces the differential Ginzburg–Landau equation. It contains the needed boundary conditions at the points of contact between the filament and the bulk superconductors. Some general properties of the solution  $\Delta(z)$  of Eq. (17) follow from the form of the functions (18) and (19). Let us write  $\Delta(z)$  in the form

$$\Delta(z) = \Delta_0(T) \left( \cos \frac{\varphi}{2} + iq(z) \sin \frac{\varphi}{2} \right) \quad (20)$$

and substitute it in Eq. (17). For the function  $q(z)$  we obtain the equation

$$q(z) = b(z) + \int_{-L/2}^{L/2} dz' q(z') K(|z - z'|), \quad (21)$$

with  $K(z)$  defined by (19) and the new out-integral function  $b(z)$ ,

$$b(z) = \lambda 2 \pi T \sum_{\omega > 0} \frac{1}{\omega} \left\langle e^{-\omega L/v_z} \sinh\left(\frac{2\omega z}{v_z}\right) \right\rangle_{v_z > 0}. \quad (22)$$

In obtaining Eq. (21) we have used the relation

$$\lambda 2 \pi T \sum_{\omega > 0} \frac{1}{\omega} = 1, \quad \text{for } T \rightarrow T_c. \quad (23)$$

It follows from (19), (21), and (22) that the function  $q(z)$  has such properties:

- i) the function  $q(z)$  is real,
- ii)  $q(z)$  does not depend on the phase  $\varphi$ ,
- iii)  $q(-z) = -q(z)$ ,  $q(0) = 0$ .

Thus, the value of the order parameter  $\Delta$  at the center of the contact always is equal to  $\Delta_0(T)\cos(\varphi/2)$ . Also, the universal phase dependence of  $\Delta(z, \varphi)$ , which is determined by (20) and i)–iii), leads (see below) to the sinusoidal current-phase dependence  $j = j_c \sin \varphi$ . It is emphasized that these general properties of the ballistic microchannel [within the considered case of “rigid” boundary conditions (10) and temperatures close to  $T_c$ ] *does not depend* on the contact length  $L$ , in particular, on the ratio of  $L/\xi_0$ .

Now we are going to obtain the Josephson current in the system. To calculate the total current  $I = Sj$  that flows through the channel at the given phase difference  $\varphi$ , we use the equation for the current density (9) and the anomalous Green’s function  $f_\omega$  (16) obtained above. The normal Green’s function  $q_\omega$  (12) in the second order in  $\Delta_0(T)$  is  $g_\omega(v_z, z) = 1 - 1/2 f_\omega(v_z, z)[f_\omega(-v_z, z)]^*$ . It is convenient to calculate the current density at the point  $z = 0$ . Using the expression for  $\Delta(z)$  (20), we obtain the general formula for the Josephson current  $I(\varphi)$  in terms of the function  $q(z)$ :

$$I(\varphi) = I_c \sin \varphi, \tag{24}$$

$$I_c = I_0 \frac{16T^2}{v_F} \sum_{\omega > 0} \left[ \frac{1}{\omega^2} \langle v_z e^{-\omega L/v_z} \rangle_{v_z > 0} + \frac{2}{\omega} \int_0^{L/2} dz q(z) \langle e^{-2\omega z/v_z} \rangle_{v_z > 0} \right]. \tag{25}$$

Here  $I_0 = \pi \Delta_0^2(T)/(4eR_0T_c)$  is the critical current at  $L = 0$ . It coincides with the result of Ref. 8 for the orifice (2) at  $T$  near  $T_c$ . Expression (25) jointly with Eq. (21) for  $q(z)$  describes the dependence of the critical current on the contact length  $I_c(L)$ . It is valid for arbitrary value of the ratio  $L/\xi_0$ . Note that in our case  $T \rightarrow T_c$ , we have the relation  $\xi_0, L \ll \xi(T)$ .

Let us introduce the dimensionless quantities

$$x = z/L, \quad l = \frac{\pi T_c L}{v_F}, \quad \frac{\omega}{\pi T_c} = 2n + 1, \quad J_c = \frac{I_c}{I_0}. \tag{26}$$

In reduced units (26), after taking the average  $\langle \dots \rangle_{v_z > 0}$ , the equations for  $q(x)$  and  $J_c$  take the form

$$q(x) = b(x) + l \int_{-1/2}^{1/2} dx' q(x') K(|x - x'|), \tag{27}$$

$$J_c = \frac{8}{\pi^2} \sum_{n=0}^N \left\{ \frac{\exp[-l(2n+1)][1-l(2n+1)]}{(2n+1)} - l^2 Ei[-l(2n+1)] + 4l \int_0^{1/2} dx q(x) \frac{\exp[-2l(2n+1)x]}{(2n+1)} + 2lx Ei[-2l(2n+1)x] \right\}, \tag{28}$$

where

$$b(x) = \lambda \sum_{n=0}^N \left\{ \frac{2 \exp[-l(2n+1)] \sinh[2l(2n+1)x]}{(2n+1)} + l(2n+1)(1-2x) Ei[-l(2n+1)(1-2x)] + l(2n+1)(1+2x) Ei[-l(2n+1)(1+2x)] \right\}, \tag{29}$$

$$K(x) = -2\lambda \sum_{n=0}^N Ei[-2l(2n+1)x]. \tag{30}$$

The function  $Ei(x) = \int_{-\infty}^x [(\exp t)/t] dt$  is the integral exponential. The upper limit  $N$  in the sums over  $n$  is related to the cutoff frequency  $\omega_D$  in the BCS model,  $N \approx \omega_D/T_c$ . The value of the coupling constant  $\lambda$  is related to  $N$  by Eq. (23) or, in reduced units,

$$2\lambda \sum_{n=0}^N \frac{1}{(2n+1)} = 1.$$

In the weak-coupling limit of  $\lambda \ll 1$ , we have  $N \gg 1$ .

In the general case of the arbitrary value of the parameter  $l$  ( $l \approx L/\xi_0$ ) Eq. (27) is a convenient starting point for the numerical calculation of the function  $J_c(l)$ . We consider here two limiting cases,  $l \gg 1$  and  $l \ll 1$ .

For a long microbridge with  $l \gg 1$  we seek a solution of Eq. (27) in the form  $q(x) = \alpha x$ . Substituting this  $q(x)$  in Eq. (27), we find  $\alpha = 2 + O(1/l)$ . Calculating  $J_c$  (28) with  $q(x) = 2x$ , we find that the order parameter and the critical current are

$$\Delta(z) = \Delta_0 \left( \cos \frac{\varphi}{2} + i \frac{2z}{L} \sin \frac{\varphi}{2} \right), \quad L \gg \xi_0, \tag{31}$$

$$I_c(L) = \frac{14}{3\pi^2} \zeta(3) I_0 \frac{\hbar v_F}{T_c L}, \quad L \gg \xi_0. \tag{32}$$

Expressions (31) and (32) coincide with the solution of GL equations (with effective boundary conditions for the order parameter  $\Delta$ ) for the clean superconducting microbridge.<sup>12</sup> Thus, our microscopic approach with the boundary conditions (10) for the Green’s functions (not for  $\Delta$ ) gives the results of the phenomenological theory at  $L \gg \xi_0$ .

For a short microbridge with  $l \ll 1$ , in zero approximation on  $l$  we find that  $q(x) = 0$  [ $\Delta(z) = \Delta_0 \cos(\varphi/2)$ ],  $J_c = 1$  or, in dimension units,  $I_c(0) = I_0$ , in agreement with formula (2). The corrections for the zero approximation depend on the value of the product  $lN$ . For very small  $l \ll T_c/\omega_D$  (i.e.,  $L \ll a_D \approx v_F/\omega_D$ ), the product  $lN$  is small, although  $N \gg 1$ . As a result, when  $q(x, l)$  and  $J_c(l)$  are calculated in the region  $L < a_D$ , the cutoff in the sums over  $n$  must be taken into account. Apparently, when the cutoff frequency appears explicitly but not through the value of  $T_c$ , the applicability of the BCS theory becomes questionable. More rigorous consideration, based on the Eliashberg theory of superconductivity,<sup>13</sup> is needed in this case. Nevertheless, by using the BCS model with cutoff frequency we assume qualitatively to take into account the retardation effects of electron-

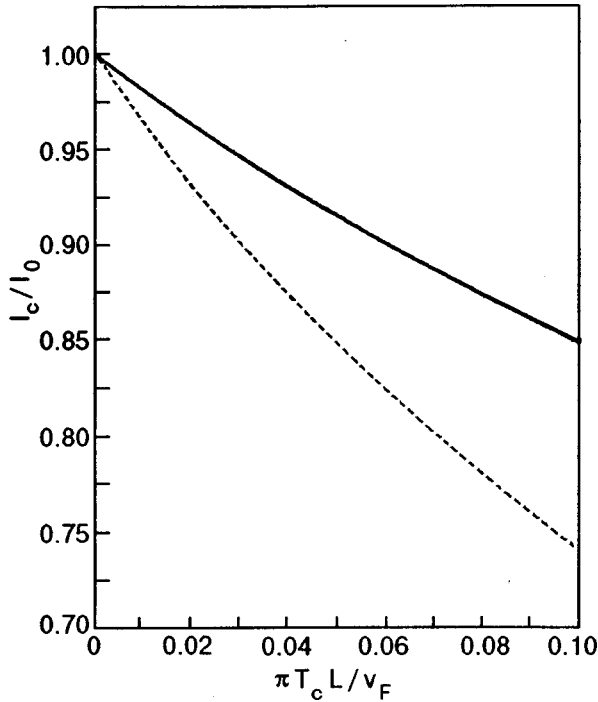


FIG. 2. Dependence of the critical current  $I_c$  on the contact length  $L$  for the microbridge (solid line). The coupling constant  $\lambda = 0.2$ . For comparison, the dependence  $I_c(L)$  for SNS contact ( $\lambda = 0$  inside the channel) is shown (dashed line).

phonon coupling in our problem. In the domain which is defined by the following inequalities:  $IN \ll 1$ ,  $N \gg 1$ ,  $l \ll 1$ , the functions  $b(x)$  (29) and  $K(x)$  (30) have the asymptotic behavior:

$$b(x) = 4\lambda IN \left\{ x \ln(IN) + x(C + \ln 2) + \frac{1}{4} \left[ \ln \left( \frac{1+2x}{1-2x} \right) + 2x \ln(1-4x^2) \right] \right\}, \quad (33)$$

$$K(|x|) = -2\lambda N [\ln(2IN|x|) - 1], \quad (34)$$

where  $C \approx 0.577$  is the Euler constant. As follows from Eqs. (33) and (34), in this case the integral term in Eq. (27) is small, and calculating the critical current in the first approximation on the small parameter  $IN$ , we set  $q(x) = b(x)$ . As a result, we have

$$\Delta(z) = \Delta_0(T) \left( \cos \frac{\varphi}{2} + ib(z/L) \sin \frac{\varphi}{2} \right), \quad L \ll a_D, \quad (35)$$

where  $b(x)$  is defined by expression (33),

$$I_c(L) = I_0 \left( 1 - \frac{8}{\pi\lambda} \frac{T_c L}{v_F} \right), \quad L \ll a_D. \quad (36)$$

In the region  $\{l \ll 1 \text{ and } IN \ll 1\}$  the integral term in Eq. (27) is numerically small as compared with the out-integral term  $b(x)$ . Using in Eq. (27) the  $q(x) = b(x)$  as a rough approximation, we calculate the function  $J_c(l)$  shown in Fig. 2.

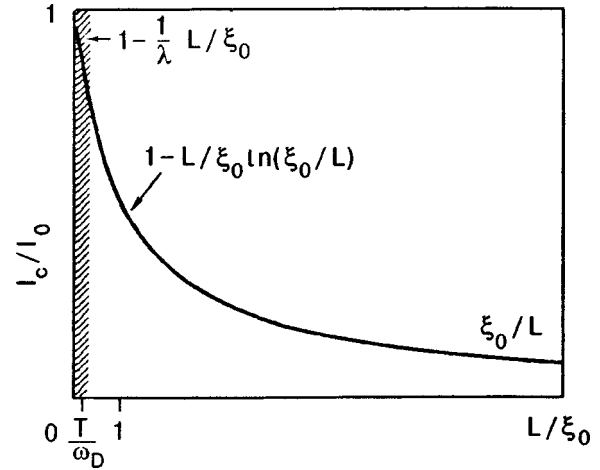


FIG. 3. Dependence of the critical current on the length of the bridge. The asymptotic behavior for short and long bridges is shown. The hatched region corresponds to the ultrashort microbridge,  $L \lesssim v_F/\omega_D$ .

For the case  $l \ll 1$  and  $IN \gg 1$ , we set  $N = \infty$  in the equation for  $q(x)$  and  $J_c(l)$ . The corrections for the critical current in this region of length  $L$  can be estimated as

$$I_c \approx I_0 \left( 1 - \text{const} \frac{L}{\xi_0} \ln \frac{\xi_0}{L} \right), \quad a_D \ll L \ll \xi_0. \quad (37)$$

The expressions (32), (36), and (37) describe the dependence of the critical current on the contact length in the limiting cases of short and long channels. With increasing length  $L$ , the critical current decreases. For ultrasmall  $L \lesssim a_D$  the value of  $\delta I_c/I_0 \sim (1/\lambda)(L/\xi_0)$  directly depends on the BCS coupling constant  $\lambda$ , and consequently it is sensitive to the effects of the strong electron-phonon coupling.

#### 4. CONCLUSION

We have studied the size dependence of the Josephson critical current in ballistic superconducting microbridges. Near the critical temperature  $T_c$ , the Eilenberger equations have been solved self-consistently. The closed integral equation for the order parameter  $\Delta$  (17) and the formula for the critical current  $I_c$  (25) are derived. Equations (17) and (25) are valid for the arbitrary microbridge length  $L$  in the scale of the coherence length,  $\xi_0 \sim v_F/T_c$ . In strongly inhomogeneous microcontact geometry they replace the differential Ginzburg–Landau equations and can be solved numerically. In the limiting cases  $L \gg \xi_0$  and  $L \ll \xi_0$ , we obtained the analytical expressions for  $\Delta$  inside the weak link and for the  $I_c(L)$ . The dependence of  $I_c$  on  $L$  is shown schematically in Fig. 3. For a long microbridge,  $L \gg \xi_0$ , the critical current  $\sim 1/L$  is in correspondence with the phenomenological analysis. The main interest lies in the region  $L \lesssim \xi_0$ , where a microscopic theory is needed. We have calculated the corrections for the KO theory,<sup>8</sup> which are connected with the finite value of the contact size. The expression (2) for the Josephson current was obtained in Ref. 8 in zeroth approximation on the contact size. For the  $L \ll \xi_0$  we find that  $\delta I_c/I_0 \sim (-L/\xi_0) \ln(\xi_0/L)$ , where  $I_0$  is the value of the critical current in KO theory. Thus, the corrections for the value  $I_0$  are small when  $L \ll \xi_0$ , but the derivative  $dI_c/dL$

has a singularity at  $L=0$ . This singularity is smeared if we take into account the finite value of the ratio  $T_c/\omega_D$ . For an ultrashort microchannel,  $L \lesssim a_D \sim v_F/\omega_D$  (the hatched region in Fig. 3), the length dependence of the critical current is  $\delta I_c/I_0 \sim -L/(\lambda \xi_0)$  ( $\lambda$  is the electron-phonon coupling constant). In the very small microcontacts we have a unique situation in which the disturbance of the superconducting order parameter can be localized on the length  $a_D$ , making essential the effects of retardation of electron-phonon interaction. The ballistic flight of electrons through the channel is a dynamic process with characteristic frequency  $\omega_0 \sim v_F/L$ . For  $L$  smaller than  $a_D$  this frequency is comparable with the Debye frequency  $\omega_D$ .

In summary, the critical current  $I_c$  for the finite contact's size is smaller than  $I_0$ . At the same time, the normal-state resistance  $R_N$  of the ballistic microchannel does not depend on the length  $L$  and remains equal to the Sharvin resistance  $R_0$  (3). As a result, the value of the product  $I_c R_N$  is not equal to  $\pi \Delta_0^2/4eT_c$  and depends on the contact size. We have considered here the quasi-classical case  $L \gg \hbar/p_F$ . In the quantum regime,  $L \sim \hbar/p_F$ , the Sharvin resistance  $R_0$  in Eq. (2) is substituted by the quantized resistance of the contact, as was first shown by Beenakker and Houten.<sup>14</sup> It follows from our analysis that for such small microcontacts with  $L \lesssim a_D$  the rigorous calculation of the Josephson current requires taking into account the retardation effects.

We wish to thank M. R. H. Khajepour for useful discussions. This work has been supported in part by the Institute for Advanced Studies in Basic Sciences at Zanjan, Iran.

\*E-mail: omelyanchouk@ilt.kharkov.ua

- 
- <sup>1</sup>B. D. Josephson, *Weakly Coupled Superconductors, Superconductivity*, R. D. Parks (Ed.), Marcel Dekker (1969), Vol. 1.
- <sup>2</sup>L. G. Aslamazov and A. I. Larkin, JETP Lett. **9**, 87 (1969). See also K. K. Likharev, Rev. Mod. Phys. **51**, 101 (1979).
- <sup>3</sup>M. Poza *et al.*, Phys. Rev. B **58**, 11173 (1998).
- <sup>4</sup>C. J. Muller, J. M. van Ruitenbeek, and L. J. de Jongh, Physica C **191**, 485 (1992).
- <sup>5</sup>A. I. Yanson, G. Rubio Bollinger, H. E. van der Brom, N. Agrait, and J. M. van Ruitenbeek, Nature (London) **395**, 783 (1998).
- <sup>6</sup>H. Ohishi, Yu. Kondo, and K. Takayanagi, Nature (London) **395**, 780 (1998).
- <sup>7</sup>I. K. Yanson, Fiz. Nizk. Temp. **4**, 141 (1978) [Sov. J. Low Temp. Phys. **4**, 69 (1978)].
- <sup>8</sup>I. O. Kulik and A. N. Omelyanchouk, Fiz. Nizk. Temp. **4**, 296 (1978) [Sov. J. Low Temp. Phys. **4**, 142 (1978)].
- <sup>9</sup>Yu. V. Sharvin, Zh. Éksp. Teor. Fiz. **48**, 984 (1965) [Sov. Phys. JETP **21**, 655 (1965)].
- <sup>10</sup>G. Eilenberger, Z. Phys. **214**, 195 (1968).
- <sup>11</sup>A. I. Larkin and Yu. N. Ovchinnikov, Zh. Éksp. Teor. Fiz. **73**, 299 (1977) [Sov. Phys. JETP **46**, 155 (1977)].
- <sup>12</sup>I. O. Kulik and A. N. Omelyanchouk, Zh. Éksp. Teor. Fiz. **68**, 2139 (1975) [Sov. Phys. JETP **41**, 1071 (1975)].
- <sup>13</sup>G. M. Eliashberg, Sov. Phys. JETP **38**, 969 (1960); **39**, 1437 (1960).
- <sup>14</sup>C. W. J. Beenakker and H. van Houten, Phys. Rev. Lett. **66**, 3056 (1991).

This article was published in English in the original Russian journal. It was edited by S. J. Amoretty.

## Dynamics and drag of a vortex in type II superconductor with weak inhomogeneities

A. Yu. Galkin

*Institute of Metal Physics, National Academy of Sciences of the Ukraine, 252142 Kiev, Ukraine*

B. A. Ivanov

*Institute of Magnetism, National Academy of Sciences of the Ukraine, 252142 Kiev, Ukraine\**

(Submitted April 20, 1999)

Fiz. Nizk. Temp. **25**, 1161–1169 (November 1999)

The dynamics of the Abrikosov vortex lattice and a single vortex in a type II superconductor with defects is studied taking into account inertial as well as gyroscopic (Hall) properties. The spectrum of normal modes in the absence of defects has two branches. In the limit of small  $k$ , one of the branches is gapless and has a quadratic dispersion relation, while the other branch has a finite gap. In the limit of large  $k$ , the dispersion relations for both modes become linear (acoustic). It is shown that the interaction with defects in a moving vortex or a vortex lattice excites oscillations corresponding to these modes. This creates an additional energy dissipation channel for translation motion of the vortex. In the case of a single vortex, the corresponding drag force diverges as  $V^{-1/2}$  for  $V \rightarrow 0$ , i.e., prevails over the regular force of viscous friction for small velocities. © 1999 American Institute of Physics.  
[S1063-777X(99)00411-9]

The dynamics of vortices and vortex lattices in superconductors, their pinning at defects, and depinning processes determine basic physical properties of type II superconductors, which are important for their applications (see the review by Blatter *et al.*<sup>1</sup>). Vortex dynamics in various ordered media (superconductors and superfluid phases of <sup>4</sup>He and <sup>3</sup>He) is a complex phenomenon which should be generally analyzed taking into account inertial and dissipative properties of vortices, the presence of a gyroscopic force (Hall force in the case of superconductors) as well as defects. Among other things, these properties are manifested in special collective modes existing in the vortex system. These modes were observed in resonance experiments with <sup>4</sup>He.<sup>2</sup> The interest to these mode as applied to high  $T_c$  superconductors (HTSC) has increased considerably in recent years in connection with experiments<sup>3</sup> on magnetic absorption in  $\text{Bi}_2\text{Si}_2\text{CaCu}_2\text{O}_{8+x}$ , in which resonance associated with normal vortex modes was observed. However, induced motion of vortices in the vortex lattices of HTSC is usually described in the purely dissipative approximation without taking into account the peculiarities in the response of the system with local modes (see the review by Blatter *et al.*<sup>1</sup>).

In this communication, we analyze the dynamics of the vortex lattice and a single vortex in a superconductor taking into account inertial as well as gyroscopic (Hall) properties of the superconductor with defects. In the absence of defects, the spectrum of normal modes of vortices has two branches. For small wave vectors  $q$ , one of the branches is gapless and has a quadratic dispersion relation, while the other has a finite gap. For large values of  $q$ , the dispersion relation for both modes becomes linear (acoustic).

The interaction with defects in a moving vortex or vortex lattice induces oscillations corresponding to these modes. This creates an additional dissipation channel for the energy

of translational motion of the vortex. Since the dispersion relation is gapless, such a dissipation appears at an infinitely small vortex velocity  $V$ . It differs from zero even if we disregard the initial dissipation in the equation of motion for the vortex. In this case, the vortex is decelerated due to the fact that the energy of its translational motion is transferred irreversibly to elementary excitations (normal modes quanta).

The type of this drag force depends considerably on the spacing between vortices. When the density of vortices is high, they interact strongly and form a lattice. The vortex lattice can be three-dimensional (3D) or two-dimensional (2D), the latter case (of so-called pancake vortices<sup>1</sup>) being typical of strongly anisotropic superconductors. Our analysis proves that in both cases the contribution of interaction with defects to the dissipation of a moving vortex lattice is small, but it increases upon a decrease in the density of the lattice. Thus, the effect is the strongest for weakly interacting vortices. In the case of a solitary vortex, the additional contribution to the drag force diverges as  $V \rightarrow 0$ . The latter statement is in qualitative agreement with the conclusion drawn by Koshelev and Vinokur,<sup>4</sup> according to which the amplitude of forced oscillations of vortices in a vortex lattice moving in the presence of defects increases upon a decrease in the velocity of the lattice.

### DYNAMICS OF VORTEX LATTICE

Let us consider the dynamics of a vortex lattice (formed by Abrikosov vortices parallel to the  $z$ -axis) in the absence of a perturbation. The low-frequency dynamics of a vortex lattice can be described on the basis of an effective equation for the 2D vector  $\mathbf{u} = \mathbf{u}(x, y, z, t)$  lying in the  $(x, y)$  plane and describing the displacement of the vortex lattice<sup>1</sup> (Fig. 1).

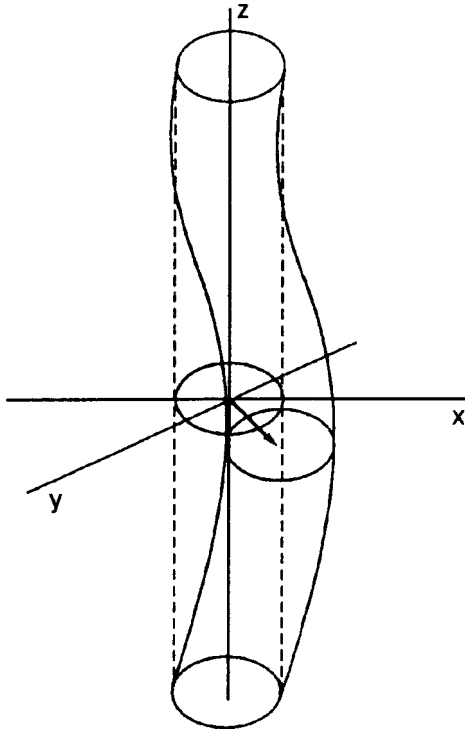


FIG. 1. Undeformed vortex (dashed cylinder) and deformed vortex (solid curves); vector  $\mathbf{u}(z,t)$  is shown by an arrow.

The nondissipative dynamics of  $\mathbf{u}$  is determined by the following Lagrangian:

$$L(\dot{\mathbf{u}}) = \int dx dy dz \left[ \frac{\rho}{2} \dot{\mathbf{u}}^2 + \frac{H}{2} (u_x \dot{u}_y - u_y \dot{u}_x) \right] - W\{\mathbf{u}\}. \tag{1}$$

Here  $\dot{\mathbf{u}} = \partial \mathbf{u} / \partial t$ ;  $\rho$  and  $H$  are the mass and Hall constant of vortices in the lattice per unit volume,  $W\{\mathbf{u}\}$  is the energy of the deformed lattice,

$$W(\mathbf{u}) = \int dx dy dz \left[ \frac{1}{2} c_{11} \left( \frac{\partial u_x}{\partial x} + \frac{\partial u_y}{\partial y} \right)^2 + \frac{1}{2} c_{66} \left( \frac{\partial u_x}{\partial y} - \frac{\partial u_y}{\partial x} \right)^2 + \frac{1}{2} c_{44} \left( \frac{\partial \mathbf{u}}{\partial z} \right)^2 \right] + U_{\text{imp}}(\mathbf{u}), \tag{1a}$$

which is written as in the theory of elasticity, and  $c_{11}$ ,  $c_{44}$ , and  $c_{66}$  are elastic moduli of the lattice. The term  $U_{\text{imp}}$  defines the energy of interaction of a vortex with defects (its structure will be considered later). The rate of energy dissipation in the system is determined by the dissipative function i.e.,  $dE/dt = -2Q(\dot{\mathbf{u}})$ . In the theory of elasticity, this rate is equal to zero in the case of translational motion of the lattice as a single entity, and hence the density of dissipative function  $Q(\dot{\mathbf{u}})$  is proportional to  $[\partial^2 \mathbf{u} / \partial x_i \partial t]^2$ . The situation for a lattice formed by macroscopic objects of the type of vortices or dislocations is different. Each vortex moving in the medium experiences the action of a drag force, and the rate of its energy dissipation is proportional to  $(\partial \mathbf{u} / \partial t)^2$ . For this reason, we choose the dissipative function in the form

$$Q = \frac{\beta}{2} \int dx dy dz \dot{\mathbf{u}}^2, \tag{2}$$

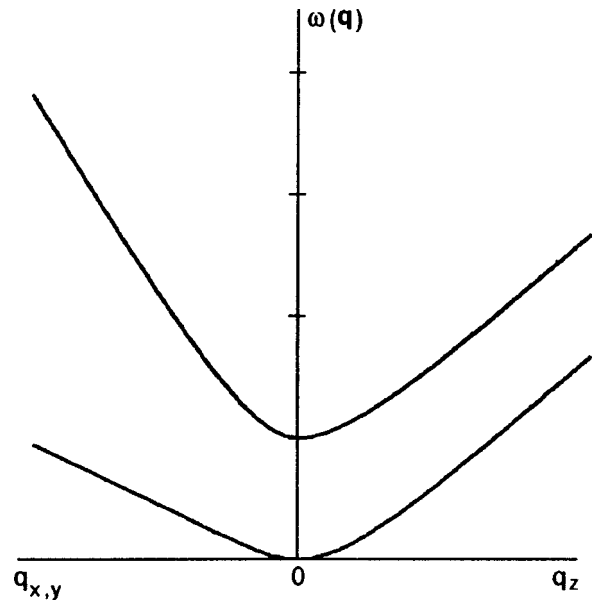


FIG. 2. Dispersion relation shown schematically for vortex lattice vibrations during the propagation of a wave along the vortex axis (right branches) and at right angles to it (left branches).

where  $\beta$  is the dissipation coefficient per unit volume.

Expressions (1) and (2) are written for a 3D vortex lattice. We can easily go over to other interesting cases like a 2D lattice (pancake vortices) or a solitary vortex. It is sufficient to carry out the substitution  $\int dx dy dz \{ \dots \} \rightarrow \int dx dy \{ \dots \}$  (2D case) or  $\int dx dy dz \{ \dots \} \rightarrow \int dz \{ \dots \}$  (solitary vortex) and omit the terms with the derivatives of  $\mathbf{u}$  with respect to  $z$  (2D case) or with respect to  $x, y$  (solitary vortex). We must also assume that  $\rho$ ,  $\beta$ , etc. describe typical values per unit area of the lattice (2D case) or per unit length of a solitary vortex. For example, in the important case of a solitary vortex, we must carry out substitutions of the type  $\rho \rightarrow \rho a_v^2$ ,  $\beta \rightarrow \beta a_v^2$ ,  $c_{44} \rightarrow k$ , where  $\kappa$  is the energy per unit length of the vortex and  $a_v^2$  the area of the vortex lattice per vortex.

The equations of motion for the variable  $\mathbf{u}$  can be derived by variation of Eqs. (1) and (2),  $\delta L / \delta \mathbf{u} - \delta Q / \delta \dot{\mathbf{u}} = 0$ . In the absence of interaction with defects, the equation of motion for a vortex lattice can be written in the form

$$\begin{aligned} \rho \ddot{\mathbf{u}} + H(\mathbf{e}_x \dot{u}_y - \mathbf{e}_y \dot{u}_x) + \beta \dot{\mathbf{u}} - c_{44} \frac{\partial^2 \mathbf{u}}{\partial z^2} - \mathbf{e}_x \left[ c_{11} \frac{\partial}{\partial x} \left( \frac{\partial u_x}{\partial x} + \frac{\partial u_y}{\partial y} \right) + c_{66} \frac{\partial}{\partial y} \left( \frac{\partial u_x}{\partial y} - \frac{\partial u_y}{\partial x} \right) \right] - \mathbf{e}_y \left[ c_{11} \frac{\partial}{\partial y} \left( \frac{\partial u_x}{\partial x} + \frac{\partial u_y}{\partial y} \right) - c_{66} \frac{\partial}{\partial x} \left( \frac{\partial u_x}{\partial y} - \frac{\partial u_y}{\partial x} \right) \right] = 0. \tag{3} \end{aligned}$$

In the nondissipative limit ( $\beta = 0$ ), this equation describes the normal vibrations of the lattice. In the case of small dissipation, the corresponding dispersion relation  $\omega = \omega(\mathbf{q})$  is strongly anisotropic (Fig. 2) and is given by the following cumbersome formula

$$\rho\omega^2 = c_{44}q_z^2 + \frac{1}{2}(c_{11} + c_{66})q_\perp^2 + \frac{H^2}{2\rho} \pm \left[ \left( \frac{H^2}{2\rho} \right)^2 + \frac{H^2}{2\rho} [2c_{44}q_z^2 + (c_{11} + c_{66})q_\perp^2] + \frac{1}{4}(c_{11} - c_{66})^2 q_\perp^4 \right]^{1/2}, \quad (4)$$

where  $q_\perp^2 = q_x^2 + q_y^2$  and the signs “+” and “-” correspond to two vibrational branches. In the limit of small  $q_z$  and  $q_\perp$ , the expressions for frequencies of the upper and lower branches are simplified considerably:

$$\omega_{(-)}^2 = \frac{1}{H^2} (c_{44}q_z^2 + c_{66}q_\perp^2)(c_{44}q_z^2 + c_{11}q_\perp^2), \quad (5a)$$

$$\omega_{(+)}^2 = \frac{H^2}{\rho^2} + \frac{2}{\rho} c_{44}q_z^2 + \frac{1}{\rho} q_\perp^2 (c_{11} + c_{66}). \quad (5b)$$

Expression (5a) corresponds to the low-frequency gapless mode. For small  $q_z$  and  $q_\perp$ , the dispersion relation for this mode is quadratic in the components of  $\mathbf{q}$  and independent of the vortex mass. For a wave propagating along the vortex (the limiting case  $q_\perp \rightarrow 0$ ) the result coincides with that obtained long ago by De Gennes and Matricon<sup>5</sup> for a solitary vortex, i.e.,  $\omega_{(-)} \rightarrow q_z^2 \kappa / H_1$ , where the Hall constant  $H_1$  of the solitary vortex is introduced.

Formula (5b) for small  $q$  describes the mode with a finite gap, i.e.,  $\omega_{(+)} \rightarrow H/\rho + [2c_{44}q_z^2 + (c_{11} + c_{66})q_\perp^2]/2\rho$ . The limiting value of frequency for this mode is determined by the Hall constant  $H$  and mass  $\rho$ , i.e.,  $\omega_{(+)} \rightarrow H/\rho$  for  $q \rightarrow 0$ . Thus, this mode corresponds to the cyclotron motion of vortices in the lattice in the homogeneous case ( $q=0$ ). Cyclotron motion of a vortex in superfluid systems and superconductors has been considered by many authors from the microscopic point of view.<sup>6</sup> It was also observed for ferromagnets<sup>7</sup> and antiferromagnets in an external magnetic field.<sup>8</sup> It should be noted that sometimes another cyclotron frequency  $\omega_c$  is introduced for superconductors,<sup>9</sup> which is determined by the cyclotron motion of electrons and has a finite value even when the vortex mass is not taken into account. A different mechanism of gap formation in the spectrum of normal modes in the lattice, namely, the long-range interaction between vortices, was considered by Sonin.<sup>10</sup> Naturally, this mechanism does not work for normal modes of oscillations of a solitary vortex in contrast to the cyclotron mechanism.

The above specific features (quadratic dispersion relation and the presence of a gap) are due to the gyroscopic force. Only in the limit of large  $q$ ,  $cq^2 \gg H/\rho$ , gyroscopic force is insignificant, and the dispersion relation for both modes is transformed to a linear (quasi-acoustic) relation typical of lattice systems. The corresponding velocity of sound strongly depends on the direction of wave propagation:

$$\omega_{(\pm)}^2 = \frac{1}{2\rho} [2c_{44}q_z^2 + (c_{66} + c_{11})q_\perp^2] \pm \frac{1}{2\rho} |c_{66} - c_{11}| q_\perp^2.$$

If the wave propagates along vortices, both branches naturally correspond to transverse oscillations with the

velocity of sound  $s_z = \sqrt{c_{44}/\rho}$ . The two branches corresponding to the propagation in a direction perpendicular to vortices for  $cq^2 \gg H/\rho$  describe longitudinal and transverse waves with velocities  $s_l = \sqrt{c_{11}/\rho}$  and  $s_t = \sqrt{c_{66}/\rho}$  respectively.

Let us consider the interaction between the vortex lattice and the defects in the crystal. For definiteness, we assume that the presence of defects leads to a coordinate dependence of the local critical temperature  $T_c$ . This can be taken into account by introducing the coordinate-dependent coefficient  $[a_0 + F(\mathbf{r})]|\psi|^2$  into the Ginzburg–Landau expansion.<sup>1</sup>

We start from the case of a single vortex located in equilibrium at a certain site  $\mathbf{I}$  of the vortex lattice. For definiteness, we assume that the distribution of the order parameter in the vortex does not change during the motion of a vortex and is described by a known function  $f(r_\perp)$ .<sup>11</sup> Thus, taking into account the displacement of the vortex, we can write  $|\psi|^2 = |\psi_0|^2 f(r_\perp)$ , where  $r_\perp = [(x - l_x - u_x)^2 + (y - l_y - u_y)^2]^{1/2}$ . In this case, the energy  $U_{\text{imp}}$  associated with crystal inhomogeneities can be written in terms of the function  $f(r_\perp)$  in the form of a functional of the vortex displacement:

$$U_{\text{imp}} = \int d\tilde{x} d\tilde{y} dz f(r_\perp) F[x + l_x + u_x(\mathbf{r}, t), y + l_y + u_y(\mathbf{r}, t), z],$$

where  $\tilde{x} = x - l_x - u_x(\mathbf{r}, t)$ ,  $\tilde{y} = y - l_y - u_y(\mathbf{r}, t)$ .

It is convenient to write the expression for  $U_{\text{imp}}$  in the form of the Fourier expansion in  $x$  and  $y$ :

$$U_{\text{imp}} = \frac{1}{S} \sum_{q_x, q_y} f(q_\perp) \int dz F(q_x, q_y, z) \times \exp\{-i\mathbf{q}_\perp \cdot \mathbf{I} - i\mathbf{q}_\perp \cdot \mathbf{u}(\mathbf{r}, t)\}, \quad (6)$$

where  $\mathbf{q}_\perp = (q_x, q_y, 0)$ ,  $S = L_x L_y$  is the area of the superconductor,  $f(q_\perp)$  is the form factor of the vortex, and

$$F(q_x, q_y, z) = \int d\xi d\eta F(\xi, \eta, z) e^{iq_x \xi + iq_y \eta},$$

$$f(x, y) = \sum_{q_x, q_y} f(q_\perp) e^{iq_x x + iq_y y}.$$

Taking this expression into account, we can write the equation of motion of the vortices in the presence of defects in the form (3) with an additional force  $\mathcal{F}_{\text{imp}}$  on the right-hand side:

$$\mathbf{F}_{\text{imp}} = \sum_{q_x, q_y} i\mathbf{q}_\perp f(q_\perp) F(q_x, q_y, z) \exp(i\mathbf{q}_\perp \cdot \mathbf{u}). \quad (7)$$

A general solution of this nonlinear equation with coefficients depending on  $z$  cannot be obtained. However, we can carry out a complete analysis assuming that deviations from the rectilinear uniform motion of vortices due to defects are small. Putting  $\mathbf{u} = \mathbf{e}_x Vt + \tilde{\mathbf{u}}(\mathbf{r}, t)$  and linearizing (3) and (7) in  $\tilde{\mathbf{u}}$ , we obtain for  $\tilde{\mathbf{u}}$  the following linear equation with a right-hand side:

$$\rho \ddot{\tilde{\mathbf{u}}} + H[\mathbf{e}_2 \times \dot{\tilde{\mathbf{u}}}] + \beta \dot{\tilde{\mathbf{u}}} + \kappa \frac{\partial^2 \tilde{\mathbf{u}}}{\partial z^2} = \frac{1}{\Omega} \sum_{\mathbf{q}} i\mathbf{q}_\perp f(q_\perp) F(\mathbf{q}) \times \exp(i\mathbf{q}_\perp \cdot \mathbf{I} + iq_z z) - iq_x Vt. \quad (8)$$

where  $\Omega = L_x L_y L_z$  is the volume of the superconductor.

This equation describes induced oscillations of a vortex, and its solution can easily be obtained by the method of Fourier transformation. Substituting the solution of this equation into the dissipative function, we obtain additional contribution to the vortex energy dissipation associated with the fact that the motion of the vortex in the presence of a defect is not rectilinear and uniform. Since the value of  $\tilde{\mathbf{u}}$  averaged over  $z$  and  $t$  vanishes, this contribution is quadratic in the amplitude of forced oscillations of the vortex.

Clearly, the same expression (8) is valid for each of the vortices forming the lattice. In order to describe the force acting per unit volume of the lattice in the vicinity of a given point  $\mathbf{r}$  in the macroscopic limit, it is sufficient to carry out the substitution  $\mathbf{q}_\perp \cdot \mathbf{1} + q_z z \rightarrow \mathbf{q} \cdot \mathbf{r}$  in (8) and divide (7) by the area  $a_v^2$  per vortex. This gives

$$(\mathcal{F}_{\text{imp}})_{\text{lat}} = \frac{1}{a_v^2 \Omega} \sum_{\mathbf{q}} i \mathbf{q}_\perp f(q_\perp) F(\mathbf{q}) \exp(i \mathbf{q} \cdot \mathbf{r} - i q_x V t). \quad (8a)$$

### CALCULATION OF DISSIPATION FOR VORTEX LATTICE

In order to analyze specifically the contribution to the drag of a vortex lattice, we shall assume that inhomogeneity is due to the system of point defects whose size is smaller than the radius of the vortex core. In this case, the function  $F(x, y, z)$  in (5) can be written as the sum of Dirac delta functions:

$$F(\mathbf{r}) = \sum_a \alpha \delta(\mathbf{r} - \mathbf{r}_a).$$

Here  $\mathbf{r}_a$  is the coordinate of the  $a$ th defect and  $\alpha$  characterizes the intensity of interaction of the defect with the order

parameter (we assume for simplicity that the value of  $\alpha$  is the same for all defects). Such a model correctly describes any defect whose size is smaller than the coherence length  $\xi$  of the superconductor. Typical examples of such defects in HTSC are oxygen vacancies.<sup>1</sup>

In this case, the expression (8a) for the force  $\mathcal{F}_{\text{imp}}$  acting per unit volume of the lattice can be written in the form

$$\mathbf{F}_{\text{imp}} = \frac{1}{a_v^2} \frac{\alpha}{\Omega} \sum_a \sum_{\mathbf{q}} i \mathbf{q}_\perp f(q_\perp) e^{i \mathbf{q}_\perp \cdot \mathbf{r}_a} e^{i \mathbf{q} \cdot \mathbf{r} - i q_x V t}.$$

Solving this equation for  $\tilde{\mathbf{u}}$ , we obtain

$$\tilde{u}_{x,y} = \frac{1}{a_v^2} \frac{\alpha}{\Omega} \sum_a \sum_{\mathbf{q}} f(q_\perp) e^{i \mathbf{q}_\perp \cdot \mathbf{r}_a} \times \frac{A_{x,y}(\mathbf{q}_\perp) + i B(\mathbf{e}_{x,y}[\mathbf{e}_z \times \mathbf{q}])}{A_x A_y - B^2} e^{-i \mathbf{q} \cdot \mathbf{r} - i q_x V t}, \quad (9)$$

where

$$\begin{aligned} A_x &= (c_{11} q_\perp^2 + c_{44} q_z^2) + i \beta q_x V - \rho (q_x V)^2; \\ A_y &= (c_{66} q_\perp^2 + c_{44} q_z^2) + i \beta q_y V - \rho (q_y V)^2; \\ B &= q_x V H. \end{aligned}$$

It should be noted that the condition  $A_x A_y - B^2 = 0$  for  $\beta \rightarrow 0$  determines the dispersion relation (4) for oscillations of the vortex lattice derived above. For  $\beta \neq 0$ , the denominator in formula (9) does not vanish for any value of  $\mathbf{q}$ .

Substituting expression (9) into the dissipative function and carrying out averaging over defects with the help of the relation  $\sum_a \exp(i \mathbf{q} \cdot \mathbf{r}_a) = N \delta_{\mathbf{q},0}$ , where  $N$  is the number of defects and  $\delta_{\mathbf{q},0}$  is the Kronecker symbol, we can easily find the dependence of the drag force on the velocity of the vortex:

$$\begin{aligned} Q(V) &= \frac{1}{a_v^4} \frac{C_{\text{imp}}}{(2\pi)^2} V^2 \alpha^2 \beta \int dq_x dq_y dq_z q_\perp^2 q_x^2 f^2(q_\perp) \\ &\times \frac{q_x^2 V^2 (\beta^2 + H^2) + (c_{44} q_z^2 + c_{11} q_y^2 + c_{66} q_x^2 - \rho q_x^2 V^2)^2 + (c_{11} - c_{66})^2 q_x^2 q_y^2}{[\rho^2 (q_x V)^4 - H^2 (q_x V)^2 - \rho \hat{C}_q (q_x V)^2 + \hat{C}_{1q} \hat{C}_{2q} - (\beta q_x V)^2]^2 + (\beta q_x V)^2 [\hat{C}_q - 2\rho (q_x V)^2]^2}. \end{aligned} \quad (10)$$

Here  $C_{\text{imp}} = N/\Omega$  is the concentration of defects, and the following notation has been introduced to simplify the relation:

$$\begin{aligned} \hat{C}_q &= \hat{C}_{1q} + \hat{C}_{2q}, \quad \hat{C}_{1q} = c_{11} q_\perp^2 + c_{44} q_z^2, \\ \hat{C}_{2q} &= c_{66} q_\perp^2 + c_{44} q_z^2. \end{aligned}$$

Direct evaluation of this integral leads to cumbersome expressions, and we shall confine our further analysis to limiting relations between the parameters of the problem such as viscosity, Hall constant and vortex mass, and to the case of small velocities. Before discussing specific results, however, we shall make a general statement concerning the depen-

dence of the additional drag force  $\Delta F(V) = Q(V)/V$  [ $Q(V)$  is the dissipative function (10)] on the velocity of vortices and on the parameters of the problem.

The factor  $\beta V^2$  appearing in (10) in front of the integral can be interpreted so that the quantity  $Q(V) \sim \beta V^2$ , which in turn leads to a linear dependence  $F(V) \sim \beta V$  of the drag force on velocity. Clearly, the inclusion of vibrations of vortices associated with interaction with defects gives only a small correction to the conventional initial drag force. However, the integral in (10) contains singularities due to which the additional relaxation channel in (10) can become significant and even decisive.

As a matter of fact, the additional drag does not vanish even in the limiting case of small dissipation ( $\beta \rightarrow 0$ , while  $\rho$

and  $H$  are finite). At first glance, this appears as paradoxical. However, such a collisionless (Landau) damping associated with pumping of energy of one vibrational mode to the other is encountered in many branches of physics. This is just the situation observed in our case the action of defects on vortices for small  $\beta$  leads to the excitation of weakly attenuating normal vibrations of vortices in the lattice. Let us consider this conclusion in greater detail.

Expression (10) contains  $\beta$  in the combination  $\beta\{\beta^2 + F^2[\mathbf{q}, (q_x V)^2]\}$  (see (10)) where the function  $F$  is such that the condition  $F[\mathbf{q}, (q_x V)^2] = 0$  with the substitution  $q_x V \rightarrow \omega$  defines the frequencies of normal modes of vortex vibrations in the lattice [cf. (4) and (10)]. For  $\beta \rightarrow 0$ , the expression (10) is transformed into the  $\delta$ -function  $\delta\{F[\mathbf{q}, (q_x V)^2]\}$ . After simple transformations, this expression can be reduced to the sum of two  $\delta$ -functions of the type  $\delta[(q_x V)^2 - \omega_{(\pm)}^2(\mathbf{q})]$ , where  $\omega_{(\pm)}(\mathbf{q})$  are the frequencies of normal modes (4). Since at least one of the equations  $q_x V = \omega_{(-)}(\mathbf{q})$  or  $q_x V = \omega_{(+)}(\mathbf{q})$  has a solution for any value of velocity, the value of  $Q(V)$  can be finite even for  $\beta \rightarrow 0$ . A similar result was obtained in an analysis of the drag of domain walls in magnets with microscopic defects.<sup>12,13</sup> It can be explained as follows: the action of defects on vortices leads to excitation of weakly attenuating natural vibrations of vortices, and hence to irreversible transfer of the energy of translational motion of the vortex to the energy of these vibrations.

The physical meaning of this result becomes clearer if we formulate it in the language of quantum mechanics.<sup>11</sup> Let us go over to a reference frame moving with the vortices. In this reference frame, defects move at a velocity  $-\mathbf{V} = -V\mathbf{e}_x$  parallel to the  $x$ -axis and can transfer the momentum  $\mathbf{q}$  to the vortex lattice (we put  $\hbar = 1$ ) only simultaneously with the energy  $\mathbf{q} \cdot \mathbf{V} = q_x V$ . This momentum is redistributed between the lattice as a whole and an elementary excitation, and the energy is transferred to the elementary excitation. In particular, for a single vortex the situation is quite simple: the vortex acquires a momentum in a direction perpendicular to its axis ( $z$ -axis), and the wave propagating along the vortex acquires a component of the momentum along the  $z$ -axis. It can easily be seen that the arguments of the  $\delta$ -functions written above determine the corresponding laws of conservation of energy and momentum during the generation of a vibrational quantum corresponding to a certain normal mode. Dissipation is due to irreversible transfer of kinetic energy of the vortex to such excitations.

The calculation for small velocities leads to the expression  $\Delta F(V) \sim V^3/C$ , where  $C$  is a certain combination of the quantities  $c_{11}$  and  $c_{66}$ . Consequently, in contrast to the case of domain walls<sup>12,13</sup> for which  $\Delta F(V) \rightarrow \text{const}$  for  $V \rightarrow 0$ , the corresponding correction to drag force for small velocities is smaller than the standard term of the type  $\beta V$ . However, this correction contains the quantity  $C \sim 1/a_v^2$  in the denominator and increases upon a decrease in the density of vortices in the lattice. It follows hence that as we go over to a solitary vortex for which  $C \propto 1/a_v^2 \rightarrow 0$ , the exponent of the velocity  $V$  in the  $F(V)$  dependence must become smaller than three.

A more standard result appears when  $\beta$  is finite. In this case, we find as a result of simple but cumbersome evalua-

tion of the integral in (10) that the correction to drag force is linear in  $V$  for small velocities:

$$\Delta F(V) = -(\Delta B_{3D})V,$$

$$\Delta B_{3D} = \frac{1}{a_v^4} C_{\text{imp}} \frac{\beta \pi \alpha^2}{4 c_{44}^{1/2} c_{66}^{3/2}} \int dq_x dq_y |f(q_\perp)|^2 \frac{q_x^2}{q_\perp}.$$

Since  $c_{66} \propto B \propto a_v^{-2}$  and  $c_{44} \propto B \propto a_v^{-4}$  ( $B$  is the induction in the superconductor),<sup>1</sup> the quantity  $\Delta B_{3D} \propto a_v$  as for  $\beta = 0$  and diverges for  $(1/a_v^2) \rightarrow 0$ . Consequently, the correction  $\Delta F(V)$  becomes more significant as the density of vortices decreases. An analysis proved that the corresponding contributions become equal ( $\Delta B_{3D} \sim \beta$ ) only for small values of density for which the interaction between vortices can be neglected, and they can be regarded as independent.

Let us make a transition to the case of a solitary vortex: the dependence corresponds to the limit  $c_{66} \rightarrow 0$  in the formula for  $\Delta B_{3D}$  written above. Since the quantity  $\Delta B_{3D}$  formally diverges, the dependence of  $\Delta F(V)$  for a solitary vortex must become stronger than linear (it should be expected that  $\Delta F(V) \propto V^\sigma$ ,  $\sigma < 1$ ).

The analysis of a 2D lattice proved that such lattices obey the same regularities as in the 3D case. For example, the corresponding correction to drag force for low velocities and a finite  $\beta$  is smaller than  $\beta V$ . For this reason, we shall not discuss details and go over to an analysis of a solitary vortex for which the contribution  $\Delta F(V)$  has the maximum value.

### DRAG OF A SOLITARY VORTEX

For a solitary vortex, we must assume in the integral (10) that the quantities  $H$  and  $\rho$  correspond to unit length of the vortex (see (3)) and put  $\hat{C}_{1q} = \hat{C}_{2q} = \kappa q_z^2$ , where  $\kappa$  is the energy per unit vortex length. In this case, the dependence of the integrand on  $\mathbf{q}$  is simplified significantly, and  $Q(V)$  can be calculated in detail. For example, if we disregard inertial properties of the vortex (i.e., put  $\rho = 0$ ), we can determine the  $Q(V)$  dependence exactly. For all values of velocity and any relation between  $H$  and  $\beta$ , the additional drag force is proportional to  $V^{-1/2}$ :

$$F(V) = \eta V^{-1/2} = C_{\text{imp}} A \xi^{-1/2} \frac{\pi \alpha^2}{2 \sqrt{2} \kappa V} \frac{1}{\sqrt{H^2 + \beta^2}}$$

$$\times [(\sqrt{H^2 + \beta^2} + H)^{1/2} + (\sqrt{H^2 + \beta^2} - H)^{1/2}] \quad (11)$$

and the coefficient  $\eta$  is finite for  $\beta \rightarrow 0$ ,  $H \neq 0$  as well as for  $H \rightarrow 0$ ,  $\beta \neq 0$ .

We have introduced here the notation  $A \xi^{-1/2} = \int dq_x dq_y \times \sqrt{q_x q_\perp^2} |f(q_\perp)|^2$ , where  $\xi$  is the coherence length. Considering that the vortex form factor  $f(q_\perp)$  is a function localized in the region  $\xi q_\perp \leq 1$ ,  $f(q_\perp) \sim \xi^2$  for  $q_\perp \rightarrow 0$  and  $f(q_\perp) \rightarrow 0$  for  $\xi q_\perp \gg 1$  [see (11)], we find that  $A$  is a constant of the order of unity.

An analysis of the effect of inertial properties of the vortex will be carried out assuming that  $\beta \ll H$ , but without requiring that any inequalities are satisfied for other param-

eters of the problem. In this case, the integral with respect to  $q_z^2$  was evaluated exactly using  $\delta$ -functions and the following compact expression was obtained:

$$\begin{aligned}
 Q(V) = & \frac{C_{\text{imp}}\alpha^2}{\sqrt{\kappa}} \int_0^\infty dq_x \int_{-\infty}^\infty dq_y q_\perp^2 f^2 \\
 & \times (q_\perp) \frac{q_x V}{\sqrt{H(q_x V) + \rho(q_x V)^2}} + 2 \frac{C_{\text{imp}}\alpha^2}{\sqrt{\kappa}} \\
 & \times \int_{(H/\rho V)}^\infty dq_x \int_{-\infty}^{+\infty} dq_y q_\perp^2 f^2 \\
 & \times (q_\perp) \frac{q_x V}{\sqrt{\rho(q_x V)^2 - H(q_x V)}}. \quad (12)
 \end{aligned}$$

The first term in this expression is due to excitation of oscillations of the activationless mode, while the second term is associated with the activation mode. For small velocities  $V \ll H\xi/\rho$ , the integration in the second integral is carried out over the region  $q_x > 1/\xi$ . In this region, the function  $f(q_\perp)$  is exponentially small, and hence the contribution from the second term is insignificant. However, the first term associated with elementary excitations with activationless dispersion relation gives a significant contribution to  $\Delta F(V) = Q(V)/V$  for an indefinitely small velocity. It can easily be seen that this contribution diverges for  $V \rightarrow 0$ . In the limiting case  $\rho \ll H\xi/V$ , we naturally arrive again at the formula (11) for  $\beta = 0$ , in which  $F(V)$  does not depend on  $\rho$ . Inertial properties of the vortex are manifested only for  $V > H\xi/\rho$ . In this case, the divergence of  $F(V)$  is stronger than in (11):  $F(V) \propto 1/V$ . However, this case corresponds to too high velocities and will not be considered here.

Thus, for arbitrary relations between dynamic parameters  $\rho$ ,  $\kappa$ , and  $\beta$  of the solitary vortex and a small vortex velocity  $V \ll H\xi/\rho$ , the additional drag force is described by formula (11), i.e.,  $\Delta F(V) \propto V^{-1/2}$  and diverges for  $V \rightarrow 0$ . Taking into account the ordinary viscous drag force acting on the vortex, we can write the resultant force in the form  $F(V) = \beta V + \eta/V^{1/2}$ , where  $\beta$  is the viscosity introduced in (2), and  $\eta$  is defined by formula (11). It follows hence that for small velocities  $V < V^*$ , the value of  $\Delta F$  is larger than  $\beta V$  even if the coefficient of  $V^{-1/2}$  is quite small.

Let us estimate the characteristic velocities of the vortex, i.e., the quantities  $H\xi/\rho$  and  $V^* = (\eta/\beta)^{2/3}$ . The quantity  $H\xi/\rho$  turns out to be larger than ordinary velocities of vortex lattices, while  $V^*$  is obviously smaller than  $H\xi/\rho$  if only due to the fact that it contains small parameters  $C_{\text{imp}}$  and  $\alpha$ . In accordance with formulas (11) and (12), the characteristic velocity  $V^*$  for small velocities and any relation between  $\beta$  and  $H$  is defined as

$$V^* = \left( \frac{AC_{\text{imp}}\alpha^2}{2\beta\sqrt{\kappa}\xi \max\{\beta, H\}} \right)^{2/3}, \quad (13)$$

where  $A$  is a numerical factor of the order of unity and  $\xi$  the coherence length.

In order to obtain estimates, we choose conventional expressions for phenomenological parameters of the problem

in terms of microscopic characteristics of the superconductor (see, for example, Refs. 1 and 11). We write  $\kappa = (\Phi_0/4\pi\lambda)^2$ , where  $\lambda$  is the depth of magnetic field penetration in the superconductor and  $\Phi_0$  the magnetic flux quantum. For the quantity  $\alpha$ , we put  $\alpha = (H_{cm}^2/8\pi) \times (\Delta T_c/T_{c0})a^3$ , where  $H_{cm} = \Phi_0/2\pi\lambda\xi$  is the thermodynamic critical field of the superconductor,  $\Delta T_c/T_c$  the relative suppression of the superconducting transition temperature at a defect, and  $a^3$  is the volume corresponding to a defect (the value of  $a$  is of the order of atomic spacing). The gyroscopic constant  $H$  is determined by the number density  $n$  of superconducting electrons,  $H = \pi\hbar n$ ,  $n = mc^2/4\pi\lambda^2 e^2$ , where  $\hbar$  is Planck's constant,  $m$  and  $e$  are the electron mass and charge, and  $c$  is the velocity of light. Finally, the viscosity  $\beta$  is primarily determined by the metal resistivity  $\rho_n$  in the normal state, and hence we can write<sup>1</sup>  $\beta = H_{c2}\Phi_0/c^2\rho_n$ , where  $H_{c2}$  is the upper critical field,  $H_{c2} = \Phi_0/2\pi\xi^2$ . This gives

$$\begin{aligned}
 V^* &= \frac{a^4 c^2 \rho_n}{64\pi^{5/3} \lambda^2 \xi} \left( \frac{C_{\text{imp}}}{2} \right)^{2/3} \left( \frac{\Delta T_c}{T_{c0}} \right)^{4/3} \quad \text{for } \beta \gg H, \\
 V^* &= \frac{a^4 c^2}{64\pi^2} \left( \frac{C_{\text{imp}} e \rho_n}{2\lambda^2 \xi^{5/2} \sqrt{m\hbar}} \right)^{2/3} \left( \frac{\Delta T_c}{T_{c0}} \right)^{4/3} \quad \text{for } \beta \ll H. \quad (14)
 \end{aligned}$$

If we take the characteristic values of HTSC of the YBCO type, i.e.,  $\rho_n = 5 \cdot 10^{-15}$  s,  $a = 10^{-8}$  cm,  $\xi = 10^{-7}$  cm,  $\lambda/\xi = 10^2$ , and assume that  $\Delta T_c/T_c \sim 10^{-1}$ , the values of  $V^*$  do not differ significantly for  $\beta < H$  and  $\beta > H$  and can be estimated as

$$V^* \sim [C_{\text{imp}}^{2/3} (10^{-11} - 10^{-12})] \text{ cm/s},$$

where the value of  $C_{\text{imp}}$  is measured in  $\text{cm}^{-3}$ . For a reasonable value of  $C_{\text{imp}} \sim 10^{15} \text{ cm}^{-3}$ , which corresponds, for example, to the equivalent density of dislocations  $C_{\text{disl}} \sim 10^{10} \text{ cm}^{-2}$ , the value of  $V^* \sim 10^{-1} - 10^{-2} \text{ cm/s}$ , which is even larger than ordinary values of vortex velocity in superconductors.

## DISCUSSION OF RESULTS

Thus, the correction to the drag force acting on a vortex and associated with collective modes induced during the motion of the vortex through a system of defects is small for a dense vortex lattice, but has a singularity  $F(V) \propto 1/\sqrt{V}$  for  $V \rightarrow 0$  in the case of a solitary vortex. The dependence of drag force on velocity is stronger than that obtained in Ref. 4. This is due to the fact that we proceed from the realistic model of vortex interaction with defects and not from the model of random force as in Ref. 4.

The nonmonotonic dependence of drag force on velocity can lead to singularities of the induced motion of vortices. The drag force acting on a moving vortex if we take into account the excitation of natural vibrational mode can be presented in the form

$$F = \beta V + \eta/\sqrt{V},$$

where the first term describes "conventional" viscous drag and the quantity  $\eta$  is defined by formula (11). This must lead

to singularities in the velocity of induced motion of a vortex under the action of the external force  $F_e$  (transport current), which is defined as  $F_e = F(V)$ . It can be easily seen that this equation has two solutions, the solution corresponding to the upper branch existing only for a velocity larger than the characteristic value  $V^* = (\eta/\beta)^{2/3}$  introduced above [see (11)].

The steady-state motion for a negative differential mobility  $(1/\beta)_{\text{dif}} = dV/dF_e$  is usually unstable.<sup>14</sup> Since the condition  $dV/dF_e > 0$  is satisfied only for the upper branch of the function  $F(V)$ , the steady-state motion of the vortex is possible only for  $V > V^*$ . Thus, this singularity must be manifested in the form of an abrupt jump on the dependence  $V(F_e)$ , which in fact coincides with the current–voltage characteristic of the superconductor.

It should also be noted that the theory developed above is not confined only to vortices in superconductors and can be applied for vortex-like objects in any ordered medium. The only condition is that a vortex must possess gyroscopic properties. It was mentioned above, however, that gyroscopic dynamics is typical of many models of ordered media. Apart from the examples considered above, we can mention Bloch lines, viz., specific vortex-like objects existing in domain walls of ferromagnets and characterized by experimentally established gyroscopic properties, which can be used as carriers of information in memory devices (see Ref. 14).

The authors are grateful to V. G. Bar'yakhtar, V. M. Pan, and A. L. Kasatkin for fruitful discussions.

<sup>\*</sup>E-mail: vbaryakhtar@bitp.kiev.ua

- <sup>1</sup>G. Blatter, M. V. Feigel'man, V. B. Geshkenbein *et al.*, Rev. Mod. Phys. **66**, 1125 (1994).
- <sup>2</sup>R. J. Donnelly, in *Quantized Vortices in Helium II*, edited by A. M. Goldman, P. V. E. McClintock, and M. Springford (Cambridge University Press, Cambridge, 1991).
- <sup>3</sup>O. K. C. Tsui, N. P. Ong, Y. Matsuda *et al.*, Phys. Rev. Lett. **73**, 724 (1994).
- <sup>4</sup>A. E. Koshelev and V. M. Vinokur, Phys. Rev. Lett. **73**, 3580 (1994).
- <sup>5</sup>P. G. de Gennes and J. Matricon, Rev. Mod. Phys. **36**, 45 (1964).
- <sup>6</sup>E. Šimànek, Phys. Lett. A **194**, 323 (1994); P. Ao and X.-M. Zhu, Physica C **282**, 367 (1997); E. Demircan, P. Ao, and Q. Niu, Phys. Rev. B **54**, 10027 (1996); G. E. Volovik, Pis'ma Zh. Eksp. Teor. Fiz. **65**, 201 (1997) [JETP Lett. **65**, 217 (1997)].
- <sup>7</sup>G. M. Wysin, Phys. Rev. B **54**, 15156 (1996); B. A. Ivanov, H. J. Schnitzer, F.-G. Mertens, and G. M. Wysin, Phys. Rev. B **58**, 8464 (1998).
- <sup>8</sup>B. A. Ivanov and D. D. Sheka, Phys. Rev. Lett. **72**, 404 (1994).
- <sup>9</sup>N. B. Kopnin, A. V. Lopatin, E. B. Sonin, and K. B. Traito, Phys. Rev. Lett. **74**, 4527 (1995).
- <sup>10</sup>E. B. Sonin, Phys. Rev. Lett. **79**, 3732 (1997).
- <sup>11</sup>P. de Gennes, *Superconductivity of Metals and Alloys* (New York, 1966).
- <sup>12</sup>A. V. Zuev and B. A. Ivanov, Zh. Eksp. Teor. Fiz. **82**, 1679 (1982) [Sov. Phys. JETP **55**, 971 (1982)].
- <sup>13</sup>B. A. Ivanov and S. N. Lyakhimets, IEEE Trans. Magn. **30**, 824 (1994).
- <sup>14</sup>V. G. Bar'yakhtar, M. V. Chetkin, B. A. Ivanov, and S. N. Gadetskii, *Dynamics of Topological Magnetic Solitons* (Springer-Verlag, Berlin, 1993).

Translated by R. S. Wadhwa

## LOW-TEMPERATURE MAGNETISM

### Description of critical behavior of Ising ferromagnet in the $\rho^6$ model approximation taking into account confluent correction. I. Region above the phase transition point

I. V. Pylyuk

*Institute for Condensed Matter Physics, National Academy of Sciences of the Ukraine, 290011 Lviv, Ukraine\**

(Submitted December 15, 1998; revised June 9, 1999)

Fiz. Nizk. Temp. **25**, 1170–1185 (November 1999)

The behavior of a 3D Ising system at temperatures above  $T_c$  is studied in the approximation of sextic distribution for modes of spin moment density oscillations ( $\rho^6$  model). An original method is developed in this higher non-Gaussian approximation for calculating the thermodynamic characteristics of the 3D Ising model near  $T_c$  taking into account the first confluent correction. The contributions to the thermodynamic functions of an Ising ferromagnet (free energy, entropy, internal energy, and specific heat) from the short-wave and long-wave modes of spin density oscillations are considered separately. A nonuniversal factor determined by microscopic characteristics of the system is singled out in the expressions for leading critical amplitudes and the amplitudes of the confluent correction. Numerical estimates of the critical region size, phase transition temperature, leading critical amplitudes, and the amplitudes of the correction to scaling of specific heat and susceptibility of the system are given for different values of effective radius of the exponentially decreasing interaction potential. © 1999 American Institute of Physics. [S1063-777X(99)00511-3]

#### INTRODUCTION

The description of phase transitions and critical phenomena, i.e., the construction of a microscopic theory of phase transitions is a fundamental problem in physics. It includes a wide range of questions associated with the study of physical systems such as liquids, ferromagnets and ferroelectrics, binary alloys, polymers, and liquid crystals. Phase transitions are considered in low-temperature physics, solid-state physics, physical chemistry, metal physics, and biology. These phenomena are widely used in engineering. Persistent scientific interest to this problem is stimulated by exceptional significance of these phenomena for modern technology, their complexity near the phase transition point, the difficulties of their theoretical description and experimental investigation in view of increasing role of large-scale fluctuations and large relaxation times.

Recent comprehensive and intense studies of phase transitions have made it possible to formulate new concepts revealing the essence of critical phenomena and to develop a powerful mathematical apparatus for their description. The problem mentioned above was considered in a number of monographs and review articles. Most authors studying the theory of phase transitions paid special attention to determining the universality class of the systems, an analysis of symmetry properties irrespective the characteristics of the initial Hamiltonian, the types of solutions of recurrence relations (RR), and the calculation of critical exponents. Important experimental results have been obtained in this field. Universal ratios and combinations of critical amplitudes of thermo-

dynamic characteristics of spin systems, including the 3D Ising model (which is a key model of phase transition) are calculated. The problem of dependence of critical amplitudes on the microscopic characteristics of the system required a consistent analysis and could be solved successfully together with the main problem in the theory of phase transitions, i.e., derivation of explicit expressions for thermodynamic characteristics of the system near the phase transition point as functions of temperature and microscopic characteristics. Considerable progress in the solution of this problem were made by using the method of collective variables (CV) generalized by Yukhnovskii<sup>1-4</sup> to the case of spin systems. The term collective variables is applied to a special class of variables specific for each individual physical system. The set of CV contains variables associated with order characteristics. For this reason, the phase space of CV is most natural for describing a phase transition. For magnetic systems, the CV  $\rho_{\mathbf{k}}$  are the variables associated with modes of spin moment density oscillations, while the order parameter is associated with the variable  $\rho_0$  in which the subscript "0" corresponds to the peak of the Fourier transform of the interaction potential.

This paper is devoted to statistical description of the main properties of a 3D Ising ferromagnet by the CV method taking into account the microscopic characteristics of the system. The obtained results can be used for interpreting experimental results concerning the behavior of real materials in the vicinity of the second-order phase transition point, and the computational technique proposed here for thermodynamic characteristics can be used for calculating their thermodynamic functions in the critical region. The original

technique developed in this work for computing a one-component spin system may be generalized to the case of a system with an  $n$ -component order parameter (see, for example, Ref. 3). Such an  $n$ -component model for  $n=2$  can be used advantageously for describing a Bose liquid (phase transition in liquid  $^4\text{He}$ ) and a plane rotator.

## 1. BASIC RELATIONS

We consider a three-dimensional Ising model on a simple cubic lattice with period  $c$ . The Hamiltonian of the model has the form

$$H = -\frac{1}{2} \sum_{\mathbf{j}, \mathbf{l}} \Phi(|\mathbf{j}-\mathbf{l}|) \sigma_{\mathbf{j}} \sigma_{\mathbf{l}}, \quad (1)$$

where  $\Phi(|\mathbf{j}-\mathbf{l}|)$  is the potential of interaction of particles at sites  $\mathbf{j}$  and  $\mathbf{l}$ ,  $\sigma_{\mathbf{j}}$  is the operator of the  $z$ -component of spin at the  $\mathbf{j}$ th site, having two eigenvalues  $+1$  and  $-1$ . The interaction potential is an exponentially decreasing function

$$\Phi(r_{\mathbf{j}\mathbf{l}}) = A \exp\left(-\frac{r_{\mathbf{j}\mathbf{l}}}{b}\right). \quad (2)$$

Here  $A$  is a constant,  $r_{\mathbf{j}\mathbf{l}}$  the separation between particles, and  $b$  the radius of effective interaction. For the Fourier transform of the interaction potential, we use the approximation

$$\tilde{\Phi}(k) = \begin{cases} \tilde{\Phi}(0)(1-2b^2k^2), & k \leq B', \\ 0, & B' < k \leq B, \end{cases} \quad (3)$$

where  $B$  is the boundary of Brillouin half-zone ( $B = \pi/c$ ),  $B' = (b\sqrt{2})^{-1}$ ,  $\tilde{\Phi}(0) = 8\pi A(b/c)^3$ .

We shall use here the method of collective variables (CV),<sup>3</sup> which allows us to calculate approximately the expression for partition function and to obtain, in addition to universal quantities (critical exponents), complete expressions for thermodynamic functions near the phase transition temperature  $T_c$ .

In the CV representation for the partition function of the 3D Ising model, we have

$$Z = \int \exp\left[\frac{1}{2} \sum_{\mathbf{k}} \beta \tilde{\Phi}(k) \rho_{\mathbf{k}} \rho_{-\mathbf{k}}\right] J(\rho) (d\rho)^N. \quad (4)$$

Here the summation over the wave vectors  $\mathbf{k}$  is carried out within the first Brillouin zone,  $\beta = 1/(kT)$  is the reciprocal thermodynamic temperature, and the CV  $\rho_{\mathbf{k}}$  are introduced with the help of relations of the type of an analytic functional for operators of spin moment density oscillation modes

$$\begin{aligned} \hat{\rho}_{\mathbf{k}} &= (\sqrt{N})^{-1} \sum_{\mathbf{l}} \sigma_{\mathbf{l}} \exp(-i\mathbf{k}\cdot\mathbf{l}), \\ J(\rho) &= 2^N \int \exp\left[2\pi i \sum_{\mathbf{k}} \omega_{\mathbf{k}} \rho_{\mathbf{k}} + \sum_{n=1}^{\infty} (2\pi i)^{2n} N^{1-n} \right. \\ &\quad \left. \times \frac{\mathcal{M}_{2n}}{(2n)!} \sum_{\mathbf{k}_1, \dots, \mathbf{k}_{2n}} \omega_{\mathbf{k}_1} \dots \omega_{\mathbf{k}_{2n}} \delta_{\mathbf{k}_1 + \dots + \mathbf{k}_{2n}}\right] (d\omega)^N \end{aligned} \quad (5)$$

is the Jacobian of transition from the set  $N$  spin variables  $\sigma_{\mathbf{l}}$  to the set of CV  $\rho_{\mathbf{k}}$ , and  $\delta_{\mathbf{k}_1 + \dots + \mathbf{k}_{2n}}$  is the Kronecker symbol. The variables  $\omega_{\mathbf{k}}$  are conjugate to  $\rho_{\mathbf{k}}$ , and cumulants  $\mathcal{M}_{2n}$  assume constant values (see Ref. 3). The expression for the partition function (4) cannot be calculated exactly due to the presence of an infinitely large number of terms in the exponent (5). For this reason, approximations limiting the number of terms in the exponent of the integrand in (5) are used. A certain approximation of the integrand in the expression for  $J(\rho)$  determines the choice of the model for calculating the explicit form of the Jacobian of the transition (models  $\rho^4$ ,  $\rho^6$ , etc.). For  $n=1$ , we obtain the Gaussian approximation. It leads to classical values of critical exponents. An important condition in describing the critical properties of the Ising model is the use of non-Gaussian densities of measures. The simplest approximation permitting an analysis beyond the classical behavior corresponds to  $n=2$  and is based on quartic density of measure ( $\rho^4$  model). This approximation is used for calculating basic critical exponents of thermodynamic characteristics, complete expressions for these characteristics taking into account confluent corrections, and for analyzing the relation for critical amplitudes (see, for example, Refs. 5–7). In view of approximate calculation of partition function confined to the  $\rho^4$  model, the obtained results (critical exponents, amplitudes, and thermodynamic functions) contain a certain dependence on the renormalization group (RG) parameter  $s$ . This dependence becomes much weaker as the form of the non-Gaussian density of measure becomes more complicated (transition to more complicated models  $\rho^6$  [ $n=3$ , see (5)],  $\rho^8$ , and  $\rho^{10}$ ). This is confirmed by an analysis of the behavior of the critical exponent of correlation length  $\nu$  for the models  $\rho^{2m}$  ( $m=3,4,5$ )<sup>8–12</sup> as well as by a direct comparison of the curves describing the temperature dependences of thermodynamic characteristics calculated in the models  $\rho^4$  and  $\rho^6$  for various values of the parameter  $s$ .<sup>13,14</sup> The dependence of the results of calculations on the parameter  $s$  is studied and quite controllable. For each of the  $\rho^{2m}$  models, there exists a preferred value of the parameter  $s = s^*$  ( $s^* = 3.5862$  for the  $\rho^4$  model,  $s^* = 2.7349$  for the  $\rho^6$  model,  $s^* = 2.6511$  for the  $\rho^8$  model, and  $s^* = 2.6108$  for the  $\rho^{10}$  model) nullifying the average value of the coefficient in the term with the second power of the effective density of measure at a fixed point. The values of  $s$  close to  $s^*$  are optimal for the given method of calculations. The difference form of RR between the coefficients of effective non-Gaussian densities of measures (expansions for the functions appearing in these relations) operates successfully just in this region of  $s$ . For such definite methods of division of the phase space of CV into layers (values of  $s$  close to  $s^*$ ), we obtain reliable results matching with the experimental data and the results of theoretical investigations.<sup>3,13,14</sup> In this paper, the results of calculations based on the  $\rho^6$  model taking into account the sextic density of measure while integrating the partition function are given for values of  $s$  equal to 2, 2.7349, and 3 (i.e., optimal values for the given method of calculations).

In our earlier publication,<sup>15</sup> we proposed a new method of calculation of the equation of state of a 3D Ising system on microscopic level in the approximation of the above-

mentioned  $\rho^6$  model, which attracts the attention of many scientists even today (see, for example, Ref. 16 in which the equation of state for systems of universality class of the 3D Ising model is analyzed by using the field-theory approach with RG technique). The correctness of the choice of the  $\rho^6$  model for investigations is confirmed in Ref. 17 where the effective potential is studied for the scalar field theory in three dimensions in symmetric phase. In this case, probabilistic distributions of average magnetization in the 3D Ising model in an external field obtained with the help of the Monte Carlo method were used. Tsy-pin<sup>17</sup> proved that the term with the sixth power of the variable in the effective potential plays an important role. The values of universal four- and six-point coupling constants were calculated. Dimensionless six- and eight-point effective coupling constants were calculated by Sokolov *et al.*<sup>18</sup> in the three-loop approximation.

In this paper, the  $\rho^6$  model is used for developing the method of calculation of expressions for thermodynamic functions of the 3D Ising system taking into account the terms determining the correction to scaling. The calculations are made above the phase transition temperature  $T_c$  (high-temperature range). The obtained expressions for basic critical amplitudes and the amplitudes of the first confluent correction make it possible to analyze their dependence on microscopic characteristics of the system (the range  $b$  of potential and the lattice constant  $c$ ).

We shall proceed from the expression for partition function in the approximation of the  $\rho^6$  model. Putting  $n=3$  in (5) and carrying out integration in (4) with respect to the variables  $\rho_{\mathbf{k}}$  and  $\omega_{\mathbf{k}}$  with indices  $B' < k \leq B$ , followed by the integration with respect to  $N'$  variables  $\omega_{\mathbf{k}}$ , we obtain

$$\begin{aligned}
 Z &= 2^{N'} 2^{(N'-1)/2} e^{a'_0 N'} \\
 &\times \int \exp \left[ -\frac{1}{2} \sum_{k \leq B'} d'(k) \rho_{\mathbf{k}} \rho_{-\mathbf{k}} \right. \\
 &\left. - \sum_{l=2}^3 \frac{a'_{2l}}{(2l)!(N')^{l-1}} \right. \\
 &\left. \times \sum_{k_1, \dots, k_{2l} \leq B'} \rho_{\mathbf{k}_1} \dots \rho_{\mathbf{k}_{2l}} \delta_{\mathbf{k}_1 + \dots + \mathbf{k}_{2l}} \right] (d\rho)^{N'}. \quad (6)
 \end{aligned}$$

Here  $N' = N s_0^{-3}$ ,  $s_0 = B/B' = \pi\sqrt{2}b/c$ , and

$$d'(k) = a'_2 - \beta \tilde{\Phi}(k). \quad (7)$$

The coefficients  $a'_{2l}$  are defined as

$$\begin{aligned}
 a'_0 &= \ln Q(\mathcal{M}), \quad Q(\mathcal{M}) = (12s_0^3)^{1/4} \pi^{-1} I_0(\eta', \xi'), \\
 a'_2 &= (12s_0^3)^{1/2} F_2(\eta', \xi'), \\
 a'_4 &= 12s_0^3 C(\eta', \xi'), \\
 a'_6 &= (12s_0^3)^{3/2} N(\eta', \xi')
 \end{aligned} \quad (8)$$

and are functions of  $s_0$ , i.e., of the ratio  $b/c$  (see Table I). In this expressions, the role of the arguments is played by the quantities

TABLE I. Values of coefficients  $a'_{2l}$  for various  $b$ .

$b$	$a'_0$	$a'_2$	$a'_4$	$a'_6$
$b_I$	-1.0196	0.7023	0.2212	0.4379
$b_{II}$	-0.9863	0.7820	0.2163	0.3895
$b_{III}$	-0.9764	0.8083	0.2086	0.3547
$c$	-0.9218	0.9887	0.0220	0.0031
$2c$	-0.9193	0.9986	0.0028	0.0000
$5c$	-0.9190	0.9999	0.0002	0.0000
$7c$	-0.9189	1.0000	0.0000	0.0000

$$\eta' = \sqrt{3} s_0^{3/2}, \quad \xi' = \frac{8\sqrt{3}}{15 s_0^{3/2}}. \quad (9)$$

The special function  $C(\eta', \xi')$  and  $N(\eta', \xi')$  have the form

$$\begin{aligned}
 C(\eta', \xi') &= -F_4(\eta', \xi') + 3F_2^2(\eta', \xi'), \\
 N(\eta', \xi') &= F_6(\eta', \xi') - 15F_4(\eta', \xi')F_2(\eta', \xi') \\
 &\quad + 30F_2^3(\eta', \xi'), \quad (10)
 \end{aligned}$$

where

$$\begin{aligned}
 F_{2l}(\eta', \xi') &= I_{2l}(\eta', \xi') / I_0(\eta', \xi'), \\
 I_{2l}(\eta', \xi') &= \int_0^\infty t^{2l} \exp(-\eta' t^2 - t^4 - \xi' t^6) dt. \quad (11)
 \end{aligned}$$

It can be seen from Table I that  $a'_2 \rightarrow 1$  for  $b \gg c$ ,  $a'_{2l} \rightarrow 0$  for  $l \geq 2$ , and the integrand in formula (6) has a form close to the Gaussian distribution. In the case when the range of the potential and the lattice constant are commensurate, the coefficients  $a'_{2l}$  differ from zero for all values of  $l \geq 0$ , and we must take into account in the exponent of the integrand in (6) the terms proportional to higher degrees of the variable  $\rho_{\mathbf{k}}$  in addition to the Gaussian terms. Henceforth, we shall consider just this case. The value of  $b = b_I = c/(2\sqrt{3})$  corresponds to the interaction between nearest neighbors,  $b = b_{II} = 0.3379c$  to the interaction between the nearest and next-nearest neighbors, and  $b = b_{III} = 0.3584c$  to the nearest, next-nearest, and third neighbors.<sup>19</sup>

The increase in the number of terms in expressions (5) and (6) corresponds to a complication of the form of the non-Gaussian density of measure (complication of the model). Critical phenomena in a 3D Ising ferromagnet in the CV method can be described quantitatively even in the  $\rho^6$  model approximation. The confinement to the quartic approximation in formulas (5) and (6) allows us to go beyond the classical analysis and to describe all qualitative aspects of the second-order phase transition, while the sextic approximation ensures a more adequate quantitative description of the critical properties of a spin system. This is confirmed by calculations as well as an analysis of the behavior of the coefficients in the initial expression for partition function and the critical exponent of the correlation length  $\nu$  for the sequence of  $\rho^4$ ,  $\rho^6$ ,  $\rho^8$ , and  $\rho^{10}$  models<sup>3,8-12</sup> as well as by the calculation and comparison of thermodynamic functions for the models<sup>13,14</sup>  $\rho^4$  and  $\rho^6$  and by comparison of the results of our calculations with other available data (see, for example, Refs. 13 and 14). The analysis of the above-mentioned

sequence of the model was necessary for estimating the convergence of the procedure for calculating the critical exponent  $\nu$ , for finding its dependence on the RG parameter  $s$ , and for establishing whether it is expedient to use higher densities of measures. It was found that as the form of the density of measure becomes more complicated, the dependence of the critical exponent  $\nu$  on the RG parameter  $s$  becomes weaker gradually, and starting from the sextic density of measure, the value of the exponent  $\nu$ , having a tendency to saturation with increasing  $m$  (which characterizes the order of the  $\rho^{2m}$  model or determines the summation limit in formula (5),  $m=2,3,4,5$ ) changes insignificantly. It is also interesting that the numerical values of the coefficients  $a'_{2l}$  appearing for  $m \geq 3$ , in the partition function (relations similar to (8) and (6)) vary insignificantly upon an increase in the order of the density of measure, i.e., upon an increase in the number of terms in (5).

An advantage of the CV method in the description of phase transitions is the presence of a variable associated with the order parameter among the CV  $\rho_{\mathbf{k}}$ . Such a variable for the Ising model is  $\rho_0$ . We cannot single out the contribution from  $\rho_0$  alone in expression (6) since all the variables  $\rho_{\mathbf{k}}$  are interconnected. We shall use the method of ‘‘layer-by-layer’’ integration of (6) with respect to variables  $\rho_{\mathbf{k}}$  proposed by Yukhnovskii.<sup>3</sup> The integration begins from the variables  $\rho_{\mathbf{k}}$  with a large value of  $k$  (of the order of the Brillouin half-zone boundary) and terminates at  $\rho_{\mathbf{k}}$  with  $k \rightarrow 0$ . For this purpose, we divide the phase space of the CV  $\rho_{\mathbf{k}}$  into layers with the division parameter  $s$ . In each  $n$ th layer (corresponding to the region of wave vectors  $B_{n+1} < \mathbf{k} \leq B_n$ ,  $B_{n+1} = B_n/s$ ,  $s > 1$ ), the Fourier transform of the potential  $\Phi(k)$  is replaced by its average value (arithmetic mean in the given case). As a result of step-by-step calculation of partition function, the number of integration variables in the expression for this quantity decreases gradually. After the integration over  $n+1$  layers of the CV space, we obtain

$$Z = 2^N 2^{(N_{n+1}-1)/2} Q_0 Q_1 \dots Q_n [Q(P_n)]^{N_{n+1}} \times \int \mathcal{W}_6^{(n+1)}(\rho) (d\rho)^{N_{n+1}}. \tag{12}$$

Here  $N_{n+1} = N' s^{-3(n+1)}$ , and

$$\begin{aligned} Q_0 &= [e^{a'_0} Q(d)]^{N'}, \quad Q_1 = [Q(P) Q(d_1)]^{N_1}, \dots, \\ Q_n &= [Q(P_{n-1}) Q(d_n)]^{N_n}, \\ Q(d_n) &= 2(24/a_4^{(n)})^{1/4} I_0(h_n, \alpha_n), \\ Q(P_n) &= \pi^{-1} [s^3 a_4^{(n)} / C(h_n, \alpha_n)]^{1/4} I_0(\eta_n, \xi_n). \end{aligned} \tag{13}$$

The basic arguments

$$h_n = d_n(B_{n+1}, B_n) \left( \frac{6}{a_4^{(n)}} \right)^{1/2}, \quad \alpha_n = \frac{\sqrt{6}}{15} \frac{a_6^{(n)}}{(a_4^{(n)})^{3/2}} \tag{14}$$

are determined by the mean value of the coefficient  $d_n(k)$  in the  $n$ th layer of the phase space of CV, i.e., by  $d_n(B_{n+1}, B_n)$  as well as the quantities  $a_4^{(n)}$  and  $a_6^{(n)}$ . The effective sextic density of measure of the  $(n+1)$ th block structure  $\mathcal{W}_6^{(n+1)}(\rho)$  has the form

$$\begin{aligned} \mathcal{W}_6^{(n+1)}(\rho) &= \exp \left[ -\frac{1}{2} \sum_{\mathbf{k} \leq B_{n+1}} d_{n+1}(k) \rho_{\mathbf{k}} \rho_{-\mathbf{k}} \right. \\ &\quad \left. - \sum_{l=2}^3 \frac{a_{2l}^{(n+1)}}{(2l)! N_{n+1}^{l-1}} \right. \\ &\quad \left. \times \sum_{k_1, \dots, k_{2l} \leq B_{n+1}} \rho_{\mathbf{k}_1} \dots \rho_{\mathbf{k}_{2l}} \delta_{\mathbf{k}_1 + \dots + \mathbf{k}_{2l}} \right]. \end{aligned} \tag{15}$$

Here  $B_{n+1} = B' s^{-(n+1)}$ ,  $d_{n+1}(k) = a_2^{(n+1)} - \beta \Phi(k)$ ,  $a_{2l}^{(n+1)}$  are renormalized values of the coefficients  $a'_{2l}$  after integration over  $n+1$  layers of the phase space of CV. The intermediate variables  $\eta_n$ ,  $\xi_n$  are functions of  $h_n$  and  $\alpha_n$  and are defined as

$$\begin{aligned} \eta_n &= (6s^3)^{1/2} F_2(h_n, \alpha_n) [C(h_n, \alpha_n)]^{-1/2}, \\ \xi_n &= \frac{\sqrt{6}}{15} s^{-3/2} N(h_n, \alpha_n) [C(h_n, \alpha_n)]^{3/2}, \end{aligned} \tag{16}$$

where the form of the special functions  $C(h_n, \alpha_n)$  and  $N(h_n, \alpha_n)$  is defined in (10). The coefficients  $d_n(B_{n+1}, B_n)$ ,  $a_4^{(n)}$ , and  $a_6^{(n)}$  are connected with the coefficients for the  $n+1$ th layer through the recurrence relations (RR)<sup>11,20,21</sup> whose solutions<sup>15,21</sup> are used for calculating the free energy of the system.

The basic idea of the calculation of explicit expressions for free energy and other thermodynamic functions of the system near  $T_c$  on microscopic level ( $\tau < \tau^* \sim 10^{-2}$ ,  $\tau = (T - T_c)/T_c$ ) lies in the separate inclusion of contributions from short-wave and long-wave modes of spin moment density oscillations.<sup>3,5,22</sup>

Short-wave modes are characterized by a RG symmetry and are described by a non-Gaussian density of measure. They correspond to the region of critical regime (CR) observed above as well as below  $T_c$ . In this case, the RG method is used (see, for example, Ref. 23). The calculation of the expression describing the contribution from short-wave modes of spin moment density oscillations to free energy involves the summation of partial free energies over the layers of the phase space of CV up to the point at which the system leaves the CR region. In this case, it is important to obtain an explicit dependence on the number of the layer. For this purpose the solutions of RR are used. Taking into account the larger eigenvalue ( $E_1 > 1$ ) of the RG linear transformation matrix, we can describe the main singularity for specific heat near  $T_c$ . Smaller eigenvalues ( $E_2 < 1$  and  $E_3 < 1$ ) are responsible for the emergence of corrections to scaling. The inclusion of short-wave modes of spin density oscillations leads to a renormalization of the dispersion of the distribution describing long-wave modes. For  $T > T_c$ , these modes correspond to the region of limiting Gaussian regime (LGR). The way in which the contribution from long-wave modes of oscillations to free energy of the system is taken into account differs qualitatively from the method of calculating the short-wave component of the partition function. The calculation of this contribution is based on the use of the Gaussian density of measure as the basis density. We

TABLE II. Values of  $n_0$  and  $\tau^*$  for large values of the interaction potential range  $b$  and the RG parameter  $s=3$ .

$b$	$n_0$	$\tau^*$
$4c$	7	$0.8266 \times 10^{-8}$
$5c$	8	$0.6274 \times 10^{-9}$
$7c$	9	$0.4680 \times 10^{-10}$

have developed a direct method of calculations with the results obtained by taking into account the short-wave modes as initial parameters.

It should be noted that our calculations are valid in a small neighborhood of  $T_c$ . The solutions of RR make it possible to calculate the size of this critical region. Indeed, using these solutions and the conditions for the existence of CR (the exit from this regime for  $n \rightarrow 1$ , described by terms proportional to  $E_1^n$ , does not prevail over the entry to this regime, which is described by terms proportional to,  $E_2^n$  and  $E_3^n$ ), we can determine the temperature range  $\tau < \tau^*$  in which the CR corresponding to the presence of strongly correlated spin blocks takes place. The value of  $\tau^*$  is equal to the magnitude of the smallest root of the three equations obtained on the basis of solutions of RR. The value of  $\tau^*$  determined in this way is of the order of a few hundredths for commensurate  $b$  and  $c$ . For large values of  $b$ , it is important to take correctly into account the entry in the CR. In this case, the value of  $\tau^*$  can be obtained by imposing the condition that the entry to CR prevails over the exit from this regime for  $n \rightarrow n_0$ , where the layer number  $n_0$  as a function of  $b$  can be determined from RR,<sup>11,20,21</sup> for example, proceeding from the relation for  $a_4^{(n)}$  (see Table II). The data contained in Table II show that the critical region is practically absent for large  $b$ . This is not surprising since the condition  $b \gg c$  corresponds to the transition to the model with long-range interaction, which is based on the Gaussian distribution of spin moment density oscillation modes (see (6) and Table I) and demonstrates the classical critical behavior.

Calculating separately the contributions  $F_{CR}$  and  $F_{LGR}$  to free energy from short-wave and long-wave modes of spin moment density oscillations at  $T > T_c$ , we can obtain the complete expression for the free energy of the system:

$$F = F_0 + F_{CR} + F_{LGR}. \quad (17)$$

Here  $F_0 = -kTN \ln 2$  is the free energy of  $N$  noninteracting spins. Let us calculate the contributions  $F_{CR}$  and  $F_{LGR}$ .

## 2. CALCULATION OF CONTRIBUTION FROM SHORT-WAVE MODES OF SPIN MOMENT DENSITY OSCILLATIONS TO THERMODYNAMIC FUNCTIONS OF THE SYSTEM

It is convenient to write the partition function of the model in the form<sup>13,14,24</sup>

$$Z = 2^N Z_{CR} Z_{LGR}, \quad (18)$$

where the first factor corresponds to noninteracting spins. The quantity  $Z_{CR}$  describes the contribution of short-wave fluctuations of  $\rho_{\mathbf{k}}$  with  $k \in [B_{m_\tau}, B']$  (the CR region). The number  $m_\tau$  of the layer in the CV space appearing in the expression  $B_{m_\tau} = B' s^{-m_\tau}$ , and characterizing the point of the

exit of the system from the CR  $m_\tau$ , will be defined later. The factor  $Z_{LGR}$  contains contributions from long-wave fluctuations with  $k \in [0, B_{m_\tau}]$  and corresponds to the LGR.

Let us consider the quantity  $Z_{CR}$ . It is defined as

$$Z_{CR} = \prod_{n=0}^{m_\tau} \left[ \frac{2}{\pi} \left( \frac{24}{C(\eta_{n-1}, \xi_{n-1})} \right)^{1/4} \times I_0(h_n, \alpha_n) I_0(\eta_{n-1}, \xi_{n-1}) \right]^{N_n}. \quad (19)$$

In order to calculate  $Z_{CR}$ , we must present the right-hand side of formula (19) in the form of an explicit function of the layer number  $n$ . It should be noted that  $\eta_{-1} \equiv \eta'$  and  $\xi_{-1} \equiv \xi'$  in (19) for  $n=0$ . In the CR region, the basic  $(h_n, \alpha_n)$  and intermediate  $(\eta_n, \xi_n)$  arguments are close to their values at a fixed point  $h^{(0)}, \alpha^{(0)}$  and  $\eta^{(0)}, \xi^{(0)}$ . Consequently, the functions of these arguments can be approximated in this case by power series in deviations of these arguments from their fixed values.<sup>25</sup> Intermediate arguments and their functions can be presented in terms of deviations of the basic arguments from their values at a fixed point. Using the relations for  $I_0(h_n, \alpha_n)$ ,  $I_0(\eta_{n-1}, \xi_{n-1})$ ,  $C(\eta_{n-1}, \xi_{n-1})$  taking into account the squares of deviations of basic arguments,<sup>13,25</sup> we calculate from (19) the free energy corresponding to the  $n$ th phase layer:

$$F_n = -kTN_n [f_{CR}^{(0)} + \varphi_1(h_{n-1} - h^{(0)}) + \varphi_2(\alpha_{n-1} - \alpha^{(0)}) + \varphi_3(h_n - h^{(0)}) + \varphi_4(\alpha_n - \alpha^{(0)}) + \varphi'_1(h_{n-1} - h^{(0)})^2 + \varphi'_2(\alpha_{n-1} - \alpha^{(0)})^2 + \varphi'_3(h_n - h^{(0)})^2 + \varphi'_4(\alpha_n - \alpha^{(0)})^2 + \varphi'_5(h_{n-1} - h^{(0)})(\alpha_{n-1} - \alpha^{(0)}) + \varphi'_6(h_n - h^{(0)})(\alpha_n - \alpha^{(0)})], \quad (20)$$

$$f_{CR}^{(0)} = \ln \left( \frac{2(24)^{1/4}}{\pi} \right) - (1/4) \ln P_{40} + \ln I_0^* + \ln I_0^{**},$$

$$\varphi_k = b_k + P_{4k}/4, \quad k=1,2,$$

$$\varphi_3 = -F_2^*, \quad \varphi_4 = -F_6^*,$$

$$\varphi'_k = b'_k - \frac{1}{2} b_k^2 - P'_{4k}/4 + P_{4k}^2/8,$$

$$\varphi'_3 = F_4^*/2 - F_2^{*2}/2, \quad \varphi'_4 = F_{12}^*/2 - F_6^{*2}/2,$$

$$\varphi'_5 = b'_3 - b_1 b_2 - P'_{43}/4 + P_{41} P_{42}/4,$$

$$\varphi'_6 = F_8^* - F_2^* F_6^*.$$

The quantities appearing in  $f_{CR}^{(0)}$ ,  $\varphi_i$ , and  $\varphi'_i$  are ultimately functions of the basic arguments at a fixed point. They are given in the above-mentioned publications.<sup>13,25</sup>

The partial free energy of the  $n$ th layer of the phase space of CV taking into account the explicit dependence on  $n$  can be written in the form

$$F_n = -kTN' s^{-3n} [f_{CR}^{(0)} + f_{CR}^{(1)}(u^{(0)})^{-1/2} c_1 E_1^n + f_{CR}^{(2)} \times (u^{(0)})^{-1} c_2 E_2^n + f_{CR}^{(3)}(u^{(0)})^{-3/2} c_3 E_3^n + f_{CR}^{(4)} \times (u^{(0)})^{-3/2} c_1 c_2 E_1^n E_2^n + f_{CR}^{(5)}(u^{(0)})^{-5/2} c_1 c_2^2 E_1^n E_2^{2n}]$$

$$\begin{aligned}
 &+ f_{\text{CR}}^{(6)}(u^{(0)})^{-2}c_2^2E_2^{2n} + f_{\text{CR}}^{(7)}(u^{(0)})^{-1}c_1^2E_1^{2n} + f_{\text{CR}}^{(8)} \\
 &\times (u^{(0)})^{-2}c_1^2c_2E_1^{2n}E_2^n + f_{\text{CR}}^{(9)}(u^{(0)})^{-3} \\
 &\times c_1^2c_2^2E_1^{2n}E_2^{2n}. \tag{21}
 \end{aligned}$$

Here

$$\begin{aligned}
 f_{\text{CR}}^{(k)} &= H_k(\varphi_3 + \varphi_1/E_k) + L_k(\varphi_4 + \varphi_2/E_k), \quad k=1,2,3, \\
 f_{\text{CR}}^{(4)} &= H_4[\varphi_3 + \varphi_1/(E_1E_2)] + L_4[\varphi_4 + \varphi_2/(E_1E_2)] \\
 &+ 2H_1H_2[\varphi'_3 + \varphi'_1/(E_1E_2)] + 2L_1L_2[\varphi'_4 \\
 &+ \varphi'_2/(E_1E_2)] + (H_1L_2 + H_2L_1)[\varphi'_6 \\
 &+ \varphi'_5/(E_1E_2)], \\
 f_{\text{CR}}^{(5)} &= H_5[\varphi_3 + \varphi_1/(E_1E_2^2)] + L_5[\varphi_4 + \varphi_2/(E_1E_2^2)] \\
 &+ 2(H_1H_6 + H_2H_4)[\varphi'_3 + \varphi'_1/(E_1E_2^2)] + 2(L_1L_6 \\
 &+ L_2L_4)[\varphi'_4 + \varphi'_2/(E_1E_2^2)] + (H_1L_6 + H_6L_1 \\
 &+ H_2L_4 + H_4L_2)[\varphi'_6 + \varphi'_5/(E_1E_2^2)], \\
 f_{\text{CR}}^{(6)} &= H_6(\varphi_3 + \varphi_1/E_2^2) + L_6(\varphi_4 + \varphi_2/E_2^2) + H_2^2(\varphi'_3 \\
 &+ \varphi'_1/E_2^2) + L_2^2(\varphi'_4 + \varphi'_2/E_2^2) + H_2L_2(\varphi'_6 + \varphi'_5/E_2^2), \\
 f_{\text{CR}}^{(7)} &= H_7(\varphi_3 + \varphi_1/E_1^2) + L_7(\varphi_4 + \varphi_2/E_1^2) + H_1^2(\varphi'_3 \\
 &+ \varphi'_1/E_1^2) + L_1^2(\varphi'_4 + \varphi'_2/E_1^2) + H_1L_1(\varphi'_6 + \varphi'_5/E_1^2), \\
 f_{\text{CR}}^{(8)} &= H_8[\varphi_3 + \varphi_1/(E_1^2E_2)] + L_8[\varphi_4 + \varphi_2/(E_1^2E_2)] \\
 &+ 2(H_1H_4 + H_2H_7)[\varphi'_3 + \varphi'_1/(E_1^2E_2)] + 2(L_1L_4 \\
 &+ L_2L_7)[\varphi'_4 + \varphi'_2/(E_1^2E_2)] + (H_1L_4 + H_4L_1 \\
 &+ H_2L_7 + H_7L_2)[\varphi'_6 + \varphi'_5/(E_1^2E_2)], \\
 f_{\text{CR}}^{(9)} &= H_9[\varphi_3 + \varphi_1/(E_1E_2)^2] + L_9[\varphi_4 + \varphi_2/(E_1E_2)^2] \\
 &+ (2H_1H_5 + 2H_2H_8 + H_4^2 + 2H_6H_7)[\varphi'_3 \\
 &+ \varphi'_1/(E_1E_2)^2] + (2L_1L_5 + 2L_2L_8 + L_4^2 + 2L_6L_7) \\
 &\times [\varphi'_4 + \varphi'_2/(E_1E_2)^2] + (H_1L_5 + H_5L_1 + H_2L_8 \\
 &+ H_8L_2 + H_4L_4 + H_6L_7 + H_7L_6)[\varphi'_6 \\
 &+ \varphi'_5/(E_1E_2)^2]. \tag{22}
 \end{aligned}$$

The expressions for the quantities  $H_i$  and  $L_i$  are given in Refs. 13, 14, and 26 for three coordinates of the fixed point (including  $u^{(0)}$ ), and the coefficients of the solutions of RR

$$c_1 = \tilde{c}_1 \beta \tilde{\Phi}(0) \tau, \quad c_2 = c_{20} [\beta \tilde{\Phi}(0)]^2, \quad c_3 = c_{30} [\beta \tilde{\Phi}(0)]^3,$$

where  $\tilde{c}_1 = \tilde{c}_1^{(0)} + \tilde{c}_1^{(1)} \tau$ ,  $c_{20} = c_{20}^{(0)} + c_{20}^{(1)} \tau + c_{20}^{(2)} \tau^2$ ,  $c_{30} = c_{30}^{(0)} + c_{30}^{(1)} \tau + c_{30}^{(2)} \tau^2$ , are given in Refs. 21, 24 and 26. It should be emphasized that a typical feature of the solutions of RR is a specific temperature dependence of the coefficient  $c_1$ . On the basis of the expression for  $c_1$ , we obtain an equation for the quantity  $\beta_c \tilde{\Phi}(0)$  determining the phase transition temperature (see Ref. 21). The dependence of  $\beta_c A$  [ $A$  is the

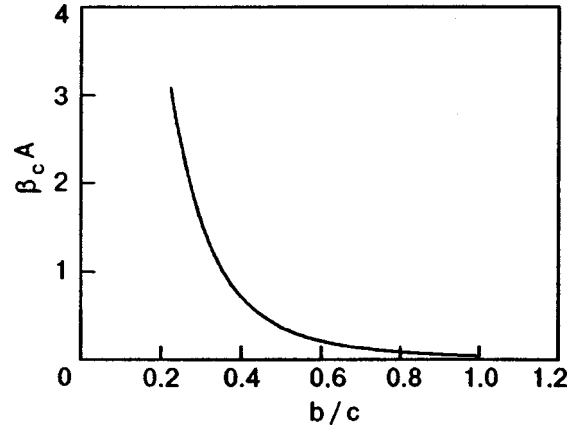


FIG. 1. Dependence of reciprocal phase transition temperature on the ratio of the interaction potential range to the lattice constant.

constant appearing in the interaction potential (2)] on the ratio of the potential range  $b$  to the lattice constant  $c$  is shown in Fig. 1 for  $s=3$ .

Thus, the partial free energy  $F_n$  of the  $n$ th layer contains the term  $f_{\text{CR}}^{(0)}$  which is independent on the number  $n$  of the layer and is a universal quantity, and the terms containing the dependence on  $n$ . In contrast to  $f_{\text{CR}}^{(0)}$ , these terms depend on microscopic characteristics of the Hamiltonian of the system.

Carrying out summations of expression (21) for  $F_n$  over the layers of the phase space of CV, we can calculate  $F_{\text{CR}}$ :

$$F_{\text{CR}} = F'_0 + F'_{\text{CR}}, \tag{23}$$

$$F'_0 = -kTN'[\ln Q(\mathcal{M}) + \ln Q(d)],$$

$$F'_{\text{CR}} = \sum_{n=1}^{m_\tau} F_n.$$

The layer number  $m_\tau$  determining the point of exit of the system from the CR region at  $T > T_c$  can be found from the condition<sup>15,26</sup>

$$\frac{r_{m_\tau+1} - r^{(0)}}{r^{(0)}} = -\delta, \tag{24}$$

where  $\delta$  is a constant ( $\delta \ll 1$ ),  $r^{(0)}$  is a coordinate of the fixed point, and  $r_n$  characterizes the coefficient of the sextic density of measure of the  $n$ th block structure of the second power of the variable and is determined with the help of solutions of RR (see, for example, Ref. 26). In our numerical calculations, we shall put  $\delta=1$ . In this case,  $r_{m_\tau+1} = 0$  or  $d_{m_\tau+1}(0) = r_{m_\tau+1} s^{-2(m_\tau+1)} = 0$  and the curves  $d_n(k)$  are situated above the abscissa axis for all  $n > m_\tau$ . On the basis of (24), we obtain the explicit form of equation for  $m_\tau$ :

$$\begin{aligned}
 \tilde{c}_1 \tau E_1^{m_\tau+1} &= f_0 \delta - c_{20} w_{12}^{(0)} \varphi_0^{-1/2} E_2^{m_\tau+1} \\
 &- c_{30} w_{13}^{(0)} \varphi_0^{-1} E_3^{m_\tau+1}. \tag{25}
 \end{aligned}$$

The temperature-independent quantities  $w_{12}^{(0)}$  and  $w_{13}^{(0)}$  as well as the quantities  $f_0$  and  $\varphi_0$  characterizing the coordinates of the fixed point  $r^{(0)}$ ,  $u^{(0)}$  are given in Ref. 26. In the region  $\tau \ll 1$ , it is convenient to use the method of successive approximations for solving Eq. (25), taking into account the

fact that  $E_2^{m_\tau+1} \ll 1$  and  $E_3^{m_\tau+1} \ll 1$ . In the zeroth approximation, Eq. (25) can be written in the form of the equation

$$\tilde{c}_1 \tau E_1^{m_\tau^{(0)+1}} = f_0 \delta, \tag{26}$$

whose solution is given by

$$m_\tau^{(0)} = -\frac{\ln \tau}{\ln E_1} + m_0 - 1. \tag{27}$$

Here

$$m_0 = m_c, \quad m_c = \frac{\ln(f_0 \delta / \tilde{c}_1^{(0)})}{\ln E_1}. \tag{28}$$

The first approximation is written taking into account the smallness of terms proportional to  $E_2^{m_\tau+1}$  and  $E_3^{m_\tau+1}$  for which the zeroth approximation is used, i.e., the right-hand side of Eq. (25) contains terms proportional to

$$\begin{aligned} E_2^{m_\tau^{(0)+1}} &= E_2^{m_0} \tau^{\Delta_1}, \quad E_3^{m_\tau^{(0)+1}} = E_3^{m_0} \tau^{\Delta_2}, \\ \tilde{c}_1 \tau E_1^{m_\tau+1} &= f_0 \delta - c_{20} w_{12}^{(0)} \varphi_0^{-1/2} E_2^{m_\tau^{(0)+1}} \\ &\quad - c_{30} w_{13}^{(0)} \varphi_0^{-1} E_3^{m_\tau^{(0)+1}}. \end{aligned} \tag{29}$$

It should be noted that in the right-hand side of this equation we neglect the term proportional to  $E_3^{m_\tau^{(0)+1}}$  since we take into account in these calculations only the first confluent correction (which is determined by the term proportional to  $\tau^{\Delta_1}$ ,  $\Delta_1 = -\ln E_2 / \ln E_1$ ) and disregard the second confluent correction (which is determined by the term proportional to  $\tau^{\Delta_2}$ ,  $\Delta_2 = -\ln E_3 / \ln E_1$ ). This is due to the fact that the contribution from the first confluent correction to thermodynamic functions of the model near  $T_c$  is more significant than the small contribution from the second correction ( $\tau \ll 1$ ,  $\Delta_1$  is of the order of 0.5, and  $\Delta_2 > 2$ , see Refs. 13 and 14). Solving Eq. (29), we obtain

$$m_\tau = m_\tau^{(0)} + m_{\Delta_1} \tau^{\Delta_1}, \tag{30}$$

$$m_{\Delta_1} = \frac{m_2}{\ln E_1}, \quad m_2 = -c_{\Delta_1} \Phi_0,$$

$$c_{\Delta_1} = c_{20}^{(0)} \left( \frac{\tilde{c}_1^{(0)}}{f_0 \delta} \right)^{\Delta_1}, \quad \Phi_0 = \frac{w_{12}^{(0)}}{f_0 \delta \sqrt{\varphi_0}}.$$

It should be emphasized that in a higher-order approximation, Eq. (25) leads to a solution of the type (30), where terms proportional to  $\tau^{2\Delta_1}$ , etc., appear additionally; in the present calculations, we neglect these terms also.

Having obtained expression (30) for  $m_\tau$ , we return to the calculation of expression (23) for  $F_{CR}$ . Taking into account (30) as well as the relations

$$\begin{aligned} E_1^{m_\tau+1} &= \frac{f_0 \delta (1 + m_2 \tau^{\Delta_1})}{\tilde{c}_1 \tau}, \quad E_2^{m_\tau^{(0)+1}} = \left( \frac{\tilde{c}_1^{(0)}}{f_0 \delta} \right)^{\Delta_1} \tau^{\Delta_1}, \\ s^{-3(m_\tau+1)} &= s^{-3(m_\tau^{(0)+1})} (1 + \mathcal{N}_1^+ \tau^{\Delta_1}), \\ s^{-3(m_\tau^{(0)+1})} &= s^{-3m_0} \tau^{3\nu}, \quad s^{-3m_0} = c_\nu^3, \end{aligned}$$

$$c_\nu = \left( \frac{\tilde{c}_1^{(0)}}{f_0 \delta} \right)^\nu, \quad \nu = \frac{\ln s}{\ln E_1},$$

$$\mathcal{N}_1^+ = -3\nu m_2 = 3\nu c_{\Delta_1} \Phi_0, \tag{31}$$

we obtain

$$\begin{aligned} F_{CR} &= -kTN' [\gamma_0 + \delta_0 - \gamma_3^{(CR)(0)+} \tau^{3\nu} \\ &\quad - \gamma_3^{(CR)(1)+} \tau^{3\nu + \Delta_1}], \end{aligned} \tag{32}$$

where

$$\begin{aligned} \gamma_0 &= s^{-3} \left[ \frac{f_{CR}^{(0)}}{1-s^{-3}} + \frac{f_{CR}^{(1)} \varphi_0^{-1/2} \tilde{c}_1 \tau E_1}{1-E_1 s^{-3}} + \frac{f_{CR}^{(2)} \varphi_0^{-1/2} c_{20} E_2}{1-E_2 s^{-3}} \right. \\ &\quad + \frac{f_{CR}^{(3)} \varphi_0^{-3/2} c_{30} E_3}{1-E_3 s^{-3}} + \frac{f_{CR}^{(4)} \varphi_0^{-3/2} \tilde{c}_1 \tau c_{20} E_1 E_2}{1-E_1 E_2 s^{-3}} \\ &\quad + \frac{f_{CR}^{(5)} \varphi_0^{-5/2} \tilde{c}_1 c_{20}^2 \tau E_1 E_2^2}{1-E_1 E_2^2 s^{-3}} + \frac{f_{CR}^{(6)} \varphi_0^{-2} c_{20}^2 E_2^2}{1-E_2^2 s^{-3}} \\ &\quad + \frac{f_{CR}^{(7)} \varphi_0^{-1} \tilde{c}_1^2 \tau^2 E_1^2}{1-E_1^2 s^{-3}} + \frac{f_{CR}^{(8)} \varphi_0^{-2} \tilde{c}_1^2 c_{20}^2 \tau^2 E_1^2 E_2}{1-E_1^2 E_2 s^{-3}} \\ &\quad \left. + \frac{f_{CR}^{(9)} \varphi_0^{-3} \tilde{c}_1^2 c_{20}^2 \tau^2 E_1^2 E_2^2}{1-E_1^2 E_2^2 s^{-3}} \right], \end{aligned} \tag{33}$$

$$\delta_0 = \ln Q(\mathcal{M}) + \ln Q(d),$$

$$\gamma_3^{(CR)(l)+} = c_\nu^3 c_{\Delta_1}^l \bar{\gamma}_3^{(CR)(l)+}, \quad l=0,1,$$

$$\bar{\gamma}_3^{(CR)(0)+} = \gamma^+, \quad \bar{\gamma}_3^{(CR)(1)+} = \gamma_{\Delta_1}^+ - \Phi_0 (\gamma_{11}^+ - 3\nu \gamma^+).$$

Here

$$\begin{aligned} \gamma^+ &= \frac{f_{CR}^{(0)}}{1-s^{-3}} + \frac{f_{CR}^{(1)} \varphi_0^{-1/2} f_0 \delta}{1-E_1 s^{-3}} + \frac{f_{CR}^{(7)} \varphi_0^{-1} (f_0 \delta)^2}{1-E_1^2 s^{-3}}, \\ \gamma_{\Delta_1}^+ &= \frac{f_{CR}^{(2)} \varphi_0^{-1}}{1-E_2 s^{-3}} + \frac{f_{CR}^{(4)} \varphi_0^{-3/2} f_0 \delta}{1-E_1 E_2 s^{-3}} + \frac{f_{CR}^{(8)} \varphi_0^{-2} (f_0 \delta)^2}{1-E_1^2 E_2 s^{-3}}, \\ \gamma_{11}^+ &= \frac{f_{CR}^{(1)} \varphi_0^{-1/2} f_0 \delta}{1-E_1 s^{-3}} + \frac{2 f_{CR}^{(7)} \varphi_0^{-1} (f_0 \delta)^2}{1-E_1^2 s^{-3}}. \end{aligned} \tag{34}$$

Let us single out explicitly the temperature in  $\gamma_0$  and  $\delta_0$  in (33). As a result, we can write for the coefficient  $\gamma_0$

$$\gamma_0 = \gamma_0^{(0)} + \gamma_0^{(1)} \tau + \gamma_0^{(2)} \tau^2, \tag{35}$$

$$\begin{aligned} \gamma_0^{(0)} &= s^{-3} \left[ \frac{f_{CR}^{(0)}}{1-s^{-3}} + \frac{f_{CR}^{(2)} \varphi_0^{-1} c_{20}^{(0)} E_2}{1-E_2 s^{-3}} + \frac{f_{CR}^{(3)} \varphi_0^{-3/2} c_{30}^{(0)} E_3}{1-E_3 s^{-3}} \right. \\ &\quad \left. + \frac{f_{CR}^{(6)} \varphi_0^{-2} (c_{20}^{(0)})^2 E_2^2}{1-E_2^2 s^{-3}} \right], \end{aligned}$$

$$\begin{aligned} \gamma_0^{(1)} = & s^{-3} \left[ \frac{f_{\text{CR}}^{(1)} \varphi_0^{-1/2} \tilde{c}_1^{(0)} E_1}{1 - E_1 s^{-3}} + \frac{f_{\text{CR}}^{(2)} \varphi_0^{-1} c_{20}^{(1)} E_2}{1 - E_2 s^{-3}} \right. \\ & + \frac{f_{\text{CR}}^{(3)} \varphi_0^{-3/2} c_{30}^{(1)} E_3}{1 - E_3 s^{-3}} + \frac{f_{\text{CR}}^{(4)} \varphi_0^{-3/2} \tilde{c}_1^{(0)} c_{20}^{(0)} E_1 E_2}{1 - E_1 E_2 s^{-3}} \\ & + \frac{f_{\text{CR}}^{(5)} \varphi_0^{-5/2} \tilde{c}_1^{(0)} (c_{20}^{(0)})^2 E_1 E_2^2}{1 - E_1 E_2^2 s^{-3}} \\ & \left. + \frac{2 f_{\text{CR}}^{(6)} \varphi_0^{-2} c_{20}^{(0)} c_{20}^{(1)} E_2^2}{1 - E_1 E_2^2 s^{-3}} \right], \\ \gamma_0^{(2)} = & s^{-3} \left[ \frac{f_{\text{CR}}^{(1)} \varphi_0^{-1/2} \tilde{c}_1^{(1)} E_1}{1 - E_1 s^{-3}} + \frac{f_{\text{CR}}^{(2)} \varphi_0^{-1} c_{20}^{(2)} E_2}{1 - E_2 s^{-3}} \right. \\ & + \frac{f_{\text{CR}}^{(3)} \varphi_0^{-3/2} c_{30}^{(2)} E_3}{1 - E_3 s^{-3}} \\ & + \frac{f_{\text{CR}}^{(4)} \varphi_0^{-3/2} [\tilde{c}_1^{(0)} c_{20}^{(1)} + \tilde{c}_1^{(1)} c_{20}^{(0)}] E_1 E_2}{1 - E_1 E_2 s^{-3}} \\ & + \frac{f_{\text{CR}}^{(5)} \varphi_0^{-5/2} [2 \tilde{c}_1^{(0)} c_{20}^{(0)} c_{20}^{(1)} + \tilde{c}_1^{(1)} (c_{20}^{(0)})^2] E_1 E_2^2}{1 - E_1 E_2^2 s^{-3}} \\ & + \frac{f_{\text{CR}}^{(6)} \varphi_0^{-2} [(c_{20}^{(1)})^2 + 2 c_{20}^{(0)} c_{20}^{(2)}] E_2^2}{1 - E_2^2 s^{-3}} \\ & + \frac{f_{\text{CR}}^{(7)} \varphi_0^{-1} (\tilde{c}_1^{(0)})^2 E_1^2}{1 - E_1^2 s^{-3}} + \frac{f_{\text{CR}}^{(8)} \varphi_0^{-2} (\tilde{c}_1^{(0)})^2 c_{20}^{(0)} E_1^2 E_2}{1 - E_1^2 E_2 s^{-3}} \\ & \left. + \frac{f_{\text{CR}}^{(9)} \varphi_0^{-3} [\tilde{c}_1^{(0)}]^2 (c_{20}^{(0)})^2 E_1^2 E_2^2}{1 - E_1^2 E_2^2 s^{-3}} \right]. \end{aligned}$$

For  $\delta_0$ , we obtain

$$\delta_0 = \delta_0^{(0)} + \delta_0^{(1)} \tau + \delta_0^{(2)} \tau^2, \tag{36}$$

$$\delta_0^{(0)} = \ln Q(\mathcal{M}) + \ln Q(d; T_c),$$

$$\delta_0^{(1)} = - \frac{\sqrt{6}}{(a'_4)^{1/2}} (1 - \bar{q}) \beta_c \Phi(0) F_2(h_c; \alpha),$$

$$\begin{aligned} \delta_0^{(2)} = & - \frac{3}{a'_4} (1 - \bar{q})^2 [\beta_c \Phi(0)]^2 [F_2^2(h_c, \alpha) - F_4(h_c, \alpha)] \\ & + \frac{\sqrt{6}}{(a'_4)^{1/2}} (1 - \bar{q}) \beta_c \Phi(0) F_2(h_c, \alpha), \quad \bar{q} = \frac{1 + s^{-2}}{2}, \end{aligned}$$

$$h_c = \frac{\sqrt{6}}{(a'_4)^{1/2}} [a'_2 - \beta_c \Phi(0) (1 - \bar{q})], \quad \alpha = \frac{\sqrt{6}}{15} \frac{a'_6}{(a'_4)^{3/2}}.$$

Thus, for the free energy of the CR we have

$$\begin{aligned} F_{\text{CR}} = & -kTN' [\gamma_0^{(\text{CR})} + \gamma_1 \tau + \gamma_2 \tau^2 - \gamma_3^{(\text{CR})(0)+} \tau^{3\nu} \\ & - \gamma_3^{(\text{CR})(1)+} \tau^{3\nu + \Delta_1}], \end{aligned} \tag{37}$$

$$\gamma_0^{(\text{CR})} = \gamma_0^{(0)} + \delta_0^{(0)}, \quad \gamma_k = \gamma_0^{(k)} + \delta_0^{(k)}, \quad k = 1, 2.$$

The coefficients  $\gamma_0^{(\text{CR})}$ ,  $\gamma_1$ , and  $\gamma_2$  [see (37)] as well as  $m_2$  and  $\mathcal{N}_1^+$  [see (30) and (31)] are not universal since they contain the quantities  $\tilde{c}_1^{(l)}$ ,  $c_{20}^{(i)}$ ,  $c_{30}^{(i)}$  ( $l=0,1$ ;  $i=0,1,2$ ),

depending on microscopic characteristics of the Hamiltonian. The coefficients  $\gamma_3^{(\text{CR})(l)+}$  ( $l=0,1$ ) are given in (33). Here the quantities  $\bar{\gamma}_3^{(\text{CR})(l)+}$  do not depend on microscopic characteristics, i.e., are universal relative to these characteristics.

Using  $F_{\text{CR}}$ , we can calculate other thermodynamic functions of the system in the CR region at  $T > T_c$ . For the entropy  $S_{\text{CR}} = -\partial F_{\text{CR}} / \partial T$ , internal energy  $U_{\text{CR}} = F_{\text{CR}} + TS_{\text{CR}}$ , and specific heat  $C_{\text{CR}} = T \partial S_{\text{CR}} / \partial T$  we obtain

$$\begin{aligned} S_{\text{CR}} = & kN' [s^{(\text{CR})(0)} + c_0 \tau + u_3^{(\text{CR})(0)+} \tau^{1-\alpha} \\ & + u_3^{(\text{CR})(1)+} \tau^{1-\alpha + \Delta_1}], \\ U_{\text{CR}} = & kTN' [\gamma_1 + u_1 \tau + u_3^{(\text{CR})(0)+} \tau^{1-\alpha} \\ & + u_3^{(\text{CR})(1)+} \tau^{1-\alpha + \Delta_1}], \end{aligned} \tag{38}$$

$$C_{\text{CR}} = kN' [c_0 + c_3^{(\text{CR})(0)+} \tau^{-\alpha} + c_3^{(\text{CR})(1)+} \tau^{\Delta_1 - \alpha}],$$

where

$$\begin{aligned} s^{(\text{CR})(0)} = & \gamma_0^{(\text{CR})} + \gamma_1, \quad c_0 = 2(\gamma_1 + \gamma_2), \\ u_3^{(\text{CR})(l)+} = & c_\nu^3 c_{\Delta_1}^l \bar{u}_3^{(\text{CR})(l)+}, \quad l = 0, 1, \\ \bar{u}_3^{(\text{CR})(0)+} = & -3\nu \bar{\gamma}_3^{(\text{CR})(0)+}, \\ \bar{u}_3^{(\text{CR})(1)+} = & -(3\nu + \Delta_1) \bar{\gamma}_3^{(\text{CR})(1)+}, \\ u_1 = & \gamma_1 + 2\gamma_2, \quad c_3^{(\text{CR})(l)+} = c_\nu^3 c_{\Delta_1}^l \bar{c}_3^{(\text{CR})(l)+}, \\ \bar{c}_3^{(\text{CR})(0)+} = & -3\nu(3\nu - 1) \bar{\gamma}_3^{(\text{CR})(0)+}, \\ \bar{c}_3^{(\text{CR})(1)+} = & -(3\nu + \Delta_1)(3\nu + \Delta_1 - 1) \bar{\gamma}_3^{(\text{CR})(1)+}, \\ \alpha = & 2 - 3\nu. \end{aligned} \tag{39}$$

### 3. CALCULATION OF THE CONTRIBUTION OF LONG-WAVE MODES OF SPIN DENSITY OSCILLATIONS TO THE THERMODYNAMIC CHARACTERISTICS OF THE SYSTEM

The contribution of long-wave modes of spin moment density oscillations to the free energy of the 3D Ising model ( $k < B' s^{-m} \tau$ ) taking into account the first confluent correction is calculated according to the scheme proposed in Refs. 3, 13, 14, and 24. After the exit from the CR, the system goes over to the LGR. In this case, while calculating the partition function component  $Z_{\text{LGR}}$  from (18), it is convenient to single out two regions of values of wave vectors. The first is the transition region (TR) corresponding to values of  $\mathbf{k}$  close to  $B_{m_\tau}$ , while the second is the Gaussian region corresponding to small values of wave vector ( $k \rightarrow 0$ ). After the integration of partition function in several layers of the phase space of CV, which follow the point of exit from the CR and determine the size of the TR, the system is described by a Gaussian density of measure. Thus, we can write

$$Z_{\text{LGR}} = Z_{\text{LGR}}^{(1)} Z_{\text{LGR}}^{(2)}. \tag{40}$$

#### Transition region (TR)

This region corresponds to  $\bar{m}_0$  layers of the phase space of CV. The lower boundary of the TR is determined by the point of exit of the system from the CR region ( $n = m_\tau + 1$ ). The upper boundary corresponds to the layer  $m_\tau$

+ $\tilde{m}_0+1$ . The latter determines the beginning of the Gaussian region in which the Gaussian distribution of spin moment density oscillation modes is observed. A transition of the system to the LGR region is accompanied by an increase in the value of  $h_n$  as a function of  $n$ .<sup>24</sup> Consequently, the condition for obtaining  $\tilde{m}_0$  is the equality

$$|h_{m_\tau+\tilde{m}'_0}| = \frac{A_0}{1-s^{-3}}, \tag{41}$$

where  $A_0$  is a large number ( $A_0 \geq 10$ ). The value of  $\tilde{m}'_0$  determined from (41) actually determines the number  $\tilde{m}_0$  (see Ref. 26).

Let us calculate the contribution  $F_{\text{LGR}}^{(1)}$  to free energy from the layers of the phase space of CV immediately beyond the point of exit from the CR, which corresponds to the contribution  $Z_{\text{LGR}}^{(1)}$  from the TR to partition function. It has the form

$$F_{\text{LGR}}^{(1)} = -kTN_{m_\tau+1} \sum_{m=0}^{\tilde{m}_0} s^{-3m} f_{\text{LGR}_1}(m), \tag{42}$$

$$f_{\text{LGR}_1}(m) = \ln\left(\frac{2}{\pi}\right) + \frac{1}{4} \ln 24 - \frac{1}{4} \ln C(\eta_{m_\tau+m}, \xi_{m_\tau+m}) \\ + \ln I_0(h_{m_\tau+m+1}, \alpha_{m_\tau+m+1}) \\ + \ln I_0(\eta_{m_\tau+m}, \xi_{m_\tau+m}).$$

It follows from Refs. 3, 27–30 containing the results of numerical calculations of the partition function in the Ising model as well as the results of analysis of RR that the evolution of the coefficients of effective densities of measures with increasing number of the layer in the TR is successfully described by solutions of the RG type. Consequently,  $F_{\text{LGR}}^{(1)}$  can be calculated by using the solutions of RR. On the basis of expansions for functions appearing in the expressions for the intermediate arguments  $\eta_{m_\tau+m}$ ,  $\xi_{m_\tau+m}$ , and  $f_{\text{LGR}_1}(m)$  (42) given in Refs. 13 and 25, we can obtain the following relation<sup>26</sup> accurate to within  $\tau^{\Delta_1}$ :

$$f_{\text{LGR}_1}(m) = f_{\text{LGR}_1}^{(0)}(m) + f_{\text{LGR}_1}^{(1)}(m) \tau^{\Delta_1}, \tag{43}$$

$$f_{\text{LGR}_1}^{(0)}(m) = \ln\left(\frac{2}{\pi}\right) + \frac{1}{4} \ln 24 - \frac{1}{4} \ln C(\eta_{m_\tau+m}^{(0)}, \xi_{m_\tau+m}^{(0)}) \\ + \ln I_0(h_{m_\tau+m+1}^{(0)}, \alpha_{m_\tau+m+1}^{(0)}) \\ + \ln I_0(\eta_{m_\tau+m}^{(0)}, \xi_{m_\tau+m}^{(0)}),$$

$$f_{\text{LGR}_1}^{(1)}(m) = \varphi_1^{(m_\tau+m)} h_{m_\tau+m}^{(0)} h_{m_\tau+m}^{(1)} \\ + \varphi_2^{(m_\tau+m)} \alpha_{m_\tau+m}^{(0)} \alpha_{m_\tau+m}^{(1)} \\ + \varphi_3^{(m_\tau+m+1)} h_{m_\tau+m+1}^{(0)} h_{m_\tau+m+1}^{(1)} \\ + \varphi_4^{(m_\tau+m+1)} \alpha_{m_\tau+m+1}^{(0)} \alpha_{m_\tau+m+1}^{(1)},$$

$$\varphi_k^{(m_\tau+m)} = b_k^{(m_\tau+m)} + P_{4k}^{(m_\tau+m)}/4, \quad k=1,2,$$

$$\varphi_3^{(m_\tau+m+1)} = -F_2^{*(m_\tau+m+1)}, \quad \varphi_4^{(m_\tau+m+1)} = -F_6^{*(m_\tau+m+1)}.$$

The quantities  $b_k^{(m_\tau+m)}$  and  $P_{4k}^{(m_\tau+m)}$  depend on  $F_{2l}^{*(m_\tau+m)} = I_{2l}^{*(m_\tau+m)}/I_0^{*(m_\tau+m)}$ , where

$$I_{2l}^{*(m_\tau+m)} = \int_0^\infty x^{2l} \exp(-h_{m_\tau+m}^{(0)} x^2 - x^4 - \alpha_{m_\tau+m}^{(0)} x^6) dx, \tag{44}$$

as well as on  $F_{2l}^{***(m_\tau+m)} = I_{2l}^{***(m_\tau+m)}/I_0^{***(m_\tau+m)}$ , where

$$I_{2l}^{***(m_\tau+m)} = \int_0^\infty x^{2l} \exp(-\eta_{m_\tau+m}^{(0)} x^2 - x^4 - \xi_{m_\tau+m}^{(0)} x^6) dx. \tag{45}$$

The coefficients of the expressions

$$h_{m_\tau+m} = h_{m_\tau+m}^{(0)} (1 + h_{m_\tau+m}^{(1)} \tau^{\Delta_1}), \\ \alpha_{m_\tau+m} = \alpha_{m_\tau+m}^{(0)} (1 + \alpha_{m_\tau+m}^{(1)} \tau^{\Delta_1}) \tag{46}$$

appearing in (43) are defined in Ref. 26, and the quantities  $\eta_{m_\tau+m}^{(0)}$  and  $\xi_{m_\tau+m}^{(0)}$  appearing in (45) can be expressed in terms of  $F_{2l}^{*(m_\tau+m)}$ . An important point in the calculation of  $f_{\text{LGR}_1}(m)$  is the representation of special functions in the form of power series in small deviations of basic arguments  $h_{m_\tau+m}$  and  $\alpha_{m_\tau+m}$  from their values in the zeroth approximation, i.e., from  $h_{m_\tau+m}^{(0)}$  and  $\alpha_{m_\tau+m}^{(0)}$  from (46). It should be recalled that in the CR region we took into account the deviations of the basic arguments  $h_n$  and  $\alpha_n$  ( $n \leq m_\tau$ ) from their values  $h^{(0)}$  and  $\alpha^{(0)}$  at a fixed point. In the summation over  $m$  in  $F_{\text{LGR}}^{(1)}$  (42), we must use for  $\tilde{m}_0$  the integer closest to  $\tilde{m}'_0$ . The final result for  $F_{\text{LGR}}^{(1)}$  assumes the form

$$F_{\text{LGR}}^{(1)} = -kTN' [f_{\text{TR}}^{(0)} \tau^{3\nu} + f_{\text{TR}}^{(1)} \tau^{3\nu+\Delta_1}], \tag{47}$$

$$f_{\text{TR}}^{(l)} = c_\nu^3 c_{\Delta_1}^l \bar{f}_{\text{TR}}^{(l)}, \quad l=0,1,$$

$$\bar{f}_{\text{TR}}^{(0)} = \sum_{m=0}^{\tilde{m}_0} s^{-3m} f_{\text{LGR}_1}^{(0)}(m), \quad \bar{f}_{\text{TR}}^{(1)} = \bar{f}_{\text{TR}_1} + 3\nu\Phi_0 \bar{f}_{\text{TR}}^{(0)},$$

$$\bar{f}_{\text{TR}_1} = c_{\Delta_1}^{-1} \sum_{m=0}^{\tilde{m}_0} s^{-3m} f_{\text{LGR}_1}^{(1)}(m).$$

Let us now calculate the contribution of long-wave modes of oscillations to free energy of the system in the range of wave vectors

$$k \leq B' s^{-m'_\tau}, \quad m'_\tau = m_\tau + \tilde{m}_0 + 2. \tag{48}$$

### Region of small values of wave vector ( $k \rightarrow 0$ )

Introducing an infinitely weak external magnetic field  $\mathcal{H}$  (or  $h = \mu_B \mathcal{H}$ ,  $\mu_B$  is the Bohr magneton), we obtain the following expression for the free energy component corresponding to  $Z_{\text{LGR}}^{(2)}$  from (40):

$$F_{\text{LGR}}^{(2)} = \frac{1}{2} kT \left[ N_{m'_\tau} \ln P_2^{(m'_\tau-1)} \right. \\ \left. + \sum_{k=0}^{B_{m'_\tau}} \ln \tilde{d}_{m'_\tau}(k) - \frac{\beta^2 N h^2}{\tilde{d}_{m'_\tau}(0)} \right]. \tag{49}$$

Here

$$P_2^{(m'_\tau-1)} = 2h_{m'_\tau-1} F_2(h_{m'_\tau-1}, \alpha_{m'_\tau-1}) \times [d_{m'_\tau-1}(B_{m'_\tau}, B_{m'_\tau-1})]^{-1},$$

$$\tilde{d}_{m'_\tau}(k) = [P_2^{(m'_\tau-1)}]^{-1} + \beta \tilde{\Phi}(B_{m'_\tau}, B_{m'_\tau-1}) - \beta \tilde{\Phi}(k). \tag{50}$$

For  $d_{m'_\tau-1}(B_{m'_\tau}, B_{m'_\tau-1})$ , we have the following standard representation:<sup>3,6,26</sup>

$$d_{m'_\tau-1}(B_{m'_\tau}, B_{m'_\tau-1}) = s^{-2(m'_\tau-1)}(r_{m'_\tau-1} + q). \tag{51}$$

The quantity  $q = \bar{q} \beta \tilde{\Phi}(0)$  determines the average value of potential  $\beta \tilde{\Phi}(B_{n+1}, B_n) = \beta \tilde{\Phi}(0) - q/s^{2n}$  in the  $n$ th layer (in this paper,  $\bar{q} = (1 + s^{-2})/2$  corresponds to the arithmetic mean value of  $k^2$  on the interval  $(1/s, 1)$ ).

Calculating  $P_2^{(m'_\tau-1)}$  and  $\tilde{d}_{m'_\tau}(k)$  using the expansion for  $F_2(h_{m'_\tau-1}, \alpha_{m'_\tau-1})$  from Ref. 25 and then the sum  $(1/2) \sum_{k=0}^{B_{m'_\tau}} \ln \tilde{d}_{m'_\tau}(k)$  with the help of transition to the spherical Brillouin zone and integration with respect to  $k$ , we arrive at the final formula for  $F_{LGR}^{(2)}$  (see Ref. 26):

$$F_{LGR}^{(2)} = -kTN' [f^{(0)'} \tau^{3\nu} + f^{(1)'} \tau^{3\nu+\Delta_1}] - \beta N \gamma_4^+ h^2 \tau^{-2\nu} (1 + a_\chi^+ \tau^{\Delta_1}), \tag{52}$$

$$f^{(l)'} = c_\nu^3 c_{\Delta_1}^l \bar{f}^{(l)'}, \quad l=0,1, \quad \bar{f}^{(0)'} = s^{-3(\tilde{m}_0+1)} f^{(0)},$$

$$\bar{f}^{(1)'} = \bar{f}_1' + 3\nu \Phi_0 \bar{f}^{(0)'}, \quad \bar{f}_1' = c_{\Delta_1}^{-1} s^{-3(\tilde{m}_0+1)} f^{(1)},$$

$$\gamma_4^+ = c_\nu^{-2} \bar{\gamma}_4^+ / [\beta \tilde{\Phi}(0)], \quad \bar{\gamma}_4^+ = s^{2\tilde{m}_0} / (2g_0),$$

$$a_\chi^+ = -g_1 - 2\nu c_{\Delta_1} \Phi_0,$$

where

$$f^{(0)} = -\frac{1}{2} \ln \left( \frac{s^{-2} + g_0}{g_0 + \bar{q}} \right) + \frac{1}{3} - g_0' \left[ 1 - \sqrt{g_0'} \arctan \left( \frac{1}{\sqrt{g_0'}} \right) \right], \tag{53}$$

$$f^{(1)} = \frac{1}{2} \left( \frac{g_0 g_1}{g_0 + \bar{q}} - \frac{g_1}{(g_0')^{-1} + 1} - \frac{g_0' g_1}{(g_0')^{-1} + 1} \right) - g_0' g_1 \left[ 1 - \frac{3}{2} \sqrt{g_0'} \arctan \left( \frac{1}{\sqrt{g_0'}} \right) \right],$$

$$g_0' = s^2 g_0,$$

and  $g_0$  and  $g_1$  appear in  $\tilde{d}_{m'_\tau}(k)$  and are given in Ref. 26.

On the basis of (47) and (52), we can write the following relation for the general expression  $F_{LGR} = F_{LGR}^{(1)} + F_{LGR}^{(2)}$  corresponding to the contribution to free energy from long-wave modes of spin moment density oscillations:

$$F_{LGR} = -kTN' [f_{LGR}^{(0)} \tau^{3\nu} + f_{LGR}^{(1)} \tau^{3\nu+\Delta_1}] - \beta N \gamma_4^+ h^2 \tau^{-2\nu} (1 + a_\chi^+ \tau^{\Delta_1}), \tag{54}$$

$$f_{LGR}^{(l)} = c_\nu^3 c_{\Delta_1}^l \bar{f}_{LGR}^{(l)}, \quad \bar{f}_{LGR}^{(l)} = \bar{f}_{TR}^{(l)} + \bar{f}^{(l)'}, \quad l=0,1.$$

For  $\mathcal{H} = 0$ , the entropy, internal energy, and specific heat of the system corresponding to LGR are defined by the following relations:

$$S_{LGR} = kN' [u_3^{(LGR)(0)} \tau^{1-\alpha} + u_3^{(LGR)(1)} \tau^{1-\alpha+\Delta_1}],$$

$$U_{LGR} = kTN' [u_3^{(LGR)(0)} \tau^{1-\alpha} + u_3^{(LGR)(1)} \tau^{1-\alpha+\Delta_1}], \tag{55}$$

$$C_{LGR} = kN' [c_3^{(LGR)(0)} \tau^{-\alpha} + c_3^{(LGR)(1)} \tau^{\Delta_1-\alpha}],$$

where

$$u_3^{(LGR)(l)} = c_\nu^3 c_{\Delta_1}^l \bar{u}_3^{(LGR)(l)}, \quad l=0,1,$$

$$\bar{u}_3^{(LGR)(0)} = 3\nu \bar{f}_{LGR}^{(0)},$$

$$\bar{u}_3^{(LGR)(1)} = (3\nu + \Delta_1) \bar{f}_{LGR}^{(1)}, \tag{56}$$

$$c_3^{(LGR)(l)} = c_\nu^3 c_{\Delta_1}^l \bar{c}_3^{(LGR)(l)},$$

$$\bar{c}_3^{(LGR)(0)} = 3\nu(3\nu - 1) \bar{f}_{LGR}^{(0)},$$

$$\bar{c}_3^{(LGR)(1)} = (3\nu + \Delta_1)(3\nu + \Delta_1 - 1) \bar{f}_{LGR}^{(1)}.$$

Taking into account consistently the short- and long-wave modes of spin moment density oscillations, we can now write complete expressions for free energy and other thermodynamic functions of the three-dimensional Ising model near the phase transition point.

#### 4. THERMODYNAMIC CHARACTERISTICS OF THE MODEL FOR $T > T_c$ TAKING INTO ACCOUNT FIRST CONFLUENT CORRECTION

In accordance with (17), the free energy of the system taking into account (37) and (54), assumes the following form in zero external field:

$$F = -kTN' [\gamma_0 + \gamma_1 \tau + \gamma_2 \tau^2 + \gamma_3^{(0)+} \tau^{3\nu} + \gamma_3^{(1)+} \tau^{3\nu+\Delta_1}],$$

$$\gamma_0 = s_0^3 \ln 2 + \gamma_0^{(CR)}, \quad \gamma_3^{(l)+} = c_\nu^3 c_{\Delta_1}^l \bar{\gamma}_3^{(l)+}, \tag{57}$$

$$\bar{\gamma}_3^{(l)+} = -\bar{\gamma}_3^{(CR)(l)+} + \bar{f}_{LGR}^{(l)}, \quad l=0,1.$$

The coefficients  $\gamma_1$  and  $\gamma_2$  are defined in (37). The terms proportional to integral powers of  $\tau$  in (57) appear exclusively due to inclusion of short-wave modes of oscillations. The terms proportional to  $\tau^{3\nu}$  and  $\tau^{3\nu+\Delta_1}$  (nonanalytic component of free energy) are formed as a result of inclusion of short-wave as well as long-wave modes of oscillations. The first confluent correction appears due to the smaller eigenvalue  $E_2$  of the RG linear transformation matrix taken into account in the solutions of RR.

The main advantage of the expression for  $F$  is the presence of relations connecting its coefficients with microscopic characteristics of the system and the coordinates of a fixed point of RR. The coefficients  $\gamma_3^{(l)+}$  ( $l=0,1$ ) are presented in

TABLE III. Coefficients  $\gamma_0$ ,  $\gamma_1$  and  $\gamma_2$  of free energy  $F$  (57).

$b$	$\gamma_0$	$\gamma_1$	$\gamma_2$
$s=2.0000$			
$b_I$	1.8758	-0.8032	-4.4816
$b_{II}$	2.7464	-0.7759	-3.9551
$b_{III}$	3.1962	-0.7651	-3.7548
$c$	61.1798	-0.6734	-2.0482
$2c$	486.699	-0.6701	-1.9599
$s=2.7349$			
$b_I$	1.8776	-0.7063	-4.6948
$b_{II}$	2.7496	-0.6952	-4.1735
$b_{III}$	3.2000	-0.6913	-3.9764
$c$	61.1930	-0.6924	-2.2672
$2c$	486.713	-0.6978	-2.1665
$s=3.0000$			
$b_I$	1.8789	-0.6867	-4.5304
$b_{II}$	2.7516	-0.6795	-4.0342
$b_{III}$	3.2023	-0.6773	-3.8466
$c$	61.1999	-0.7020	-2.1971
$2c$	486.720	-0.7100	-2.0936

the form of the product of the universal component  $\bar{\gamma}_3^{(l)+}$  and the nonuniversal factor depending on microscopic characteristics through  $\bar{c}_1^{(0)}$  and  $c_{20}^{(0)}$  [see (57)]. Leading critical amplitudes and the amplitudes of the confluent correction to specific heat and other thermodynamic characteristics of the system can be presented in a similar way. The values of  $\gamma_0$ ,  $\gamma_1$ , and  $\gamma_2$  are presented in Table III for different values of the parameter  $s$  and the effective range  $b$  of the potential, while the values of  $\bar{\gamma}_3^{(l)+}$  are given in Table IV. For  $s=2.7349$ , the value of the basic variable at a fixed point satisfies the condition  $h^{(0)} \approx 0$  (see, for example, Ref. 25).

The coefficients of entropy, internal energy, and specific heat can be expressed in terms of the coefficients of free energy. Taking into account the first confluent correction, we obtain the following expressions for entropy, internal energy, and specific heat of the system for  $\mathcal{H}=0$ :

$$S = kN' [s^{(0)} + c_0 \tau + u_3^{(0)+} \tau^{1-\alpha} + u_3^{(1)+} \tau^{1-\alpha+\Delta_1}],$$

TABLE V. Values of coefficients in the expressions (60) for heat capacity  $C/kN'$  and (62) for susceptibility  $\chi$ .

$b$	$A^+$	$a_c^+$	$B^+$	$\Gamma^+$	$a_\chi^+$
$s=2.0000$					
$b_I$	1.0876	-1.2609	-10.5696	1.8711	-0.0691
$b_{II}$	0.9960	-1.8262	-9.4620	1.9842	-0.1001
$b_{III}$	0.9609	-2.0389	-9.0397	2.0321	-0.1118
$c$	0.6620	-3.7773	-5.4430	2.6052	-0.2071
$2c$	0.6471	-3.8634	-5.2601	2.6450	-0.2118
$s=2.7349$					
$b_I$	0.8113	-2.3816	-10.8022	2.1659	-0.1177
$b_{II}$	0.7439	-2.7420	-9.7375	2.2948	-0.1355
$b_{III}$	0.7184	-2.8773	-9.3355	2.3488	-0.1422
$c$	0.5050	-3.9838	-5.9193	2.9709	-0.1969
$2c$	0.4944	-4.0397	-5.7286	3.0134	-0.1996
$s=3.0000$					
$b_I$	0.7238	-2.6494	-10.4343	2.4427	-0.1291
$b_{II}$	0.6644	-2.9650	-9.4274	2.5860	-0.1445
$b_{III}$	0.6420	-3.0832	-9.0478	2.6459	-0.1502
$c$	0.4558	-4.0460	-5.7981	3.3248	-0.1971
$2c$	0.4465	-4.0947	-5.6074	3.3710	-0.1995

TABLE IV. Universal parts of coefficients of the nonanalytic component of free energy.

$s$	$\bar{\gamma}_3^{(0)+}$	$\bar{\gamma}_3^{(1)+}$
2.0000	0.9699	0.6508
2.7349	1.8654	0.7263
3.0000	2.1770	0.7162

$$U = kTN' [\gamma_1 + u_1 \tau + u_3^{(0)+} \tau^{1-\alpha} + u_3^{(1)+} \tau^{1-\alpha+\Delta_1}],$$

$$C = kN' [c_0 + c_3^{(0)+} \tau^{-\alpha} + c_3^{(1)+} \tau^{\Delta_1-\alpha}]. \tag{58}$$

Here

$$s^{(0)} = \gamma_0 + \gamma_1, \quad u_3^{(l)+} = c_\nu^3 c_{\Delta_1}^l \bar{u}_3^{(l)+}, \quad l=0,1,$$

$$\bar{u}_3^{(0)+} = 3\nu \bar{\gamma}_3^{(0)+}, \quad \bar{u}_3^{(1)+} = (3\nu + \Delta_1) \bar{\gamma}_3^{(1)+}, \tag{59}$$

$$c_3^{(l)+} = c_\nu^3 c_{\Delta_1}^l \bar{c}_3^{(l)+}, \quad \bar{c}_3^{(0)+} = 3\nu(3\nu-1) \bar{\gamma}_3^{(0)+},$$

$$\bar{c}_3^{(1)+} = (3\nu + \Delta_1)(3\nu + \Delta_1 - 1) \bar{\gamma}_3^{(1)+}.$$

The coefficients  $c_0$  and  $u_1$  are given in (39).

The formula for specific heat [see (58)] for the model under investigation can be written in the form<sup>31,32</sup>

$$\frac{C}{kN'} = \frac{A^+}{\alpha} \tau^{-\alpha} (1 + \alpha a_c^+ \tau^{\Delta_1}) + B^+, \tag{60}$$

$$A^+ = c_\nu^3 \alpha \bar{c}_3^{(0)+}, \quad a_c^+ = \frac{c_{\Delta_1} \bar{c}_3^{(1)+}}{\alpha \bar{c}_3^{(0)+}}, \quad B^+ = c_0.$$

An important characteristic of the system such as susceptibility per particle

$$\chi = -\frac{1}{N} \frac{\partial^2 F_{LGR}}{\partial \mathcal{H}^2}, \tag{61}$$

can be calculated using (54). For infinitely small values of external field  $\mathcal{H}$  near  $T_c$ , it is defined as

$$\chi = \Gamma^+ \tau^{-\gamma} (1 + a_\chi^+ \tau^{\Delta_1}) \frac{\mu_B^2}{\bar{\Phi}(0)}, \quad \Gamma^+ = 2c_\nu^{-2} \bar{\gamma}_4^+, \quad (62)$$

$$a_\chi^+ = c_{\Delta_1} \bar{a}_\chi^+, \quad \bar{a}_\chi^+ = -\bar{g}_1 - 2\nu\bar{\Phi}_0,$$

$$\bar{g}_1 = \frac{g_1}{c_{\Delta_1}}, \quad \gamma = 2\nu.$$

Here the value of  $\bar{g}_1$  does not depend on microscopic characteristics and can be obtained as a result of elimination of the nonuniversal factor  $c_{\Delta_1} = c_{20}^{(0)}[\bar{c}_1^{(0)}/(f_0\delta)]^{\Delta_1}$  from  $g_1$ . The coefficient  $\bar{\gamma}_4^+$  is presented in (52).

The coefficients for specific heat  $C/kN'$  (60) and susceptibility  $\chi$  (62) are given in Table V. It should be emphasized that the calculated amplitudes  $a_c^+$  and  $a_\chi^+$  of confluent corrections are in accord with the results obtained by Liu and Fisher<sup>33</sup> who considered leading corrections to scaling amplitudes for Ising models with the interaction between nearest neighbors in sc, bcc and fcc lattices. It was proved<sup>33</sup> that the amplitudes of these corrections for susceptibility, correlation length, specific heat, and spontaneous magnetization have negative sign for all the three lattices. Liu and Fisher<sup>33</sup> also noted the agreement between the obtained results and the results of high-temperature expansions and the results of the field-theory analysis.

This research was carried out under partial financial support from the State Foundation of Fundamental Studies at the Ukrainian Ministry of Science (Project No. 2.4/173).

\*E-mail: piv@icmp.lviv.ua

<sup>1</sup>I. R. Yukhnovskii, Dokl. Akad. Nauk SSSR **232**, 312 (1977) [Sov. Phys. Dokl. **22**, 18 (1977)].

<sup>2</sup>I. R. Yukhnovskii, Teor. Mat. Fiz. **36**, 373 (1978).

<sup>3</sup>I. R. Yukhnovskii, *Second Order Phase Transitions. Method of Collective Variables* [in Russian], Naukova Dumka, Kiev (1985).

<sup>4</sup>I. R. Yukhnovskii, Riv. Nuovo Cimento **12**, 1 (1989).

<sup>5</sup>I. R. Yukhnovskii, M. P. Kozlovskii, and I. V. Pylyuk, Z. Naturforsch. **46a**, 1 (1991).

<sup>6</sup>M. P. Kozlovskii, I. V. Pylyuk, and I. R. Yukhnovskii, Teor. Mat. Fiz. **87**, 293 (1991).

<sup>7</sup>M. P. Kozlovskii, I. V. Pylyuk, and I. R. Yukhnovskii, Teor. Mat. Fiz. **87**, 434 (1991).

<sup>8</sup>I. V. Pylyuk and M. P. Kozlovskii, Preprint ITP, Acad. Sci. Ukr. SSR, ITP-87-31R, Kiev (1987).

<sup>9</sup>I. V. Pylyuk, Preprint ITP, Acad. Sci. Ukr. SSR, ITP-88-107R, Kiev (1988).

<sup>10</sup>M. P. Kozlovskii and I. V. Pylyuk, in *Proceedings All-Union Conf. on Modern Problems in Statistical Physics (Lvov, February 3–5, 1987)* [in Russian], vol. 2, Naukova Dumka, Kiev 1989.

<sup>11</sup>M. P. Kozlovskii, Teor. Mat. Fiz. **78**, 422 (1989).

<sup>12</sup>M. P. Kozlovskii and I. V. Pylyuk, Ukr. Fiz. Zh. (Russ. Ed.) **35**, 146 (1990).

<sup>13</sup>M. P. Kozlovskii and I. V. Pylyuk, Preprint ITP, Acad. Sci. Ukr. SSR, ITP-90-81R, Kiev (1990).

<sup>14</sup>M. P. Kozlovskii, I. V. Pylyuk, and V. V. Dukhovii, Condens. Matter Phys. **11**, 17 (1997).

<sup>15</sup>V. V. Dukhovii, M. P. Kozlovskii, and I. V. Pylyuk, Teor. Mat. Fiz. **107**, 288 (1996).

<sup>16</sup>R. Guida and J. Zinn-Justin, Nucl. Phys. B **489** [FS], 626 (1997).

<sup>17</sup>M. M. Tsy-pin, Phys. Rev. Lett. **73**, 2015 (1994).

<sup>18</sup>A. I. Sokolov, V. A. Ul'kov, and E. V. Orlov, J. Phys. Stud. **1**, 362 (1997).

<sup>19</sup>M. P. Kozlovskii, I. V. Pylyuk, and Z. E. Usatenko, Phys. Status Solidi B **197**, 465 (1996).

<sup>20</sup>M. P. Kozlovskii, Preprint ITP, Acad. Sci. Ukr. SSR, ITP-82-104R, Kiev (1982).

<sup>21</sup>M. P. Kozlovskii, Preprint ITP, Acad. Sci. Ukr. SSR, ITP-84-35R, Kiev (1984).

<sup>22</sup>M. P. Kozlovskii and I. V. Pylyuk, Preprint ITP, Acad. Sci. Ukr. SSR, ITP-85-23E, Kiev (1985).

<sup>23</sup>S. Ma, *Modern Theory of Critical Phenomena*, Benjamin/Cummings, Reading (USA) (1976).

<sup>24</sup>M. P. Kozlovskii and I. V. Pylyuk, Preprint ITP, Acad. Sci. Ukr. SSR, ITP-87-9R, Kiev (1987).

<sup>25</sup>I. V. Pylyuk, Ukr. Fiz. Zh. (Russ. Ed.) **41**, 885 (1996).

<sup>26</sup>I. V. Pylyuk and M. P. Kozlovskii, Preprint ICMP, National Acad. Sci. Ukraine, ICMP-97-06U, Lviv (1997).

<sup>27</sup>I. R. Yukhnovskii, M. P. Kozlovskii, and V. A. Kolomiets, Ukr. Fiz. Zh. (Russ. Ed.) **27**, 925 (1982).

<sup>28</sup>I. R. Yukhnovskii, M. P. Kozlovskii, and V. A. Kolomiets, Ukr. Fiz. Zh. (Russ. Ed.) **27**, 930 (1982).

<sup>29</sup>I. R. Yukhnovskii, M. P. Kozlovskii, and V. A. Kolomiets, Ukr. Fiz. Zh. (Russ. Ed.) **27**, 1399 (1982).

<sup>30</sup>M. P. Kozlovskii, I. V. Pylyuk, and V. A. Kolomiets, Preprint ITP, Acad. Sci. Ukr. SSR, ITP-84-177R, Kiev (1984).

<sup>31</sup>C. Bagnuls and C. Bervillier, Phys. Rev. B **24**, 1226 (1981).

<sup>32</sup>J. F. Nicoll and P. C. Albright, Phys. Rev. B **34**, 1991 (1986).

<sup>33</sup>A. J. Liu and M. E. Fisher, J. Stat. Phys. **58**, 431 (1990).

Translated by R. S. Wadhwa

## The role of chemical disorder in the magnetism of $\text{YbInCu}_4$ compound

I. V. Svechkarev and S. N. Dolya

*B. Verkin Institute for Low Temperature Physics and Engineering, National Academy of Sciences of the Ukraine, 310164 Kharkov, Ukraine\**)

(Submitted March 10, 1999)

Fiz. Nizk. Temp. **25**, 1186–1193 (November 1999)

It is found that chemical disorder in the  $\text{YbInCu}_4$  compound (especially in the Yb sublattice) considerably affects its magnetic properties due to spatial nonuniformity of the temperature  $T_V$  of the first-order valence phase transition. The evolution of the magnetic susceptibility during disordering of the stoichiometric compound  $\text{YbInCu}_4$  is described by the model expression taking into account the  $T_V$  dispersion upon the application of pressure and variation of composition of  $\text{YbIn}_{1-x}\text{Ag}_x\text{Cu}_4$  solid mixtures. The behavior of the main parameters of the system masked by blurring of the magnetic susceptibility singularity for a disordered sample during phase transition. Among other things, the value of the derivative  $dT_V/dx=203$  K is determined. The reason behind an abrupt change in the concentration dependence of dispersion and the paramagnetic Curie temperature is calculated at  $x_c \approx 0.25$ .  
© 1999 American Institute of Physics. [S1063-777X(99)00611-8]

### 1. INTRODUCTION

Unstable valence of some rare-earth elements (Ce, Sm, Eu, and Yb) is responsible for many peculiar properties of metallic or semiconducting systems containing these elements. Such properties include first-order phase transitions accompanied by an abrupt change in the valence state of ions (usually, from almost integral HF phase of heavy fermions to intermediate-valence IV phase). These transitions are isomorphic even for considerable jumps in volume (up to 15% in pure Ce),<sup>1</sup> and their phase boundary on the  $P$ - $T$  diagram terminates at the tricritical point as on the liquid-vapor diagram, followed by further continuous transition between phases,<sup>2</sup> or rather between regimes of interaction between the  $f$ -level and conduction electrons. It should be noted that Eliashberg and Capellmann<sup>3</sup> in their recent publication paid attention to the fact that the curve of first-order phase transitions is continued behind the tricritical point at the second-order transition curve, i.e., the crystal structure of phases may display differences lying apparently beyond the resolving power of direct structural investigations.

Although the fundamental relation between the jump in volume and the change in the valence state, and hence the size of the electron shell of a rare-earth ion is obvious, the trigger mechanism of the first-order phase transition, as well as the mechanism limiting the valence jump during the transition, are still disputable and give rise to new theoretical models. If we disregard some modifications, these model can be classified as follows: electron excitation from localized  $f$ -level to band states,<sup>4,5</sup> Mott transition with delocalization of the  $f$ -level itself,<sup>6,7</sup> fluctuations between configurations,<sup>8-10</sup> volume collapse due to a strong dependence of Kondo energy on volume (the KVC model),<sup>11-13</sup> and essentially band transition.<sup>14</sup>

It should be noted that not all of these models passed through quantitative testing in real systems. Even when such

a testing was carried out, its results cannot be regarded as unambiguous evidence in favor of a definite model since either not all aspects in the behavior of phase diagrams were analyzed (e.g., possible effect of a magnetic field on it as in Ref. 13), or the chosen model parameters did not correspond to reliably established facts (like the model value  $\Delta\nu \approx 1$  of valence jump adopted in Refs. 10 and 15 instead of the experimentally determined value 0.1 for  $\text{YbInCu}_4$ ). Besides, the most detailed verification of the models was carried out in Refs. 13 and 15 for different objects for which the mechanisms of transition can be different. Thus, a more detailed analysis of features of the phase diagrams and quantitative comparison of various theoretical models on the same object are required for determining the driving forces of first-order valence phase transitions along with a search for new systems with valence transitions.

The intermetallic compound  $\text{YbInCu}_4$  appears as especially attractive among such objects. This is the only compound known so far, in which the first-order valence phase transition takes place for the stoichiometric composition at atmospheric pressure and a temperature convenient for experiments ( $T_V \approx 40$  K).<sup>10,16,17</sup> Consequently, a part of the phase diagram can be obtained (at least, in principle) on an object with a high degree of perfection. Abundant experimental data with elements of analysis of transition mechanism (see Refs. 6, 18, and 19 and the literature cited therein) accumulated for this compound as well as its structural and electronic analogs are still insufficient for drawing final conclusions. Unfortunately, the value of  $T_V$  for the compound  $\text{YbInCu}_4$  decreases under pressure unlike the case in Ce-based systems. For this reason, it is still impossible to obtain the region on the phase diagram with the tricritical point, which is most important for an unambiguous verification of the models, without using solid substitutional mixtures like the quasi-binary system  $\text{YbIn}_{1-x}\text{Ag}_x\text{Cu}_4$ .<sup>18</sup> However, consequences of

chemical disorder for properties and structure of the phase diagram of this system are unknown.

Our aim is to demonstrate the importance of inclusion of disordering in compounds of the  $\text{YbInCu}_4$  for correct determination of phase boundaries. It should be noted that, for the existing method of sample preparation, the most important singularity at the phase-transition point associated with the effect of disorder was observed for a nonstoichiometric sample  $\text{Yb}_{1.2}\text{In}_{0.8}\text{Cu}_4$  which was chosen as the preferred object in subsequent investigations.<sup>10,15</sup> Recently, Sarrao *et al.*<sup>16-18</sup> successfully applied special technique for obtaining single crystals of stoichiometric composition with a high degree of ordering and exceptionally sharp jumps in properties at the phase transition point and for clarifying the microscopic pattern of sample disordering for different methods of sample preparation.<sup>20</sup>

It should be noted that essentially structural methods are not always used for detecting and identifying the type of transitions. In many cases, the study of various electronic properties sensitive to structure variations are more convenient. However, the efficiency of such investigations is determined by the existence of one-to-one correspondence between peculiarities in the behavior of electronic properties and the valence and structural states of the system. In compounds of rare-earth elements, magnetic susceptibility  $\chi$  serves in many cases as a reliably interpreted property due to large values of magnetic moments. A simple model of inclusion of disorder and estimation of its role in the magneto-volume effect  $d \ln \chi / d \ln V$  were considered in Refs. 19 and 21. In the present paper, this model is verified (Sec. 2) for available data on the dependence of magnetic susceptibility  $\chi$  on the extent of ordering in the stoichiometric compound  $\text{YbInCu}_4$  (Ref. 20) (Sec. 3) and on pressure for the nonstoichiometric composition  $\text{Yb}_{1.2}\text{In}_{0.8}\text{Cu}_4$  (Ref. 15) (Sec. 4) and is used for analyzing a system of continuous solid mixtures  $\text{YbIn}_{1-x}\text{Ag}_x\text{Cu}_4$  (Ref. 17) (Sec. 5). The main results are summarized in Sec. 6.

## 2. MODEL DESCRIPTION OF MAGNETIC SUSCEPTIBILITY OF $\text{YbInCu}_4$

The magnetic susceptibility of a perfect sample of  $\text{YbInCu}_4$  is correctly described by the following expression:<sup>19</sup>

$$\chi(T) = \chi_0 + [C/(T - \Theta) - \chi_0]W(T). \quad (1)$$

Here  $\chi_0 \propto 1/T_K^{\text{IV}}$  (Ref. 22) is the temperature-independent susceptibility,  $T_K^{\text{IV}}$  is the characteristic Kondo temperature in the IV state,  $C$  and  $\Theta$  are the Curie constant and temperature, and  $W(T)$  is a step function:

$$W(T < T_V) = 0; \quad W(T > T_V) = 1. \quad (2)$$

Such a form of the expression for susceptibility corresponds to the condition  $\Delta_{\text{CEF}} \leq T_V < T_K^{\text{IV}}$  ( $\Delta_{\text{CEF}}$  is the complete splitting of the fundamental multiplet  $J = 7/2$  of Yb by the crystal electric field (CEF)), which is observed for  $\text{YbInCu}_4$  ( $\Delta_{\text{CEF}} = 44$  K,<sup>23</sup>  $T_K^{\text{IV}} \approx 420$  K).<sup>17</sup> The values of the parameters in Eq. (1) were selected earlier by Sarrao *et al.*<sup>16</sup> and are given in Table I. The value of the magnetic moment  $\mu$  per Yb ion

TABLE I. Values of model parameters for magnetic susceptibility and  $T_V$  distribution function in  $\text{YbInCu}_4$  compounds. Sample numbers corresponds to Fig. 1.

Parameter	Sample		
	1	2	3
$C$ , emu·K/mole	2.55	2.55	2.55
$-\Theta$ , K	7.2	23	33
$\chi_0$ , $10^{-3}$ emu/mole	6.0	6.0	8.4
$n$	0	0.35	0.76
$\bar{T}_{V1}$ , K	40	41	38
$\bar{T}_{V2}$ , K	0	47	74
$\sigma_1$ , K	<1.0	1.9	2.85
$\sigma_2$ , K	0	4.9	11

following from the Curie constant is close to the value expected for  $\text{Yb}^{3+}$  in view of the small deviation of the true valence of the ion from an integer in the heavy-fermion HF phase of  $\text{YbInCu}_4$ .<sup>17,24</sup> Curve 1 in Fig. 1 shows that the results calculated by formula (1) for the chosen parameter are in good agreement with experimental data.<sup>16</sup>

Following Lawrence *et al.*,<sup>20</sup> and in accordance with structural data, we shall assume that the main reason of disorder in the stoichiometric compound  $\text{YbInCu}_4$  is the disordered distribution of atoms of the form  $(\text{Yb}_{1-x}\text{In}_x) \times (\text{In}_{1-x}\text{Yb}_x)\text{Cu}_4$  in Yb and In sublattices. It is responsible for spatial nonuniformity of the phase-transition temperature  $T_V$ . Taking into account a considerable susceptibility jump at the transition point as well as a high sensitivity of  $T_V$  to various factors (pressure, impurities, and magnetic field),<sup>15,20,24</sup> we can confine our analysis to just this mechanism of influence of lattice-site or chemical disorder on the magnetic susceptibility (1). In this case, the expression (1) remains valid if  $W(T)$  in (1) is a function of distribution of the values of  $T_V^i$  of the  $i$ th volume elements of sample. It was found<sup>19</sup> that the normal Gaussian distribution

$$W(T) = W(T, \bar{T}_V, \sigma) = \{1 + \text{erf}[(T - \bar{T}_V)/(\sqrt{2}\sigma)]\}/2 \quad (3)$$

[ $\text{erf}(x)$  is the standard error function] can serve as a satisfactory distribution function for weakly disordered  $\text{YbInCu}_4$  samples. In order to describe susceptibility in the vicinity of

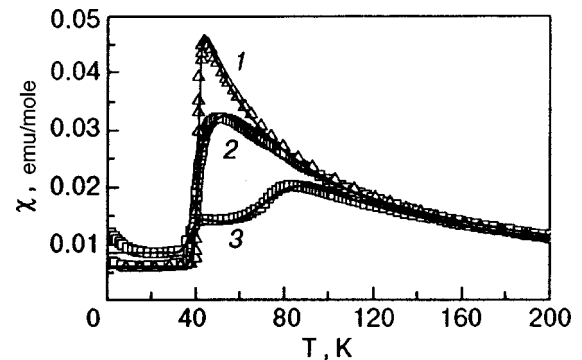


FIG. 1. Temperature dependence of magnetic susceptibility in different samples of  $\text{YbInCu}_4$  compound: for a single crystal with a high degree of perfection (curve 1), for a polycrystal (curve 2), and for a highly disordered sample (curve 3). Symbols correspond to experimental data of Ref. 20, solid curves are the results of model fitting.

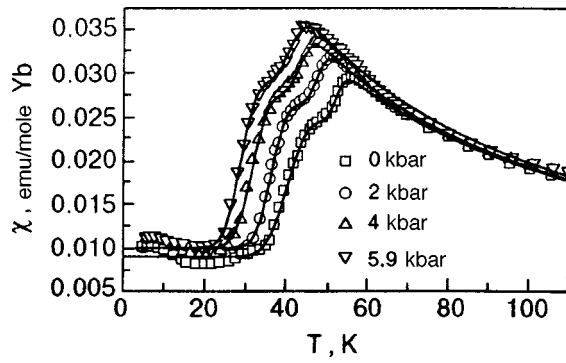


FIG. 2. Temperature dependence of magnetic susceptibility in nonstoichiometric compound  $\text{Yb}_{1.2}\text{In}_{0.8}\text{Cu}_4$  at different pressures according to experimental data of Ref. 15; solid curves are the results of model fitting.

phase transition with the help of Eqs. (1) and (3), it is sufficient to select the parameters of the distribution function, viz., a certain mean value  $\bar{T}_V$  and the dispersion  $\sigma^2$ , for asymptotic values of  $\chi_0$ ,  $\mu$ , and  $\Theta$ . We shall demonstrate the applicability and consequences of application of the proposed model from an analysis of the behavior of magnetic susceptibility as a function of ordering, applied pressure, and variation of composition.

### 3. ANALYSIS OF THE ROLE OF DISORDER IN STOICHIOMETRIC $\text{YbInCu}_4$ SAMPLES

Figure 1 shows that the peak on the temperature dependence of the magnetic susceptibility of  $\text{YbInCu}_4$  compound becomes less sharp as disordering in the sample increases and is then transformed into a two-hump curve also typical of samples with a nonstoichiometric composition (Fig. 2). There can be several reasons behind the emergence of the two humps. First, the presence of at least two types of dominating structural defects, which is quite natural for the presumed arrangement of Yb atoms in the two sublattices (Yb and In sublattice). Second, a certain stratification of the sample in composition within one structural phase for a special form of phase diagram.<sup>20</sup> Finally, the separation of the sample into two phases. In any of the versions listed above, the distribution function  $W(T)$  in (1) must contain two Gaussians of type (3) with different sets of parameters:

$$W(T) = W_1(T, \bar{T}_{V1}, \sigma_1)(1-n) + W_2(T, \bar{T}_{V2}, \sigma_2)n. \quad (4)$$

Figures 1 and 2 show the results of selection of the parameters  $\bar{T}_{Vj}$ ,  $\sigma_j$ , and  $n$  in Eqs. (1) and (4) for the best description of the  $\chi(T)$  dependences for samples with different degrees of disordering. The values of the parameters of the distribution function (4) and the magnetic parameters  $\chi_0$ ,  $\mu$ , and  $\Theta$  are given in Tables I and II.

Naturally, the distribution function (4) should also be used for describing two-hump dependences  $\chi(T)$  for nonstoichiometric samples also.

### 4. ANALYSIS OF THE EFFECT OF PRESSURE ON THE SUSCEPTIBILITY OF $\text{Yb}_{1.2}\text{In}_{0.8}\text{Cu}_4$

Figure 2 shows the temperature dependence of the magnetic susceptibility for nonstoichiometric compound

TABLE II. Values of model parameters of distribution function for nonstoichiometric compound  $\text{Yb}_{1.2}\text{In}_{0.8}\text{Cu}_4$  for different pressures (Fig. 2).

Parameter	Pressure, kbar			
	0	2	4	5.9
$n$	0.32	0.28	0.38	0.42
$\bar{T}_{V1}$ , K	40.8	36.7	32	29.2
$\bar{T}_{V2}$ , K	52	47	43.7	40.7
$\sigma_1$ , K	4	3.7	3.74	3.3
$\sigma_2$ , K	1.9	1.6	3	3.26

$\text{Yb}_{1.2}\text{In}_{0.8}\text{Cu}_4$  under different pressures (borrowed from Ref. 15) and its model description. The corresponding model parameters are given in Table II, and pressure dependences of the temperatures  $\bar{T}_{V1}$  and  $\bar{T}_{V2}$  are shown in Fig. 3. In the pressure range under investigation, these dependences are linear and have almost the same slope with the average value of  $d\bar{T}_V/dP = -2$  K/kbar. This value differs insignificantly from that obtained by Nowik *et al.*<sup>15</sup> from an analysis of displacement of singularities on the  $\chi(T)$  curve under pressure, although the shape of the curve is slightly deformed under pressure. This can be seen from the change in the parameters of the distribution function (4) in Table II. The weak but stable variation of the distribution function  $W(T)$  under pressure can be due to structural defects. Unfortunately, Nowik *et al.*<sup>15</sup> give no information concerning the reversibility of susceptibility after the removal of pressure. Subsequent measurements of the effect of pressure on the susceptibility of the compound with the stoichiometric composition give practically the same value of the derivative ( $-2$  K/kbar) for an imperfect sample for which disorder is taken into account<sup>19,21</sup> as well as a high-quality sample.<sup>18</sup>

### 5. ROLE OF DISORDER IN $\text{YbIn}_{1-x}\text{Ag}_x\text{Cu}_4$ SOLID MIXTURES

An analysis of magnetic properties of  $\text{YbIn}_{1-x}\text{Ag}_x\text{Cu}_4$  alloys is of special importance since it is generally accepted that the first-order valence phase transition in this system is transformed into a continuous transition for  $x \approx 0.25$  in view of changes in the parameters of electron-electron interaction during alloying.<sup>17</sup> Monocrystalline samples of solid mixtures in Ref. 17 were grown according to the same method under

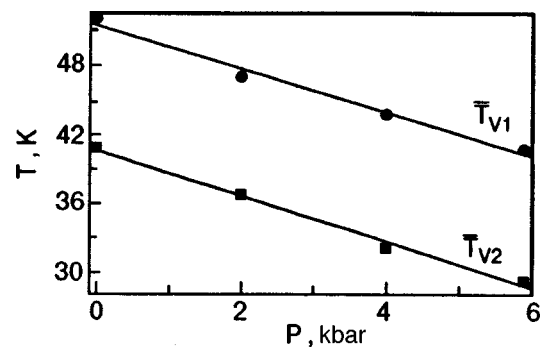


FIG. 3. Pressure dependence of model values of phase transition temperature for compound  $\text{Yb}_{1.2}\text{In}_{0.8}\text{Cu}_4$ .

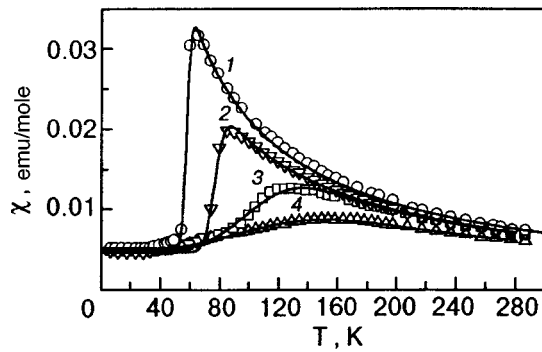


FIG. 4. Temperature dependence of magnetic susceptibility in  $\text{YbIn}_{1-x}\text{Ag}_x\text{Cu}_4$  alloys according to experimental data of Ref. 17 and their model fitting (solid curves) corresponding to the following values of concentration  $x$ : 0.1 (curve 1), 0.2 (curve 2), 0.3 (curve 3) and 0.4 (curve 4).

the InCu flux that was used for obtaining  $\text{YbInCu}_4$  compound, which ensured a high degree of sample perfection except random distribution of atoms over the sites of In–Ag sublattice. For this reason, we can confine the approximation of the  $\chi(T)$  dependences to formulas (1) and (3). The results of the approximation are shown in Fig. 4, and the obtained values of fitting parameters are given in Fig. 5.

The model used by us correctly describes the evolution of temperature dependences of susceptibility of alloys for a reasonable behavior of the parameters (at least, to values of  $x \approx 0.3$ ). For example, the linear increase in the phase-transition temperature with silver concentration  $d\bar{T}_V/dx = 203 \text{ K}$  (see Fig. 5a) is in satisfactory agreement with the data following from the measurements of elastic parameters ( $dT_V/dx = 210 \text{ K}$ ).<sup>25</sup> A weak initial increase in the quantity  $\sigma = (1 + 25x)$  (see Fig. 5b) appears as natural since disorder takes place in the In–Ag sublattice of the alloy under investigation and affects the  $f$ -states of Yb only indirectly.

The paramagnetic Curie temperature  $\Theta$  also changes insignificantly in the concentration range under investigation (Fig. 5c). However, this important parameter characterizing the interaction of the  $f$ -level with band electrons strongly depends on the accuracy of reconstruction of the  $\chi(T)$  dependences from the available data and on the choice of the temperature interval for their approximation. For this reason, the values of  $\Theta$  presented in Fig. 5c and Table II are rather qualitative estimates, and only the anomalous increase in the absolute value of  $\Theta$  as well as  $\sigma$  starting from a certain critical value  $x_c = 0.25 - 0.3$  is worth noting.

## 6. DISCUSSION OF THE RESULTS OF MODEL ANALYSIS OF SUSCEPTIBILITY

1. It should be noted above all that in our model we assume the simplest structure of the distribution function for the phase-transition temperature  $T_V$  in a spatially inhomogeneous sample. The validity of just this function is not obvious beforehand, but nevertheless the proposed model makes it possible to approximate correctly the transformation of magnetic susceptibility of the compound  $\text{YbInCu}_4$  under the action of various factors in combination with the disorder taking place or induced by these interactions. This allows us to assume that the behavior of physical parameters deter-

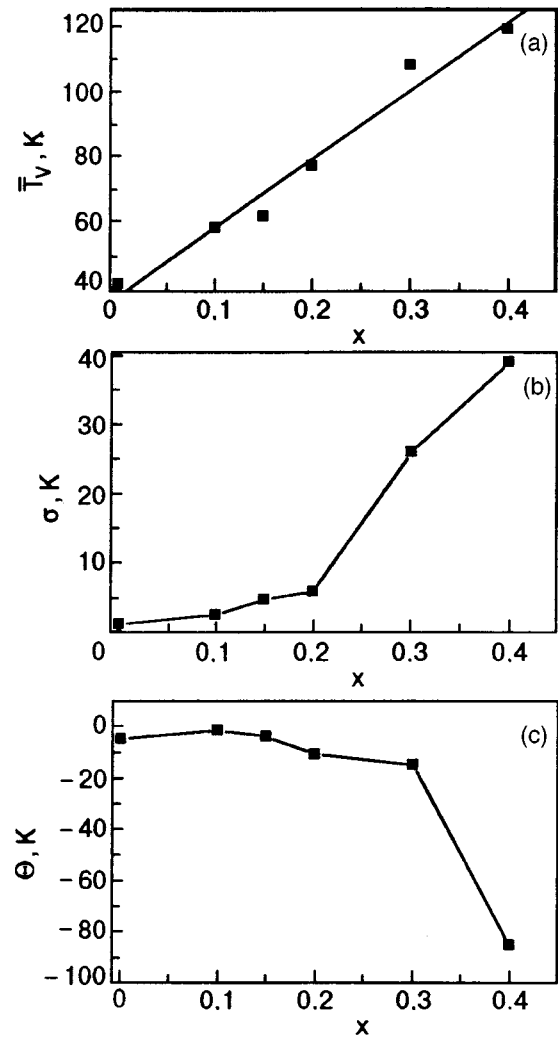


FIG. 5. Concentration dependence of model parameters calculated by formulas (1) and (3) for  $\text{YbIn}_{1-x}\text{Ag}_x\text{Cu}_4$  alloys:  $\bar{T}_V$  (a),  $\sigma$  (b) and  $\Theta$  (c).

mined as a result of such an approximation corresponds to the properties of a perfect system. It is remarkable that the spatial distribution function for Curie temperature reconstructed experimentally for some compositions of inhomogeneous Invar alloys Fe–Ni is close to the Gaussian distribution function.<sup>26</sup> Apparently, distribution (3) can indeed serve as a good initial approximation for taking into account imperfection of various systems.

2. The results of successful model fitting of temperature dependences of susceptibility correspond to the assumption that dispersion of the quantity  $T_V$  is mainly responsible for smoothing of singularities in the physical properties of disordered samples in the phase-transition region. This assumption is confirmed by an anomalous increase in the magneto-volume effect in imperfect samples in the vicinity of the phase-transition temperature<sup>27</sup> since just in this case the effect involves a strong pressure dependence of  $T_V^i$  and  $\chi(T_V^i)$  of volume elements of the sample with  $T_V^i \approx T$ . A direct microscopic evidence of dispersion of  $T_V$  is the simultaneous observation of the NMR signal from the IV and HF phases<sup>28</sup> coexisting in the temperature range  $\sim \sigma$  in the vicinity of  $T_V$ .

The value of the Curie temperature  $\Theta$  also depends on the composition and the degree of perfection of samples, but the role of its possible dispersion in (1) is considerably smaller than the effect of  $T_V$  according to estimates. For this reason, we disregard here the nonuniformity of  $\Theta$  to simplify the analysis, which does not affect semi-quantitative conclusions drawn below.

3. An increase in the extent of disorder in the stoichiometric compound, as well as deviation from stoichiometry, leads to “splitting” of  $T_V$  into two temperatures. Their identical pressure dependences speak in favor of the concentration stratification of the sample within the same structural phase rather than separation into different phases. It was presumed by Lawrence *et al.*<sup>20</sup> that such a stratification can be due to peritectic nature of the phase diagram for the compound YbInCu<sub>4</sub>. However, the shape of the phase diagram in the region of the stoichiometric composition under investigation has not been established as yet by direct structural methods, and we cannot rule out in principle the existence of two isomeric HF phases with close atomic volumes and properties, whose transition to the IV phase is controlled by the same parameters of the system, although it occurs at slightly different temperatures. In such a case, the very fact and the actual origin of phase separation of the sample are immaterial, and a distribution function of the form (3), albeit with a high dispersion,<sup>19</sup> remains valid for an adequate description of a number of its properties for a moderate disorder.

4. In the presence of stratification in the highest-temperature phase of the compound under investigation, a detailed comparison of the parameters of the  $\bar{T}_V$  distribution function for samples obtained under different conditions in different laboratories (and the more so, by different methods) is meaningful only on a qualitative level. A comparison of values of dispersion in Table II and in Fig. 5b shows that the disorder associated with imperfection of the method of preparation of stoichiometric samples is a much more important factor for the magnetism of the compound under investigation than, for example, the disorder in the In–Ag sublattice of the YbIn<sub>1-x</sub>Ag<sub>x</sub>Cu<sub>4</sub> solid mixture which cannot be eliminated in principle (it should be noted for comparison that sample 3 in Fig. 1 corresponds to  $x \approx 0.06$  in the equivalent formula for the disordered stoichiometric composition (Yb<sub>1-x</sub>In<sub>x</sub>)(In<sub>1-x</sub>Yb<sub>x</sub>)Cu<sub>4</sub> mentioned above).<sup>20</sup>

Thus, the results of analysis of the properties of alloys based on the compound YbInCu<sub>4</sub> without an appropriate control of the state of the Yb–In subsystem should be treated with care. This remark does not concern the data for YbIn<sub>1-x</sub>Ag<sub>x</sub>Cu<sub>4</sub> alloys used by us here since these data were obtained by using the standard method which minimizes the disorder in the Yb–In sublattice.<sup>17</sup>

5. The behavior of the magnetic susceptibility upon an increase in the Ag concentration up to  $x \approx 0.3$  in YbIn<sub>1-x</sub>Ag<sub>x</sub>Cu<sub>4</sub> alloys is essentially explained in the model (1), (3) only by an increase in the value of  $\bar{T}_V$  and its dispersion. Such an approach differs in principle from that used by Sarrao *et al.*<sup>17</sup> who approximated the experimental dependences  $\chi(T)$  by the theoretical curve for a Kondo impurity with  $J = 7/2$ <sup>22</sup> by selecting the characteristic temperature for

the low- and high-temperature phases separately. Thus, the evolution of asymptotic segments of the  $\chi(T)$  curves during alloying is associated, according Sarrao *et al.*,<sup>17</sup> with a variation of the parameters  $T_K^{IV}$  and  $T_K^{HF}$ . In this case, the transition temperature region, and hence the behavior of  $T_V(x)$ , which play the leading role in the proposed model of disordering are not considered.

The exaggerated opposition of the mechanisms of temperature dependence of  $\chi$  in the approaches discussed here demonstrates that the inclusion of disorder is of considerable importance. In actual practice, both mechanisms must be taken into account in the description of experimental results. In contrast to the model proposed by Sarrao *et al.*,<sup>17</sup> the model (1), (3) allows us to do this easily, but the temperature dependence of susceptibility alone is obviously insufficient for an unambiguous selection of the doubled number of parameters. According to the results obtained by us earlier,<sup>19,21</sup> the magnetovolume effect  $d \ln \chi / d \ln V$  in the alloys under investigation can successfully compensate the missing experimental information.

6. This effect would be especially helpful in the vicinity of the concentration  $x_c$  which is critical indeed for the parameters of the proposed model: for  $x > x_c$ , the concentration dependence of  $\sigma$  as well as  $\Theta$  becomes considerably stronger. The dispersion of  $\bar{T}_V$  and the characteristic of the interaction of magnetic moment with band electrons in the HF phase<sup>29</sup> ( $|\Theta| \approx T_K^{HF}$ ) are not connected directly, and we cannot establish unambiguously the reason behind such a behavior on the basis of the available data.

A possible reason can be the transformation of an abrupt phase transition at  $x_c$  into a continuous transition,<sup>17</sup> which presumes that the values of  $T_K^{IV}$  and  $T_K^{HF}$  become closer. The corresponding increase in  $|\Theta|$  in Fig. 5c does not contradict such a hypothesis and the asymptotic value of  $T_K = 143$  K for  $x = 1$ ,<sup>17</sup> and the increasing role of dispersion of the Kondo temperature can be manifested in a more rapid increase in  $\sigma$ . Although the model itself must be modified for  $x > x_c$  in the case of transformation of phase transition, the dependences in Fig. 4 following from it appear more natural than the strong and nonmonotonic changes in  $T_K^{IV}$  and  $T_K^{HF}$  in Ref. 17. The latter have no singularities for  $x_c$ , and this concentration is singled out by Sarrao *et al.*<sup>17</sup> on the basis of the change in the behavior of  $\chi(T)$  only in the transition temperature region. Naturally, the first-order phase-transition curve in Fig. 5a must terminate at  $x \approx 0.3$  for such a scenario, and its continuation beyond  $x_c$  is only the result of successful imitation of the  $\chi(T)$  dependence by the initial model (1), (3).

However, it cannot be ruled out that the observed behavior of the model parameters is due to inclusion of the additional interaction of the moments upon attainment of a certain level of band filling or coordination of impurity atoms in the nearest neighborhood of Yb (of the type of percolation effect). It is also possible that such a behavior is associated with the beginning of a certain structural randomization in the alloy involving the Yb sublattice in spite of the application of unique method of sample preparation. The list of possible scenarios is much larger, and further investigations of structural and electronic properties of the YbIn<sub>1-x</sub>Ag<sub>x</sub>Cu<sub>4</sub>

system must be carried out in the concentration range  $x \sim x_c$  for selecting the most realistic scenario. The analysis carried out by us here indicates that there are no solid grounds for assuming that the concentration  $x_c$  is the point of termination of the first-order transition curve on the  $T-x$  diagram.

## 7. CONCLUSIONS

Summarizing the results of analysis of the role of chemical disorder in the  $\text{YbInCu}_4$  compound and in  $\text{YbIn}_{1-x}\text{Ag}_x\text{Cu}_4$  alloys, we can formulate the following statements.

1. Chemical disorder (especially in the Yb sublattice) can radically change the properties of the systems under investigation due to spatial nonuniformity of the first-order valence phase transition temperature.

2. The model proposed by us earlier<sup>19</sup> with a normal Gaussian distribution for  $T_V$  describes the transformation of the magnetic susceptibility of  $\text{YbInCu}_4$  under the influence of various effects with a plausible behavior of parameters. The dependence  $T_V(x)$  obtained for the first time for  $\text{YbIn}_{1-x}\text{Ag}_x\text{Cu}_4$  alloys is close to a linear dependence with the derivative  $dT_V/dx = 203$  K.

3. The behavior of the parameters of the  $\text{YbIn}_{1-x}\text{Ag}_x\text{Cu}_4$  system changes significantly for the critical concentration  $x_c \approx 0.03$ , but it is premature to attribute this to a change in the type of phase transition. Additional investigations of structural and electronic properties of the alloys in the region of critical composition are required to rule out other scenarios.

<sup>\*</sup>E-mail: isvechkarev@ilt.kharkov.ua

<sup>1</sup>D. C. Koskenmaki and K. A. Gschneidner, Jr., in *Handbook on the Physics and Chemistry of Rare Earths*, Vol. 1 (ed. by K. A. Gschneidner, Jr. and L. Eyring), North Holland, Amsterdam (1978); J. M. Lawrence, P. S. Risenborough, and R. D. Parks, *Rep. Prog. Phys.* **44**, 1 (1981).

<sup>2</sup>Ye. G. Ponyatovskii, *Dokl. Akad. Nauk* **120**, 1021 (1958) [*Sov. Phys. Dokl.* **3**, 498 (1958)].

<sup>3</sup>G. Eliashberg and H. Capellmann, *Pis'ma Zh. Éksp. Teor. Fiz.* **67**, 111 (1998) [*JETP Lett.* **67**, 125 (1998)].

<sup>4</sup>L. M. Falicov and J. C. Kimball, *Phys. Rev. Lett.* **22**, 997 (1969); R. Ramirez and L. M. Falicov, *Phys. Rev. B* **3**, 2424 (1971).

<sup>5</sup>J. K. Freericks and V. Zlatic, *Phys. Rev. B* **58**, 322 (1998).

<sup>6</sup>B. Johansson, *Philos. Mag.* **30**, 469 (1974).

<sup>7</sup>B. Johansson and M. S. S. Brooks, in *Handbook on the Physics and Chemistry of Rare Earths*, Vol. 17 (edited by K. A. Gschneidner, Jr., L. Eyring, G. H. Lander, and G. R. Choppin), Elsevier Science Publisher B. V., Amsterdam (1993).

<sup>8</sup>M. Croft, J. A. Hodges, E. Kemly *et al.*, *Phys. Rev. Lett.* **48**, 826 (1982).

<sup>9</sup>I. Novik, *Hyperfine Interact.* **13**, 89 (1983).

<sup>10</sup>I. Felner and I. Nowik, *Phys. Rev. B* **33**, 617 (1986).

<sup>11</sup>M. Lavagna, C. Lacroix, and M. Cyrot, *J. Phys. (Paris)* **F13**, 1007 (1983).

<sup>12</sup>J. W. Allen and R. M. Martin, *Phys. Rev. Lett.* **49**, 1106 (1982).

<sup>13</sup>J. W. Allen and L. Z. Liu, *Phys. Rev. B* **46**, 5047 (1992).

<sup>14</sup>T. Jarlborg, E. G. Moroni, and C. Grimvall, *Phys. Rev. B* **55**, 1288 (1997).

<sup>15</sup>I. Novik, I. Felner, J. Voiron *et al.*, *Phys. Rev. B* **37**, 5633 (1988).

<sup>16</sup>J. L. Sarrao, C. L. Benton, Z. Fisk *et al.*, *Physica B* **223–224**, 366 (1996).

<sup>17</sup>J. L. Sarrao, C. D. Immer, C. L. Benton *et al.*, *Phys. Rev. B* **54**, 12207 (1996).

<sup>18</sup>J. L. Sarrao, A. P. Ramirez, T. W. Darling *et al.*, *Phys. Rev. B* **58**, 409 (1998).

<sup>19</sup>I. V. Svechkarev, A. S. Panfilov, S. N. Dolya *et al.*, in *Itinerant Electron Magnetism: Fluctuation Effects* (edited by D. Wagner, W. Brauneck, and A. Solontsov), Kluwer Academic Publ., Netherlands (1998); I. V. Svechkarev, A. S. Panfilov, S. N. Dolya *et al.*, *J. Phys.: Condens. Matter* (submitted).

<sup>20</sup>J. M. Lawrence, G. H. Kwei, J. L. Sarrao *et al.*, *Phys. Rev. B* **54**, 6011 (1996).

<sup>21</sup>I. V. Svechkarev, A. S. Panfilov, S. N. Dolja *et al.*, *J. Magn. Magn. Mater.* **196–197**, 893 (1999).

<sup>22</sup>V. T. Rajan, *Phys. Rev. Lett.* **51**, 308 (1983).

<sup>23</sup>A. E. Severing, E. Gratz, B. D. Rainford, and K. Yoshimura, *Physica B* **163**, 409 (1990).

<sup>24</sup>I. Felner, I. Nowik, D. Vaknin *et al.*, *Phys. Rev. B* **35**, 6956 (1987).

<sup>25</sup>S. Zherlitsyn, D. Finsterbusch, G. Bruls *et al.*, in *International Conference on Strongly Correlated Electron Systems*, Paris (1999) (unpublished).

<sup>26</sup>A. Yu. Romanov, V. P. Silin, and D. Wagner, *Phys. Lett. A* **226**, 310 (1997).

<sup>27</sup>J. M. de Teresa, Z. Arnold, A. del Moral *et al.*, *Solid State Commun.* **99**, 911 (1996).

<sup>28</sup>K. Kojima, H. Hayashi, A. Minami *et al.*, *J. Magn. Magn. Mater.* **81**, 267 (1989).

<sup>29</sup>E. Bauer, *Adv. Phys.* **40**, 417 (1991).

## ELECTRONIC PROPERTIES OF METALS AND ALLOYS

### Nonstationary effects induced by a strong direct current in a compensated metal

G. B. Tkachev

*Institute of Radiophysics and Electronics, National Academy of Sciences of the Ukraine, 310085 Kharkov, Ukraine\**

(Submitted March 1, 1999)

Fiz. Nizk. Temp. **25**, 1194–1202 (November 1999)

The existence of nonstationary electromagnetic processes in a plate of compensated metal carrying a strong direct current is established theoretically. The nonstationary effects are due to the nonlinearity caused by the influence of an inhomogeneous sign-alternating magnetic field of the current on the dynamics of charge carriers. Such an influence suppresses conductivity in the entire sample except a narrow region near the zero magnetic field plane. It is found that the current pinch formed in this region can propagate quasi-statically in the direction transverse to the current. As a result, an ac electric field component (and hence, an ac voltage across the sample) appears against the background of the applied dc electric field. The ac voltage generation can be observed experimentally in a preset current mode. © 1999 American Institute of Physics. [S1063-777X(99)00711-2]

#### INTRODUCTION

Experiments on pure metals at low temperatures revealed a number of electrodynamic effects which could not be described on the basis of conventional concepts of metals as exceptionally “linear” elements. Among first communications were those on observation of deviation of current–voltage characteristics (IVC) for thin samples from Ohm’s law towards a decrease in resistance,<sup>1,2</sup> dependence of surface impedance on the amplitude of incident wave,<sup>3</sup> and hysteretic rectification of rf current in a metal.<sup>4,5</sup> Nonlinearity was observed for such insignificant values of current or wave amplitude that it could not be due to overheating of charge carriers or other familiar sources of nonlinearity associated with electric field. It was found that the nonlinearity typical of pure samples is connected with their main property, viz., long mean free path for electrons. The mean free paths of charge carriers in pure conductors at low temperatures can be as large as a few millimeters. For this reason, the magnetic field of the current effectively bends the trajectories of particles, thus affecting the metal conductivity. Such a nonlinearity mechanism is known as magnetodynamic. In the static case, the most favorable conditions for its observation are created in thin samples whose thickness  $d$  can be smaller than the mean free path  $l$  of the carriers:

$$d \ll l. \quad (1)$$

The conductivity is determined in this case by a small group of electrons moving almost parallel to the metal surface. In view of the small number of such electrons, even a comparatively weak magnetic field of the current can noticeably affect the electrical conductivity of the sample and its IVC.

A theoretical analysis of the magnetodynamic nonlinearity effects in the static case was carried out for the first time by Kaner *et al.*,<sup>6</sup> who studied the conductivity and IVC of a

thin plane-parallel plate with diffuse boundaries. It was proved that peculiarities of the nonlinear response in the sample are associated with an alternation of the magnetic field of the current over the sample thickness. It is equal to zero at the middle of the plate and assumes equal but opposite values  $\mathcal{H}$  and  $-\mathcal{H}$  at the opposite faces of the plate:

$$\mathcal{H} = 2\pi I/c. \quad (2)$$

Here  $I$  is the current per unit width of the plate and  $c$  the velocity of light in vacuum. The alternating magnetic field of the current traps a part of electrons in the potential well. The trajectories of such particles are coiled around the zero magnetic field plane. For this reason, trapped charge carriers interact with the electric field over the entire mean free path  $l$ . As the current  $I$  increases, the number of such carriers increases due to particles that collided with the metal surface for smaller values of the current and hence could not participate effectively in the formation of the plate conductivity. Thus, trapping of electrons increases the conductivity of the sample. This is observed for quite small values of  $I$  for which the characteristic radius of curvature  $R(I)$  of electron trajectories in the magnetic field of the current is larger than the plate thickness:

$$R(I) = cp_F/e\mathcal{H}(I) \propto I^{-1}, \quad d < R(I), \quad (3)$$

where  $-e$  and  $p_F$  are the charge and Fermi momentum of an electron.

The theory constructed by Kaner *et al.*<sup>6</sup> explained the results obtained in Refs. 1 and 2 and stimulated new experimental investigations.<sup>7</sup> It was found that as the current  $I$  increases further, the resistance of thin plates attains its minimum value (when the radius  $R(I)$  becomes of the order of  $d$ ) and then starts increasing. In the region of strong currents

$$d \gg R(I) \quad (4)$$

the resistance of a conductor exhibits a tendency to a linear increase. Such a regularity is observed for metals with equal concentrations of electrons and holes (compensated metals), e.g., tungsten and cadmium (see Ref. 7).

Later, Kaner *et al.*<sup>8</sup> established theoretically that the increase in the resistance of thin samples of a compensated metal is due to a peculiar pinch effect. According to Kaner *et al.*,<sup>8</sup> in the limit of strong currents (4) all the electrons intersecting the zero magnetic field plane become trapped irrespective of the angle of incidence on the plane. As a result, their conductivity tends to saturation and becomes of the same order of magnitude as the conductivity  $\sigma = Ne^2l/p_F$  of a bulk plate ( $N$  is the charge carrier concentration). In this case, in contrast to the case of weak currents (3), the group of trapped particles occupies not all the sample, but is concentrated in a narrow central region having a width of the order of  $R(I)$ . Outside this region, charge carriers move in a dc magnetic field along trajectories resembling Larmor orbits. Their conductivity turns out to be much smaller than the conductivity of trapped particles.<sup>9</sup> As a result, a strongly nonuniform spatial distribution of current density typical of the pinch effect sets in in the plate. The width of the current pinch formed by trapped electrons decreases with increasing  $I$ . This in turn leads to an increase in the sample resistance.

The strong nonlinearity in the distribution of direct current over the sample cross section can generally lead to effects of another type, such as the instability of the static current structure, and to a transition to a nonstationary state (see Ref. 10). Such a situation was not considered as applied to the pinch effect (4), although the available experimental data indicate the evolution of nonstationary processes under the preset direct current conditions.<sup>11</sup>

The aim of the present publication is to demonstrate theoretically the possibility of a nonstationary process in a compensated metal carrying a strong direct current. The dynamics of charge carriers and their conductivity in the strongly nonuniform magnetic field of the current is analyzed in Sec. 2. It is found (see Sec. 3) that the static distribution of current in the case (4) is not the only one possible distribution. An alternative state in which the current pinch propagates in the direction transverse to the current is possible due to essentially nonlinear and nonlocal nature of conductivity. In this case, instead of a uniform electric field distribution over the plate thickness, a domain structure is formed: the propagating current pinch separates two regions with different values of electric field  $E$ . The difference in these values is proportional to the velocity of propagation. The direction of motion of the domain wall and the pinch is such that the region of a stronger electric field expels the region with a smaller value of  $E$ . The observed nonstationary process is not accompanied by Joulean losses.

## 1. FORMULATION OF THE PROBLEM: BASIC EQUATIONS AND BOUNDARY CONDITIONS

We shall assume that the required nonstationary state is quasi-static: the characteristic time  $\Delta t$  of variation of electromagnetic field is much longer than the mean free time of charge carriers:

$$\Delta t \gg \nu^{-1}, \quad (5)$$

where  $\nu$  is the frequency of bulk relaxation of particles. We shall assume that reflection of electrons at the plate boundaries is diffusive.

We introduce the Cartesian system of coordinates in which the  $x$ -axis is perpendicular to the faces of the plate, and the plane  $x=0$  is at the middle of the sample. We direct the  $y$ -axis along the current and the  $z$ -axis along the vector  $\mathbf{H}(x,t)$  of the magnetic field of the current:

$$\mathbf{H}(x,t) = \{0, 0, H(x,t)\}. \quad (6)$$

The plate is assumed to be infinitely long (the size along the  $y$ -axis) and wide (the size along the  $z$ -axis).

In order to emphasize most vividly the role of magnetodynamic nonlinearity in the phenomena under investigation, we assume a simple model of a compensated metal, i.e., assume that the electron and hole Fermi surfaces are identical spheres. The masses and mean free paths of electrons and holes are also regarded to be identical. In this case, electrons and holes make equal contributions to the electrical conductivity tensor. These contributions are mutually compensated in the nondiagonal tensor components and added in the diagonal components. Thus, the Hall effect does not take place in the metal. This means that the electric field vector  $\mathbf{E}(x,t)$  is directed along the current:

$$\mathbf{E}(x,t) = \{0, E(x,t), 0\}. \quad (7)$$

The electric  $E(x,t)$  and magnetic  $H(x,t)$  fields can be determined from Maxwell's equations, which have the following form in our geometry:

$$-\frac{\partial H(x,t)}{\partial x} = \frac{4\pi}{c} j(x,t), \quad \frac{\partial E(x,t)}{\partial x} = -\frac{1}{c} \frac{\partial H(x,t)}{\partial t}, \quad (8)$$

where  $j(x,t)$  is the current density.

Since the characteristic size  $R(I)$  of the electron orbit under the conditions (1) and (4) is much smaller than the plate thickness as well as the mean free path, we shall carry out the analysis of the distribution of current density and the fields in the main approximation in the parameters  $R(I)/d \ll 1$  and  $R(I)/l \ll 1$ . The limit  $(R(I)/d) \rightarrow 0$  corresponds to the approximation of unbounded metal. In this case, the boundary conditions for Maxwell's equations (8) can be written in the form

$$H(-\infty, t) = -H(+\infty, t) = \mathcal{H}(I). \quad (9)$$

Since we assume that the total current

$$I = \int_{-\infty}^{+\infty} dx j(x,t), \quad (10)$$

is assumed to be constant, the magnetic field  $H(x,t)$  for  $x \rightarrow \pm \infty$  is independent of time [see (9)] and is determined only by the value of  $I$  in accordance with (2).

## 2. DYNAMICS OF CONDUCTION ELECTRONS AND CURRENT DENSITY

Peculiarities of the nonlinear conductivity of a metal are determined by the shape of electron trajectories formed by the intrinsic magnetic field of the current. Let us analyze the

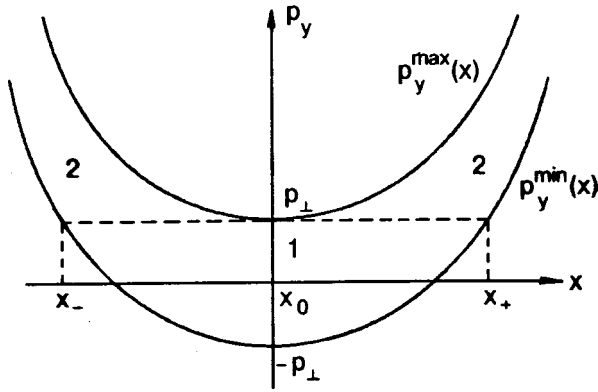


FIG. 1. Phase space \$(p\_y, x)\$. Regions of existence of trapped (1) and Larmor (2) particles.

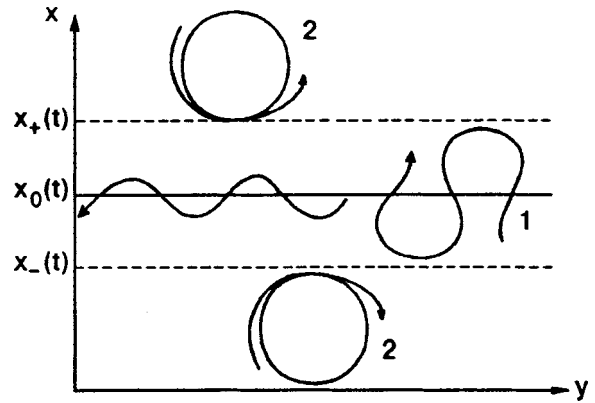


FIG. 2. Geometry of the problem. Schematic diagram of trajectories of trapped (curves 1) and Larmor (curves 2) electrons in the intrinsic magnetic field of current.

dynamics of charge carriers in a nonuniform quasi-static field \$H(x,t)\$. Since the motion of electrons and holes in the adopted model of the metal differs only in the sign of the radius of curvature of their trajectories, we shall consider only the dynamics of electrons.

The integrals of motion in a magnetic field \$H(x,t)\$ are the total energy (which will be assumed to be equal to the Fermi energy for definiteness)

$$\epsilon_F = p_F^2/2m, \tag{11}$$

and the \$y\$- and \$z\$-components of the generalized momentum, i.e.,

$$p_y = m v_y - eA(x,t)/c, \quad p_z = m v_z. \tag{12}$$

Here \$m\$ is the electron mass and \$v\_y\$ and \$v\_z\$ are the components of electron velocity. The vector potential \$\mathbf{A}(x,t)\$ is calibrated as follows:

$$A(x,t) = \{0, A(x,t), 0\}, \quad A(x,t) = \int_{x_0}^x dx' H(x',t). \tag{13}$$

The symbol \$x\_0\$ denotes the point at which the magnetic field of the current vanishes, i.e., \$H(x\_0,t) = 0\$. In the static situation, this point corresponds to the middle of the sample, i.e., \$x\_0 = 0\$. In the general case, however, the value of \$x\_0\$ depends on time and hence does not coincide with \$x = 0\$. The value of \$A(x,t)\$ is negative and attains its maximum equal to zero for \$x = x\_0(t)\$.

The velocity component \$v\_x\$ is defined as

$$v_x = \pm (1/m)[p_{\perp}^2 - (p_y + eA(x,t)/c)^2]^{1/2}, \tag{14}$$

$$p_{\perp} = (p_F^2 - p_z^2)^{1/2}.$$

The condition that the radicand in the first formula in (14) must be nonnegative can be used to find the range of admissible values of the generalized momentum \$p\_y\$:

$$p_y^{\min}(x,t) \equiv -p_{\perp} - \frac{eA(x,t)}{c} \leq p_y \leq p_{\perp} - \frac{eA(x,t)}{c} \tag{15}$$

$$\equiv p_y^{\max}(x,t).$$

This range is shown schematically in Fig. 1 in the

coordinates \$p\_y\$ and \$x\$. It can be seen that conduction electrons can be divided into two groups according to the type of motion:

(a) Trapped particles. They exist due to the alternating spatial distribution of the magnetic field of the current. Their trajectories are shown in Fig. 2 in the form of curves 1 coiling around the plane \$x = x\_0(t)\$. The half-period of motion of a trapped electron along the \$x\$-axis is given by

$$T(p_{\perp}, p_y) = \int_{x_1}^{x_2} \frac{dx'}{|v_x(x',t)|}. \tag{16}$$

According to Fig. 1, the turning points \$x\_1 < x\_2\$ are the roots of the equation

$$p_y^{\min}(x,t) = p_y. \tag{17}$$

In the momentum space \$(p\_{\perp}, p\_y)\$, this group of electrons corresponds to the region

$$-eA(x,t)/2c \leq p_{\perp} \leq p_F, \tag{18}$$

$$p_y^{\min}(x,t) \leq p_y \leq p_y^{\max}(x,t) = p_{\perp}.$$

It is important to note that trapped particles are present only in the neighborhood of the plane \$x = x\_0(t)\$, occupying the spatial region of width \$x\_+ - x\_-\$. The coordinates \$x\_{\pm}\$ of the boundaries of the region where trapped carriers exist are the roots of the equation

$$e|A(x_{\pm},t)|/2cp_F = 1. \tag{19}$$

(b) Larmor electrons. These particles move in a constant-polarity magnetic field of the current in trajectories 2 resembling circular orbits (see Fig. 2). However, in contrast to Larmor circles, their trajectories are open in view of nonuniformity of the field \$H(x,t)\$. The half-period of motion of Larmor electrons is given by (16), and according to Fig. 1, the turning points \$x\_1 < x\_2\$ can be found from the equations

$$p_y^{\max}(x,t) = p_y, \quad p_y^{\min}(x,t) = p_y. \tag{20}$$

The momentum space region \$(p\_{\perp}, p\_y)\$ occupied by this electron group is defined by the inequalities

$$0 \leq p_{\perp} \leq p_F, \max\{p_{\perp}, p_y^{\min}(x,t)\} \leq p_y \leq p_y^{\max}(x,t),$$

$$\max\{p_{\perp}, p_y^{\min}(x,t)\} = \frac{p_{\perp} + p_y^{\min}(x,t)}{2} + \frac{|p_{\perp} - p_y^{\min}(x,t)|}{2}. \tag{21}$$

The current density for the corresponding groups of particles can be determined from the solution of Boltzmann's kinetic equation which must be linearized in the electric field  $E(x,t)$ . The nonlinearity in this case is completely determined by the magnetic field  $H(x,t)$  in the Lorentz force. If we choose the generalized momentum  $p_y$  (12), the quantity  $p_{\perp}$  (14), and the electron energy as independent variables of the distribution function, the kinetic equation is transformed into an ordinary differential equation. It can be easily integrated for positive and negative values of the velocity  $v_x$  (14) separately. Integration constants are determined from the conditions of joining of the obtained solutions at the points  $x_{1,2}$  of electron turning. Omitting simple calculations, we write the final result:<sup>8</sup>

$$j_{t,L}(x,t) = \frac{3}{2\pi} \frac{\sigma}{p_F^2 l} \int_{O_{t,L}} \frac{dp_{\perp} dp_y p_{\perp} v_y(x,t)}{(p_F^2 - p_{\perp}^2)^{1/2} |v_x(x,t)|} \times \left\{ \int_{x_1}^x \frac{dx' v_y(x',t) E(x',t)}{|v_x(x',t)|} \sinh(\nu\tau(x;x')) + \frac{\cosh(\nu\tau(x_1;x))}{\cosh(\nu T)} \times \int_{x_1}^{x_2} \frac{dx' v_y(x',t) E(x',t)}{|v_x(x',t)|} \cosh(\nu\tau(x_2;x')) \right\}. \tag{22}$$

The symbols  $O_t$  and  $O_L$  denote the regions (18) and (21) of trapped and Larmor electrons in the momentum space  $(p_{\perp}, p_y)$ . The quantity

$$\tau(x;x') = \int_x^{x'} \frac{dx''}{|v_x(x'',t)|}. \tag{23}$$

is the time of motion of a particle between the points  $x$  and  $x'$ .

The parameter  $\nu\tau$  appearing in (22) has the same order of magnitude as the ratio of the characteristic radius of curvature  $R$  of electron trajectories to the mean free path  $l$  of charge carriers:

$$\nu\tau \sim R/l \ll 1. \tag{24}$$

In the main approximation in this parameter, the current density of trapped and Larmor charge carriers is independent of  $\nu\tau$ .

$$j_{t,L}(x,t) = \frac{3}{2\pi} \frac{\sigma}{p_F^3} \int_{O_{t,L}} \frac{dp_{\perp} dp_y p_{\perp} v_y(x,t)}{|v_z||v_x(x,t)| T} \times \int_{x_1}^{x_2} \frac{dx' v_y(x',t) E(x',t)}{|v_x(x',t)|}. \tag{25}$$

We transform the integral with respect to the coordinate  $x'$ . According to formulas (12) and (14), the velocity ratio  $v_y/|v_x|$  is proportional to the derivative of  $|v_x|$  with respect to the coordinate:

$$\int_{x_1}^{x_2} \frac{dx' v_y(x',t) E(x',t)}{|v_x(x',t)|} = - \frac{mc}{e} \int_{x_1}^{x_2} dx' \frac{\partial |v_x(x',t)|}{\partial x'} \frac{E(x',t)}{H(x',t)}. \tag{26}$$

We integrate the right-hand side of this equality by parts. Since the velocity component  $v_x$  vanishes at the turning points  $x_1$  and  $x_2$ , the nonintegral term vanishes, and the ratio (26) assumes the form

$$\int_{x_1}^{x_2} \frac{dx' v_y(x',t) E(x',t)}{|v_x(x',t)|} = \frac{mc}{e} \int_{x_1}^{x_2} dx' |v_x(x',t)| \frac{\partial}{\partial x'} \frac{E(x',t)}{H(x',t)}. \tag{27}$$

It follows hence that the asymptotic form (25) of current density differs from zero only due to the nonuniformity of the magnetic  $H(x,t)$  and electric  $E(x,t)$  fields. It should be noted that the next term in the expansion in the small parameter (24) is proportional to  $(R/l)^2 \ll 1$ . This term describes the magnetoresistance effect in the intrinsic magnetic field of the current.

### 3. SELF-SIMULATING SOLUTION OF MAXWELL'S EQUATIONS. ZERO-CURRENT RUNNING WAVE

We assume that a nonstationary process has the form of a wave of the type

$$E(x,t) = E(x-Vt), \quad H(x,t) = H(x-Vt), \tag{28}$$

propagating along the  $x$ -axis,  $V$  being the phase velocity. For a solution of the type (28), the second Maxwell equation (8) is transformed into an ordinary differential equation. Integrating it, we can find the relation between the electric and magnetic fields:

$$E(x-Vt) = E_0 + (V/c)H(x-Vt). \tag{29}$$

In this relation, the first term  $E_0$  is the integration constant. It is equal to the electric field in the static case when  $V=0$ . The second term  $(V/c)H(x-Vt)$  is the varying non-uniform field of the wave. It turns out that it does not generate current. Indeed, the electric field  $(V/c)H(x-Vt)$  nullifies the integral (27):

$$\int_{x_1}^{x_2} \frac{dx' v_y(x'-Vt)}{|v_x(x'-Vt)|} \frac{V}{c} H(x'-Vt) = \frac{mc}{e} \int_{x_1}^{x_2} dx' |v_x(x'-Vt)| \frac{\partial}{\partial x'} \frac{V}{c} = 0. \tag{30}$$

Thus, the current in a metal exists only due to the constant electric field  $E_0$ . The current density depends on time since it is a functional of the varying magnetic field  $H(x-Vt)$ . We shall write the expression for current density in terms of dimensionless variables of the self-simulating variable  $\xi$ , magnetic field  $h(\xi)$ , and the vector potential  $a(\xi)$ , which can be introduced as follows:

$$\xi = (x-Vt)/R(I), \quad h(\xi) = H(x-Vt)/\mathcal{H}(I),$$

$$a(\xi) = eA(x - Vt)/cp_F. \tag{31}$$

Taking into account (18), (21), and (31), for the current density (25) normalized to  $\sigma E_0$ , i.e.,

$$i_{t,L}(\xi) = j_{t,L}(x - Vt)/\sigma E_0, \tag{32}$$

we can write the following expressions:

$$i_t(\xi) = \int_{-a(\xi)/2}^1 \frac{dk_{\perp}k_{\parallel}}{(1-k_{\perp}^2)^{1/2}} \int_{-k_{\perp}-a(\xi)}^{k_{\perp}} \frac{dk_y\beta_y(\xi)}{|\beta_x(\xi)|\theta(k_{\perp},k_y)} \times \int_{\xi_1}^{\xi_2} \frac{d\xi'\beta_y(\xi')}{|\beta_x(\xi')|}, \quad \xi_- \leq \xi \leq \xi_+, \tag{33}$$

$$i_L(\xi) = \int_0^1 \frac{dk_{\perp}k_{\parallel}}{(1-k_{\perp}^2)^{1/2}} \int_{-a(\xi)/2+|k_{\perp}+a(\xi)/2|}^{k_{\perp}-a(\xi)} \frac{dk_y\beta_y(\xi)}{|\beta_x(\xi)|\theta(k_{\perp},k_y)} \times \int_{\xi_1}^{\xi_2} \frac{d\xi'\beta_y(\xi')}{|\beta_x(\xi')|}, \quad -\infty < \xi < +\infty. \tag{34}$$

Here  $k_{\perp,y}$ ,  $\beta_{x,y}(\xi)$  and  $\theta(k_{\perp},k_y)$  are the dimensionless momenta, velocities, and half-period of motion, respectively, of a particle:

$$k_{\perp,y} = \frac{p_{\perp,y}}{p_F}, \quad \beta_{x,y}(\xi) = \frac{v_{x,y}(x - Vt)}{v_F}, \tag{35}$$

$$\theta = \frac{2\pi e\mathcal{H}(I)}{3mc} T = \frac{2\pi}{3} \int_{\xi_1}^{\xi_2} \frac{d\xi'}{|\beta_x(\xi')|}.$$

The symbols  $\xi_{\pm} = (x_{\pm} - Vt)/R(I)$  denote dimensionless coordinates of the boundaries of the region of existence for trapped carriers in a reference frame moving with the wave, and  $\xi_{1,2} = (x_{1,2} - Vt)/R(I)$  are the turning points for an electron in the same reference frame.

Expressions (33) and (34) have completely the same structure as the formulas for static current density. However, the role of spatial coordinate is played by the self-simulating variable  $\xi$ . Thus, the problem of finding the profile of the magnetic field of the wave is exactly reduced to the solution of the magnetostatic problem:

$$-\frac{dh(\xi)}{d\xi} = \frac{2\sigma R(I)E_0}{I} i(\xi), \tag{36}$$

$$i(\xi) = \begin{cases} i_t(\xi) + i_L(\xi), & \xi_- \leq \xi \leq \xi_+, \\ i_L(\xi), & \xi \leq \xi_-, \quad \xi \geq \xi_+, \end{cases} \tag{37}$$

$$h(-\infty) = -h(+\infty) = 1.$$

Integrating the left- and right-hand sides of Eq. (36) from  $-\infty$  to  $+\infty$  and taking into account the boundary conditions (37), we obtain the following expression for the IVC of the metal:

$$E_0(I) = I \left[ \sigma R(I) \int_{-\infty}^{+\infty} d\xi i(\xi) \right]. \tag{38}$$

Taking into account this expression, we can write the magnetostatic equation (36) in the form

$$-\frac{dh(\xi)}{d\xi} = 2i(\xi) \int_{-\infty}^{+\infty} d\xi' i(\xi'). \tag{39}$$

It is natural to seek a solution of this equation, which is odd in  $\xi$  since such a solution automatically satisfies the boundary conditions (37). It should be noted that for an odd  $h(\xi)$ , the turning points  $\xi_{1,2}$  and  $\xi_{\pm}$  of trapped electrons are located symmetrically relative to  $\xi = 0$ :

$$\xi_1 = -\xi_2, \quad \xi_- = -\xi_+. \tag{40}$$

Equation (39) and expressions (33) and (34) for current density do not contain any parameters. For this reason, the IVC (38) of the metal is defined to within a numerical factor by the formula

$$E_0(I) \propto I/\sigma R(I) = 2\pi eI^2/\sigma c^2 p_F. \tag{41}$$

It follows hence that in the limit of strong currents (4), the electrical resistance of the sample increases linearly with  $I$ . It was mentioned in Introduction that such a tendency was observed experimentally.<sup>7</sup>

The type of the nonlinearity of the IVC (41) implies that the total current  $I$  flows mainly through the region having a size  $\sim R(I)$  and a high conductivity of the order of  $\sigma$ . Unfortunately, it is impossible to solve the magnetostatic equation (39) exactly and to find the current density distribution in view of extremely complicated integral relation between  $i(\xi)$  and  $h(\xi)$ . However, a qualitative analysis of the asymptotic forms (33) and (34) of current density shows that the current pinch is formed by the group of trapped charge carriers.<sup>8</sup> Trapped particles oscillating relative to plane of the zero magnetic field of the current preserve a considerable effective mean free path (of the order of  $l$ ). In this case, the contribution to the current density  $i_t(0)$  comes from all electrons irrespective of their angle of incidence on the plane  $\xi = 0$ . It follows from (33) that the value of  $i_t(0)$  is of the order of unity. The value of  $i_t(\xi)$  decreases with increasing distance from the plane  $\xi = 0$  and vanishes, by virtue of (19), at the boundaries  $\pm \xi_+$  of the region of existence of trapped carriers. The width  $2\xi_+$  of this region is of the order of unity. At the periphery ( $|\xi| \geq \xi_+$ ), the mobility of particles is suppressed by the strong constant-polarity magnetic field of the current. As a result, the dimensionless current density  $i_L(\xi)$  (34) turns out to be smaller than the value  $i_t(0)$  according to estimates.<sup>9</sup> In the limit  $|\xi| \rightarrow \infty$ , it decreases to zero over the characteristic scale  $\sim 1$  so that the total current through the metal is a finite quantity. The current density distribution can be roughly presented as follows:<sup>8</sup>

$$i(\xi) = \begin{cases} 1, & |\xi| \leq \xi_+, \\ 0, & |\xi| > \xi_+. \end{cases} \tag{42}$$

Here we assume that the entire current flows in the region occupied by trapped charge carriers:

$$\int_{-\infty}^{+\infty} d\xi i(\xi) = 2\xi_+. \tag{43}$$

Equation (39) with the current density (42) leads to the following expression for the profile of the dimensionless magnetic field  $h(\xi)$ :

$$h(\xi) = - \begin{cases} \xi/\xi_+, & |\xi| \leq \xi_+, \\ \text{sgn } \xi, & |\xi| > \xi_+. \end{cases} \tag{44}$$

We determine the quantity  $\xi_+$  from Eq. (19) after writing it in terms of the dimensionless variables (31). Solving this equation for the given distribution (44) of  $h(\xi)$ , we find that the dimensionless half-width  $\xi_+$  of the current pinch is equal to 4. Accordingly, the numerical factor in the expression (38) for IVC is equal to  $1/8$ .

Thus, the observed nonstationary process is a quasi-static propagation of high-conductivity region in a direction perpendicular to the current. This motion generates a zero-current variable component of the electric field [see (29)] owing to which the distribution of the resultant electric field acquires the form of a running domain wall of the size  $R(I)$ :

$$E(x-Vt) = \frac{\pi e I^2}{4\sigma c^2 p_F} + \frac{V}{c} \mathcal{H}(1) h\left(\frac{x-Vt}{R(I)}\right). \quad (45)$$

The direction of wave propagation corresponds to “switching” of the sample from the state with a smaller value of electric field to a state with a larger value of  $E$ . The wave velocity  $V$  is bounded by the requirement (5). Considering that the characteristic time scale  $\Delta t$  of electromagnetic field variation is  $R(I)/V$ , we can write condition (5) in the form

$$V \ll R(I) \nu. \quad (46)$$

Let us calculate Joule losses under nonstationary conditions without resorting to the model expressions (42) and (44). Using the relation (29) between the electric and magnetic fields, first Maxwell’s equation (8), and taking into account the antisymmetry of the boundary conditions (9), we arrive at the following chain of equalities:

$$\begin{aligned} & \int_{-\infty}^{+\infty} dx j(x-Vt) E(x-Vt) \\ &= -\frac{cE_0}{4\pi} \int_{-\infty}^{+\infty} dx \frac{\partial H(x-Vt)}{\partial x} - \frac{V}{4\pi} \int_{-\infty}^{+\infty} dx \\ & \quad \times H(x-Vt) \frac{\partial H(x-Vt)}{\partial x} = E_0 I. \end{aligned} \quad (47)$$

It follows hence that Joule losses are associated only with the constant electric field  $E_0$ , i.e., have the same magnitude as in the static case. This means that the motion of the electromagnetic domain wall (45) is nondissipative.

## CONCLUSION

According to the above analysis, the voltage across the sample for a given current under the conditions of pinch effect must have a constant as well as a varying component (see (45)). This conclusion is confirmed by the result of

experiments<sup>11</sup> devoted to the detailed analysis of IVC for compensated metals in the range of strong currents. However, Zakharchenko *et al.*<sup>11</sup> observed self-excited voltage oscillations, while the dependence (45) is a switching signal, i.e., is aperiodic. In our opinion, self-excited oscillations emerge as a result of the effect of sample boundaries on the dynamics of the current pinch under real conditions. This effect becomes significant when the high-conductivity region approaches the metal surface to a distance of the order of characteristic radius of curvature  $R(I)$  of electron trajectories. In the vicinity of the boundary, the current pinch must stop since the plane  $x=x_0(t)$  of zero magnetic field cannot emerge at the conductor surface by virtue of the conditions  $H(-d/2, t) = -H(d/2, t) = \mathcal{H}(I)$ . The asymmetric current distribution formed is obviously unstable, and the pinch starts moving to the opposite face of the plate. As a result, spatial oscillations of current pitch accompanied by low-frequency oscillations of voltage across the sample can appear. The need to take into account the finite thickness of the plate necessitates further theoretical investigations of nonstationary effects in metals. The reason behind the instability of static distribution of current leading to the generation of self-sustained voltage oscillations deserves special investigation.

The author is grateful to V. A. Yampol’skii for valuable remarks made during the discussion of the results of this research.

\*E-mail: tkachev@ire.kharkov.ua

<sup>1</sup>B. N. Aleksandrov, Zh. Teor. Éksp. Fiz. **43**, 1231 (1962) [Sov. Phys. JETP **16**, 871 (1962)].

<sup>2</sup>M. Yaqub and J. F. Cochran, Phys. Rev. Lett. **10**, 390 (1963).

<sup>3</sup>V. F. Gantmakher, Pis'ma Zh. Teor. Éksp. Fiz. **2**, 557 (1965) [JETP Lett. **2**, 346 (1965)].

<sup>4</sup>V. T. Dolgoplov and L. Ya. Margolin, Pis'ma Zh. Teor. Éksp. Fiz. **17**, 233 (1973) [JETP Lett. **17**, 167 (1973)].

<sup>5</sup>G. I. Babkin and V. T. Dolgoplov, Solid State Commun. **18**, 713 (1976).

<sup>6</sup>E. A. Kaner, N. M. Makarov, I. B. Snapiro, and V. A. Yampol’skii, Pis'ma Zh. Teor. Éksp. Fiz. **39**, 384 (1984) [JETP Lett. **39**, 463 (1984)].

<sup>7</sup>I. F. Voloshin, S. V. Kravchenko, N. A. Podlevskikh, and L. M. Fisher, Zh. Teor. Éksp. Fiz. **89**, 233 (1985) [Sov. Phys. JETP **62**, 132 (1985)].

<sup>8</sup>E. A. Kaner, Yu. G. Leonov, N. M. Makarov, and V. A. Yampol’skii, Zh. Teor. Éksp. Fiz. **93**, 2020 (1987) [Sov. Phys. JETP **66**, 1153 (1987)].

<sup>9</sup>N. M. Makarov, G. B. Tkachev, V. A. Yampol’skii *et al.*, J. Phys.: Condens. Matter **7**, 625 (1995).

<sup>10</sup>M. Ya. Azbel, Pis'ma Zh. Teor. Éksp. Fiz. **10**, 550 (1969) [JETP Lett. **10**, 351 (1969)].

<sup>11</sup>S. I. Zakharchenko, S. V. Kravchenko and L. M. Fisher, Zh. Teor. Éksp. Fiz. **91**, 660 (1986) [Sov. Phys. JETP **64**, 390 (1986)].

Translated by R. S. Wadhwa

## Generation of nonequilibrium phonons in Bi in a quantizing magnetic field

Yu. A. Bogod

*Weizmann Institute of Science, 76100 Rehovot, Israel\**  
 (Submitted March 2, 1999; revised April 29, 1999)  
 Fiz. Nizk. Temp. **25**, 1203–1210 (November 1999)

The voltage across a Bi single crystal in the  $[\mathbf{E} \times \mathbf{H}]$  direction (transverse voltage  $E_{\perp}$ ) is investigated in strong crossed electric  $\mathbf{E}$  and magnetic  $\mathbf{H}$  fields under phonon generation conditions. Information on electron acousto-emf  $E_e^a$  of bismuth, forming segments with a negative differential conductivity on current–voltage characteristics  $j$  vs.  $E_{\perp}$ , is obtained. Acousto-emf is measured as the absolute value of the difference in transverse voltage before and after the transition of the sample to the phonon generation mode. It is found that the dependence of acousto-emf on quantizing magnetic field is nonmonotonic. This is associated with oscillations in the electron–phonon generation rate  $\partial N_{\mathbf{q}}/\partial t$  in a magnetic field, i.e., with oscillations of the phonon–electron collision frequency  $\tau_{pe}^{-1}$ . © 1999 American Institute of Physics. [S1063-777X(99)00811-7]

### INTRODUCTION

Until recently, electroacoustic effects in semiconductors<sup>1,2</sup> and semimetals (represented by Bi which is the only material suitable for such experiments)<sup>3–5</sup> were studied by measuring, as a rule, the potential difference along the electric field in the sample. However, a number of effects associated with the generation of nonequilibrium phonons can be observed while studying the potential difference  $U_{\perp}$  transverse to current.<sup>6</sup>

Let us consider a Bi sample in strong crossed electric  $\mathbf{E}$  and magnetic  $\mathbf{H}$  fields during supersonic drift of charge carriers in the  $[\mathbf{E} \times \mathbf{H}]$  direction (phonon generation mode), i.e., under the conditions  $v_{\perp}^d = cE/H \geq s$ ;  $j \geq nes/\Omega\tau$ ;  $\Omega\tau \gg 1$ . Here,  $v_{\perp}^d$  is the drift velocity of charge carriers,  $j$  the current density,  $s$  the velocity of sound,  $\Omega$  the cyclotron frequency,  $\tau$  carrier momentum relaxation time, and  $n$  the number density of electrons.

For supersonic drift of charge carriers, the phonon flux in bismuth is formed mainly by electrons rather than holes. This conclusion is based on the ratio of the deformation potential constants for electrons  $e$  and holes  $h$ ,<sup>7</sup> and is confirmed by the experimental results.<sup>8</sup> Hence the effect of phonon generation in bismuth may be described phenomenologically with the help of the acousto-emf<sup>5,9,10</sup>  $E_e^a \cong \langle \partial \varepsilon / \partial t \rangle_{\text{ph}} / nes$  which is associated with the transfer of momentum from the electron subsystem to the phonon subsystem. Here  $\langle \partial \varepsilon / \partial t \rangle_{\text{ph}}$  is the average energy of phonons emitted by the electrons per unit time. If  $W_e$  is the specific electric power imparted to the electron subsystem, and  $\Gamma$  the coefficient which shows the part of electron power transformed into sound, we can present the acousto-emf in the form  $E_e^a \cong \Gamma W_e / nes$ . Like the acoustic absorption coefficient, the generation coefficient  $\Gamma$  is a function of the electron drift velocity.<sup>5</sup>

We shall assume that the applied longitudinal electric field  $\mathbf{E}$  is given. In this case, the increase in the bismuth resistivity  $\rho_H$  upon an increase in the transverse magnetic

field must be accompanied by a decrease in the specific power  $W_e \cong E^2 / \rho_H$ . In other words, the increase in transverse magnetic field in the phonon generation mode for a given value of the longitudinal electric field and for  $\Gamma \approx 1$  must lead to a decrease in the acousto-emf. Moreover, the peculiarities of the bismuth electron spectrum (low Fermi energy  $\varepsilon_F$  and small cyclotron masses  $m^*$ ) lead to the quantum limit in the magnetic field ( $\hbar\Omega \approx \varepsilon_F$ ) even for  $H \approx 10$  kOe.<sup>11</sup> In the quantum limit, the number of energy levels below the Fermi energy is small, and consequently their population density is quite high. Hence the oscillations of the number of electron states at the Fermi level in a magnetic field are also relatively large. This circumstance must affect noticeably the frequency  $\tau_{pe}^{-1}$  of phonon–electron collisions, which becomes a considerably nonmonotonic function of  $H$  in relatively weak magnetic fields. It follows hence that the acousto-emf

$$E_p^a \propto \langle \partial \varepsilon / \partial t \rangle_{\text{ph}} \propto \sum_{\mathbf{q}} \langle \partial N_{\mathbf{q}} / \partial t \rangle \cong \sum_{\mathbf{q}} \langle N_{\mathbf{q}} / \tau_{pe} \rangle$$

must also vary nonmonotonically in a magnetic field ( $N_{\mathbf{q}}$  is the number of phonons with momentum  $\mathbf{q}$  in the steady state).

The present paper aims at measuring the dependence  $E_e^a(H)$  and attempts to discover experimentally the properties of the acousto-emf considered above. The expression for the electron acousto-emf can be obtained from the condition of vanishing of the transverse current in the sample ( $I_{\perp} = 0$ ) under the assumption  $|E_e^a| \gg |E_h^a|$ .<sup>6</sup> It is found that  $E_e^a$  is approximately equal to the absolute magnitude of the difference  $|\Delta E_{\perp}|$  in the transverse fields before and after a transition of the sample to the phonon generation regime for a given longitudinal field  $E$ . (It should be recalled that the transverse field  $\mathbf{E}_{\perp}$  is parallel to the drift velocity, i.e.,  $\mathbf{v}_{\perp}^d \parallel [\mathbf{E} \times \mathbf{H}]$ .) Hence the necessary condition for the measurement of acousto-emf is that the time  $\tau_i$  in which the driving signal increases must be much smaller than the relaxation

time  $\tau_r$  in the phonon generation regime. For bismuth,  $\tau_r \approx 10^{-6}$  s in crossed electric and magnetic fields.<sup>4,5</sup> Consequently, and also with a view to exclude the sample heating, we used the pulsed measuring technique in our investigations. For characteristic current densities  $j \approx 10^3$  A/cm<sup>2</sup> for sound generation in bismuth, pulses of duration 5–6  $\mu$ s and a repetition rate  $\sim 0.1$  s are found to be optimal.

## EXPERIMENTAL RESULTS

Measurements were made on a bismuth single crystal of purity 99.9999% at helium temperatures in magnetic fields up to 56 kOe. The sample had the dimensions  $1 \times 1 \times 8$  mm. The longitudinal axis is parallel to the binary direction  $C_2 \parallel x$ , and the transverse edges coincide with the directions  $C_1 \parallel y$  and  $C_3 \parallel z$  ( $C_1$  and  $C_3$  are the bisector and trigonal crystallographic axes, respectively). The contacts for measuring transverse potential difference  $U_{\perp} \perp I \parallel x$  were established on opposite ends ( $C_1 C_2$  plane) along the trigonal axis  $C_3$  with the help of Wood's alloy. The longitudinal potential difference  $U \parallel I$  was measured by using the current leads situated on the end faces  $C_1 C_3$ . The magnetic field vector  $\mathbf{H}$  is parallel to the  $C_1$ -axis. The quality of the investigated bismuth single crystal could be estimated from the ratio of resistances at room temperature and at helium temperature  $R_0^{300}/R_0^{4.2} = 180$  in zero magnetic field.

In this work, measurements in the linear regime ( $j \ll nes/\Omega\tau, E \ll Hs/c$ ) were made in a direct current (Keithley 224 power supply). The voltage signal across the sample was measured by the Keithley-196 voltmeter connected to a PC-AT where the signal was converted into digital form which is convenient for data processing. In order to single out the Shubnikov–de Haas oscillations, we subtracted the monotonic part from the dependence  $\rho_{xx}(H)$ , which was approximated as a certain polynomial. In the magnetic field  $H = 56$  kOe, the ratio  $U_{\perp}(+\mathbf{H})/U_{\perp}(-\mathbf{H}) = \rho_{zx}(+\mathbf{H})/\rho_{zx}(-\mathbf{H}) = -1.4$ ,  $\rho_{zx}(+\mathbf{H}) = 0.43 \Omega \cdot \text{cm}$ , while  $\rho_{xx} = 0.38 \Omega \cdot \text{cm}$  ( $\rho_{ik}$  are components of the magnetoresistivity tensor).

In the phonon generation regime, the properties of the sample were measured in pulsed current. The pulse duration was  $\tau_p \approx 4.5\text{--}5.5 \mu\text{s}$ , while the time interval between pulses was  $\tau_b \approx 0.5 \times 10^{-1}$  s. The sample, the standard resistance  $R_N = 1 \Omega$ , and the current leads with a resistance  $R_w \approx 0.5 \Omega$  ( $R_N + R_w = R_b$  is the ballast resistance) served as the load for the pulse generator. The maximum output voltage of the generator was  $V_g = 43$  V.

Under the conditions of our experiments, the value of  $\tau_b$  is optimal in the sense that a relatively small thermal energy liberated in the sample during the pulse propagation is dissipated into the surroundings before the arrival of the next pulse. The evolution of the response signal  $U_{\perp}$  associated with the accumulation of energy in the sample can be observed on the oscillograph screen by decreasing  $\tau_b$  by a factor of 2–3. For  $\tau_b = 10^{-2}$  s, the heating of the sample by about 10 K results in the disappearance of the region with negative differential conductivity, which is typical of the phonon generation regime at 4.2 K, from the current–voltage ( $I$  vs.  $U_{\perp}$ ) characteristics.

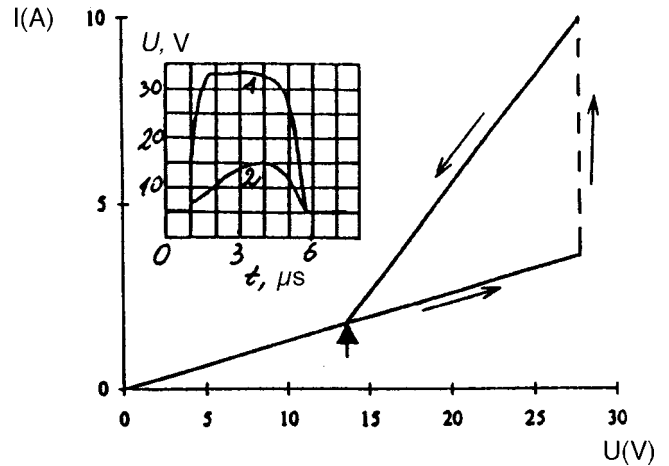


FIG. 1. Dynamic current–voltage characteristic in a magnetic field  $H = 22.7$  kOe. The inset shows the longitudinal voltage in the sample (curve 1) and the voltage across the standard resistance (curve 2).

Figure 1 shows the dynamic current–voltage ( $I$ – $U$ ) characteristic in a magnetic field 22.7 kOe, obtained under the conditions when the pulse amplitude of the longitudinal voltage across the sample is the largest. The upper pulse in the inset to Fig. 1 corresponds to the longitudinal voltage  $U$  across the sample, and the lower one corresponds to the potential difference across the standard resistance, i.e., is the oscillogram of the current. The current–voltage characteristic consists of several segments corresponding to various regions (leading edge, plateau and the trailing edge) of the voltage pulse. The build-up time of the longitudinal voltage front is  $\tau_i = 0.7 \mu\text{s}$ , and the corresponding part of the IVC is  $I$ – $U$  characteristic linear ( $\rightarrow$ , see Fig. 1). This is followed by an increase in current in the circuit at practically constant (plateau) longitudinal voltage across the sample ( $\uparrow$ ), which is associated with the transition of the sample into the phonon generation mode. The part of the IVC corresponding to the trailing edge of the pulse ( $\leftarrow$ ) has a characteristic kink<sup>3–5</sup> which is observed for a drift velocity  $v_{\perp}^d = cE_k/H \approx 0.75 \times 10^5$  cm/s of carriers close to the velocity of sound ( $U_k = 13.4$  V, Fig. 1). The kink determines the transition from the phonon generation (nonlinear) mode to the linear regime. Another method of constructing the  $I$ – $U$  characteristics is the comparison of the voltage across the sample and the current in it at a fixed instant of time for different values of the output voltage of the generator. We carried out such a comparison 3  $\mu\text{s}$  after the beginning of the pulse. The results almost coincided with the segment of the  $I$ – $U$  characteristic obtained at the rear front of the pulse mentioned above (see Fig. 1).

Thus, the relaxation time  $\tau_r$  in the phonon generation mode under the experimental conditions varies from 0.7 to 3  $\mu\text{s}$ . It should be noted that  $\tau_r$  is generally measured not from the beginning of the pulse, but from the instant when the voltage across the sample attains the value  $U_k$ . However, the value  $U_k$  of voltage in our experiments is attained almost instantaneously (see Fig. 1). The current–voltage characteristic shown in Fig. 1 is typical of the magnetic field range used in our experiments.

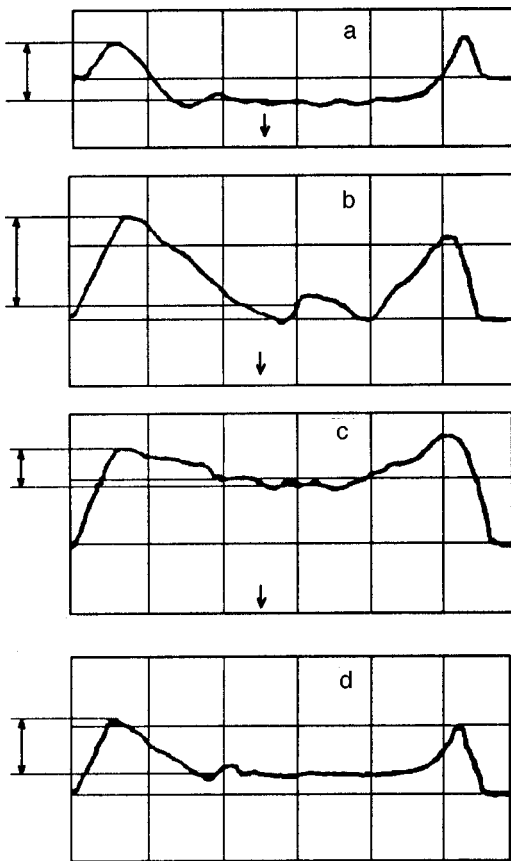


FIG. 2. Oscillograms of transverse voltage in magnetic fields, kOe: 22.7 (a,d), 29.89 (b), and 52.3 (c) in the experimental geometry  $-\mathbf{H}$  (a-c) and  $+\mathbf{H}$  (d). The scale is  $1 \mu\text{s}/\text{division}$  along the horizontal and  $2 \text{ V}/\text{division}$  along the vertical.

In accordance with what has been said earlier, the time of relaxation to the phonon generation mode for Bi samples of thickness  $\sim 1 \text{ mm}$  is close to  $1 \mu\text{s}$  for magnetic fields  $\geq 10 \text{ kOe}$ .<sup>5</sup> The peculiarities of transition of such samples to the phonon generation mode observed by many authors, viz., a decrease in the relaxation time with increasing magnetic field and quantum oscillations of relaxation time in antiphase with oscillations of the density of electron states at the Fermi surface, have typical features of the phonon-electron damping. Apparently, we are speaking of samples with a thickness exceeding the phonon-electron mean free path ( $d \gg l_{pe}$ ), and the possibility of predominant phonon-electron damping is associated with the propagation of an acoustic wave from the sample boundary in a direction opposite to the drift of a mobile charge. (A detailed discussion of mechanisms of relaxation to the phonon generation mode in Bi can be found in Ref. 5.)

Figure 2 shows signals of transverse voltage obtained in different magnetic fields for the maximum potential difference at the generator output. We shall assume (the substantiation will be given below) that the point on the oscillogram beyond which the transverse voltage starts decreasing corresponds to the beginning of the transition to the phonon generation (*nonlinear*) mode, while the realization of the *nonlinear* mode corresponds to the peak of the current through the sample (see Fig. 1). Vertical arrows in Fig. 2 show the ab-

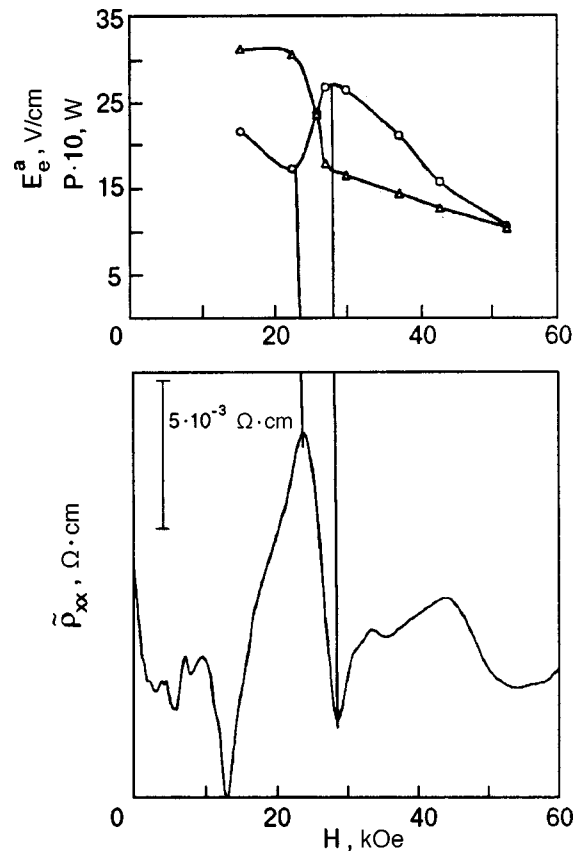


FIG. 3. Magnetic field dependences of the oscillating component of linear magnetoresistance  $\bar{\rho}_{xx}$ , acousto-emf  $E_e^a$  ( $\circ$ ), and electric power  $P$  ( $\Delta$ ).

solute value of the difference between transverse voltages at these points, i.e., the difference in voltages before and after the transition of the sample to the phonon generation mode.

The magnetic field dependence of the difference in transverse voltages (which is approximately equal to the acousto-emf  $E_e^a$ ; see below) is presented in Fig. 3. Obviously, the  $E_e^a(H)$  dependence should be determined at a constant longitudinal voltage in the conductor. However, the longitudinal voltage in the sample also change slightly for a fixed voltage at the generator output and a finite ballast resistance as a result of an increase in the Bi resistance in a magnetic field. In our opinion, these changes do not affect the acousto-emf  $E_e^a$  significantly. Indeed, the longitudinal voltage increases approximately by 30% as the magnetic field increases from 22.7 to 29.9 kOe, and by 40% when it increases to 52.3 kOe. At the same time, acousto-emf increases approximately by a factor of 1.6 in the former case and decreases virtually in the same proportion in the latter case (see Fig. 3). For this reason we assume that decisive changes in  $E_e^a$  upon an increase in  $H$ , which correlate with changes in magnetoresistance (see below), should be attributed to the effect of magnetic field on the properties of the sample.

Figure 3 also shows the magnetic field dependence of the electric power  $P$  liberated in the sample. The power was determined with the help of the approximate relation  $P \cong I_m^2 [(U_g/I_m) - R_B]$ , where  $I_m$  is the maximum value of the current pulse measured simultaneously with the transverse voltage  $U_{\perp}$ , and  $U_g = 43 \text{ V}$ . Figure 3 also illustrates

Shubnikov–de Haas oscillations  $\tilde{\rho}_{xx}(H)$  measured in the linear mode ( $\tilde{\rho}_{xx}/\rho_{xx} \leq 0.1$ ).

It can be seen that like power, acousto-emf decreases on the average upon an increase in magnetic field, depending nonmonotonically on  $H$  in the quantum limit for electrons. The minimum of  $E_e^a$  for  $H \cong 24$  kOe corresponds to the maximum of  $\rho_{xx}$ , while the maximum of  $E_e^a$  for  $H \cong 28$  kOe corresponds to the minimum of  $\rho_{xx}$ .

### DISCUSSION OF RESULTS

Let us introduce the electron acousto-emf  $E_e^a$ ,<sup>9,10</sup> assuming that the average changes in pulses of the electron and phonon subsystems per unit time in the phonon generation mode are equal:

$$\begin{aligned} \langle \partial P / \partial t \rangle_e &= -\langle \partial P / \partial t \rangle_{ph} = -\vec{q} \sum_{\mathbf{q}} \hbar q \langle \partial N_{\mathbf{q}} / \partial t \rangle \\ &= -neE_e^a. \end{aligned} \quad (1)$$

It follows hence that

$$E_e^a = \frac{\vec{q} \langle \partial \varepsilon / \partial t \rangle_{ph}}{nes}; \quad \langle \partial \varepsilon / \partial t \rangle_{ph} = \sum_{\mathbf{q}} \hbar s q \langle \partial N_{\mathbf{q}} / \partial t \rangle, \quad (2)$$

where  $N_{\mathbf{q}}$  is the distribution function for phonons with the momentum  $\mathbf{q}$  and  $\vec{q}$  is the unit vector.

We present the phonon distribution function as the sum of the equilibrium ( $N_{\mathbf{q}0}$ ) and nonequilibrium ( $N_{\mathbf{q}}^{(1)}$ ) components. In this case, for the arriving term in the kinetic equation we have

$$\sum_{\mathbf{q}} \partial N_{\mathbf{q}} / \partial t = \sum_{\mathbf{q}} a_{\mathbf{q}} (N_{\mathbf{q}0} + N_{\mathbf{q}}^{(1)}) + a_{\mathbf{q}}^f. \quad (3)$$

Here  $a_{\mathbf{q}}$  is the increment of phonon accumulation and  $a_{\mathbf{q}}^f$  the coefficient describing the interaction of electrons with zero-point vibrations of the lattice. An analysis shows (see Refs. 5, 6, and 12 for details) that the determining contribution to the sum (3) comes from nonequilibrium phonons. For this reason, we can put in relation (2)  $\partial N_{\mathbf{q}} / \partial t \cong a_{\mathbf{q}} N_{\mathbf{q}}^{(1)}$ .

Let us now suppose that a certain coefficient  $\gamma$  corresponds to the fraction of the electric power  $W_e$  introduced into the electron system, which is transformed into acoustic flux. In this case, acousto-emf can be defined (to within the terms associated with amplification of equilibrium phonons and zero-point vibrations) as<sup>5</sup>

$$E_e^a \cong (\gamma - \beta) W_e / nes, \quad (4)$$

where the coefficient  $\beta$  is associated with attenuation of sound,  $\gamma - \beta = \Gamma$ . Taking into account what has been said above, we can now write the following relation connecting, among other things, the acousto-emf  $E_e^a$  with the phonon–electron collision frequency  $a_{\mathbf{q}} = \tau_{pe}^{-1}$ :

$$\Gamma W_e \cong \sum_{\mathbf{q}} \hbar \omega_{\mathbf{q}} \langle a_{\mathbf{q}} N_{\mathbf{q}}^{(1)} \rangle \cong nes E_e^a. \quad (5)$$

The method of experimental determination of acousto-emf in Bi was proposed by the author in Ref. 6. Following Ref. 6, we shall assume that the sample is unbounded along

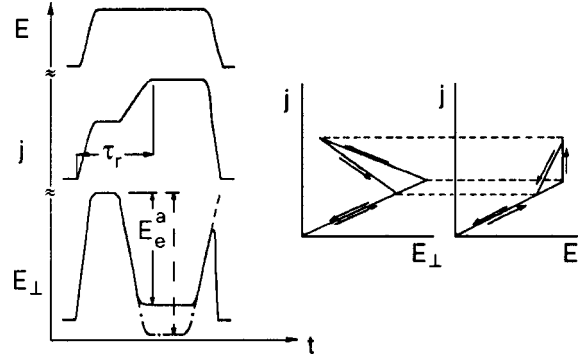


FIG. 4. Schematic diagram of electric signal pulses and current–voltage characteristics.

the  $y$ -axis ( $E_y = 0$ ) and introduce the acousto-emf for electrons drifting along the  $z$ -axis. Assuming that the acousto-emf for holes is smaller than the electron acousto-emf and neglecting diffusive effects, we can determine the transverse field  $E_{\perp}$  in the phonon generation mode from the condition that the current along the  $z$ -axis is equal to zero (see also Ref. 13):

$$\begin{aligned} E_{\perp}(\pm \mathbf{H}) &\cong \pm \left( \frac{nec}{H} \right) [\Delta n / n \pm \sin \theta (\mu_e^0 H / c)^{-1}] \\ &\quad \times E (n_e e \mu_e^H + n_h e \mu_h^H)^{-1} \mp E_e^a. \end{aligned} \quad (6)$$

Here  $\mu_{e,h}^H = \mu_{e,h}^0 / (\mu_{e,h}^0 H / c)^2$  are the average mobilities of electrons and holes along the  $z$ -axis,  $\mu_{e,h}^0$  the mobilities of electrons and holes in zero magnetic field,  $\Delta n = n_e - n_h$  is the difference in the electron and hole concentrations,  $\theta$  the possible small angle of deviation of magnetic field from the bisector axis  $C_1 \parallel y$ , and  $n_e e \mu_e^H \gg n_h e \mu_h^H$ . Let us estimate the parameters appearing in formula (6). From the experimental relation  $E_{\perp}(+\mathbf{H}) / E_{\perp}(-\mathbf{H}) = -1.4$  obtained in the linear mode for  $H = 56$  kOe (see above), we have  $|(\Delta n / n)(\sin \theta) \times (\mu_e^0 H / c)^{-1}| \approx 10$ . Putting<sup>11</sup>  $\mu_e^0 H / c \approx 10^3$  and  $\theta \approx 1^\circ$ , we obtain  $\Delta n / n \approx 10^{-3} - 10^{-4}$ .

It follows from formula (6) that the electronic acousto-emf is defined as the absolute value of the difference in transverse voltages measured before and after transition of the sample to the phonon generation regime for a given value of the longitudinal field  $E$ .

For a visual comparison with the experimental results, we present graphically the driving voltage signal  $E$  and the response signals for current  $j$  and the transverse voltage  $E_{\perp}$ . We shall assume that the relaxation time  $\tau_r$  in the phonon generation mode is much larger than the build-up time  $\tau_i$  of the driving signal pulse. To begin with, we shall also disregard relaxation effects during a transition from nonlinear to linear regime upon a decrease in the driving voltage at the trailing edge of the pulse. Further, we assume that in accordance with formula (4), the dependence of acousto-emf on the longitudinal field  $E$  is considerably nonlinear.

Figure 4 shows the pulses of  $E, j$  and  $E_{\perp}$ , as well as the dependences  $j(E)$  and  $j(E_{\perp})$ . Let us consider the pulse  $j(t)$  in the time interval in which the longitudinal voltage is constant, i.e., corresponds to the plateau of driving signal pulse. In the beginning (for  $t < \tau_i$ ), the current is independent of

time. Later (for  $t \approx \tau_r$ ), the current increases with decreasing resistance of the sample during transition to the phonon generation regime. After the transition to the nonlinear regime ( $t > \tau_r$ ), the current again becomes constant (Fig. 4). Like current, the transverse voltage is independent of time for  $\tau_i < t < \tau_r$ . Upon a transition to the phonon generation regime ( $t \approx \tau_r$ ), the electronic acousto-emf comes into play and increases, thus leading to a decrease in the value of  $E_{\perp}$  in accordance with formula (6). On completion of a transition to the nonlinear regime ( $t > \tau_r$ ), the transverse resistance becomes independent of time again ( $E_e^a = \text{const}$ ). As the driving voltage  $E$  begins to decrease (trailing edge of the pulse, Fig. 4), the acousto-emf  $E_e^a$  decreases more rapidly than the term linear in  $E$  in formula (6). As a result, the transverse voltage  $E_{\perp}$  increases, forming a peak at the trailing edge of the pulse. After transition from nonlinear to linear regime (upon a further decrease in the longitudinal voltage), the acousto-emf vanishes, and  $E_{\perp}$  decreases in proportion to  $E$  (see formula (6) and Fig. 4).

In the schematic diagram of the transverse voltage signal  $E_{\perp}$  (see Fig. 4), the vertical arrow shows the electronic acousto-emf  $E_e^a$ . The acousto-emf is measured graphically as the difference between two values of the transverse voltage. The first corresponds to the moment when the transverse voltage decreases at the beginning of a transition of the sample to the phonon generation regime. The second corresponds to the completion of the transition, which is indicated by the maximum value of the current passing through the sample. It should be recalled that this technique was used for determining the acousto-emf from the experimental oscillograms.

The current–voltage characteristics  $j(E)$  and  $j(E_{\perp})$  were constructed from a comparison of the schematic pulses of  $E, j$  and  $E_{\perp}$  in Fig. 4. The dependence  $j(E_{\perp})$  contains regions with negative differential conductivity.<sup>6</sup>

Let us compare the schematic diagrams presented in Fig. 4 with the experimental data presented in Figs. 1 and 2. A qualitative agreement of the phenomenological analysis with the experiment is beyond any doubt (we do not consider here the experimentally observed acoustoelectric vibrations<sup>5</sup>). The analogy is closer than a simple illustrative similarity. Indeed, it follows from Eq. (6) that the sign of transverse voltage may be reversed upon a transition to the phonon generation regime (dot-and-dash curve in Fig. 4). It can be seen from Eq. (6) that under the conditions considered by us, the probability of such an occurrence is higher for the magnetic field direction  $-\mathbf{H}$  than for the direction  $+\mathbf{H}$ : the term linear in  $E$  in Eq. (6) is relatively small for the direction  $-\mathbf{H}$ . This is exactly in accord with the experiment [see Figs. 2(a) and 2(d)]: the sign of transverse voltage is reversed upon inclusion of the acousto-emf for the direction  $-\mathbf{H}$  [Fig. 2(a)]. For the direction  $+\mathbf{H}$  and a given value of the driving longitudinal voltage, the sign of transverse voltage remains unchanged [Fig. 2(d)].

In the above analysis, we disregarded the possible influence of the so-called aftersound effect on the peak value of transverse voltage corresponding to the trailing edge of the driving voltage pulse (see Fig. 4). The ‘‘aftersound’’ effect is manifested in that upon a sharp decrease in the applied elec-

tric field whose value initially corresponds to supersonic drift of charge carriers, a potential difference associated with electron drag by previously excited phonons can be detected in the sample. In particular, the phonon–electron drag must induce an extra transverse emf which, being added to the voltage peak at the trailing edge of the pulse, can increase its height<sup>6</sup> (the initial segment of the possible ‘‘resultant’’ peak is shown by dashed lines in Fig. 4). Obviously, the peak height, on the one hand, must be the higher, the larger the concentration of nonequilibrium phonons [i.e., acousto-emf, see (5)]. On the other hand, a high value of acousto-emf can correspond to a high frequency of phonon–electron collisions, which hampers the formation of the ‘‘aftersound’’ peak. As a result, the combination of the two factors determines the height of observed experimental peaks (see Fig. 2).

Let us consider the effect of magnetic field on acousto-emf. It should be noted above all that in accordance with formula (4), the relative change in acousto-emf must be of the order of the relative change in the power introduced to the electron system. An experimental confirmation of this fact can be seen in Fig. 3 showing the magnetic field dependences of these quantities. It should be noted, however, that the power  $P$  in Fig. 3 was calculated from an empirical formula (see above). Consequently, we must verify that the formula conforms to a correct physical relation. Let us do this.

The emergence of the transverse field  $E_{\perp}$  in the sample due to the difference between the electron and hole concentrations as well as under the influence of the electron acousto-emf leads to the following expression for specific power:

$$W \cong (n_e e \mu_e^H + n_h e \mu_h^H)(E^2 + E_{\perp}^2), \quad (7)$$

where the quantity  $E_{\perp}$  is defined by formula (6). Putting  $n_e \approx n_h$ ,  $\mu_e^H \approx \mu_h^H$ ,  $(\mu_e^0 H/c)^{-1} \approx \Delta n/n$ ,  $E_e^a \ll E$ , we obtain

$$W \cong E^2 / \rho_H^l, \quad (8)$$

where  $\rho_H^l$  is the linear magnetoresistivity of the sample. The calculation of the power with the help of an empirical formula and formula (8) using the data presented in Fig. 1 leads to values of the same order of magnitude (they can differ approximately by a factor of 2.7). Consequently, we can assume that the convenient empirical formula used by us above is suitable for obtaining estimates.

It is well known that the density of states in a strong magnetic field is quantized, and the continuous electron spectrum splits into subbands (Landau subbands). Every time when the bottom of a Landau subband intersects the Fermi level, the electron density of states at the Fermi surface attains its maximum value. For this reason, the frequency of electron collisions also has the maximum value, and hence the transverse ( $\mathbf{H} \perp \mathbf{E}$ ) magnetoresistance has a minimum.<sup>14</sup> The maximum density of electron states at the Fermi surface must also correspond to the maximum frequency  $\alpha_q = \tau_{pe}^{-1}$  of phonon–electron collisions, and hence to the maximum acousto-emf [see (5)].

It was mentioned above that the quantum limit in magnetic field in Bi for  $\mathbf{H} \parallel C_1$  is realized for  $H \approx 10$  kOe. This circumstance is associated with small values of the Fermi energy  $\varepsilon_F \approx 10^{-14}$  erg and small cyclotron masses  $m_e^*$

$\approx 10^{-2}m_0$  ( $m_0$  is the mass of a free electron). In the quantum limit, the number of Landau levels lying below the Fermi energy is of the order of unity, and their population density is relatively high. For this reason, oscillations of the number of electron states at the Fermi surface in a magnetic field are also relatively strong. Consequently, the  $E_c^a(H)$  dependence must be essentially nonmonotonic. This is illustrated in Fig. 3 in which the maximum and minimum of transverse magnetoresistance are observed simultaneously with the minimum and maximum of acousto-emf. The minimum of  $\rho_{xx}$  near  $H=28.2$  kOe is associated with the passage of the Landau electron subbands  $0^+$ ,  $1^-$  through the Fermi level, i.e., is the last electron minimum. The next two oscillation minima of magnetoresistance for  $H=35.3$  kOe and  $H=52.6$  kOe are associated with the hole levels  $M=7^\pm$  and  $M=6^\pm$ ,<sup>11,15</sup> the + and - signs corresponding to two spin projections.

Thus, we have observed for the first time the nonmonotonic magnetic field dependence of acousto-emf associated with oscillations of the electron-phonon generation rate  $\partial N_{\mathbf{q}}/\partial t \sim a_{\mathbf{q}} N_{\mathbf{q}}^{(1)}$  as a function of  $H$ . Ideologically, this research is close to the investigations carried out in Refs. 5, and 16. In Ref. 16, quantum oscillations in the magnetic field of sound passing through a Bi crystal ( $\mathbf{H} \perp \mathbf{q}$ ,  $\mathbf{q}$  being the wave vector of the sound) were inverted after a transition of the sample to the phonon generation mode ( $cE/H > s, \mathbf{E} \perp \mathbf{H}$ ): the minimum of the transmission was replaced by maximum, and vice versa. In Ref. 5, the phonon genera-

tion coefficient  $\Gamma$  as a function of magnetic field was calculated phenomenologically with the help of  $j$  vs.  $E$  characteristics of Bi measured in a transverse magnetic field. As a result, a nonmonotonic dependence  $\Gamma(H)$  was obtained [see (5)]. The peaks of the generation coefficient corresponded to magnetoresistance minima in this case.

\*E-mail: bogod.yu@excite.com

- 
- <sup>1</sup>V. I. Pustovoi, Usp. Fiz. Nauk **97**, 257 (1969) [Sov. Phys. Usp. **12**, 105 (1969)].
  - <sup>2</sup>H. Kuzmany, Phys. Status Solidi A **25**, 9 (1974).
  - <sup>3</sup>L. Esaki, Phys. Rev. Lett. **8**, 4 (1962).
  - <sup>4</sup>T. Yamada, J. Phys. Soc. Jpn. **20**, 1647 (1965).
  - <sup>5</sup>Yu. A. Bogod, Fiz. Nizk. Temp. **8**, 787 (1982) [Sov. J. Low Temp. Phys. **8**, 393 (1982)].
  - <sup>6</sup>Yu. A. Bogod and P. Finkel, Phys. Rev. B **51**, 16568 (1995).
  - <sup>7</sup>K. Walter, Phys. Rev. **174**, 782 (1968).
  - <sup>8</sup>Yu. A. Bogod, D. V. Gitsu, and A. D. Grozav, Zh. Éksp. Teor. Fiz. **84**, 2194 (1983) [Sov. Phys. JETP **57**, 1279 (1983)].
  - <sup>9</sup>A. Wenreich, Phys. Rev. **107**, 317 (1957).
  - <sup>10</sup>H. Ozaki and N. Mikoshiba, J. Phys. Soc. Jpn. **21**, 2486 (1966).
  - <sup>11</sup>V. S. Edelman, Usp. Fiz. Nauk **123**, 257 (1977) [Sov. Phys. Usp. **20**, 819 (1977)].
  - <sup>12</sup>S. J. Miyake and R. Kubo, Phys. Rev. Lett. **9**, 82 (1962).
  - <sup>13</sup>J. E. Aubrey, J. Phys.: Metal Phys. **F1**, 493 (1971).
  - <sup>14</sup>E. Adams and T. Holstein, J. Phys. Chem. Solids **10**, 254 (1959).
  - <sup>15</sup>G. E. Smith, G. A. Baraff, and J. H. Rowell, Phys. Rev. A **135**, 1118 (1964).
  - <sup>16</sup>K. Walter, Phys. Rev. Lett. **16**, 642 (1965).

Translated by R. S. Wadhwa

## Magnetically stimulated inhomogeneity of conductivity and nonlocal transport phenomena in metals

V. R. Sobol, O. N. Mazurenko, and A. A. Drozd

*Institute of Solid State and Semiconductor Physics, National Academy of Sciences of Belarus,  
220072 Minsk, Belarus\**

(Submitted March 9, 1999; revised June 1, 1999)

*Fiz. Nizk. Temp.* **25**, 1211–1217 (November 1999)

Charge transport in a conducting medium with a magnetically stimulated inhomogeneity of kinetic coefficients along the direction of transport is investigated both experimentally and analytically. Measurements were made on samples in the form of high-purity polycrystalline aluminum plates whose conductivity inhomogeneity was simulated by the technique of curving of current lines so that the local normal component of the applied magnetic field varies according to an exponential or quadratic law. The relations describing the tensor connection between the electric field and charge flux density are used to calculate spatial dependence of the potential. The sign reversal of the electric field is described as the result of competition between the potential contributions from the current along the transverse magnetic field gradient and the Hall current at right angles to it. © 1999 American Institute of Physics.  
[S1063-777X(99)00911-1]

### INTRODUCTION

In this communication, we describe the peculiarities of dynamics of conduction electrons in metals during static charge transport under conditions of regular spatial inhomogeneity of kinetic coefficients. Earlier, we constructed<sup>1</sup> the phenomenological model describing the motion of charge carriers for linear dependence of magnetic field in the approximation of zero charge transport through lateral faces of the sample along the inward normal for spherical and closed types of constant energy surface. It was proven that there exists a nonlocal relation between the current density and magnetic field, and the current density depends considerably on the magnetic field as well as its gradient. Consequently, the electric potential is large at one of the lateral faces and small at the other. It was found<sup>2,3</sup> that an inconsistency is observed for large values and a complex (e.g., exponential) spatial dependence of the inhomogeneity between the experimental results and the theoretical model. For the sample face corresponding to a low potential level, the inconsistency is not only quantitative, but also qualitative and is the result of disparity between the boundary conditions in the model<sup>1</sup> and the actual boundary conditions in the experiment.<sup>2,3</sup>

The present paper aims at studying the kinetic phenomena in an inhomogeneous nonlinear magnetic field under appropriate boundary conditions at the lateral surface of the sample. The investigated object was polycrystalline aluminum as a typical cryoconductor. The justification for such investigations is that low-temperature electrodynamics covers a number of problems which requires not only the evaluation of effective conductivity connecting the volume-averaged current and field, but also the nature of charge flow, the of current density distribution, and the scale of its localization. The main factors involved are the conditions of interaction of conduction electrons with the surface of the

conductor and their effect on the probability density distribution function, nature and scale of inhomogeneities both intrinsic and those caused by external agencies.<sup>4–6</sup> We shall consider charge transport in a polycrystalline medium which is randomly inhomogeneous due to different orientations of crystallites, and has an additional regular macroscopic inhomogeneity of kinetic coefficients induced by the applied magnetic field. Such a formulation of the problem is justified since the development of cryogenic and electrical engineering is directed towards creating new conducting materials with complex phase composition and crystal structure. In spite of the fact that such materials are homogeneous on microscopic level, their resistive properties may change significantly because of various types of inhomogeneities existing on the macroscopic scale. For example, inhomogeneity in the properties of composite conductors is observed at the interface between two components having different values of Hall coefficient.<sup>6,7</sup> Cryoconductors based on polycrystalline aluminum are complex systems, and the spatial dependence of kinetic coefficients induced by natural inhomogeneity of the magnetic field in the bulk of the solenoid winding deteriorates their efficiency.

### EXPERIMENT

#### Simulation of regular spatial inhomogeneity of conductivity. Sample preparation

The method of curved current trajectories conforming to the bent profile of the sample, where the local normal component of the external field is defined by the curvature at a given point,<sup>1</sup> was used for simulating conductivity inhomogeneities instead of the modification of pole pieces of the electromagnet, which usually bends the magnetic lines of force and changes their density in the bulk of the sample. The samples were prepared from aluminum ingots in which

TABLE I. Characteristics of samples and field inhomogeneity parameters.

Sample Batch No.	$\rho_0$ , $10^{-10} \Omega \cdot \text{cm}$	$\lambda$ , $\text{T}^{-1}$	$k$ , $\text{T} \cdot \text{cm}^{-1}$	$\alpha$ , $\text{T} \cdot \text{cm}^{-2}$
1	2	0.3	0.9	0.1
2	2	0.4	1.0	0.5
3	3	0.4	0.7	1
4	4.5	0.5	0.15	2.6

the ratio of room temperature resistance to resistance at liquid helium temperature was 6000–15000. The field dependence  $\rho = \rho_0(1 + \lambda B)$  of the magnetoresistance of aluminum was taken into account during the analysis, where  $\rho_0$  is the diagonal component of resistance extrapolated to zero values and  $\lambda$  is a phenomenological parameter describing the degree of unsaturation associated with the presence of a narrow layer of extended and open trajectories.

The nonlinear character of spatial dependence was realized in the experiment for the local normal component of the two types of external magnetic field  $B$ , arbitrarily described as exponential and quadratic, for which the main contribution to  $B$  comes from the first and second terms in the field expansion into a series in the direction of charge transport:

$$B = B_0 \exp(dx), \quad B = B_0 + kx + \alpha \frac{x^2}{2}. \quad (1)$$

Here  $B_0$  is the magnetic field at the beginning of the working region,  $d$ ,  $k$  and  $\alpha$  are its inhomogeneity parameters. The direction of transport coincides with the  $x$ -axis, while the direction perpendicular to the lateral faces coincides with the  $y$ -axis. The characteristics of the families of samples differ from one another and are presented systematically in Table I.

The sample preparation technique, i.e., the process of computing the appropriate shape, preparation of template, preparation of the initial sample plate ( $0.2 \times 0.6 \times 3.5$  cm) with the required potential areas, formation of profile followed by annealing and preparation of potential contacts on the surface and lateral faces of the sample were identical to those used in our earlier work.<sup>1</sup>

## MEASURING PROCEDURE

The electric field potential was measured by taking into account the redistribution of the current density over the cross section, and hence traditional methods of obtaining useful signal through commutation of the magnetic field direction and direction of the current through the sample could not be used. In this case, a change in the magnetic field direction automatically leads to the sign reversal of the field gradient, and hence to a transformation of the current density distribution pattern over the cross section, when the lateral face of the sample with a high level of the signal is transformed into a face with a low signal level and vice versa. In other words, signals at the lateral faces and in the bulk of the sample change not only in sign, but also in magnitude as a result of such an operation. Only the integral Hall voltage between lateral faces remains unchanged. This fact was used for measuring and systematizing the data. In addition to

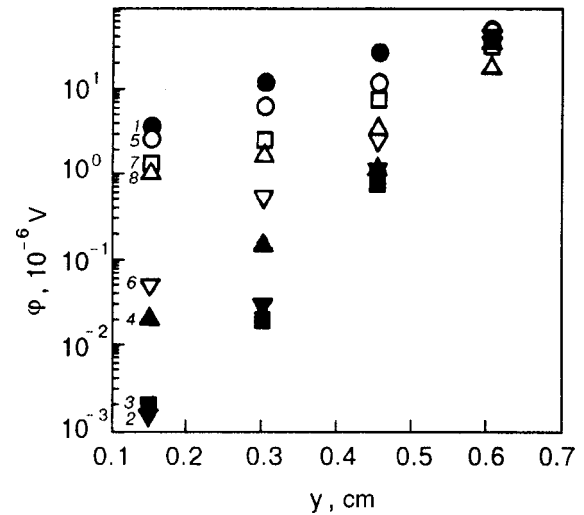


FIG. 1. Dependence of potential on coordinate along the normal to the direction of charge transport for exponential type of inhomogeneity for different values of the relative gradient  $d$  ( $\text{cm}^{-1}$ ): 0.1 (1, 5), 0.4 (2, 6), 0.6 (3, 7), 1.1 (4, 8), and local magnetic field  $B$  (in T): 6.85 (1), 6.50 (5), 6.0 (2), 5.35 (3), 5.20 (6), 4.20 (7), 3.95 (4), and 2.40 (8).

commutation, the main method used for control was the potentiality technique in which the vortex field through any closed loop is equal to zero. These circumstances impose severe constraints on the initial orientation of the sample which was carried out in two stages. In the beginning, the sample was tilted in the magnetic field plane at right angles to the transportation direction until the Hall voltage attained its maximum value. In the second stage, the sample was tilted in a plane passing through the transport direction and the magnetic field vector until the voltage across the Hall opposite faces attained its maximum value along the direction of current flow.

## DISCUSSION OF EXPERIMENTAL RESULTS

### Main regularities in the potential distribution along and across the charge flow direction

It was mentioned earlier that our experimental investigations were aimed at the spatial distribution of the potential  $\varphi(x, y)$ . The results of measurements of the potential difference between different points on the sample surface and their lateral faces make it possible to reconstruct the voltage  $\varphi$  in the direction of charge flux and at right angles to it. In Fig. 1,  $\varphi$  is plotted as a function of the transverse coordinate  $y$  for several values of the local magnetic field in samples with different inhomogeneity parameters. In this case, the potential is an increasing function of coordinates. At the same time, a qualitative difference is observed for  $\varphi(x)$  at the faces corresponding to strong and weak signals. For strong signals, the potential across the face increases for all gradient levels. The same is true for weak signals if the gradient level is low. For large gradients, the potential for a weak signal at the face is a nonmonotonic function of the coordinate  $x$  (Fig. 2). The dependences  $\varphi(x)$  for both faces are presented below together with the theoretical results. For a weak signal, the

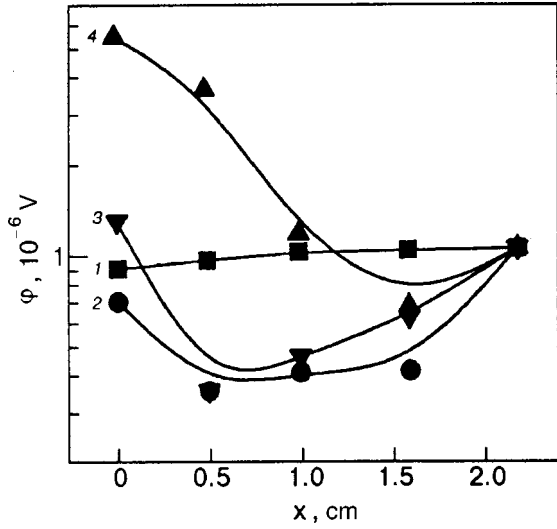


FIG. 2. Potential  $\varphi$  distribution in the direction of the current at the lateral face of the sample corresponding to a weak signal for different values of the magnetic field gradient  $d$  ( $\text{cm}^{-1}$ ): 0.1 (1), 0.4 (2), 0.6 (3), and 1.1 (4).

current flows in a weak local field over the face along the potential gradient  $\partial\varphi/\partial x$ , while the sign of the gradient is reversed upon an increase in local field.

**Analysis of the phenomenon and its interpretation**

Naturally, the above potential difference peculiarities of an electric field can be associated with the complex form of the magnetic field gradient and specific properties of the dispersion relation for charge carriers. We shall use the results<sup>1</sup> obtained for the model in which the current density in the direction of transport has the form

$$j_x = \frac{I R k}{t \rho} \frac{\exp(Rky/\rho)}{\exp(Rkb/\rho) - 1}, \quad j_y = 0. \tag{2}$$

Here,  $k = dB/dx$  is the magnetic field gradient,  $R$  the Hall constant,  $\rho$  the diagonal component of the magnetoresistance tensor,  $I$  the integral current, while  $t$  and  $b$  are the sample thickness and width. For fixed values of  $k$  and  $\rho$  over the sample volume, the current density  $j_x$  is independent of the coordinate  $x$ , and there is no transverse current. The exponent  $Rk/\rho$  determines the current localization, so that an increase in the value of  $k$  leads to an increase in the current density at the face with a strong signal, while an increase in  $\rho$  decreases this quantity. In the present form of notation, the lateral face  $y=0$  corresponds to the low potential level, while the opposite face  $y=b$  corresponds to the high potential level.

According to the model considered here, the current density is finite at lateral faces of the sample along the inward normals, and there exists a lateral Hall current which redistributes the conduction current. Assuming that there are two regions with constant gradients  $k_1$  and  $k_2$  ( $k_1 < k_2$ ), the pattern of current distribution in the interval  $\Delta x$  between these regions must be transformed. This means that the current density increases gradually in the transition region at the face  $y=b$ , and decreases at the face  $y=0$  and in its vicinity. Such

variations may occur as a result of lateral drift of carriers. The magnetic field gradient in the transition region can be presented in the form

$$k = k_1 + \frac{k_2 - k_1}{\Delta x} x, \tag{3}$$

which corresponds to a nonlinear dependence of magnetic field on the coordinate in the direction of the current realized in the experiment. Assuming that the form of  $j_x$  must correspond to the expression which is transformed into (2) upon a limiting transition, and using the continuity condition, we define the two-dimensional pattern of current flow through such a medium as follows:

$$j_x = \frac{I}{t} f(x) \frac{\exp[f(x)y]}{\exp[f(x)b] - 1},$$

$$j_y = -\frac{I}{t} f'(x) \frac{\exp[f(x)y]}{\exp[f(x)b] - 1} \left\{ y - b \frac{\exp[f(x)b]}{\exp[f(x)b] - 1} \right\},$$

$$f(x) = \frac{d}{dx} \left( \frac{RB}{\rho} \right), \quad f'(x) = \frac{d}{dx} (f(x)). \tag{4}$$

In this approximation, the integral current through the cross section is independent of coordinate  $x$  and is defined by the generator current. The direction of the transverse current is determined by the sign of the parameter  $f'(x)$ . For a dominating numerator in the component  $f(x)$ , the transverse current is collinear with the  $y$ -axis, while for a stronger dependence of denominator on coordinate  $x$  the transverse current is opposite to the  $y$ -axis. An analysis shows that the transverse current density is not constant along the  $y$ -axis and must have an extremum whose coordinate is defined by the expression

$$y_0 = b \left( 1 - \frac{1}{fb} \frac{\exp(fb) - 1 - fb}{\exp(fb) - 1} \right). \tag{5}$$

It follows hence that for small values of the parameter  $fb$ , the extremum lies in the middle ( $y_0 = b/2$ ), while for  $fb > 1$  the transverse current peak is displaced towards the face corresponding to strong signal level. Using the analytic expressions (4), we calculated the dependence of the current density along the field gradient  $j_x$  and in the transverse direction  $j_y$  for several values of the inhomogeneity parameters of the medium, conforming to the values of integral current, sample thickness and width, etc., under experimental conditions (Figs. 3, 4). The analytic characteristics were obtained by using the expression

$$f(x) = \frac{R(k + \alpha x)}{\rho_0 [1 + \lambda(B_0 + kx + \alpha(x^2/2))]^2}. \tag{6}$$

It follows from Fig. 3 that the current density  $j_y$  is a function of the parameter  $f(x)$  and decreases with increasing values of this parameter. Such a behavior corresponds to a change in the transverse current from positive to negative values characteristic of a strong dependence of resistance on field. The current density  $j_x$  (Fig. 4) is also nonmonotonic at the lateral faces of the sample as well as in the bulk. The oppo-

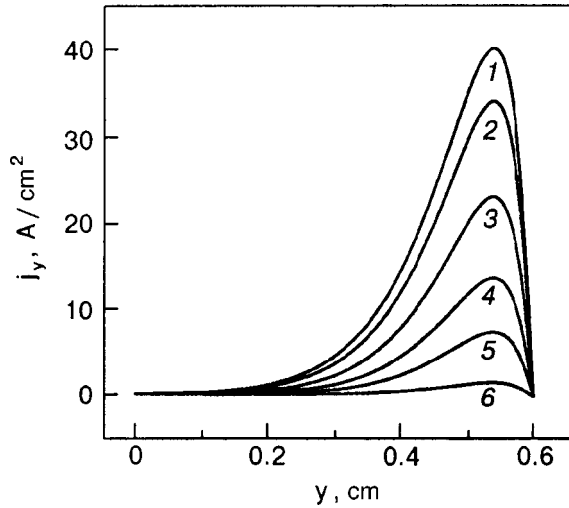


FIG. 3. Theoretical dependence of the transverse current density  $j_y$  on coordinate  $y$  for various values of the inhomogeneity parameters (6)  $f(x)$  ( $\text{cm}^{-1}$ ): 15.7 (1), 16.0 (2), 16.3 (3), 16.5 (4), 16.6 (5) and 16.7 (6).

site faces display qualitatively different behavior, and a transformation from one type to the other occurs in the intermediate region.

Starting from formulas (4) for the current density  $j_x$  and  $j_y$  and the conditions of tensor coupling between the electric field and current, we can easily reconstruct the dependence of the electric field potential  $\varphi(x,y)$  over the bulk. Among other things, for the nonlinear type of inhomogeneity analyzed here, the potential can be written in the form

$$\varphi(x,y) = \frac{I}{t} R \left( B_0 + kx + \frac{\alpha x^2}{2} \right) \exp[f(x)(y-b)]. \quad (7)$$

This expression was obtained in the approximation  $f(x)b > 1$ . Such a form of distribution describes the spatial non-monotonic dependence of potential on coordinate  $x$ . Indeed, for the lateral face of the sample corresponding to the high potential level, we can write

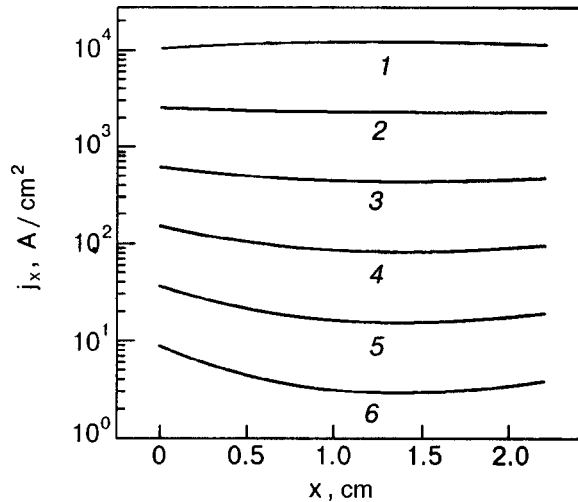


FIG. 4. Analytic distribution of the current density  $j_x$  along field gradient for various values of the transverse coordinate  $y$  (cm): 0.6 (1), 0.5 (2), 0.4 (3), 0.3 (4), 0.2 (5), 0.1 (6).

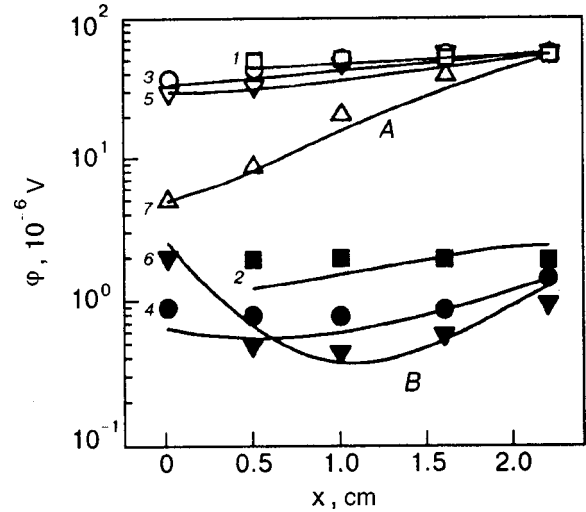


FIG. 5. Potential  $\varphi$  as a function of coordinate along the current direction at the lateral faces (A is the sample face corresponding to a strong signal, and B to the weak signal) for various inhomogeneity parameters  $k$  (T/cm) and  $\alpha$  ( $\text{T}/\text{cm}^2$ ): 0.9, 0.1 (1, 2), 1.0, 0.5 (3, 4), 0.7, 1.0 (5, 6), 0.15, 2.6 (7). The symbols correspond to the experiment and the lines to the theory.

$$\varphi(x,y=b) = \frac{I}{t} R \left( B_0 + kx + \frac{\alpha x^2}{2} \right). \quad (8)$$

For the lateral face corresponding to a low signal level, we have

$$\varphi(x,y=0) = \frac{1}{t} R \left( B_0 + kx + \frac{\alpha x^2}{2} \right) \exp[-f(x)b], \quad (9)$$

where two competing factors are responsible for nonmonotonicity. If  $\exp[f(x)b]$  is larger than unity, we can write without any loss of generality a more symmetrized expression for spatial dependence  $\varphi(x,y)$ , which ensures the fulfillment of the normalization condition for current and is a continuation of the previous model:

$$\varphi(x,y) = \frac{I}{t} R \left( B_0 + kx + \frac{\alpha x^2}{2} \right) \frac{\exp[f(x)y]}{\exp[f(x)b] - 1}. \quad (10)$$

Using the expression obtained for potential, we calculated spatial dependence  $\varphi(x,y)$  at the lateral faces of the sample, as well as at right angles to the transport. Figures 5 and 6 show the most typical experimental and the corresponding analytic dependences of the potential  $\varphi(x,y=0)$ ,  $\varphi(x,y=b)$  and  $\varphi(x=\text{const}, y)$ , calculated by using formula (10) when the transverse magnetic field gradient is a linear function of the coordinate. The results of theoretical and experimental studies reveal that while determining the dependence of the potential difference along the  $x$  coordinate, we must take into account the contribution to the electric field from transverse current on the whole, since the Hall component  $\rho_{xy}$  of the resistivity is larger than the diagonal component  $\rho_{xx}$  by a factor of  $\omega\tau$  (where  $\omega$  is the cyclotron frequency and  $\tau$  the relaxation time), and hence the quantity  $\rho_{xy}j_y$  may influence the overall field pattern considerably. This is especially important for the sample face corresponding to a low signal level, where the current density components in the direction of the current and at right angles to it

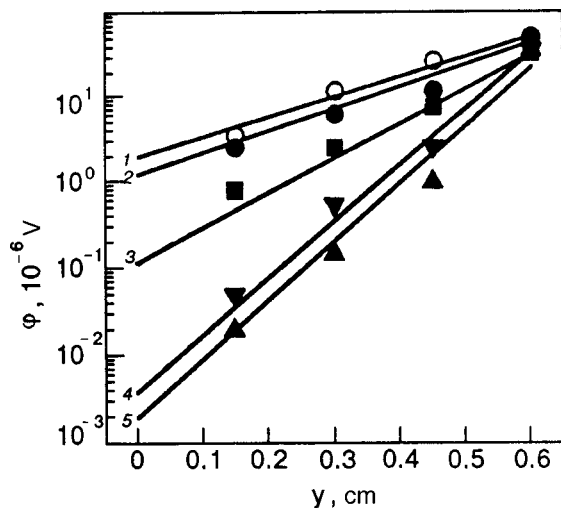


FIG. 6. Dependence of potential  $\varphi$  on transverse coordinate for various values of the inhomogeneity parameters  $k$  (T/cm) and  $\alpha$  (T/cm<sup>2</sup>): 0.9, 0.1 (1, 2), 0.7, 1.0 (3), 1.0, 0.5 (4), 0.15, 2.6 (5) and for various values of the local magnetic field  $B$  (T): 6.75 (1), 5.8 (2), 4.34 (3), 4.73 (4), and 3.09 (5). The symbols correspond to the experiment and the lines to the theory.

may become comparable. Note that in the approximation  $\exp[f(x)b] \gg 1$ , the behavior of the potential at the face corresponding to a strong signal is analogous to the analytic expression obtained earlier<sup>1</sup> for an exponential type of inhomogeneity, where it was postulated that there is no transverse current along the inward normal to this face. Such an assumption is valid for high inhomogeneity levels since the nature of potential under such conditions is determined predominantly by the component  $j_x$ . If the transverse current is disregarded for the face  $y=0$ , the variation of  $\varphi$  is qualitatively identical with the behavior at the face  $y=b$  observed experimentally only in the case when inhomogeneity and nonlinearity of the magnetic field are small. It can be stated that the reversal of the sign of the electric field component at the face corresponding to a weak signal is the result of competition between two opposite contributions during redistribution of the current density  $j_x$  on account of a lateral drift of carriers which leads to the emergence of the current  $j_y$ .

It should be specified that for high inhomogeneity levels, when the magnetic field varies by several hundred percent over the sample, the exponential index may become comparable with unity or even smaller than it. Under such conditions, the analytic expression for potential has a more complicated form. It should be noted that the experimental pattern may also be affected by the motion of charges in the direction of the magnetic field, which was disregarded in the model approximation. An analysis of this effect is beyond the scope of the present work and requires independent investigations.

## CONCLUSION

Two factors affecting the charge flow, viz., the spatial nonlinearity of transverse magnetic field in the direction of charge transport and the dependence of resistance on magnetic field, are considered in the problem of charge transport in a plate-shaped cryoconductor made of normal metal (polycrystalline aluminum sample). These factors stimulate the emergence of additional processes of redistribution of current density in the transverse direction, thus leading to the reversal of electric field at one of the lateral faces of the sample.

The analytic model is constructed in the two-dimensional approximation. It is found that the behavior of potential at the sample face corresponding to a strong signal is determined to a considerable extent by the coordinate dependence of the magnetic field defining the local value of the nondiagonal Hall component of the resistivity tensor. For the face corresponding to a low potential level, transverse Hall current plays a significant role.

This research was based on a consideration of the specific features of kinetic phenomena in conductors made of a normal metal in polycrystalline state. The main regularities of charge transport in a nonuniform magnetic field may be adapted to other cryoconductors since the formation of resistive properties in a magnetic field is qualitatively similar for them, and the prevailing quantitative differences associated with the layer thickness of open orbits are taken into consideration in the model.

This research was supported financially by the Belarus Foundation of Fundamental Research.

\*E-mail: sobol@ifftp.bas-net.by

<sup>1</sup>O. N. Mazurenko, V. R. Sobol, and A. A. Drozd, *Fiz. Nizk. Temp.* **21**, 78 (1995) [*Low Temp. Phys.* **21**, 59 (1995)].

<sup>2</sup>O. N. Mazurenko and A. A. Drozd, *Czech. J. Phys.* **46**(S5), 2549 (1996).

<sup>3</sup>V. R. Sobol, O. N. Mazurenko, and A. A. Drozd, *Proceedings ICECI 16/ICVC*, Kitakyushu, Japan 1996.

<sup>4</sup>M. Ya. Azbel and V. G. Peschansky, *Zh. Éksp. Teor. Fiz.* **49**, 572 (1965) [*Sov. Phys. JETP* **22**, 399 (1965)].

<sup>5</sup>M. Ya. Azbel and V. G. Peschansky, *Zh. Éksp. Teor. Fiz.* **55**, 1980 (1968) [*Sov. Phys. JETP* **28**, 1045 (1968)].

<sup>6</sup>Yu. A. Dreizin and A. M. Dykhne, *Zh. Éksp. Teor. Fiz.* **63**, 242 (1972) [*Sov. Phys. JETP* **36**, 127 (1972)].

<sup>7</sup>M. P. Krefta, O. R. Christianson, and J. H. Parker, *Cryogenics* **36**, 291 (1996).



monic interaction between acoustic phonons and  $\Pi_2^j$  the interaction between acoustic phonons and phonon density fluctuations in the vicinity of the defects. Lines with arrows in Eq. (4) correspond to Green's function  $\bar{G}^{(+,-)}$ , while the vertex  $U_j$  emerges as a result of summation of "fan-shaped" plots and describes processes of inverse coherent scattering of phonons by defects (see, for example, Refs. 11–14). The contributions of  $l$ - and  $b$ -modes to the processes of anharmonic interaction and to the vertex  $U_j$  during computations are assumed to be independent.

Let us now consider explicit expressions for the vertex  $U_j$  under the following conditions:

$$q_l^j(\omega_1) \ll 1, \quad \omega \tau_i^j \ll 1,$$

where  $l_j(\omega_1) = v_j(\omega_1) \tau_i^j(\omega_1)$  is the elastic mean free path, and  $v_j$  the group velocity of quasiparticles. It was shown in Ref. 13 that

$$U_j(\mathbf{k}, \mathbf{k}'; \omega, \omega_1) = \frac{\Gamma_j}{N} \left[ 1 - \frac{\Gamma_j}{N} \sum_{\mathbf{k}_1} \bar{G}_j^+(\mathbf{k}_1, \omega_1) \times \bar{G}_j^-(\mathbf{k}_1 - \mathbf{q}, \omega_1 - \omega) \right]^{-1}, \quad (5)$$

$$\mathbf{q} = \mathbf{k} + \mathbf{k}'.$$

This equation contains the quantity  $\Gamma_j = \omega_1 [\pi \tau_i^j(\omega_1) g_j(\omega_1^2)]^{-1}$ , i.e., the initial vertex describing a single elastic scattering of low-frequency phonons with quasimomenta  $\mathbf{k}$  and  $-\mathbf{k}$ .

In the standard approximation, the anharmonic interaction parameter  $\Phi_j^{(3)}$  has the form

$$\Phi_j^{(3)}(\mathbf{k}, \mathbf{k}_1, \mathbf{k}_2) = -i \tilde{\gamma}_3 \omega_j(\mathbf{k}) \omega_j(\mathbf{k}_1) \omega_j(\mathbf{k}_2), \quad (6)$$

$$\tilde{\gamma}_3 = \gamma_3 \sqrt{\gamma_{\parallel}^2 \gamma_{\perp}}.$$

Here,  $\gamma_{\parallel}, \gamma_{\perp}$  ( $\gamma_{\parallel} \gg \gamma_{\perp}$ ) and  $\gamma_3$ , are the effective harmonic and anharmonic force constants.

Taking into consideration Eqs. (4)–(6), the expressions for  $\Pi_1^j$  and  $\Pi_2^j$  can be presented in the form

$$\Pi_1^j(\mathbf{k}, \omega) \approx i \tilde{\gamma}_3^2 \omega_j^2(\mathbf{k}) \int_0^{\infty} \frac{d\omega_1}{2\pi} \int_0^{\infty} \frac{d\omega_2}{2\pi} \delta(\omega + \omega_2 - \omega_1) \times 2[n(\omega_2) - n(\omega_1)] \frac{1}{N} \times \sum_{\mathbf{k}_1, \mathbf{k}_2} \omega_j^2(\mathbf{k}_1) \omega_j^2(\mathbf{k}_2) \bar{G}_j^{(+)}(\mathbf{k}_1, \omega_1) \times \bar{G}_j^{(-)}(\mathbf{k}_2, \omega_2) \Delta(\mathbf{k} + \mathbf{k}_1 + \mathbf{k}_2), \quad (7)$$

$$\Pi_2^j(\mathbf{k}, \omega) \approx i \tilde{\gamma}_3^2 \omega_j^2(\mathbf{k}) \int_0^{\infty} \frac{d\omega_1}{2\pi} \int_0^{\infty} \frac{d\omega_2}{2\pi} \delta(\omega + \omega_2 - \omega_1) \times 2[n(\omega_2) - n(\omega_1)] F_j(\omega_1) \times \sum_{\mathbf{q} \leq \mathbf{q}_c} U_j(\mathbf{q}; \omega_1, \omega). \quad (8)$$

The quantity  $F_j$  is defined as

$$F_j(\omega_1) = \frac{1}{N} \sum_{\mathbf{k}_1} [\omega_j^2(\mathbf{k}_1) \bar{G}_j^{(-)}(\mathbf{k}_1, \omega_1) \bar{G}_j^{(+)}(\mathbf{k}_1, \omega_1)]^2, \quad (9)$$

where  $n(\omega)$  is Planck's equilibrium distribution function for phonons. While writing this equation, we disregarded the small terms  $\mathbf{q}$  in the arguments of Green's functions. In lattices with strongly anisotropic force of interaction between atoms, summation in Eq. (8) over  $\mathbf{q}$  has an upper limit really set by two small quantities  $q_{\parallel, \perp}^{(\parallel, \perp)} \approx \pi/l_{\parallel, \perp}^{(j)}(\omega_1)$  (it is assumed that diffusion takes place over distances larger than the elastic mean free path). If  $a \approx b$ , the mean free paths  $l_{\parallel, \perp}^{(j)} = v_{\parallel, \perp}^{(j)} \tau_i^{(j)}(\omega_1)$ . If, however, the unit cell parameters  $a$  and  $b$  are quite different, i.e.,  $a \ll b$ , a situation may arise in which  $q_j^{(\perp)} \approx \pi/b$ .

In order to proceed further, we must determine the phonon mode frequencies. It was mentioned in the Introduction that the lattice is assumed to be tetragonal with unit cell parameters  $a$  and  $b$ . It is assumed that the effective interaction between atoms in the basal plane  $xOy$  (denoted as  $(\parallel)$ ) is much stronger than along the  $z$ -axis  $(\perp)$ . The interaction along the  $z$ -axis is be central. In such a situation, we encounter three characteristic force parameters satisfying the inequality

$$|\Phi_{xx\perp}^{0s}| \ll |\Phi_{zz\perp}^{0s}| \ll |\Phi_{zz\parallel}^{0s}|. \quad (10)$$

These force parameters have three effective frequencies corresponding to them:  $\omega_{\perp}^2 \ll \omega_2^2 \ll \omega_{\parallel}^2$ .

Taking into consideration the interaction between near-est neighbors only, we can write for the  $l$ -mode

$$\omega_l^2(\mathbf{k}) \approx v_{\parallel}^{(l)2} k_{\parallel}^2 + 2\omega_{\perp}^2 \sin^2\left(\frac{bk_{\perp}}{2}\right), \quad (11)$$

where  $v_{\parallel}^{(l)} \approx \omega_{\parallel} a/2$  is the velocity of sound in the  $l$ -mode. For the  $b$ -mode, the dispersion relation can be defined as

$$\omega_b^2(\mathbf{k}) = \omega_{\perp}^2 b^2 k_{\parallel}^2 + \left(\frac{\omega_{\parallel} a^2}{\pi}\right)^2 k_{\parallel}^4 + 2\omega_2^2 \sin^2\left(\frac{bk_{\perp}}{2}\right) \quad (12)$$

(see details in Ref. 2 as well as in Ref. 13).

We shall consider only the  $l$ -mode in details. The computations for the  $b$ -mode can be carried out in an analogous manner. In the last section of this paper, we shall mention some differences in the qualitative behavior of the sound absorption coefficient for  $l$ - and  $b$ -modes.

In the first place, it can be shown that in the polar approximation we obtain<sup>11,12</sup> instead of Eq. (9)

$$F_l(\omega_1) \approx \frac{\pi}{4} g_l(\omega_1) \tau_i^{(l)3}(\omega_1), \quad (13)$$

where  $g_l(\omega_1) = (\pi \omega_{\parallel}^2)^{-1}$  is the partial density of states.

Second, we can write the following approximate expression for the vertex part of  $U_l$  in the frequency region where the phonon modes act like quasi-two-dimensional excitations, i.e., where the inequality  $\omega_1^2 > 2\omega_{\perp}^2$  is satisfied<sup>13</sup>:

$$U_i(\mathbf{q}; \omega; \omega_1) \approx \frac{\omega_1}{\pi g_{\parallel}(\omega_1^2) \tau_i^{2(l)}(\omega_1)} \times \frac{1}{-i\omega + D_{\parallel}^{0(l)}(\omega_1) q_{\parallel}^2 + 2D_{\perp}^{0(l)} \sin^2(q_{\perp} b/2)}, \quad (14)$$

where

$$D_{\parallel}^{0(l)}(\omega_1) = \frac{v_{\parallel}^{(l)2} \tau_i^{(l)}(\omega_1)}{2}, \quad D_{\perp}^{0(l)}(\omega_1) = \frac{\omega_{\perp}^4 \tau_i^{(l)}(\omega_1)}{4\omega_1^2} \quad (15)$$

are the diffusion coefficient tensor components. It is assumed that  $\omega \approx \omega_1(\mathbf{k})$ .

It is well known that the real and initial phonon diffusion coefficients  $D_{\parallel,\perp}^{(j)}$  and  $D_{\parallel,\perp}^{0(j)}$  are connected with equations of the type

$$D_{\parallel} = D_{\parallel}^0 - \frac{a^2 b}{\pi g_{\parallel}(\omega_1)} \times \int d^3 q \frac{D_{\parallel}}{-\omega + D_{\parallel} q_{\parallel}^2 + 2D_{\perp} \sin^2(q_{\perp} b/2)}, \quad (16)$$

$$D_{\perp} = D_{\perp}^0 - \frac{a^2 b}{\pi g_{\parallel}(\omega_1)} \times \int d^3 q \frac{D_{\perp}}{-i\omega + D_{\parallel} q_{\parallel}^2 + 2D_{\perp} \sin^2(q_{\perp} b/2)} \quad (17)$$

(similar relations for the phonon gas in an isotropic lattice and electrons in an anisotropic system were considered in Refs. 9 and 16).

It is convenient to consider the factors

$$\alpha_{\parallel,\perp}^{(l)}(\omega, \omega_1) \equiv D_{\parallel,\perp}^{(l)}(\omega, \omega_1) / D_{\parallel,\perp}^{0(l)}(\omega_1). \quad (18)$$

It follows from (16) and (17) that

$$\alpha_{\parallel} = \alpha_{\perp} = \alpha.$$

In this case,  $\alpha^{(l)}$  satisfies the relation

$$\alpha(\omega, \omega_1) = 1 - \frac{a^2 b}{g_{\parallel}(\omega_1)} \int_{-\pi/b}^{\pi/b} \frac{dq_{\perp}}{2\pi} \times \int_0^{\pi/l} \frac{dq_{\parallel}^2}{2\pi^2} J(\omega, q_{\parallel}, q_{\perp}), \quad (19)$$

where

$$J(\omega, q_{\parallel}, q_{\perp}) = \frac{1}{-i\omega/\alpha + D_{\parallel}^{0(l)} q_{\parallel}^2 + 2D_{\perp}^{0(l)} \sin^2(q_{\perp} b/2)}.$$

It can be shown that

$$\begin{aligned} \alpha^{(l)}(\omega, \omega_1) &\approx 1 - \frac{1}{\pi \omega_1 \tau_i^{(l)}(\omega_1)} \ln \frac{2}{\tau_i^{(l)}(\omega_1) D_{\perp}^{0(l)}(\omega_1)} \\ &+ \frac{1}{\pi \omega_1 \tau_i^{(l)}(\omega_1)} \left( \frac{-2i\omega}{D_{\perp}^{(l)}(\omega_1)} \right)^{1/2} \\ &= \alpha_0^{(l)}(\omega_1) + \frac{1}{\pi \omega_1 \tau_i^{(l)}(\omega_1)} \left( \frac{-2i\omega}{D_{\perp}^{(l)}(\omega_1)} \right)^{1/2}. \end{aligned} \quad (20)$$

Taking all that has been stated above into consideration, we can determine the imaginary parts of the mass operator  $\Pi^j$  in the limit of low frequencies. Substitution of (2) into (7) leads to the following relation for  $\text{Im } \Pi_1^j$ :

$$\begin{aligned} \text{Im } \Pi_1^j(\mathbf{k}, \omega) &\approx 2\tilde{\gamma}_3^2 \omega \omega_j^2(\mathbf{k}) \frac{1}{T} \sum_{\mathbf{k}_1} \omega_j^2(\mathbf{k}_1) n[\omega_j(\mathbf{k}_1)] \\ &\times [n[\omega_j(\mathbf{k}_1)] + 1] \tau_i^{(j)}[\omega_j(\mathbf{k}_1)]. \end{aligned} \quad (21)$$

At extremely low temperatures, the sum in (21) is divergent like thermal conductivity which also diverges due to the same mechanism of phonon scattering. A finite value of sound absorption can be obtained by taking into account the anharmonic attenuation of thermal phonons and their scattering at the sample boundary. Relation (21) is valid at intermediate temperatures, when the mean free path of thermal phonons is sensitive to defects.<sup>17</sup> For the quantity  $\text{Im } \Pi_2^j$ , we use the results obtained by Volfhardt and Wolfe<sup>18,19</sup> who proposed a self-consistent generalization of a number of overlapping diagrams for the irreducible vertex  $U$ . Taking all this into consideration, we replace the initial diffusion coefficients  $D^0$  by the real diffusion coefficients  $D$ . Substituting (9) into (8) and using (18), we carry out computations analogous to those in Ref. 13. This gives

$$\begin{aligned} \text{Im } \Pi_2^j(\mathbf{k}, \omega) &\approx \frac{\tilde{\gamma}_3^2 a^2 \omega \omega_j^2(\mathbf{k})}{2T} \\ &\times \int_{\omega_j^0}^{\omega_j^*} \frac{d\omega_1}{2\pi} n(\omega_1) [n(\omega_1) + 1] \\ &\times \frac{\omega_1^2 \tau_i^{(j)}(\omega_1)}{D_{\parallel}^{(j)}(\omega, \omega_1)} \left[ \ln \frac{2}{\tau_i^{(j)}(\omega_1) D_{\perp}^{0(j)}(\omega_1)} \right. \\ &\left. - \text{Re} \left( \frac{-2i\omega}{\alpha_0 D_{\perp}^{0(j)}(\omega_1)} \right)^{1/2} \right]. \end{aligned} \quad (22)$$

The frequency  $\omega_j^0$  appearing in this expression separates the regions of quasi-three-dimensional (a small frequency region near zero) and quasi-two-dimensional behavior of the vibrational spectrum of a layered lattice. As far as the frequency  $\omega_j^*$  ( $\omega_j^* \gg \omega_j^0$ ) is concerned, it defines the threshold of phonon mobility and is determined from the condition of vanishing of the true diffusion coefficient.

Using Eq. (20), we obtain the following relations for  $\alpha^{(l)}$  near the threshold. If

$$(\pi \omega_1 \tau_i^{(l)}(\omega_1))^{-1} \ll \alpha_0^{(l)} \ll 1 \quad (23)$$

or the condition

$$\alpha_0^{(l)} \ll (\pi \omega_1 \tau_i^{(l)}(\omega_1))^{-1} \ll 1, \quad \omega \ll \alpha_0^{(l)3} D_{\perp}^{0j} [\pi \omega_1 \tau_i^{(l)}(\omega_1)]^2, \quad (24)$$

is satisfied, we can write

$$\alpha^{(l)} \approx \frac{2}{\omega_l^*} (\omega_l^* - \omega_1). \quad (25)$$

If inequalities of the type

$$\alpha_0^{(l)} \ll [\pi \omega_1 \tau_i^{(l)}(\omega_1)]^{-1} \ll 1, \quad \omega \gg [\pi \omega_1 \tau_i^{(l)}(\omega_1)]^2 \alpha_0^{3j} D_{\perp}^{0(l)}(\omega_1), \quad (26)$$

hold, we get

$$\alpha^{(l)} \approx \left[ \frac{2}{D_{\perp}^0(\omega_j)} \frac{-i\omega}{[\pi \omega_1 \tau_i^{(l)}(\omega_1)]^2} \right]^{1/3}. \quad (27)$$

Let us now consider the shear modes briefly. It should be emphasized that all the main expressions (20)–(22) for longitudinal and flexural modes have the same structure, the difference being only in the representations for the initial diffusion coefficients. In accordance with Ref. 13, we have

$$\{D_{\parallel}^{0(b)}, D_{\perp}^{0(b)}\} \approx \left\{ \frac{1}{g_b(\omega)} \frac{\pi \tau_i^{(b)}(\omega)}{4 \omega_{\parallel} \omega_2} \times \left[ \frac{16 \omega_{\parallel} \omega a^2}{3 \pi^2}, \frac{\omega_2^2 b^2 \pi}{4} \right] \right\}; \quad (28)$$

The density of states is described by the formula  $g_b(\omega_1) = \pi(8\omega_1\omega_{\parallel})^{-1}$ . Moreover, the  $l$ - and  $b$ -modes are defined in different frequency intervals:  $2\omega_{\perp}^2 < \omega_1^2 < \omega_{\parallel}^2$  and  $2\omega_2^2 < \omega_1^2 < \omega_{\parallel}^2$ . Hence the results obtained above for  $l$ -modes, including relations (25) and (27), can be extended to the case of  $b$ -modes.

### LOW-FREQUENCY SOUND ABSORPTION COEFFICIENT

Let us begin with the case of a harmonic lattice. We consider the dispersion relation for the effective frequency  $\tilde{\omega}_{\mathbf{k}}$  and the attenuation of vibrational modes (the subscript  $j$  is omitted). This equation has the form

$$\tilde{\omega}_{\mathbf{k}}^2 - \omega_{\mathbf{k}}^2 - i \frac{2\tilde{\omega}_{\mathbf{k}}}{\tau_i(\omega_{\mathbf{k}})} = 0.$$

We put

$$\omega_{\mathbf{k}}(\mathbf{k} \rightarrow 0) = v_{\parallel(\perp)} k^*, \quad \mathbf{k}^* = \mathbf{k} + i\Delta\mathbf{k}.$$

It can be shown that

$$\Delta k = \lim_{\omega \rightarrow 0} \frac{1}{v_{\parallel(\perp)} \tau_i(\omega)}, \quad (29)$$

( $v$  is the phonon group velocity and  $\tau_i$  the Rayleigh-type lifetime).

The absorption coefficient of low-frequency modes is defined by the relation

$$\Gamma_0 = \text{Im}|\mathbf{k}^*|,$$

where  $\mathbf{k}^*$  is the complex wave vector of the mode propagating through the crystal (see, for example, Ref. 11). Note that

according to Eq. (29), the factor  $\Gamma_0 (= \Delta k)$  is proportional to  $\omega^2 g_j(\omega)$ . Taking into consideration the explicit form of  $g_j(\omega)$  (see Ref. 13), we find that  $\Gamma_0 \approx \omega^3$  for longitudinal modes and  $\Gamma_0 \approx \omega^2$  for flexural modes. The factor  $\Gamma_0$  does not depend on temperature.

Let us now consider the case of an anharmonic crystal. The dispersion equation can be written in the form

$$\tilde{\omega}_{\mathbf{k}}^2 - \omega_{\mathbf{k}}^2 - i \frac{2\omega}{\tau_i(\omega_{\mathbf{k}})} - i \text{Im} \Pi^j(\omega(\mathbf{k})) = 0,$$

where

$$\text{Im} \Pi^j = \text{Im} \Pi_{(1)}^j + \text{Im} \Pi_{(2)}^j.$$

where the subscripts 1 and 2 indicate the contributions from standard and nonstandard diagrams (4). This leads to the following approximate relation for the reciprocal relaxation time:

$$\frac{1}{\tau} = \frac{1}{\tau_i} + \frac{\text{Im} \Pi^j}{2\omega_j(\mathbf{k})}.$$

It follows from this relation that the factor  $1/\tau$  in the anharmonic lattice depends on temperature.

Let us consider the temperature dependence of the ultrasound absorption coefficient

$$\bar{\Gamma}_j = \Gamma_{j,0} + \Delta\Gamma_j(T)$$

for the  $j$ -polarization mode. In accordance with the above, we can write

$$\Delta\Gamma_j(T) \approx \frac{\text{Im} \Pi^j[\omega(\mathbf{k})]}{2\omega_j(\mathbf{k})}, \quad \Delta\Gamma_j = \Delta\Gamma_j^{(1)} + \Delta\Gamma_j^{(2)}.$$

Let us analyze this expression for the sound absorption coefficient in the case of strong localization of phonon modes. For this purpose, we use the expressions (20), (25), and (27), and (28). It turns out that if the inequalities ( $c\varepsilon^2 \gg 1; T \leq 0,1\Theta_j\Theta_j$ ) is the Debye temperature) and  $D_{\perp}^{0j}(\omega) \tau_i^{(j)}(\omega) \leq 0,1$  are satisfied, the inequality  $\Delta\Gamma_j^{(2)} \gg \Delta\Gamma_j^{(1)}$  holds for acoustic frequencies in the megahertz range. In other words, the temperature dependence of the sound absorption coefficient is determined by the processes of scattering at phonon density fluctuations in the vicinity of defects.

The following circumstance must be noted. Suppose that the inequality (26) is satisfied. In this case, if the frequency  $\omega$  of sound exceeds a certain critical value  $\omega_c = [\pi \omega_T \tau_i^{(j)} \times (\omega_T)]^2 \alpha_0^{(l)3} D_{\perp}^{0j}(\omega_T)$ , the anharmonic part of the attenuation coefficient for  $l$ - and  $b$ -modes near the mobility threshold depends on frequency as  $\Delta\Gamma_j \sim \omega^{5/3}$ . (If the inequality (24) is satisfied, we obtain  $\Delta\Gamma_j \sim \omega^2$ .) Thus a strong localization may change the frequency dependence for  $\Gamma_j$  observed in the case of a harmonic lattice.

Let us compare  $\Delta\Gamma_j^{(1)}$  and  $\Delta\Gamma_j^{(2)}$  in the dominating phonon approximation ( $\omega_1 \approx T$ ). It can be shown by using Eqs. (21) and (22) that if the condition  $D_{\perp}^0 \ll D_{\parallel}^0$  is satisfied, we can write for longitudinal and flexural modes

$$\frac{\Delta\Gamma_j - \Delta\Gamma_j^{(1)}}{\Delta\Gamma_j^{(1)}} = \frac{\Delta\Gamma_j^{(2)}}{\Delta\Gamma_j^{(1)}} = \frac{1 - \alpha^j(\omega, \omega_T)}{\alpha^j(\omega, \omega_T)}.$$

As the dominating phonon frequency  $\omega_T$  approaches the threshold frequency  $\omega_j^*$ , the factor  $\Delta\Gamma$  becomes nonanalytic:  $\Delta\Gamma_j \sim (\omega_j^* - \omega_T)^{-1}$ .

Let us estimate the contribution of the weak localization of phonon modes to the sound absorption coefficient. For simplicity, we use the dominating phonon approximation again. Putting the factor  $\alpha$  in (18) approximately equal to unity, we compare  $\Delta\Gamma_j^{(1)}$  and  $\Delta\Gamma_j^{(2)}$ . Using (21), (22) and (28), we obtain

$$\frac{\Delta\Gamma_j^{(2)}}{\Delta\Gamma_j^{(1)}} \approx c\varepsilon^2 \left( \frac{T}{\Theta_j} \right)^2 \ln 2(\tau_i^{(j)}[\omega_T]D_{\perp}^0(\omega_T))^{-1},$$

which means that the contribution is just a few percent of  $\Delta\Gamma_j^{(1)}$ .

Let us summarize the main conclusions. We have considered the effect of phonon density fluctuations on reciprocal lifetime  $1/\tau$  in the longwave limit for the case of low temperatures  $T \leq 0.1\Theta_j$ . To determine the mass operator, we analyzed processes associated with cubic anharmonism. Moreover, the emergence of two-phonon coherent states in the localization regime was also taken into consideration. It was shown that specific interference phenomena lead to noticeable renormalizations. The theory developed by us was used to discuss the peculiarities of temperature and frequency dependence of the reciprocal ultrasound attenuation length  $\Gamma$ .

We are not aware of any experimental works to which

the theory developed in this communication could be applied.

\*E-mail: zhernov@kurm.polyn.kiae.su

- 
- <sup>1</sup>I. M. Lifshits, Zh. Éksp. Teor. Fiz. **22**, 475 (1952) (before AIP translations).  
<sup>2</sup>A. M. Kosevich, *Theory of Crystal Lattice* [in Russian], Vyssha Shkola, Kharkov (1988).  
<sup>3</sup>E. S. Syrkin and S. B. Feodos'ev, Fiz. Nizk. Temp. **5**, 1069 (1979) [Sov. J. Low Temp. Phys. **5**, 506 (1979)].  
<sup>4</sup>M. A. Ivanov and Yu. V. Skripnik, Fiz. Tverd. Tela (Leningrad) **32**, 2965 (1990) [Sov. Phys. Solid State **32**, 1722 (1990)].  
<sup>5</sup>M. A. Ivanov and A. M. Kosevich *et al.*, Fiz. Nizk. Temp. **19**, 434 (1993) [Low Temp. Phys. **19**, 305 (1993)].  
<sup>6</sup>T. R. Kirkpatrick, Phys. Rev. B **31**, 5746 (1985).  
<sup>7</sup>E. Akkermans and R. Maynard, Phys. Rev. B **32**, 7860 (1985).  
<sup>8</sup>Qian-Jin Chu and Zhao-Oing Zhag, Phys. Rev. B **38**, 4906 (1988).  
<sup>9</sup>H. Bottger and M. Theuerkauf, Phys. Status Solidi B **150**, 73 (1988).  
<sup>10</sup>M. P. van Albada, M. B. van der Mark, and A. Lagendik, in *Scattering and Localization of Classical Waves in Random Media* [ed. by P. Shjeng], World Scientific, Singapore (1989).  
<sup>11</sup>A. P. Zhernov and E. P. Chulkin, Zh. Éksp. Teor. Fiz. **109**, 602 (1996) [JETP **82**, 321 (1996)].  
<sup>12</sup>A. P. Zhernov and E. P. Chulkin, Phys. Status Solidi B **193**, 67 (1996).  
<sup>13</sup>A. P. Zhernov and E. P. Chulkin, Fiz. Tverd. Tela (St. Petersburg) **40**, 132 (1998) [Phys. Solid State **40**, 118 (1998)].  
<sup>14</sup>A. P. Zhernov and E. P. Chulkin, Zh. Éksp. Teor. Fiz. **113**, 930 (1998) [JETP **86**, 507 (1998)].  
<sup>15</sup>Yu. A. Barabanenkov and M. Yu. Barabanenkov, Zh. Éksp. Teor. Fiz. **113**, 432 (1998) [JETP **86**, 237 (1998)].  
<sup>16</sup>V. N. Prigodin and Yu. A. Firsov, J. Phys. C **17**, L979 (1984).  
<sup>17</sup>R. Berman, *Thermal Conduction*, Oxford University Press, Oxford (1976).  
<sup>18</sup>D. Volfhardt and P. Wolffe, Phys. Rev. Lett. **45**, 842 (1980).  
<sup>19</sup>D. Volfhardt and P. Wolffe, Phys. Rev. B **22**, 4666 (1980).

Translated by R. S. Wadhwa

## Low-frequency dynamics of cubic crystals with next-nearest neighbor interaction

E. V. Manzheliĭ and E. S. Syrkin

*B. Verkin Institute of Low-Temperature Physics and Engineering, National Academy of Sciences of Ukraine, 310164 Kharkov, Ukraine\**

(Submitted April 28, 1999; revised July 12, 1999)

*Fiz. Nizk. Temp.* **25**, 1224–1236 (November 1999)

The influence of next-nearest neighbor interaction on the dispersion characteristics of simple cubic, bcc, and fcc lattices is studied. It is shown that the next-nearest neighbor interaction affects significantly the dynamic characteristics of the above systems. In the scalar model describing the one-magnon excitations in magnetically ordered Heisenberg systems, the inclusion of the second coordination sphere can lead to the emergence of a minimum and an additional peak on the dispersion curves inside the Brillouin zone and to the disappearance of divergence of the density of states. In some cubic lattice models, the inclusion of next-nearest neighbor interaction may lead to a significant variation of the “anisotropy parameter:” in the longwave limit, two transverse branches may coincide or differ sharply from each other, depending on the relation between the force constants characterizing the interaction between the nearest and next-nearest neighbors. © 1999 American Institute of Physics. [S1063-777X(99)01111-1]

### INTRODUCTION

In order to study the spectra of quasiparticle excitations, it is extremely important to estimate the effective range of atomic interaction in the objects under consideration. Even in the case of short-range forces only (e.g., those described by the Lennard–Jones potential), the results obtained by taking into consideration interactions with nearest neighbors only are absolutely unsatisfactory in some cases. For example, the vector models of a simple cubic (sc) and a body-centered cubic (bcc) crystals with such an interaction are simply unstable in lattice dynamics (see, for example, Ref. 1).

The inclusion of the next-nearest neighbors into consideration leads to a whole range of qualitatively new results or to a much better agreement with the experiment. The description of shear waves in highly anisotropic crystals is possible only if the next-nearest neighbors are taken into consideration.<sup>2</sup> The next-nearest neighbors also play a significant part in studies of spin wave in magnetically ordered systems. For example, it has been shown experimentally<sup>3</sup> that the exchange integrals of interaction between the nearest and next-nearest neighbors are nearly identical in magnetic semiconductors EuO and EuS, while those between third and subsequent neighbors are negligibly small. Moreover, the exchange integrals of interaction between the nearest and next-nearest neighbors may be of the same or opposite signs. It was shown earlier by Petrova and Syrkin<sup>4,5</sup> that for interaction attenuating exponentially with distance, it is important to take into consideration next-nearest neighbors for studying vibrational excitations as well as spin waves. The role of distant neighbors was emphasized in numerical computations and experimental investigations of the dispersion relations for a number of metals with bcc structure<sup>6,7</sup> and solidified inert gases (fcc structure).<sup>8</sup>

In this communication, we report on the results of

investigations of the vibrational characteristics of sc, bcc and fcc lattices for an arbitrary ratio of the constants of interaction between the nearest and next-nearest neighbors. The cubic symmetry is possessed by a wide range of materials like molecular crystals, metals, superconductors, magnetically ordered systems, etc. We considered vector as well as scalar (one-component) models of the cubic lattice. The use of the scalar model is justified for a number of reasons. Upon an appropriate change in the notation, the results obtained for this model can be used for studying spin waves in magnetically ordered crystals. Moreover, real semi-infinite crystals may contain one-component surface waves of the SH type (Gulyaev–Bleustein waves in piezoelectrics<sup>9,10</sup> and Alldredge–Gel’fgat waves in conventional crystals.<sup>11,12</sup>) We considered in detail cases in which the inclusion of interaction with next-nearest neighbors qualitatively changes the investigated characteristics. For example, the peak of the dispersion curve is displaced inward into the Brillouin zone, splitting of vibrational branches takes place, and the lattice stability emerges or vanishes. We also analyzed the variation of elastic moduli of cubic lattices on account of interaction with next-nearest neighbors, and the corresponding variation of the dynamic characteristics of cubic lattices in the long-wave limit.

### 1. MATRICES OF FORCE CONSTANTS OF CUBIC LATTICES AND THE RELATION BETWEEN THESE CONSTANTS AND PAIRED POTENTIAL

According to the Born–von Carman lattice dynamics theory, the forces of interaction between two atoms in a monatomic crystal in the harmonic approximation have the form  $\Phi_{ik}(n, n')u_k(n')$ , (i.e., the force acting on an atom at the  $n$ th site in the  $i$ th direction), while the atom at the  $n'$ th site is displaced through a distance  $u(n')$  in the  $k$ th direction. Thus, the  $3 \times 3$  matrix  $\Phi_{ik}$  is a set of elastic constants of

interaction between atoms at the sites  $n$  and  $n'$ . Taking into account the interaction between the nearest and next-nearest neighbors, the matrices  $\Phi_{ik}^{nn'}$  for cubic lattices can be presented in the form<sup>1,6</sup>

$$\begin{aligned} \Phi_{ik}[0,a(1,0,0)] &= \begin{pmatrix} \alpha_1 & 0 & 0 \\ 0 & \beta_1 & 0 \\ 0 & 0 & \beta_1 \end{pmatrix} \\ \Phi_{ik}[0,a(1,1,0)] &= \begin{pmatrix} \alpha_2 & \gamma_2 & 0 \\ \gamma_2 & \alpha_2 & 0 \\ 0 & 0 & \beta_2 \end{pmatrix}; \end{aligned} \quad (1)$$

for a simple cubic lattice with the nearest neighbors at the  $a(100)$ -type sites and the next nearest neighbors at the  $a(110)$ -type sites ( $a$ -edge of the cube);

$$\begin{aligned} \Phi_{ik}\left(0, \frac{a}{2}(1,1,1)\right) &= \begin{pmatrix} \alpha_1 & \beta_1 & \beta_1 \\ \beta_1 & \alpha_1 & \beta_1 \\ \beta_1 & \beta_1 & \alpha_1 \end{pmatrix} \\ \Phi_{ik}[0,a(1,0,0)] &= \begin{bmatrix} \alpha_2 & 0 & 0 \\ 0 & \beta_2 & 0 \\ 0 & 0 & \beta_2 \end{bmatrix}; \end{aligned} \quad (2)$$

for a bcc lattice with the nearest neighbors at the  $(a/2)(111)$  sites and the next nearest neighbors at the  $a(100)$  sites; and

$$\begin{aligned} \Phi_{ik}\left(0, \frac{a}{2}(1,1,0)\right) &= \begin{pmatrix} \alpha_1 & \gamma_1 & 0 \\ \gamma_1 & \alpha_1 & 0 \\ 0 & 0 & \beta_1 \end{pmatrix} \\ \Phi_{ik}(0,a(1,0,0)) &= \begin{pmatrix} \alpha_2 & 0 & 0 \\ 0 & \beta_2 & 0 \\ 0 & 0 & \beta_2 \end{pmatrix} \end{aligned} \quad (3)$$

for an fcc lattice with the nearest neighbors at the  $a/2(110)$  sites and the next nearest neighbors at the  $a(100)$  sites.

Analyzing the arrangement and number of nearest and next-nearest neighbors, we observe that the effect of next-nearest neighbors in an fcc crystal must be weaker than in sc or bcc crystals. Indeed, although the next-nearest neighbors (12 atoms) in sc crystals are more distant, their number is double that of the nearest neighbors (six atoms). The open bcc structure has six next-nearest neighbors at a distance only 15% larger than the distance between eight nearest neighbors, while the close-packed fcc structure has six next-nearest neighbors which are farther than the 12 nearest neighbors by 40%.

Each of the matrices (1), (2) and (3) must be supplemented by the self-action matrix  $\Phi_{ik}^{0,0}$  (translational invariance condition)<sup>1</sup>:

$$\Phi_{ik}(0,0) = \alpha_0 \begin{pmatrix} 1 & 0 & 0 \\ 0 & 1 & 0 \\ 0 & 0 & 1 \end{pmatrix},$$

where  $\alpha_0$  has the following form for various lattices:

$$\alpha_0 = 2(\alpha_1 + 2\beta_1) + 4(\alpha_2 + 2\beta_2) \quad (4)$$

for sc lattice;

$$\alpha_0 = 8\alpha_1 + 2(\alpha_2 + 2\beta_2) \quad (5)$$

for bcc lattice; and

$$\alpha_0 = 4(\beta_1 + 2\alpha_1) + 2(\alpha_2 + 2\beta_2) \quad (6)$$

for fcc lattice.

The elements of the force matrix  $\Phi_{ik}^{nn'}$  may be connected with the derivatives of the paired potential. Let  $f(|\mathbf{R}_n - \mathbf{R}_{n'}|)$  be the potential of paired interaction between atoms, which depends only on the separation between them ( $\mathbf{R}_n$  is the radius vector of the atom at site  $n$ ). The total potential energy  $U$  of the lattice has the form

$$U = \frac{1}{2} \sum_{n \neq n'} f(|\mathbf{R}_n - \mathbf{R}_{n'}|). \quad (7)$$

We can present  $\mathbf{R}_n$  in the form  $\mathbf{R}_n = \mathbf{r}_n + \mathbf{u}_n$ , where  $\mathbf{r}_n$  is the radius-vector of the  $n$ th atom in the equilibrium state and  $\mathbf{u}_n$  is its displacement. In this case,

$$\begin{aligned} U &= \frac{1}{2} \sum_{n \neq n'} f(|\mathbf{r}_n - \mathbf{r}_{n'} + \mathbf{u}_n - \mathbf{u}_{n'}|) \\ &= \frac{1}{2} \sum_{\mathbf{r}} \sum_{\mathbf{D} \neq 0} f(|\mathbf{D} + \mathbf{d}|), \end{aligned} \quad (8)$$

where  $\mathbf{r} = \mathbf{r}_{n'}$ ;  $\mathbf{D} = \mathbf{r}_n - \mathbf{r}_{n'}$ ;  $\mathbf{d} = \mathbf{u}_n - \mathbf{u}_{n'}$ .

We expand  $f(|\mathbf{D} + \mathbf{d}|)$  into a power series in  $\mathbf{d}$  up to the second-order term:

$$\begin{aligned} f(\mathbf{D} + \mathbf{d}) &= f(\mathbf{D}) + f'(\mathbf{D})(\mathbf{v} \cdot \mathbf{d}) \\ &\quad + \frac{1}{2} \left( f''(\mathbf{D}) - \frac{f'(\mathbf{D})}{D} \right) (\mathbf{v} \cdot \mathbf{d})^2 + \frac{1}{2} \frac{f'(\mathbf{D})}{D} d^2, \end{aligned} \quad (9)$$

where  $D = |\mathbf{D}|$  and  $\mathbf{v} = \mathbf{D}/D$ .

Thus the total lattice energy can be presented in the form

$$U = U_0 + U_1 + U_2. \quad (10)$$

Here,

$$U_0 = \frac{1}{2} \sum_{\mathbf{r}} \sum_{\mathbf{D}} f(\mathbf{D}) = N \sum_{\mathbf{D}} f(\mathbf{D}), \quad (11)$$

$N$  is the number of atoms in the crystal,

$$U_1 = \frac{1}{2} \sum_{\mathbf{r}} \sum_{\mathbf{D}} f'(\mathbf{D})(\mathbf{v} \cdot \mathbf{d}) = \sum_{\mathbf{D}} f'(\mathbf{D}) \sum_{\mathbf{r}} (\mathbf{v} \cdot \mathbf{d}) = 0; \quad (12)$$

and

$$U_2 = \frac{1}{4} \sum_{\mathbf{r}} \sum_{\mathbf{D}} \left\{ \left[ f''(\mathbf{D}) - \frac{f'(\mathbf{D})}{D} \right] (\mathbf{v} \cdot \mathbf{d})^2 + \frac{f'(\mathbf{D})}{D} d^2 \right\}. \quad (13)$$

(Note that  $U_0$  does not depend on  $\mathbf{d}$ , and the equality of the expression (12) to zero does not mean that  $f'(\mathbf{D}) = 0$ ).

The elements of the force matrix  $\Phi_{ik} \mathbf{r} \mathbf{r}'$  are obtained from the condition

$$\begin{aligned} \Phi_{ik}^{\mathbf{r}\mathbf{r}'} &= \frac{\partial^2 U}{\partial u_i^k \partial u_{\mathbf{r}'}^k} = \frac{\partial^2 U_2}{\partial u_{\mathbf{r}'}^k \partial u_{\mathbf{r}'}^k} = \delta_{\mathbf{r}\mathbf{r}'} \sum_{\mathbf{D}} \left\{ f''(\mathbf{D}) v_i v_k \right. \\ &\quad \left. - \frac{f'(\mathbf{D})}{D} (v_i v_k - \delta_{ik}) \right\} - f''(|\mathbf{r} - \mathbf{r}'|) \\ &\quad \times v_i^{\mathbf{r} - \mathbf{r}'} v_k^{\mathbf{r} - \mathbf{r}'} + \frac{f'(|\mathbf{r} - \mathbf{r}'|)}{|\mathbf{r} - \mathbf{r}'|} (v_i^{\mathbf{r} - \mathbf{r}'} v_k^{\mathbf{r} - \mathbf{r}'} - \delta_{ik}). \end{aligned} \quad (14)$$

Thus, for fcc crystals, we obtain from (14) the following relations between force constants (3) and derivatives of the paired potential:

$$\begin{aligned} \alpha_1 &= - \left( f''(\mathbf{D}) - \frac{f'(\mathbf{D})}{2D} \right), \\ \beta_1 &= - \frac{f'(\mathbf{D})}{D}, \quad \gamma_1 = - \left( f'' + \frac{f'(\mathbf{D})}{2D} \right), \\ \alpha_2 &= - f''(2\mathbf{D}), \quad \beta_2 = - \frac{f'(2\mathbf{D})}{2D}. \end{aligned} \quad (15)$$

Before going over to specific computations, we note that an analysis of the dynamic properties in the general form is quite cumbersome in view of the large number of independent parameters. In the present communication, we shall consider only the case of central forces, i.e., we shall assume that  $f'(D) = f'(2D) = 0$ . In this case, the number of independent parameters for each structure is reduced to just two. We shall analyze the role of the next-nearest neighbors by complicating the model gradually.

## 2. DISPERSION RELATIONS FOR CUBIC LATTICES IN THE SCALAR MODEL

Let us consider the effect of interaction with next-nearest neighbors on the dispersion relations of cubic lattices in the scalar model. This model describes the vibrations of a crystal lattice in which all atoms are displaced in the same direction, and the displacement of an atom from the equilibrium position is described by a scalar quantity. It was mentioned above that for an appropriate change in the notation, such a model can be used to describe one-magnon states in a magnetically ordered medium.<sup>13</sup>

The equation of motion of the atoms at the  $n$ th crystal lattice site in the harmonic approximation has the form

$$m \frac{\partial^2 u(n, t)}{\partial t^2} = - \sum_{n'} A(n, n') u(n', t). \quad (16)$$

Here the force constant  $A(n, n')$  describes the force acting on the atom at the  $n$ th site if the atom at the site  $n'$  is displaced by a unit element of length. Taking the interaction with two coordination spheres into consideration, we can present Eq. (16) in the form

$$\begin{aligned} m \frac{\partial^2 u(n, t)}{\partial t^2} &= - \sum_{\delta_1} A(n, n + \delta_1) u(n + \delta_1) \\ &\quad - \sum_{\delta_2} A(n, n + \delta_2) u(n + \delta_2), \end{aligned} \quad (17)$$

where  $\delta_1$  and  $\delta_2$  correspond to the first and second coordination spheres.

The condition of periodicity of the crystal lattice leads to the equality

$$A(n, n') = A(n - n'), \quad (18)$$

while the invariance of the crystal energy relative to the displacement as a whole gives

$$\sum_{\delta_i} A(n + \delta_i) = 0, \quad (i = 1, 2). \quad (19)$$

Considering the periodicity of the lattice, we seek the solution of Eq. (17) in the form

$$u(n, t) = u \exp[i(\mathbf{k} \cdot \mathbf{r} - \omega t)], \quad (20)$$

where  $\mathbf{k} = (k_x, k_y, k_z)$  is the wave vector and  $\mathbf{r}$  the radius vector of the  $n$ th site. As a result, Eq. (16) is reduced to the linear equation

$$m \omega^2 u - A(\mathbf{k}) u = 0, \quad (21)$$

where  $A(\mathbf{k}) = \sum_{\mathbf{r}} A(n) \exp(i\mathbf{k} \cdot \mathbf{r})$ .

We can now go over directly to an analysis of the dispersion relations for the scalar models of cubic lattices. We shall consider in detail the high-symmetry directions along which the peak of the dispersion curve is displaced inward into the Brillouin zone, since the emergence in the continuous spectrum of a point at which  $\partial\omega/\partial k = 0$  is extremely important. We shall also consider the cases when the lattice loses stability as a result of interaction with next-nearest neighbors.

### Simple cubic lattice

In the scalar model, the dispersion relation for an sc lattice involving first and second coordination spheres has the form

$$\begin{aligned} \lambda \equiv \frac{m \omega^2}{A_s} &= 2(3 - \cos ak_x - \cos ak_y - \cos ak_z) \\ &\quad + 4\theta_s(3 - \cos ak_x \cos ak_y - \cos ak_x \cos ak_z \\ &\quad - \cos ak_y \cos ak_z), \end{aligned} \quad (22)$$

where  $A_s$  is the force constant of interaction with the nearest neighbors, and  $\theta_s = B_s/A_s$  the ratio of force constant  $B_s$  of interaction with the next-nearest neighbors to the force constant of interaction with the nearest neighbors.

Let us study the stability of sc lattice in the scalar model taking into account the interaction with next-nearest neighbors. It can be seen from the dispersion relation (22) that for  $A_s > 0$ , the scalar model of an sc lattice is stable ( $\omega^2 > 0$ ), unlike the vector model, even if the interaction with the nearest neighbors only is taken into consideration. If the constant of interaction with the next-nearest neighbors is negative, the natural vibration frequencies for the sc lattice may turn out to be imaginary, i.e., the lattice will be unstable in this case. We shall show that the sc lattice becomes unstable for  $\theta_s < -1/4$ . For this purpose, we shall consider  $\theta_s$  as a parameter and determine the value of the wave vector for which the

difference in the contributions from the interaction between the nearest and next-nearest neighbors to the square of the frequency is maximum. For this purpose, we shall determine all stationary points for the function  $\lambda(k_x, k_y, k_z)$ , i.e., the points at which all partial derivatives of the function  $\lambda(k_x, k_y, k_z)$  vanish. Next we determine the minimal value of  $|\theta_s|$  for which the frequency of vibrations at these points is smaller than zero. Thus, we must solve a system of three trigonometric equations

$$\begin{cases} \frac{\partial \lambda}{\partial k_x} = 2a \sin ak_x + 4\theta_s a \sin ak_x (\cos ak_y + \cos ak_z) = 0 \\ \frac{\partial \lambda}{\partial k_y} = 2a \sin ak_y + 4\theta_s a \sin ak_y (\cos ak_x + \cos ak_z) = 0 \\ \frac{\partial \lambda}{\partial k_z} = 2a \sin ak_z + 4\theta_s a \sin ak_z (\cos ak_x + \cos ak_y) = 0 \end{cases} \quad (23)$$

together with the inequality

$$\lambda(k_x, k_y, k_z) < 0. \quad (24)$$

By way of an example, let us find some points satisfying the system of equations (23), and the corresponding values of  $\theta_s$  for which the inequality (24) is satisfied.

1. Let

$$\begin{aligned} \sin ak_x = 0, \quad \cos ak_x = 1, \quad \sin ak_y = 0, \\ \cos ak_y = -1, \quad \sin ak_z = 0, \quad \cos ak_z = -1. \end{aligned}$$

In this case,  $\theta_s < -1/2$ .

2. Let

$$\begin{aligned} \sin ak_x = 0, \quad \cos ak_x = 1, \quad \sin ak_y = 0, \\ \cos ak_y = 1, \quad \sin ak_z = 0, \quad \cos ak_z = -1. \end{aligned}$$

In this case,  $\theta_s < -1$ .

3. For

$$\sin ak_x = 0, \quad \cos ak_x = 1, \quad \sin ak_y \neq 0, \quad \sin ak_z \neq 0,$$

the system of equations (23) is transformed into

$$\begin{cases} \sin ak_y + 2\theta_s \sin ak_y (1 + \cos ak_z) = 0 \\ \sin ak_z + 2\theta_s \sin ak_z (1 + \cos ak_y) = 0 \end{cases}.$$

The solutions of this system of equations have the form

$$\cos ak_y = \cos ak_z = \frac{1 + 2\theta_s}{2\theta_s}.$$

The conditions  $\cos ak_y > -1$  and  $\cos ak_z > -1$  lead to the inequality  $\theta_s < -1/4$ . For the above solutions of the system of equations (23) and for  $\theta_s < -1/4$ , the function  $\lambda(k_x, k_y, k_z)$  is negative.

Taking into consideration all compatible solutions of the system of equations (23) and the inequality (24) in an analogous manner and choosing the smallest value of  $|\theta_s|$ , it can be shown that the sc lattice becomes unstable for  $\theta_s < -1/4$ .

The position of the peak on the dispersion curve and its amplitude may depend on the ratio of constants of interaction with the nearest and next-nearest neighbors. We shall

consider the dispersion relations for the sc lattice along the high-symmetry directions as functions of the parameter  $\theta_s$ , indicating the direction along which the dispersion curve peak is displaced from the Brillouin zone boundary.

In the direction  $\mathbf{k} = (k, 0, 0)$ , the dispersion relation is described by the expression

$$\lambda = 2(1 - \cos ak) + 8\theta_s(1 - \cos ak). \quad (25)$$

It can be seen from this equation that the inclusion of interaction with next-nearest neighbors does not violate the monotonicity of the dispersion relation. The maximum frequency is attained at the zone boundary. For this direction,  $\lambda_{m,k(1,0,0)} = 4 + 16\theta_s$ . Here and below,  $\lambda_{m,k}$  is the maximum value of  $\lambda$  in the direction under consideration.

For the direction  $\mathbf{k} = k/\sqrt{2}(1, 1, 0)$ , the dispersion relation has the form

$$\lambda = 4(1 - \cos ak) + 4\theta_s(3 - \cos^2 ak - 2 \cos ak). \quad (26)$$

In this direction, the peak of the dispersion curve may be displaced into the Brillouin zone only for such values of  $\theta_s$  ( $\theta_s < -1/4$ ) for which the lattice becomes unstable (see above). Thus, for this direction also, the inclusion of interaction with next-nearest neighbors does not violate the monotonicity of the dispersion relation. In this case,

$$\lambda_{m,k/\sqrt{2}(1,1,0)} = 8 + 16\theta_s.$$

For  $\mathbf{k} = (k/\sqrt{3})(1, 1, 1)$ , we have

$$\lambda = 6(1 - \cos ak) + 6\theta_s(1 - \cos 2ak). \quad (27)$$

For  $\theta_s > 1/4$ , the peak of the dispersion curve is displaced into the Brillouin zone and is attained at the point  $k_0 = (1/a)\arccos(-1/4\theta_s)$  and

$$\lambda_{m,k/\sqrt{3}(1,1,1)} = \frac{3 + 24\theta_s + 48\theta_s^2}{4\theta_s}.$$

For  $\theta_s < 1/4$ , the peak of the dispersion curve is situated at the boundary of the Brillouin zone  $k_0 = \pi/a$  and  $\lambda_{m,k/\sqrt{3}(1,1,1)} = 12$ .

Thus, in contrast to the directions  $\mathbf{k} = (k, 0, 0)$  and  $\mathbf{k} = k/\sqrt{2}(1, 1, 0)$ , the inclusion of interaction with next-nearest neighbors in the direction  $\mathbf{k} = k/\sqrt{3}(1, 1, 1)$  leads to a displacement of the dispersion curve peak into the Brillouin zone.

### Body-centered cubic lattice

The dispersion relation for a bcc lattice in the scalar model is described by the expression

$$\begin{aligned} \lambda \equiv \frac{m\omega^2}{A_b} = 8 \left( 1 - \cos \frac{ak_x}{2} \cos \frac{ak_y}{2} \cos \frac{ak_z}{2} \right) \\ + 2\theta_b(3 - \cos ak_x - \cos ak_y - \cos ak_z), \end{aligned} \quad (28)$$

where  $A_b$  is the force constant of interaction with the nearest neighbors, and  $\theta_b = B_b/A_b$  the ratio of force constant  $B_b$  of interaction with the next-nearest neighbors to the force constant of interaction with the nearest neighbors.

Unlike the vector model, the scalar model of the bcc lattice with interaction between the nearest neighbors only is

stable. This model may become unstable if interaction with the next-nearest neighbors is taken into account. Analyzing the stability of the bcc lattice in the same way as the stability of the sc lattice, it can be shown that the bcc lattice becomes unstable for  $\theta_b < -2/3$ .

It should also be noted that the inclusion of the second coordination sphere in a bcc crystal results in the disappearance of divergence of the density of vibrations at the middle of the spectrum. If interaction with nearest neighbors only is taken into consideration, it follows from (28) that for  $ak_x = \pi$  and for arbitrary values of  $k_y$  and  $k_z$  (as well as for cyclic permutation of the wave vector components)  $\lambda = 8 = \lambda_{\max}/2$ , where  $\lambda_{\max}$  is the maximum value of  $\lambda(k)$  when interaction with the nearest neighbors only is taken into account. Consequently, the middle of the frequency spectrum corresponds to an infinite set of states, which leads to the divergence of the density of states for  $\lambda = \lambda_{\max}/2$ .<sup>13,14</sup> It follows from the dispersion relation (28) that this nonphysical divergence disappears when interaction with next-nearest neighbors is taken into consideration.

Interaction with next-nearest neighbors can also affect the form of the dispersion curve significantly. We shall show this by considering the example of high-symmetry directions.

In the direction  $\mathbf{k} = (k, 0, 0)$ , the dispersion relation has the form

$$\lambda = 8 \left( 1 - \cos \frac{ak}{2} \right) + 2\theta_b(1 - \cos ak). \quad (29)$$

The quantity  $\lambda(k)$  attains its peak in this direction at the boundary of the Brillouin zone for  $\theta_b < 1$ , and  $\lambda_{m,k(1,0,0)} = 16$ . For  $\theta_b > 1$ , the dispersion curve peak is displaced into the Brillouin zone and is attained at the point  $k_0 = (2/a)\arccos(-1/\theta_b)$ ; and

$$\lambda_{m,k(1,0,0)} = 4 \frac{(1 + \theta_b)^2}{\theta_b}.$$

For the direction  $\mathbf{k} = (k/\sqrt{2})(1, 1, 0)$ , the dispersion relation has the form

$$\lambda = 4(1 - \cos ak) + 4\theta_b(1 - \cos ak) \quad (30)$$

and  $\lambda_{mk/\sqrt{2}(1,1,0)} = 8 + 8\theta_b$ . It can be seen that for this direction, the interaction with the next-nearest neighbors does not violate the monotonicity of the dispersion relation.

In the direction  $\mathbf{k} = (k/\sqrt{3})(1, 1, 1)$ , the dispersion relation has the form

$$\lambda = 8(1 - \cos^3 ak/2) + 6\theta_b(1 - \cos ak). \quad (31)$$

In this direction,  $\partial\lambda/\partial k = 0$  at the points  $k_1 = \pi/a$  and  $\cos ak_2/2 = \theta_b$ , as well as at the Brillouin zone boundaries ( $k_3 = 0, k_4 = 2\pi/a$ ). At the point  $k_1$ , the function  $\lambda(k)$  assumes the form  $\lambda(k_1) = 8 + 12\theta_b$ , while the value of this function at the point  $k_2$  is  $\lambda(k_2) = 8 + 12\theta_b - 4\theta^3$ .

At the upper boundary of the Brillouin zone, the function  $\lambda(k)$  assumes the value  $\lambda(k_4) = 16$ .

It can be seen that in the interval  $-2/3 < \theta_b < 0$ , the dispersion relation (31) has a peak at the point  $k_2$  and a minimum at the point  $k_1$ . For  $0 < \theta_b < 1$ , the dispersion curve peak is situated inside the Brillouin zone at the point  $k_1$ , and

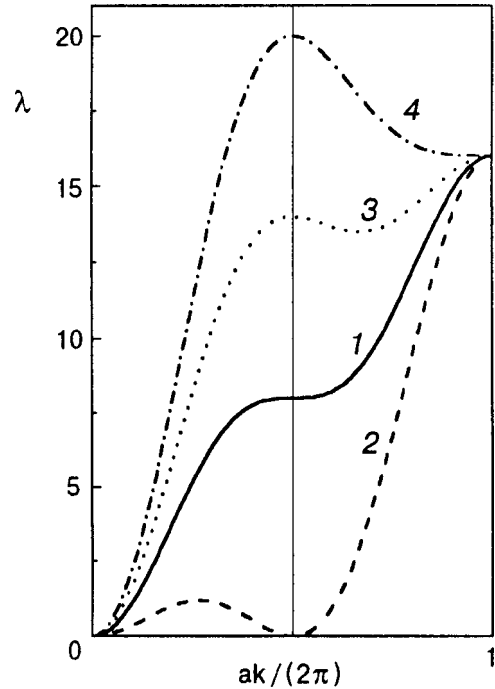


FIG. 1. Dispersion curves for a bcc lattice obtained in the scalar model along the [111] direction. Curves 1–4 correspond to  $\theta_b = 0, -2/3, 0.5$  and  $1$ , respectively.

the minimum at the point  $k_2$ . For  $\theta_b > 1$ , the function  $\lambda(k)$  has a peak at the point  $k_1$  and a minimum at the boundary of the Brillouin zone (see Fig. 1).

Thus, it can be seen that unlike the sc lattice, the bcc lattice may exhibit in the direction  $\mathbf{k} = 1/\sqrt{3}(1, 1, 1)$  an additional peak as well as an additional minimum inside the Brillouin zone in the lattice stability region as a result of the inclusion of an indefinitely small interaction with the next-nearest neighbors. Moreover, the inclusion of an indefinitely small interaction with the next-nearest neighbors leads to the disappearance of the divergence of vibrational density at the middle of the phonon spectrum.

### Face-centered cubic lattice

The dispersion relation for an fcc lattice has the form

$$\lambda \equiv \frac{m\omega^2}{A_f} = 4 \left( 3 - \cos \frac{ak_x}{2} \cos \frac{ak_y}{2} - \cos \frac{ak_x}{2} \cos \frac{ak_z}{2} - \cos \frac{ak_y}{2} \cos \frac{ak_z}{2} \right) + 2\theta_f \left( 3 - \cos ak_x - \cos ak_y - \cos ak_z \right), \quad (32)$$

where  $A_f$  is the force constant of interaction with the nearest neighbors, and  $\theta_f = B_f/A_f$  the ratio of force constant  $B_f$  of interaction with the next-nearest neighbors to the force constant of interaction with the nearest neighbors.

The fcc lattice is stable when the interaction with nearest neighbors only is taken into consideration. Analyzing the stability of the fcc lattice in the same way as the sc lattice, it can be shown that the fcc lattice is unstable for  $\theta_f < -1$ .

It can also be seen easily that the dispersion curve peak and its position may depend on the ratio of the constants of interaction with the nearest and next-nearest neighbors. We shall analyze the dispersion relation (32) for an fcc lattice along the high-symmetry directions and show that the inclusion of an indefinitely small interaction with the next-nearest neighbors may displace the dispersion curve peak into the Brillouin zone.

In the direction  $\mathbf{k}=(k,0,0)$ , the dispersion relation has the form

$$\lambda = 4 \left( 1 - \cos \frac{ak}{2} \right) + 2\theta_f(1 - \cos ak). \quad (33)$$

For  $\theta_f > 1$ , the frequency peak is displaced away from the Brillouin zone and is attained at the point  $k_0 = (2/a)\arccos(-1/\theta_f)$ , and

$$\lambda_{m,k(1,0,0)} = \frac{4(1 + \theta_f)^2}{\theta_f^2}.$$

For  $\theta_f < 1$ , we have  $\lambda_{m,k(1,1,0)} = 8\theta_f$ .

For the direction  $\mathbf{k}=(k/\sqrt{2})(1,1,0)$ , the dispersion relation has the form

$$\lambda = 4 \left( 3 - \cos^2 \frac{ak}{2} - 2 \cos \frac{ak}{2} \right) + 2\theta_f(1 - \cos ak). \quad (34)$$

For an indefinitely small value of  $\theta_f$ , the peak of the dispersion curve is displaced into the Brillouin zone and is attained at the point  $k_0 = (2/a)\arccos(-1/(2\theta_f + 1))$ . In this case,

$$\lambda_{m,k/\sqrt{2}(1,1,0)} = \frac{16(1 + \theta_f)^2}{1 + 2\theta_f}.$$

For the direction  $\mathbf{k}=(k/\sqrt{3})(1,1,1)$ , the dispersion relation has the form

$$\lambda = 6(1 - \cos ak) + 6\theta_f(1 - \cos ak). \quad (35)$$

In this direction, the inclusion of interaction with the next-nearest neighbors does not violate the monotonicity of  $\lambda(k)$  and

$$\lambda_{m,k/\sqrt{3}(1,1,1)} = 12 + 12\theta_f.$$

It should be reiterated that the fcc lattice has a high-symmetry direction  $\mathbf{k}=k/\sqrt{2}(1,1,0)$  along which the dispersion relation peak is displaced into the Brillouin zone for an arbitrarily small value of the constant of interaction with the next-nearest neighbors.

Thus, it can be seen that the inclusion of interaction with the next-nearest neighbors for positive force constants may lead to a displacement of the dispersion curve peak of cubic lattices into the Brillouin zone and to the emergence of an additional minimum on the dispersion curve in the Brillouin zone. Moreover, the inclusion of the second coordination sphere changes the maximum vibrational frequency. In the case of negative force constants of interaction with next-nearest neighbors (exchange integral in magnetically ordered systems), it is shown that the sc lattice remains stable for  $\theta_s > -1/4$ , while the bcc and fcc lattices remain stable for  $\theta_b > -2/3$  and  $\theta_f > -1$ , respectively. It was shown above that the inclusion of interaction with the next-nearest neigh-

bors in the case of the scalar model removes the divergence of the vibrational density for a bcc crystal in the middle of the frequency spectrum. The effect of interaction with the next-nearest neighbors on the dynamic properties of the cubic lattices is not confined to these facts. Thus, the dispersion relation for an fcc crystal along the line  $k_x + k_y = \pi/a$  is independent of  $k_z$ . This leads to the emergence of a singularity in the density of vibrations at the upper boundary of the phonon spectrum. If the interaction with the next-nearest neighbors is taken into consideration, this singularity disappears and the density of states vanishes at the upper boundary of the spectrum.<sup>15</sup> Interaction with the next-nearest neighbors also affects considerably the properties of surface waves. For example, no surface waves are formed in the nearest-neighbor model for an sc lattice with surface plane of the type (1,0,0). Surface waves emerge as the interaction with next-nearest neighbors is taken into consideration in this geometry. Presenting the displacement of the  $n$ th layer of atoms in the form  $u_n = u_0 q^n$ , we can easily show that  $q = 1$  in the nearest-neighbor model, while the inclusion of interaction with the next-nearest neighbors gives

$$q = \frac{1 + 2\theta_s(\cos ak_x + \cos ak_y)}{1 + 4\theta_s} < 1.$$

For fcc and bcc lattices, the inclusion of interaction with the next-nearest neighbors transforms one-partial surface waves into two-partial waves, i.e., the surface waves have the form  $u_n = u_1 q^n + u_2 q^n$ .<sup>16</sup>

### 3. DISPERSION RELATIONS FOR CUBIC LATTICES IN THE VECTOR MODEL

Let us consider models in which the displacement  $\mathbf{u}(n)$  of an atom at the  $n$ th site is a vector quantity. In the harmonic approximation, the equation of motion for an atom in the crystal lattice at the site  $n$  has the form

$$m \frac{\partial^2 u_i(n,t)}{\partial t^2} = - \sum_{n'k} \Phi_{ik}(n,n') u_k(n',t), \quad (36)$$

where  $\Phi_{ik}(n,n')$  is the matrix of force constants, and the coordinate indices  $i,k=1,2,3$ . Taking into account the interaction with next-nearest neighbors, we can present the equation of motion (36) in the form

$$m \frac{\partial^2 u_i(n,t)}{\partial t^2} = - \sum_{\delta_1 k} \Phi_{ik}(n,n + \delta_1) u_k(n + \delta_1) - \sum_{\delta_2 k} \Phi_{ik}(n,n + \delta_2) u_k(n + \delta_2). \quad (37)$$

Here  $\delta_1$  and  $\delta_2$  correspond to the first and second coordination spheres. The condition of periodicity of the crystal lattice leads to a relation analogous to (18):

$$\Phi_{ik}(n,n') = \Phi_{ik}(n - n'). \quad (38)$$

The solution of Eq. (36) is sought in the form

$$u_i(n,t) = u_i \exp(i(\mathbf{k} \cdot \mathbf{r} - \omega t)), \quad (39)$$

where  $\mathbf{k}(k_x, k_y, k_z)$  is the wave vector and  $\mathbf{r}$  the radius-vector of the site  $n$ . As a result, we arrive at the system of equations

$$[m\omega^2 \delta_{ik} - L_{ik}(\mathbf{k})]u_k = 0, \tag{40}$$

where the dynamic matrix

$$L_{ik}(\mathbf{k}) = \sum_{\mathbf{r}} \Phi_{ik}(n) \exp(i\mathbf{k} \cdot \mathbf{r}). \tag{41}$$

Solution of the system of equations (40) leads to the dispersion relations. We shall consider below these dispersion relations for lattices with cubic symmetry in the high-symmetry directions.

**Simple cubic lattice**

The sc lattice structure is possessed by a wide range of materials, including TlBr, TlI, NH<sub>4</sub>Cl, CuPd, CuZn ( $\beta$ -brass) and one of the phases of C<sub>60</sub>. We shall use the matrices (1)

in the case of central interaction with the nearest and next-nearest neighbors. Denoting by  $\varepsilon_s$  and  $\delta_s$  the force constants of central interaction between the nearest and next-nearest neighbors respectively, we can write for the matrices (1)  $\alpha_1 = \varepsilon_s$ ,  $\alpha_2 = \delta_s$ ,  $\beta_1 = 0$ ,  $\beta_2 = 0$  and  $\alpha_2 = \gamma_2$ .

In this case, the dynamic matrix  $L_{ik}^{(1)}(\mathbf{k})$  of interaction with the nearest neighbors has the form

$$L_{ik}^{(1)} = 2\varepsilon_s \begin{pmatrix} 1 - \cos ak_x & 0 & 0 \\ 0 & 1 - \cos ak_y & 0 \\ 0 & 0 & 1 - \cos ak_z \end{pmatrix}. \tag{42}$$

The dynamic matrix  $L_{ik}^{(2)}(\mathbf{k})$  of interaction with the next-nearest neighbors has the form

$$L_{ik}^{(2)}(\mathbf{k}) = 4\delta_s \begin{pmatrix} 2 - \cos ak_x(\cos ak_y + \cos ak_z) & \sin ak_x \sin ak_y & \sin ak_x \sin ak_z \\ \sin ak_x \sin ak_y & 2 - \cos ak_y(\cos ak_x + \cos ak_z) & \sin ak_y \sin ak_z \\ \sin ak_x \sin ak_z & \sin ak_y \sin ak_z & 2 - \cos ak_z(\cos ak_y + \cos ak_x) \end{pmatrix}. \tag{43}$$

Let us analyze the form of the dispersion relations for different directions of  $\mathbf{k}$ .

In the direction  $\mathbf{k} = (k, 0, 0)$ , the dispersion relation has the form

$$\lambda_l = (2 + 8\mu_s)(1 - \cos ak),$$

$$\lambda_{t1} = \lambda_{t2} = 4\mu_s(1 - \cos ak),$$

where  $\lambda_l$  corresponds to longitudinal vibrations with frequency  $\omega_l$ ,  $\lambda_{t,i} (i = 1, 2)$  corresponds to transverse vibrations with frequency  $\omega_{t,i}$ ,  $a$  is the lattice constant,  $\lambda_{l(i)} \equiv m\omega_{l(i)}^2/\varepsilon_s$ , and  $\mu_s = \delta_s/\varepsilon_s$ . It can be seen that transverse vibrations are determined only by the interaction with the next-nearest neighbors. Thus, the model becomes stable if the interaction with next-nearest neighbors is taken into consideration.

For the direction  $\mathbf{k} = (k/\sqrt{2})(1, 1, 0)$ , the dispersion curves assume the form

$$\lambda_l = 2(1 - \cos ak) + 4\mu_s(2 - \cos 2ak - \cos ak),$$

$$\lambda_{t1} = 2(1 - \cos ak) + 4\mu_s(1 - \cos ak),$$

$$\lambda_{t2} = 8\mu_s(1 - \cos ak).$$

In this case, one of the branches of transverse vibrations is determined by the interaction with the nearest and next-nearest neighbors, while the other branch is determined only by interaction with the second coordination sphere.

For the direction  $\mathbf{k} = (k/\sqrt{3})(1, 1, 1)$ , we can write

$$\lambda_l = 2(1 - \cos ak) + 8\mu_s(1 - \cos 2ak),$$

$$\lambda_{t1} = \lambda_{t2} = 2(1 - \cos ak) + 2\mu_s(1 - \cos 2ak).$$

It can be seen clearly that inclusion of interaction with the second coordination sphere leads to a splitting of the triply degenerate mode into a longitudinal and a doubly degenerate

transverse modes, and may also lead to a displacement of the peak of  $\lambda_l(k)$  from the Brillouin zone boundary. For  $\mu_s > 1/16$ , the peak on the curve  $\lambda_l(k)$  is displaced into the Brillouin zone (see Fig. 2), while a similar displacement of

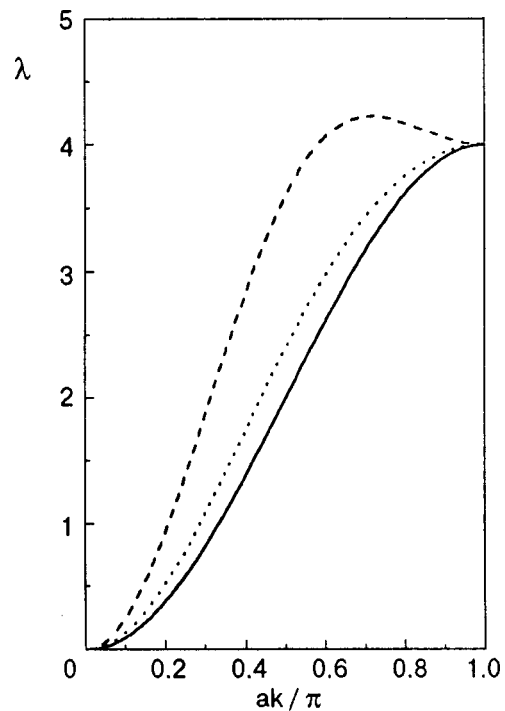


FIG. 2. Dispersion curves for an sc lattice along the [111] direction. The solid curve is a triply degenerate dispersion curve obtained by taking into account the interaction with nearest neighbors only ( $\mu_s = 0$ ). The dashed curve corresponds to the branch of longitudinal vibrations and was obtained by taking into account the interaction with next-nearest neighbors ( $\mu_s = 0.1$ ). The dotted curve corresponds to a double degeneracy of the transverse vibrational branch ( $\mu_s = 0.1$ ).

the  $\lambda_l(k)$  peak occurs for  $\mu_s > 1/4$ .

To analyze the elastic stability, we express the elastic moduli  $C_{xxxx} = C_{11}$ ,  $C_{xxyy} = C_{12}$ ,  $C_{xyxy} = C_{44}$ . (Voigt's notation<sup>17</sup>) in terms of the force constants. For the sc lattice, we can write

$$C_{11} = \frac{\varepsilon_s + 4\delta_s}{a}, \quad C_{12} = \frac{2\delta_s}{a}, \quad C_{44} = \frac{2\delta_s}{a}. \quad (44)$$

Naturally, the Cauchy condition (inclusion of central forces only) is observed for the sc lattice, as also for the other two cases considered by us:

$$C_{12} = C_{44}. \quad (45)$$

Moreover, it follows from the condition of elastic stability<sup>17</sup>

$$C_{44} > 0 \quad (46)$$

that  $\delta_s > 0$ .

The anisotropy parameter for a cubic symmetry crystal has the form

$$\eta = \frac{C_{11} - C_{12}}{2C_{44}} = \frac{C_{t1}^2}{C_{t2}^2}, \quad (47)$$

where  $C_{t1} = \sqrt{(C_{11} - C_{12})/2\rho}$ ,  $C_{t2} = \sqrt{C_{44}/\rho}$  are the transverse velocities of sound in a cubic crystal, and  $\rho$  is the density of the crystal. For the sc lattice, the anisotropy parameter  $\eta$  has the form

$$\eta = \frac{\varepsilon_s + 2\delta_s}{4\delta_s}. \quad (48)$$

It follows from Eq. (48) that  $\eta \gg 1$  for a weak interaction with the next-nearest neighbors, i.e., the sc lattice in the longwave limit corresponds to a highly anisotropic medium. For  $\delta_s = \varepsilon_s/2$ , the sc lattice in the longwave limit will correspond to an isotropic medium ( $\eta = 1$ ). Earlier, it was shown by Kosevich *et al.*<sup>18</sup> that a change in the anisotropy parameter over such a wide range in the theory of elasticity leads to significant variation of the properties of surface waves in crystals of cubic symmetry: the penetration depth and the velocity of propagation of the waves changes, and a transition from the conventional Rayleigh wave to a generalized wave occurs.

### Body-centered cubic lattice

The body-centered cubic lattice is possessed by a very wide range of materials like Fe, Nb, V, Mo, SF<sub>6</sub>, Na, Ta, Nb, Cr, and one of the solid <sup>3</sup>He phases. For the case of central interaction in the force matrices of a bcc crystal<sup>2</sup> considered by us,  $\alpha_1 = \beta_1 = \varepsilon_b$ ,  $\alpha_2 = \delta_b$ ,  $\beta_2 = 0$ . For such a relation between the parameters, the dynamic matrix of interaction with the nearest neighbors has the form

$$L_{ik}^{(1)} = \varepsilon_b \begin{pmatrix} 1 - \cos \frac{ak_x}{2} \cos \frac{ak_y}{2} \cos \frac{ak_z}{2} & \cos \frac{ak_z}{2} \sin \frac{ak_x}{2} \sin \frac{ak_y}{2} & \cos \frac{ak_y}{2} \sin \frac{ak_x}{2} \sin \frac{ak_z}{2} \\ \cos \frac{ak_z}{2} \sin \frac{ak_x}{2} \sin \frac{ak_y}{2} & 1 - \cos \frac{ak_x}{2} \cos \frac{ak_y}{2} \cos \frac{ak_z}{2} & \cos \frac{ak_x}{2} \sin \frac{ak_y}{2} \sin \frac{ak_z}{2} \\ \cos \frac{ak_y}{2} \sin \frac{ak_x}{2} \sin \frac{ak_z}{2} & \cos \frac{ak_x}{2} \sin \frac{ak_y}{2} \sin \frac{ak_z}{2} & 1 - \cos \frac{ak_x}{2} \cos \frac{ak_y}{2} \cos \frac{ak_z}{2} \end{pmatrix}. \quad (49)$$

The dynamic matrix of interaction with the next-nearest neighbors can be represented in the form

$$L_{ik}^{(2)} = 2\delta_b \begin{pmatrix} 1 - \cos ak_x & 0 & 0 \\ 0 & 1 - \cos ak_y & 0 \\ 0 & 0 & 1 - \cos ak_z \end{pmatrix}. \quad (50)$$

Let us analyze the dispersion relations for the bcc lattice taking into account the interaction with the nearest and next-nearest neighbors.

In the direction  $\mathbf{k} = (k, 0, 0)$ , the dispersion relations have the form

$$\lambda_l = 8 \left( 1 - \cos \frac{ak}{2} \right) + 2\mu_b (1 - \cos ak),$$

$$\lambda_{t1} = \lambda_{t2} = 8 \left( 1 - \cos \frac{ak}{2} \right).$$

Here,  $\lambda_{l(t)} \equiv m\omega_{l(t)}^2/\varepsilon_b$ ,  $\mu_b = \delta_b/\varepsilon_b$ . It can be seen that the inclusion of interaction with the next-nearest neighbors leads to a splitting of the triply degenerate mode into a longitudinal and a doubly degenerate transverse modes. For  $\mu_b > 1$ , the peak on the longitudinal vibrations curve is displaced into the Brillouin zone. The experimentally determined dispersion curves for Fe, Nb, V, Mo, and Cr have a peak on the longitudinal vibrational branch along  $\mathbf{k} = (k, 0, 0)$  in the Brillouin zone, while for Na and Ta, for example, the peak on the longitudinal branch is attained at the edge of the band.<sup>6,7</sup>

For the direction  $\mathbf{k} = (k/\sqrt{2})(1, 1, 0)$ , the dispersion relations have the form

$$\lambda_l = 8 \left( 1 - \cos \frac{ak}{2} \right) + 2\mu_b (1 - \cos ak),$$

$$\lambda_{t1} = 4(1 - \cos ak), \quad \lambda_{t2} = 2\mu_b (1 - \cos ak).$$

It can be seen that as in the case of an sc lattice, one of the branches of transverse vibrations is determined by a weak

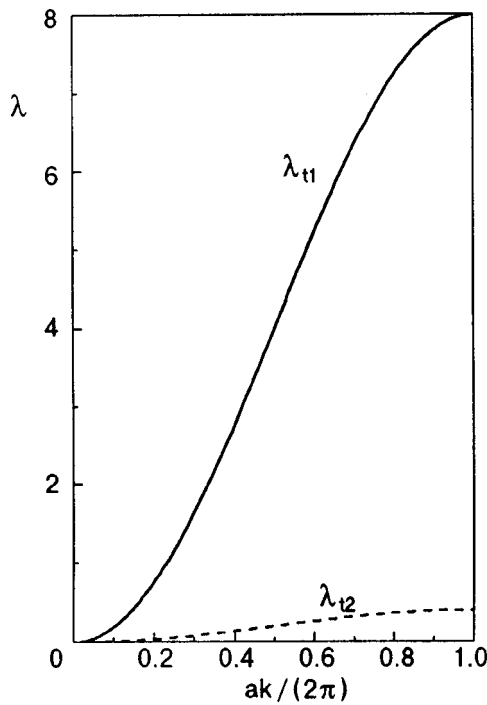


FIG. 3. Transverse branches of vibrations of a bcc lattice along the [110] direction for  $\mu_b=0.1$  (highly anisotropic medium).

interaction with the next-nearest neighbors, while the other is defined by a strong interaction with the nearest neighbors (see Fig. 3).

For the direction  $\mathbf{k}=(k/\sqrt{3})(1,1,1)$ , the dispersion relations have the form

$$\lambda_l = 2 \left( 4 - \cos \frac{ak}{2} - 3 \cos \frac{3ak}{2} \right) + 2\mu_b(1 - \cos ak),$$

$$\lambda_{l1} = \lambda_{l2} = 8 \left( 1 - \cos \frac{ak}{2} \right) + 2\mu_b(1 - \cos ak).$$

For this direction, the inclusion of interaction with the next-nearest neighbors does not lead to a qualitative variation of the dispersion relation. It should be observed that for  $\mu_b > 1$ , the peak on the curve of transverse vibrations is displaced into the Brillouin zone.

We shall now analyze the anisotropy parameter for the bcc lattice. The elastic moduli of a bcc crystal have the form

$$C_{11} = \frac{2(\varepsilon_b + \delta_b)}{a}, \quad C_{12} = \frac{2\varepsilon_b}{a}, \quad C_{44} = \frac{2\varepsilon_b}{a}. \quad (51)$$

The anisotropy parameter for a bcc crystal can be presented in terms of the force constants:

$$\eta = \delta_b / 2\varepsilon_b. \quad (52)$$

If we disregard the role of the next-nearest neighbors,  $C_{11} - C_{12}$  vanishes (elastic instability), while a variation of the ratio  $\delta_b/\varepsilon_b$  may transform (in the longwave limit) a highly anisotropic crystal into an isotropic one. It follows from formula (52) that for  $\delta_b \ll \varepsilon_b$ , a bcc crystal is a highly anisotropic medium ( $\eta \ll 1$ ) in the longwave limit. For  $\delta_b = 2\varepsilon_b$ , the anisotropy parameter  $\eta = 1$  (the medium is isotropic). In other words, the parameter  $\eta$  may change over a

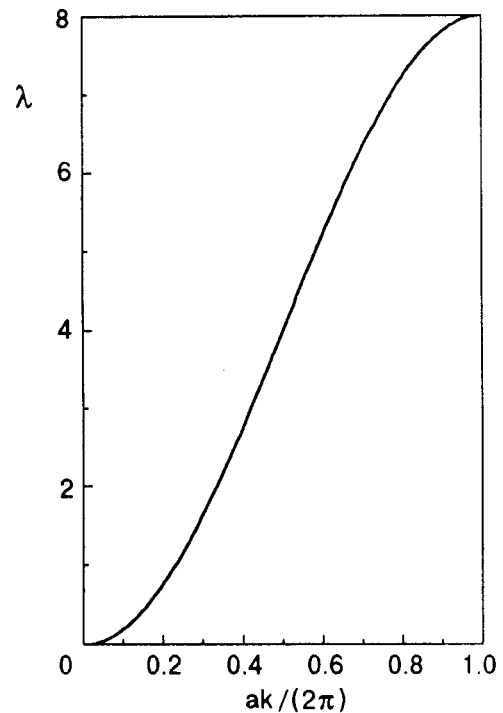


FIG. 4. Doubly degenerate transverse branch of vibrations of a bcc crystal along the [110] direction for  $\mu_b=2$  (isotropic medium).

wide range, as in the case of an sc lattice, depending on the ratio of the constants of interaction between the nearest and next-nearest neighbors (see Figs. 3 and 4). It was shown by Tyson<sup>6</sup> and by Gospodarev and Syrkin<sup>7</sup> that for a number of bcc metals, the constants of interaction with the next-nearest neighbors may turn out to be more than twice as large as the constants of interaction with the nearest neighbors.

**Face-centered cubic lattice**

Like the structures considered above, the fcc structure is quite widespread. Solidified inert gases, Ag, Ni, Cu, and Pa all have the fcc lattice. For a central interaction between the nearest and next-nearest neighbors in the force matrices (3) of an fcc crystal,  $\beta_1=0$ ,  $\alpha_1 = \gamma_1 = \varepsilon_f$ ,  $\beta_2=0$ , and  $\alpha_2 = \delta_f$ . Interaction with the next-nearest neighbors does not affect significantly the fcc lattice spectrum. It should only be remarked that in the direction  $\mathbf{k}=(k,0,0)$ , the peak of the longitudinal vibrations curve is displaced from the Brillouin zone boundary for  $\delta_f > \varepsilon_f$ . In the direction  $\mathbf{k}=(k/\sqrt{2})(1,1,0)$ , the peak of one of the branches of transverse vibrations is displaced into the Brillouin zone for  $\delta_f > 0.5\varepsilon_f$ . Thus, it can be seen that for  $\delta_f \ll \varepsilon_f$  the dispersion relations for an fcc crystal can be described quite accurately by taking into account interaction with the nearest neighbors only.

As in the case of sc and bcc lattices, let us analyze the condition of elastic stability of an fcc lattice (for an arbitrary ratio of the constants of interaction between nearest and next-nearest neighbors). The elastic moduli for an fcc crystal can be represented in the form

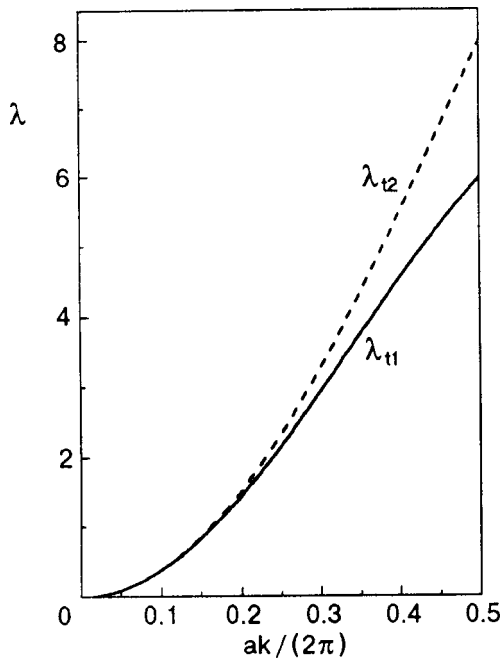


FIG. 5. Transverse branches of vibrations of an fcc lattice along the [110] direction for  $\mu_f=0.5$  (isotropic medium).

$$C_{11} = \frac{4(\epsilon_f + \delta_f)}{a}, \quad C_{12} = \frac{2\epsilon_f}{a}, \quad C_{44} = \frac{2\epsilon_f}{a}. \quad (53)$$

It follows from this relation that for  $\epsilon_f > 0$ , the fcc lattice remains stable for  $\delta_f > -\epsilon_f$ . The anisotropy parameter for an fcc crystal has the form

$$\eta = \frac{\epsilon_f + 2\delta_f}{2\epsilon_f}. \quad (54)$$

It follows from this expression that in the longwave limit, the fcc crystal is anisotropic for  $\delta_f \neq \epsilon_f/2$  and isotropic for  $\delta_f = \epsilon_f/2$ .

By way of an illustration of this fact, let us consider the dispersion relation for the transverse vibrations in the direction  $\mathbf{k} = k/\sqrt{2}(1,1,0)$ :

$$\lambda_{t1} = 4 \left( 1 - \cos \frac{ak}{2} \right) + 2\mu_f(1 - \cos ak),$$

$$\lambda_{t,2} = 8 \left( 1 - \cos \frac{ak}{2} \right).$$

Here,  $\mu_f = \delta_f/\epsilon_f$ . It can be seen that in the longwave limit ( $ak \ll 1$ ), the dispersion relations for transverse branches coincide for  $\delta_f = \epsilon_f/2$  (see Fig. 5), while for  $ak \gg 1$  these relations are not identical. If the conditions corresponding to an isotropic medium are satisfied for sc and bcc lattices, the transverse branches coincide for all values of  $k$  (see Fig. 4). The dispersion relations for an fcc crystal are presented in Fig. 6 for the case  $\delta_f = (0.1)\epsilon_f$ . Such a relation between the force constants corresponds to solidified inert gases.<sup>19</sup>

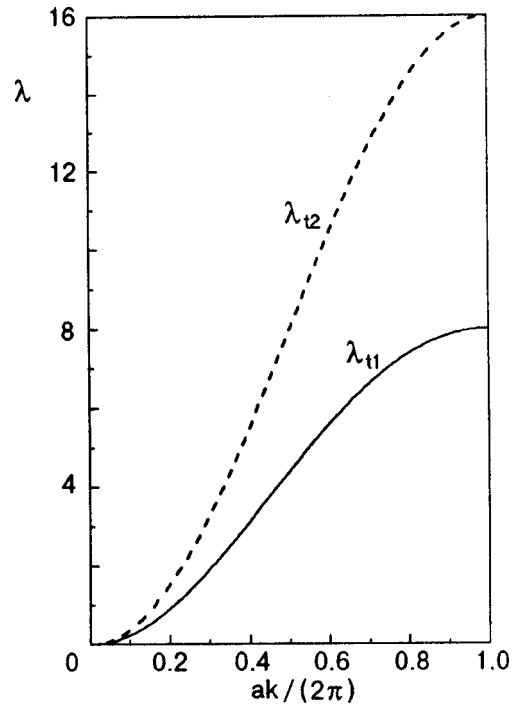


FIG. 6. Transverse branches of vibrations of an fcc lattice along the [110] direction for  $\mu_f=0.1$  (highly anisotropic medium).

### CONCLUSIONS

The role of the next-nearest neighbors is found to be extremely important for studying the vibrational spectrum of cubic lattices.

In scalar models, the inclusion of the second coordination sphere may be manifested in the displacement of the peak of dispersion curves into the Brillouin zone, and also leads to the disappearance of ‘‘nonphysical’’ singularities in the vibration density: at the upper boundary of the continuous spectrum in fcc crystals and in the middle of the spectrum for bcc crystals.

In vector models of cubic lattices, the inclusion of interaction with the next-nearest neighbors may lead to a variation of the ‘‘anisotropy parameter’’ over a wide range: in the longwave limit, the two transverse branches may coincide (isotropic medium) or differ significantly (highly anisotropic medium) depending on the ratio of the force constants of interaction between nearest and next-nearest neighbors. Among other things, this result makes it possible to determine the nature of propagation of acoustic surface waves in cubic crystals in the longwave approximation with the help of microscopic characteristics like force constants of interaction between the nearest and next-nearest neighbors. An analysis carried out within the framework of the theory of elasticity shows that in strongly anisotropic crystals, the penetration depth of a Rayleigh wave increases while the velocity of its propagation decreases and its polarization becomes almost linear rather than elliptic as in the case of weakly anisotropic crystals.

Moreover, the next-nearest neighbors can either ensure lattice stability or, on the other hand, make the lattice unstable. The analysis carried out in this work also shows that

the interaction of the third and subsequent neighbors cannot lead to such radical variations in the phonon spectrum.

The authors are indebted to A. M. Kosevich for fruitful critical remarks on the initial version of this paper.

\*)E-mail: emanzhelii@ilt.kharkov.ua

<sup>1</sup>G. Leibfried, *Microscopic Theory of Mechanical and Thermal Properties of Crystals*, in *Handbuch der Physik*, Vol. 7, Pt. 1, edited by S. Flügge, Springer-Verlag, Berlin, 1957.

<sup>2</sup>A. M. Kosevich, *Theory of Crystal Lattice* [in Russian], Vyssha Shkola, Kharkov (1988)

<sup>3</sup>H. G. Bohn, A. Kollmar, and W. Zinn, *Phys. Rev. B* **30**, 6504 (1984).

<sup>4</sup>T. G. Petrova and E. S. Syrkin, *Fiz. Nizk. Temp.* **17**, 411 (1991) [*Sov. J. Low Temp. Phys.* **17**, 215 (1991)].

<sup>5</sup>T. G. Petrova and E. S. Syrkin, *Phys. Stat. Sol.* **104**, 375 (1981).

<sup>6</sup>W. R. Tyson, *Appl. Phys.* **47**, 459 (1976).

<sup>7</sup>I. A. Gospodarev and E. S. Syrkin, *Poverkhnost'* **4**, 8 (1987).

<sup>8</sup>G. K. Horton and J. W. Leech, *Proc. Phys. Soc.* **82**, 816 (1963).

<sup>9</sup>Yu. V. Gulyaev, *Pis'ma Zh. Éksp. Teor. Fiz.* **9**, 63 (1969) [*JETP Lett.* **9**, 37 (1969)].

<sup>10</sup>J. L. Bleustein, *Appl. Phys. Lett.* **13**, 412 (1968).

<sup>11</sup>G. P. Alldredge, *Phys. Lett.* **41A**, 281 (1972).

<sup>12</sup>I. M. Gel'fgat, *Fiz. Tverd. Tela (Leningrad)* **19**, 1711 (1977) [*Sov. Phys. Solid State* **19**, 998 (1977)].

<sup>13</sup>Yu. A. Izyumov and M. V. Medvedev, *Theory of Magnetically Ordered Crystals Containing Impurities*, Consultants Bureau, New York (1973).

<sup>14</sup>V. I. Peresada, V. N. Afanas'ev, and V. S. Borovikov, *Fiz. Nizk. Temp.* **1**, 461 (1975) [*Sov. J. Low Temp. Phys.* **1**, 227 (1975)].

<sup>15</sup>A. M. Kosevich, M. L. Polyakov, and E. S. Syrkin, *Fiz. Nizk. Temp.* **15**, 1194 (1989) [*Sov. J. Low Temp. Phys.* **15**, 658 (1989)].

<sup>16</sup>A. M. Kosevich, E. S. Syrkin, and A. V. Tutov, *Acoust. Imaging* [in press].

<sup>17</sup>F. I. Fedorov, *Theory of Elastic Waves in Crystals*, Plenum Press, New York, 1968.

<sup>18</sup>A. M. Kosevich, Yu. A. Kosevich, and E. S. Syrkin, *Zh. Éksp. Teor. Fiz.* **88**, 1089 (1985) [*Sov. Phys. JETP* **61**, 639 (1985)].

<sup>19</sup>A. I. Karasevskii and V. V. Lubashenko, *Phys. Status Solidi B* **194**, 483 (1996).

Translated by R. S. Wadhwa

## ERRATA

**Erratum: Growth and dissolution kinetics of  $^3\text{He}$  inclusions in phase-separated  $^3\text{He}$ - $^4\text{He}$  solid mixtures [Low Temp. Physics 25, 592–606 (August–September 1999)]**

A. N. Gan'shin, V. N. Grigor'ev, V. A. Maïdanov, N. F. Omelaenko, A. A. Penzev,  
E. Ya. Rudavskii, A. S. Rybalko, and Yu. A. Tokar  
Fiz. Nizk. Temp. **25**, 1237 (November 1999)

© 1999 American Institute of Physics. [S1063-777X(99)01211-6]

Due to a production error, Fig. 21 was erroneously replaced with a copy of Fig. 23. The correct Fig. 21 is presented below.

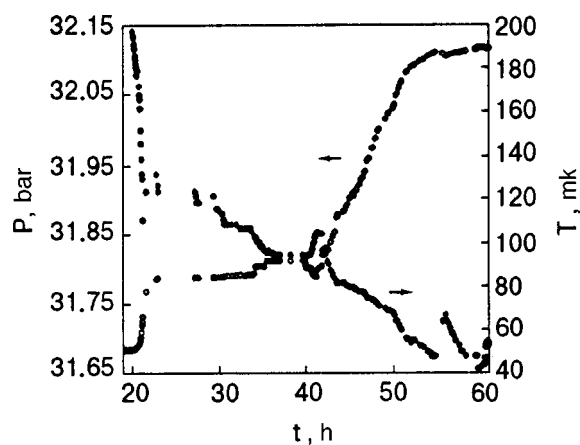


FIG. 21. Thermogram of the cooling of a crystal and the corresponding pressure change illustrating the layering at 100 mK and the fusion of  $^3\text{He}$  cluster formation upon further cooling,  $V=20.54\text{ cm}^3/\text{mole}$ .